UNIVERSITY OF CALIFORNIA
RIVERSIDE

Entanglement, Symmetry Factorization, and Topological States of Matter: From Theory to Applications

A Dissertation submitted in partial satisfaction
of the requirements for the degree of

Doctor of Philosophy

in

Physics

by

Pak Kau Lim

December 2024

Dissertation Committee:
Professor Michael Mulligan, Chairperson
Professor Jeffrey Teo
Professor Leonid Pryadko

The Dissertation of Pak Kau Lim is approved:

Committee Chairperson

University of California, Riverside

Acknowledgments

I am deeply grateful to my advisors, without whose help I would not be here.

I am grateful to Mike (Michael Mulligan) for financially supporting my research and always amazing me with his insightful questions. Mike gave me the freedom to choose my own research topics and was always there for me. I valued his advice and clever insights.

I am indebted to Jeffrey (Jeffrey Teo) for his patience in teaching me physics and technical subjects. I learned a lot from our weekly chats. During our meetings, he would scribe math equations that I would spend days or weeks deciphering and deriving new materials. I enjoyed the time we spent working together, despite my struggles with writing, especially those eureka moments when we resolved mathematically related technical issues, and even our heated arguments. Throughout working with them, I learned the value of making good mistakes.

I am grateful to Leonid (Professor Leonid Pryadko), who taught me three quarters of Statistical Mechanics. I enjoyed his classes and exam questions. More importantly, he kindly accepted me into his group. While I left to work on topological states of matter in my second year, he later welcomed me back to continue my research on quantum error correction. Through this, I felt like I finally found my place in physics, researching on something more practical and important that utilized my training in mathematics and physics. He has always been welcoming in his office to discuss physics, mathematics, and programming. This last year of my PhD has been the most precious and meaningful time, despite many personal challenges.

I am particularly thankful to Kirill Shetengel for introducing me to quantum entanglement, anyons, and fusion rules. I am forever indebted to Professor Randall Leveque, who expressed interest in working with me on applied numerical analysis and computational fluid dynamics while I was at the University of Washington (UW). When I decided to switch to theoretical physics, he introduced me to a physicist from the Physics Department and generously wrote me a letter of recommendation to assist with my transition. I kept my promise to him and published at least three solid theoretical papers in physics during my PhD.

I am deeply thankful to my dearest friends Ava Mauro and Rocío González, with whom I studied pure mathematics at Boston University. They helped me through the pandemic lockdown, especially Ava, who I shared my various writings and letters with, providing me with valuable and heartfelt feedback.

I also express my gratitude to my friends from the UW. Despite being graduate students from different departments, I learned a tremendous amount about mathematics and honed my math skills studying with Donsub Rim and Hai Zhu. I cherish the fond memories of a summer when we read through Evans' partial differential equations and Jackson's electrodynamics together.

Additionally, I am grateful to Ting Lin, Shehlit Chang, and Liyuan Zheng. We took various graduate classes together at UW, from electrodynamics to quantum field theory to particle phenomenology. We spent countless hours competing and collaborating on homework. Despite our occasionally furious discussions, thanks to Shehlit, we have remained close friends and appreciated each other's differences. Honestly, without their friendship and support,

I wouldn't have made it to my PhD in physics. I am also very grateful to Liyuan for his friendly lunch and badminton invitations, and his generous help when I was studying for my GRE subject exam.

I also appreciate my former labmate and dear friend, Alex Hostiuc. His occasional visits from Seattle to Riverside, his concern and support when I was feeling down, his ceaseless jokes, and his hospitality when I visited him in Seattle brightened my life.

I would like to acknowledge a couple more friends in Riverside. I thank Yinan Dong for her care when I got sick with COVID-19 from a conference, and for not making me feel left out. She is one of the kindest and most caring people I have ever met. I also thank Ming-Feng for taking me to the hospital and waiting for my surgery during the pandemic. It's been fun hanging out with him and celebrating our graduation together.

To my beloved grandma, Xìng Chen, for her unconditional love, who taught me to be kind and gentle and encouraged me to pursue my dreams. To my parents and my brother, for their understanding and support throughout this journey.

ABSTRACT OF THE DISSERTATION

Entanglement, Symmetry Factorization, and Topological States of Matter: From Theory to Applications

by

Pak Kau Lim

Doctor of Philosophy, Graduate Program in Physics
University of California, Riverside, December 2024
Professor Michael Mulligan, Chairperson

This thesis investigates the intricate relations between entanglement, symmetry factorization, and topological states of matter, advancing our understanding from the theoretical aspects of the emergent behavior of gapped electronic systems to potential applications in quantum information or computing. Our findings span four key areas.

First, we use the entanglement negativity to measure the multipartite entanglement arising from cutting and gluing $(2+1)$-dimensional topological fluids. We focus on the entangling properties of Abelian general Laughlin states and non-Abelian general Moore-Read states, where we analyze the real-space structure of their ground state wavefunctions. We find that while the conventional disentangling condition is necessary and sufficient for disentangling general Abelian Laughlin states and untwisted Moore-Read states, it fails for twisted Moore-Read states. Even when this condition is met, the twisted Moore-Read states remain

entangled due to the presence of the Ising twisted field, which scrambles the associated reduced density matrix. We conjecture that such obstruction to disentanglement prevails among any non-Abelian topological fluids.

Second, we investigate the topological states of matter that emerge from the symmetry factorization of E_8 bosonic integer quantum Hall states. These states are built up on the exactly solvable coupled-wire formalism. We factorize the E_8 Kac-Moody current into sub-currents that are governed by Lie groups, preserving the total chiral central charge of the E_8. This technique circumvent the challenges in mathematically describing strongly interacting bosons, leading to the bosonic analog of fractional quantum Hall states that conserve charge and momentum symmetries. The resulting states support a rich variety of emergent topological orders.

Third, we extend our studies of symmetry factorization to classical Lie groups, $SU(N)$ and $SO(N)$ at level 1. This provides us with a microscopic understanding of the emergence of quantum Hall states, topological insulators, and quantum spin liquids with non-Abelian excitations like the Majorana, metaplectic, and Fibonacci types. We discover a theorem of branching rule from these classical Lie group symmetry embeddings via the coupled-wire construction. The theorem states that the pairing of various anyons and anti-anyon from the embedded subgroups can be glued together, forming local chain operators that can be expressed as products of their parent state's current operators, which do not appear in the tensor product of current operators of the embedded symmetries.

Finally, we investigate topological defects in quantum Low-Density Parity-Check (qLDPC) codes. We showed how quantum information encoded by defects paves the way to non-local quantum error corrections in qLDPC codes. Our analysis reveals the relation between such qubit-carrying defects and the general topological entanglement entropy, demonstrating that the non-local error correction feature in the qLDPC is validated by entanglement entropy that is both finite and nonzero.

Contents

List of Figures

List of Tables

Chapter 1

Introduction

1.1 Quantum Entanglement

The concept of quantum parallelism is based on the foundational of quantum entanglement. Quantum entanglement describes a non-classical correlation between two quantum systems even if they are separated in long distance. This phenomenon, known as the quantum non-locality, implies that the state of a particle or qubit is intrinsically linked to the state of another. Two particles or qubits are entangled meaning that their combined state cannot be separated into a product of individual particle or single qubit state. Take for example the Bell state $|\psi\rangle = \frac{1}{\sqrt{2}}(|00\rangle + |11\rangle)$. This state cannot be expressed as a product of any two single-qubit states, such as $a|0\rangle + b|1\rangle$ and $c|0\rangle + d|1\rangle$ for $a, b, c, d \in \mathbb{C}$. An attempt to do so would imply that both $ad = bc = 0$ and $ac = bd = 1/\sqrt{2}$, which is impossible. When information is being encoded in an entangled state like $|\psi\rangle$, measuring one part of

the system (e.g., measuring the first qubit) will immediately inform us about the state of the other part. For example, if we measure the first qubit and obtain $|0\rangle$, the second qubit will collapse to $|0\rangle$. Coversly, if the first qubit is measured and found to be $|1\rangle$, the second qubit will be $|1\rangle$. This characteristic enables us to manipulate information simultaneously across multiple qubits. The more qubits that can be entangled, the larger the capacity for performing large-scale computation in a highly correlated manner. This avoids the need to address the qubits one by one as is required with classical computer bits. Entanglement allows for the creation of complex, intertwined quantum states that can be used to solve certain problems more efficiently than classical computers.

1.1.1 Quantum Entanglement Measurement

One convenient way to measure quantum entanglement is by using von Neumann entropy. The goal is to quantify how entangled qubits are between two subsystems, A and B, or equivalently expressing $|\psi\rangle = \frac{1}{\sqrt{2}}(|0_A 0_B\rangle + |1_A 1_B\rangle)$. This can be done by first computing the density matrix $\rho = |\psi\rangle\langle\psi|$ of the Bell state and then tracing out qubits in subsystem B to obtain the reduced density matrix ρ_A:

$$\rho_A = \frac{1}{2} \sum_{j=0,1} \langle j| \left(|00\rangle\langle 00| + |00\rangle\langle 11| + |11\rangle\langle 00| + |11\rangle\langle 11|\right) |j\rangle. \tag{1.1}$$

The von Neumann entropy is given by

$$S_A = -\operatorname{tr}(\rho_A \ln \rho_A) = -\sum_j \lambda_j \ln \lambda_j \tag{1.2}$$

where λ_j is the eigenvalues of ρ_A. For our Bell state here, it has $S_A = \ln 2$. This is because an entangled Bell state cannot be expressed as a tensor product of single qubit whose reduced density matrix each has a trace of unity. Thus a state that is not entangled will have zero von Neumann entropy. In a general quantum system, its state can be described by the density matrix ρ, a positive semi-definite Hermitian operator by choice of a basis in the underlying Hilbert space. The von Neumann entropy of the reduced density matrix ρ_A is thereby a measure of bipartite entanglement. An alternative bipartite measure is the Renyi entropy of order ℓ

$$S_\ell(\rho_A) = \frac{1}{1-\ell} \log_2 \mathrm{Tr}\left[(\rho_A)^\ell\right] = \frac{1}{1-\ell} \log_2 \left(\sum_i (|\lambda_i|^2)^\ell \right). \tag{1.3}$$

When $\ell = 0$, Renyi entropy counts the number of non-zero eigenvalues of ρ_A. When ℓ approaches infinity, it measures the largest eigenvalues of ρ_A. As $\ell \to 1$, Renyi entropy is reduced to the von Neumann entropy. Thus, the Renyi entropy provides information about the entanglement spectrum of the measured state. However, these bipartite entanglement measures fails to distinguish entanglement arising from classical and quantum correlations when studying mixed states.

Consider a quantum system divided into three regions A, B, and C. If the ground state of $A \cup B$ overlaps with region C, then the reduced density matrix of $A \cup B$ is mixed. To quantify the entanglement between regions A and B, one can use the logarithmic measure of entanglement negativity. But first, we introduce the concept of separability in terms of mixed state. A pure state $|\psi\rangle \in \mathcal{H}_A \otimes \mathcal{H}_B$ is separable if it can be decomposed into a tensor

product of two states $|\psi_A\rangle \in \mathcal{H}_A$ and $|\psi_B\rangle \in \mathcal{H}_B$. A state is entangled if it cannot be written in the form of a tensor product as demonstrated in Section 1.1.

Now, a general (or a mixed) state $|\Psi\rangle$ in Hilbert space $\mathcal{H}_{A\cup B} = \mathcal{H}_A \otimes \mathcal{H}_B$ after tracing out C can be expressed as

$$|\Psi\rangle = \sum_{i,j} \Omega^i_j |e_i\rangle \otimes |f_j\rangle, \tag{1.4}$$

with some fixed orthonormal bases $\{e_{i=1,\ldots,m}\} \in \mathcal{H}_A$ and $\{f_{j=1,\ldots,n}\} \in \mathcal{H}_B$, and a m-by-n matrix Ω_{ij}. The reduced density matrix is therefore

$$\rho_{A\cup B} = \sum_{i,j,k,\ell} \tilde{\Omega}^{ik}_{j\ell} |e_i\rangle\langle e_k| \otimes |f_j\rangle\langle f_\ell|, \tag{1.5}$$

with $\tilde{\Omega}^{ik}_{j\ell} = \Omega^i_j (\Omega^k_\ell)^\dagger$. We say the state $\rho_{A\cup B} \in \mathcal{H}_A \otimes \mathcal{H}_B$ is separable, if it can be expressed as a sum of direct products [Per96]

$$\rho_{A\cup B} = \sum_\lambda \omega_\lambda \rho_{A,\lambda} \otimes \rho_{B,\lambda} \tag{1.6}$$

for some positive weights ω_λ that are equivalent to positive eigenvalues of $\rho_{A\cup B}$ satisfying $\sum_\lambda \omega_\lambda = 1$. One can then define a partial transposition of $\rho_{A\cup B}$ as follows

$$\rho^{T_B}_{A\cup B} = \sum_{i,j,k,\ell} \tilde{\Omega}^{ik}_{j\ell} |e_i\rangle\langle e_k| \otimes (|f_j\rangle\langle f_\ell|)^T = \sum_{i,j,k,\ell} \tilde{\Omega}^{ik}_{\ell j} |e_i\rangle\langle e_k| \otimes |f_\ell\rangle\langle f_j|. \tag{1.7}$$

It is evident from (1.6) and (1.7) that if the state $\rho_{A\cup B}$ is separable, then its eigenvalues will remain positive semi-definite. This is the Peres-Horodecki criterion [Per96, HHH96].

Indeed, we can measure the separability using the trace norm $||X||_1 = \mathrm{tr}\sqrt{X^\dagger X}$ for matrix X. This operation sums over the singular values of X. If X is the density matrix of state with only positive semi-definite eigenvalues, $||X||_1 = 1$. To make the measurement more effective, we compute the entanglement negativity

$$\mathcal{E}_{A:B}(\rho_{A\cup B}) = \ln ||\rho_{A\cup B}^{T_B}||_1. \tag{1.8}$$

So a state that is separable or disentangled will have zero entanglement negativity. In addition, if a state is classically correlated, take for example

$$\rho = \frac{1}{2}\left(|00\rangle\langle 00| + |11\rangle\langle 11|\right), \tag{1.9}$$

its entanglement negativity will also be zero. This is because the partial transposition procedure will not affect the positive semi-definiteness of the density matrix of a classical correlated state.

1.1.2 Roles of Quantum Entanglement Measures

Entanglement entropy has been calculated in (2+1)D topological quantum field theories TQFTs [KP06a, LW06, DFLN08a]. For gapped Hamiltonians, the von Neumann entropy measure can be used to distinguish between short-range and long-range topological orders by a correction term coined the topological entanglement entropy (TEE). Here in this thesis, we refer the long-range topological order as those in the fractional quantum Hall (FQH) states support non-trivial quasi-particle excitations or anyons. In contrast, short-range

topological order includes states like the integer quantum Hall (IQH) states. The term TEE was first discovered by Kitaev and Preskill [KP06a], and by Levin and Wen [LW06]. The von Neumann entropy takes the general form

$$S = \alpha L - \gamma. \tag{1.10}$$

The first term of the entropy follows the area law, with L being the system circumference length and α a non-universal constant. The second term is the TEE given by

$$\gamma = \ln \mathcal{D} = \ln \sqrt{\sum_j d_j^2}. \tag{1.11}$$

Here, $\mathcal{D}$ is the total quantum dimension, and d_j are quantum dimensions that characterize anyons, and defined rigorously according to (1.20). However, γ itself cannot separate Abelian anyons from non-Abelian anyons.

By calculating the entanglement negativity of two adjacent non-contractible regions A and B on a torus,

$$\mathcal{E}_{A:B}(\rho_{A\cup B}^{T_B}) = \alpha(l_A + l_B) - \ln \mathcal{D} + \ln \left(\sum_j |\psi_j|^2 d_j \right) \tag{1.12}$$

Wen, Matsuura and Ryu [WMR16] shows it can be used to distinguish between Abelian and non-Abelian theory. ψ_j is a complex amplitude that depends on the choice of ground state of a Chern-Simons field theory (see also [DFLN08a]). These complex amplitudes satisfy $\sum_j |\psi_j|^2 = 1$. The subscript j denotes the super selection sector of the associate anyon. α

is again some non-universal constant and $l_{A(B)}$ the open boundary length of region $A(B)$. The last term of (1.12) vanished in the Abelian theory since $d_j = 1$ for all its supersectors j, but not for the non-Abelian theory.

Using the exactly solvable coupled-wire model and entanglement negativity [KML02, TK14a], we demonstrate in Chapter 2 how non-Abelian states and their non-trivial quasi-particles constrain many-body wavefunctions from being disentangled. Our approach utilizes the cut-and-glue method [CHM15] to partition torus states into multiple cylinder states. In a separate project, presented in Chapter 5, we also addresses the amount of entanglement is required to encode logical qubits, enableing non-local quantum error correction in general quantum low-density parity-check (LDPC) codes [LSP21].

1.2 Topological Order and Quantum Computing

Quantum computers hold the promise of revolutionizing computation by solving problems that are intractable for classical computers. In computational complexity theory, given an input, a decision problem provides output of yes or no. The simplest example is to know whether a given natural number is a prime. A nondeterministic polynomial time (NP) problem refers to a computational device that can explore many different solutions simultaneously, with any given solution being verifiable in polynomial time. This is the NP-complexity class and coined the NP problem. More concretely, such a device can guess integers that factorize the natural number, and these guesses can then be verified in polynomial time. It is clear that all problems that can be solved in polynomial time (the P class)

must be contained in the NP-class. The hardest NP problem is called NP-complete. An algorithm that is capable of solving NP-complete problem can therefore solve any problems in the NP-class. In computational complexity theory, it is often asked whether there exists a polynomial time algorithm that can solve the NP-complete problem. This is the most important open problem in computer science, known as the P=NP problem, . We are yet to learn whether a quantum computer is capable of solving NP-complete problem. However, while classical computers struggle with NP-hard problems, a quantum computer can indeed offer a quantum speed up.

1.2.1 The Promise of Quantum Parallelism

Current computing devices utilize parallelism extensively, especially in applications like artificial intelligence. However, the parallelism achieved in quantum computing is fundamentally different and far more powerful than classical computers. This is due to the coherent sum of entangled qubits, allowing a quantum computer to perform a massive number of computations simultaneously. This powerful parallelism was first harnessed by Peter Shor, who developed a quantum algorithm for prime factorization, now known as Shor's algorithm [Sho97]. (The same example we previously discussed can also be treated as finding the prime factorization of a natural number N.) His algorithm demonstrated that quantum computers could solve prime factorization exponentially faster with time complexity of $\mathcal{O}((\log_2 N)^2(\log_2 \log_2 N)(\log_2 \log_2 \log_2 N))$ steps as comparing to the best known classical algorithm, such as the General Number Field Sieve (GNFS), which have time complexity

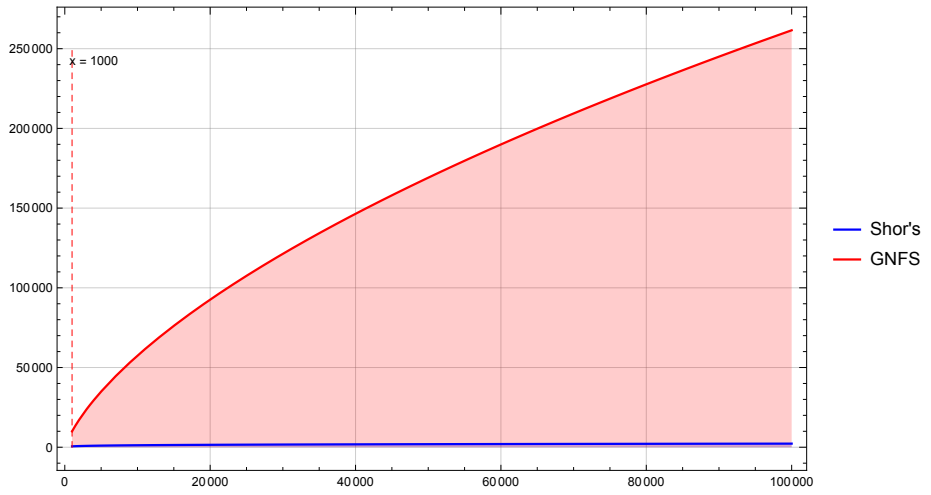

Figure 1.1: Time complexity comparision using upto 17-bit integers between the Shor's algorithm and GNFS. The red dashline indicates the comparison starting at integer 1000.

of $\mathcal{O}\left(\exp\left(\left(\frac{64}{9}\log_2 N\right)^{1/3}(\log_2\log_2 N)^{2/3}\right)\right)$ as demonstrated in Fig 1.1. Here we demonstrate Shor's algorithm by factorizing an integer $N = 15$. Number theory tells us that we can reduce the problem of finding an integer that divides N by finding the periods p of $f(x) = a^x \mod N$. We start with an initial guess of the integer $a = 2$. Next we apply $f(x)$ to superposition states. By restricting $2^q > N^2$, we have

$$\frac{1}{\sqrt{q}}\sum_{x=0}^{q-1}|x\rangle|f(x)\rangle = \frac{1}{\sqrt{8}}\left(|0\rangle|1\rangle + |1\rangle|2\rangle + |2\rangle|4\rangle + |3\rangle|8\rangle + |4\rangle|1\rangle + |5\rangle|2\rangle + |6\rangle|4\rangle + |7\rangle|8\rangle\right). \tag{1.13}$$

Assume we measured $|1\rangle$ for the second qubit. This leaves us with state $\left(|0\rangle + |4\rangle\right)/\sqrt{2}$. Its Quantum Fourier Transform (QFT) is given by

$$\frac{1}{4}\sum_{y=0}^{7}\left(1 + e^{2\pi i 4y/8}\right)|y\rangle = \frac{1}{\sqrt{4}}\left(|0\rangle + |2\rangle + |4\rangle + |6\rangle\right). \tag{1.14}$$

Supposed we measure $|k = 2\rangle$ in (1.14). The k-root of unity implies that we have $k/q = 1/p = 1/4$. Thus, we obtain the period $p = 4$. Number theory tells us that N divides $(a^p - 1) = (a^{p/2} - 1)(a^{r/2} + 1)$. Let the prime factorization in N be $N = \Pi_j p_j^{e_j}$, where p_j are prime factors of N. Since N divides the product $(a^{p/2} + 1)(a^{p/2} - 1)$, there must exist a prime p_ℓ that divides $a^{p/2} + 1$, or $a^{p/2-1}$, or both. So we can write $a^{p/2} + 1 = p_\ell k_\ell$ for some integer k_ℓ. By factoring out p_ℓ from N, we then consider $k_\ell(a^{p/2} - 1)$. If $k_\ell \neq 1$, there must be another prime factor of N that divides $k_\ell(a^{p/2} - 1)$. We can repeat this process for each prime factor of N, eventually showing that the product of all prime factors of N must divide either $(a^{p/2} + 1)$, or $(a^{p/2} - 1)$, or both. Thus, we conclude that N must be factored by one of $a^{p/2} \pm 1$. Therefore, we have $2^2 \pm 1 = 3, 5$ which factorize 15.

Shor's algorithm can be adapted to solve other problems, such as the discrete logarithm problem, which involve finding q in $a^q \equiv b \mod c$ for some integers a, b, c. His prime factorization algorithm opened up new avenues in information science and led to the development of many other quantum algorithms that leverage this inherent parallelism.

1.2.2 Scalability Challenges in Quantum Computing

However, to break a RSA encryption, by factoring a $K = 2048$-bit number, it needs a total number of $5K + 1 = 10,241$ logical qubits that is roughly 10 millions of physical qubits [BCDP96]. The biggest obstacle is the susceptibility of encoding qubits to environmental noise, leading to decoherence and loss of encoded information. Building a practical quantum computer involves overcoming this decoherence. Technologies like superconducting qubits,

trapped ions, and laser-based systems have shown promise, but they require sophisticated quantum error correction techniques to be fault-tolerant. Even with these advancements, the most coherent devices, such as IBM's Osprey, currently host a maximum of 433 physical qubits[IBM22] for fault-tolerant operations. Therefore, they are far from capable of cracking a 2048-bit RSA encryption. Despite their potential, quantum computers face significant challenges, particularly regarding scalability.

1.2.3 Non-Abelian Anyons and Topological Quantum Computing

A functional quantum computer will require a set of robust physical qubit to encode information and a set of quantum logical gates to operate on qubits. The basic set of quantum gates for a single qubit include the Pauli matrices, a Hadamard gate

$$H = \frac{1}{\sqrt{2}} \begin{bmatrix} 1 & 1 \\ 1 & -1 \end{bmatrix} \tag{1.15}$$

that maps basis $|0\rangle \rightarrow \frac{|0\rangle+|1\rangle}{\sqrt{2}}$ and $|1\rangle \rightarrow \frac{|0\rangle-|1\rangle}{\sqrt{2}}$, and a phase shift gate

$$P = \begin{bmatrix} 1 & 0 \\ 0 & e^{i\varphi} \end{bmatrix} \tag{1.16}$$

that manipulates quantum phase $e^{i\varphi}$ of the $|1\rangle$ qubit. Last but not least, we must include the fundamental control NOT gate, or simply CNOT gate for two qubits

$$\text{CNOT} = \begin{bmatrix} 1 & 0 & 0 & 0 \\ 0 & 1 & 0 & 0 \\ 0 & 0 & 0 & 1 \\ 0 & 0 & 1 & 0 \end{bmatrix}. \tag{1.17}$$

that is used for creating entanglement between qubits and performing conditional operations. For example, it creates entanglement between the control qubit $|+\rangle = \frac{1}{\sqrt{2}}(|0\rangle + |1\rangle)$ and the target qubit $|0\rangle$ by acting on $|\Psi\rangle = |+\rangle \otimes |0\rangle$ and transforming it into maximal entangled state

$$|\psi\rangle = \frac{1}{\sqrt{2}}(|00\rangle + |11\rangle). \tag{1.18}$$

Being an entangled state, $|\psi\rangle$ cannot be decomposed into product of single qubits. In addition, it possesses entanglement entropy of

$$S_A = -\operatorname{Tr}(\rho_A \ln \rho_A) = \ln 2, \tag{1.19}$$

where $\rho_A = \operatorname{Tr}_B(\rho)$ is the reduced density matrix and $\rho = |\psi\rangle\langle\psi|$ the density matrix. The CNOT gate can be used in conjunction with other single-qubit gates to construct more complex quantum gates. For example, multiqubit gates can be decomposed into a sequence of CNOT gates and single-qubit gates. This makes the CNOT gate one of the fundamental

building blocks for quantum circuits. In general, any quantum gate can be decomposed into a sequence of gates from a finite set known as universal quantum gates.

One of the most promising aspects of quantum computing is the presence of exotic particles known as anyons, particularly non-Abelian anyons, such as Fibonacci anyons. Unlike classical bits or even conventional quantum bits (qubits), anyons exhibit unique properties that make them particularly useful for quantum computation. The topological nature of anyons (see Figure 1.2) provides robustness against environmental fluctuations and noise.

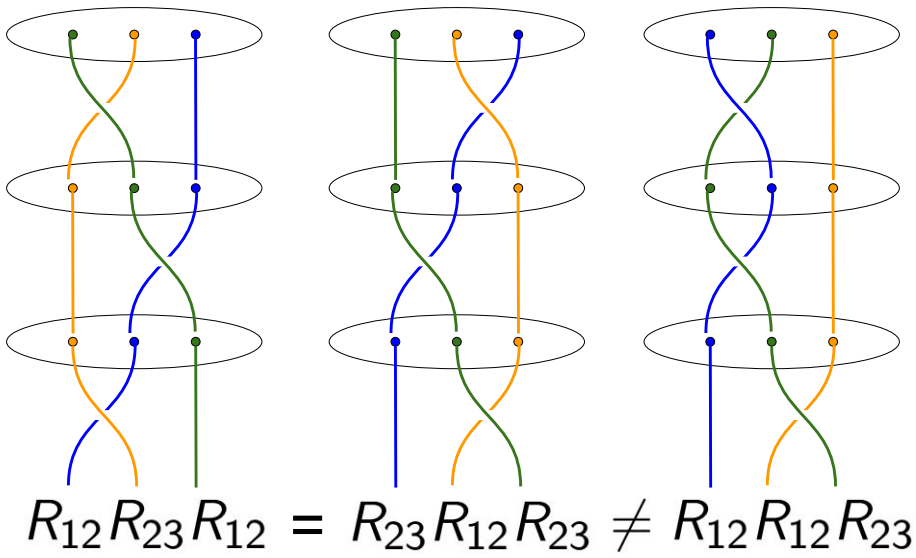

Figure 1.2: Consider three anyons, labeled 1, 2, and 3. The braiding matrix R_{12} describes the exchange of anyons 1 and 2, while R_{23} describes the exchange of anyons 2 and 3. The braiding pattern between $R_{12}R_{23}R_{12}$ and $R_{23}R_{12}R_{23}$ are topological equivalent in $2+1$D spacetime. This can be seen by noting that anyons in the middle slice of the first braiding sequence (the very left hand side) can be moved around to resemble the second sequence. On the other hand $R_{12}R_{12}R_{23}$ exhibits a very different braiding pattern compared to the others.

This means that the resulting qubits and quantum gates are inherently protected from decoherence, making topological quantum computers more scalable and reliable than their conventional counterparts. Here we assume that readers are familiar with the concept of anyons, fusion, and braiding [Kit06]. Anyons can be used to build anyon qubits through their fusion properties. Assume we have anyons a, b. The number of ways a and b fuse into c can be described in terms of the fusion coefficient or tensor N_{ab}^{c}:

$$a \times b = \sum_{c} N_{ab}^{c} c. \tag{1.20}$$

$N_{ab}^{c} = (N_a)_b^c$ is a matrix that depends on anyon a. The largest eigenvalue of N_a defines the quantum dimension d_a of anyon a. An Abelian anyon has quantum dimension one. All non-Abelian anyons have $d_a > 1$.

A particular interest among anyons is the Fibonacci anyons. Fibonacci anyons τ obey the fusion rule of $\tau \times \tau = 1 + \tau$ with 1 referring to the vacuum of the theory. Following (1.20), the quantum dimension of a Fibonacci anyon is given by the golden ratio, $d_\tau = \frac{1+\sqrt{5}}{2}$. The fusing behavior of three Fibonacci anyons is particularly useful for building anyon qubits, and their braiding can be used to construct universal quantum gates.

Here we provide a brief review of Fibonacci anyon model. A three Fibonacci anyons fusion can be used to construct a qubit system [TTWL08, Rou20] as shown in Figure. 1.3 Since braiding preserve anyon charge, one can prepare the state in such a way that the final outcome is τ. So the non-computational state $|NC\rangle$ in single qubit can be ignored. Braiding in three Fibonacci anyons can be accomplished by operation of the R-matrix as demonstrate

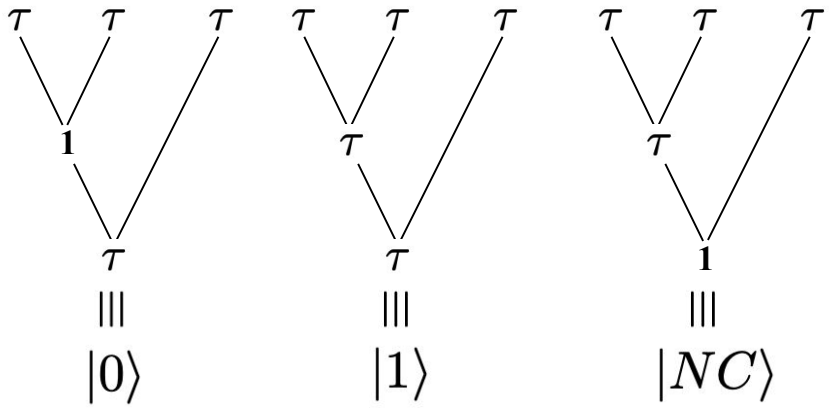

Figure 1.3: Qubit $|0\rangle$, $|1\rangle$ encoded in three Fibonacci anyon fusion. $|NC\rangle$ is a non-computational state.

in Figure.1.4. Any single qubit quantum gates can be constructed through operations of R_{12} and R_{23}, such as the Hadamard gate through a sequence of braiding operations [Rou20, aFLH+22]:

$$\begin{aligned} H = (R_{12})^4(R_{23})^{-2}(R_{12})^2(R_{23})^{-2}(R_{12})^2(R_{23})^2(R_{12})^{-2} \\ \times (R_{23})^4(R_{12})^2(R_{23})^{-2}(R_{12})^{-2}(R_{23})^2(R_{12})^2. \end{aligned} \tag{1.21}$$

Therefore, by harnessing non-Abelian anyons, we can create a new class of quantum computers that are not only powerful but also resilient to errors, paving the way for building scalable and practical quantum computers.

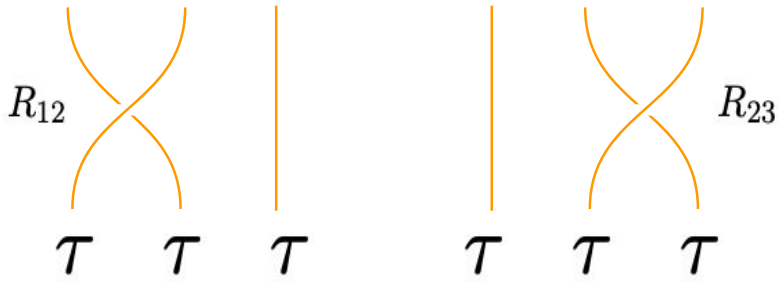

Figure 1.4: Braiding three Fibonacci anyons. The R_{12} matrix interchanges the first and second Fibonacci anyons in a counterclockwise mannar. Similary, the R_{23} matrix exchanges the second and third Fibonacci anyons.

1.3 Exactly Solvable Coupled-Wire Models and Experimental Motivation

To fully explore the existence of anyons and their potential in quantum computing, it is crucial to understand their microscopic origins. In Chapter 3 and 4, we introduce a universal framework: based on symmetry factorization of Lie groups and the exactly solvable coupled-wire model construction [KML02, TK14a]. By selecting different interactions between electronic wires, this model can simulate a wide range of electronic systems, such as spin liquids, superconducting states, quantum Hall states, and even some exotic bosonic fractional quantum Hall states [LQHT19, SSCT19, TH23, LMT23]. These states exhibit a variety of topological orders, including emergent Majorana fermions, Dirac fermions, Ising anyons, Fibonacci anyons, and metaplectic anyons [LMT23]. This framework provides a

unified approach to understanding the electronic origins of topological states of matter, which is of significant theoretical interest.

1.3.1 Symmetry Factorization

For example a coupled-wire model based on the parton construction of $\mathrm{U}(N)_1/\mathbb{Z}_N = \mathrm{U}(1)_N \times \mathrm{SU}(N)_1$ supports parton fractional quantum Hall (FQH) Abelian states at filling $\nu = 1/6$, which emerge from the transition between integer quantum Hall (IQH) and Laughlin states at filling $\nu = 1/3$. The term "parton" loosely refers to the splitting of an electron or an integral combination of electrons into products of non-local quasiparticles. Symmetry factorization allows partition of $\mathrm{SU}(N)_1$ into subgroups of $\mathrm{SU}(m)_n \times \mathrm{SU}(n)_m$ given N is a product of integers m and n, both greater than one. By constructing a microscopic Hamiltonian associated with Lie algebra factorizations $\mathcal{G} = \mathcal{G}^A \times \mathcal{G}^B$, we can obtain various topological states that arise from conformal field theories (CFTs) described by the Wess-Zumino-Witten (WZW) Kac-Moody (KM) current algebras. This process provides a pathway to describe strongly interacting electrons and bosons, assuming that current-current backscatterings within the general WZW KM algebra open up a finite mass gap.

By current algebra [FMS12], we refer to the operator product expansion (OPE) identity

$$J_a(z)J_b(w) = \frac{k\delta_{ab}}{(z-w)^2} + \sum_c i f^{abc} \frac{J_c(w)}{(z-w)} + \dots \tag{1.22}$$

satisfied by current operators $\mathbf{J}_\mathcal{G}$, defined on a Lie algebra $\mathcal{G}$ at general level k. f^{abc} is the structure constant of the Lie algebra $\mathcal{G}$. The current $\mathbf{J}_\mathcal{G}$ is spanned by the Cartan

generators and roots (ladder operators) of $\mathcal{G}$. An element J_a of the current is then either some p^{th} Cartan generator labeled by $[\mathtt{H}_{\mathcal{G}}]_p$ or a ladder operator $[\mathtt{E}_{\mathcal{G}}]_{\boldsymbol{\alpha}}$ associates with a root $\boldsymbol{\alpha}$ in $\mathcal{G}$. The number of Carton generator is given by the rank of $\mathcal{G}$, while the number of roots equals to the dimension of $\mathcal{G}$ subtracting off its rank. The CFTs here are considered on a compactified string of circumference l along the spatial $\mathtt{x}$-coordinate, and with Wick rotated time $\tau = it$ pointing at the radial direction. The complex space-time parameters are explicitly defined by $z, w = e^{2\pi(\tilde{v}\tau + i\mathtt{x})/l}$. $\tilde{v}$ is the propagating velocity of a chiral mode in the $\mathtt{x}$-direction.

Symmetry factorization follows from the conformal embedding $\mathcal{G} \supseteq \mathcal{G}^A \times \mathcal{G}^B$ in affine Lie algebrasb [NS90, NT92, FMS12]. From the exceptional E_8 at level 1, we have bipartited the E_8 symmetry [LMT23] into elements given by the set

$$\left\{ \begin{array}{ccccc} SU(3) \times E_6, & SU(2) \times E_7, & SU(5) \times SU(5), & SO(M) \times SO(16-M), \\ & G_2 \times F_4, & U(1)_8 \times SU(8), & SU(2)_4 \times Sp(8) \end{array} \right\}. \tag{1.23}$$

In the classical regime, we have symmetry factorization of the A, B, and D series:

$$\begin{aligned} &\mathrm{SU}(mn)_1 \supseteq \mathrm{SU}(m)_n \times SU(n)_m, \\ &\mathrm{SO}(mn)_1 \supseteq \mathrm{SO}(m)_n \times SO(n)_m, \\ &\mathrm{SO}(4mn)_1 \supseteq \mathrm{Sp}(2m)_n \times \mathrm{Sp}(2n)_m. \end{aligned} \tag{1.24}$$

Under conformal embedding, the WZW KM currents from $\mathcal{G}^A$ and $\mathcal{G}^B$ are orthogonal to each other, meaning their mutual OPE $\mathbf{J}_{\mathcal{G}_A} \cdot \mathbf{J}_{\mathcal{G}_B}$ must contain only nonsingular terms.

Thus, the energy-momentum tensors of the Lie algebras satisfy $T_{\mathcal{G}}(z) = T_{\mathcal{G}^A}(z) + T_{\mathcal{G}^B}(z)$. The energy-momentum tensors $T(z)$ can be calculated using the Sugawara construction

$$T(z) = \frac{1}{2(k+g)} \sum_a : J_a J_a : (z) \tag{1.25}$$

which sums over all normal-ordered current products labeled by $: J_a(z) J_a(z) :$. Here, g is the dual Coxeter number of the Lie algebra, independent of any level k. Also follow from the Sugawara construction is the description of the central charge of $\mathcal{G}$:

$$c_{\mathcal{G}} = \frac{k \dim \mathcal{G}}{k+g}. \tag{1.26}$$

The dimension of the Lie algebra is denoted by $\dim\mathcal{G}$. Evidently, the central charge of $\mathcal{G}$ must equal that of $\mathcal{G}^A \times \mathcal{G}^B$ in conformal embedding.

1.3.2 Coupled-Wire Construction

In this thesis, we establish a general edge conformal field theories (CFTs) of (3.1) and (4.1) using symmetry factorization across the A, B, D, and E_8 classes, all of level 1. This is done under the assumption that finite energy gap formation is possible due to backscattering in WZW Kac-Moody current algebras. We construct the edge CFTs from the WZW current algebras using an exactly solvable coupled-wire model. The WZW KM currents can be bosonized (as the CFT is prescribed on a ring with periodic boundary conditions) and cast into vertex operators. The coupled-wire Hamiltonian can then be configured accordingly through current-current interactions among wires to support either deconfined or confined

topological phases. For a confined topological phase of $\mathcal{G}$, it is described by a full interwire backscattering of current $\mathbf{J}_{y,\mathcal{G}}$:

$$\begin{aligned} \mathcal{H}[\mathcal{G}]_{\text{edge}} &= \mathcal{H}_0 + \mathcal{H}^{\mathcal{G}}_{\text{inter}}, \\ \mathcal{H}^{\mathcal{G}}_{\text{inter}} &= u_{\text{inter}} \sum_y \mathbf{J}^R_{y,\mathcal{G}} \cdot \mathbf{J}^L_{y+1,\mathcal{G}}. \end{aligned} \tag{1.27}$$

$\mathcal{H}_0$ is the bare Hamiltonian density that originates from electron density-density interactions. Its form will become clear later. For the deconfined phases, the coupled-wire Hamiltonian is

$$\mathcal{H}[\mathcal{G}^A] = \mathcal{H}_0 + \mathcal{H}^{\mathcal{G}^A}_{\text{inter}} + \mathcal{H}^{\mathcal{G}^B}_{\text{intra}}. \tag{1.28}$$

The current-current backscatterings between adjacent wires of adjacent bundle y and $y+1$ (interwire backscattering), and between adjacent wires within a bundle y (intrawire backscattering) are given by the following Hamiltonian densities

$$\begin{aligned} \mathcal{H}^{\mathcal{G}^A}_{\text{inter}} &= u_{\text{inter}} \sum_y \mathbf{J}^R_{y,\mathcal{G}^A} \cdot \mathbf{J}^L_{y+1,\mathcal{G}^A}, \\ \mathcal{H}^{\mathcal{G}^B}_{\text{intra}} &= u_{\text{intra}} \sum_y \mathbf{J}^R_{y,\mathcal{G}^B} \cdot \mathbf{J}^L_{y,\mathcal{G}^B}. \end{aligned} \tag{1.29}$$

The construction of the edge CFT described by WZW current algebra $\mathcal{G}^B$ follows directly from (1.28) and (1.29) by interchanging the inter and intrawire backscatterings between the A and B sectors. Conceptually, these intra and inter-wire interactions effectively glue the compactified 1D wires together, forming a close geometric bulk resembling a torus. For an open geometry like a cylinder, the intrawire backscattering gaps out the bulk and

leave us with a gappless edge theory described by the chiral CFT of a Lie subgroup. Edge theories can be constructed using the vertex operator algebras. The topological phase of matter in the bulk are facilitated by its unitary modular tensor category. The relationship between gapped bulk and the gappless edges is established through the bulk-boundary correspondence[CCM+14].

The assumption of gappability in current-current backscatterings enables the construction of exactly solvable coupled-wire models. These models allow us to analytically solve for ground state wavefunctions and study the entanglement properties of various topological fluids. Consequently, our framework offers us a robust platform for understand the general disentangling property of topological fluids, as motivated by [LATM21].

1.3.3 Experimental Motivation

The practical implementation of coupled-wire models poses several challenges. The analytical construction of these models relies on low-energy approximations and strong-coupling limits, rendering the actual microscopic systems being studied obscure. Consequently, the precise range of interaction strengths required for the emergence of states such as fractional quantum Hall remains undetermined. However, recent experimental advancement has provide novel insight to the strong tunneling regime demonstrating the possibility of probing fractional quantum Hall state using coupled-wire model in ultra cold-atom experiment [CER20]. The investigation shed light on the microscopic relevance and possible experimental realization of coupled-wire model in cold-atom setups.

Chapter 2

DISENTANGLING TOPOLOGICAL FLUIDS

This chapter was previous published as [Pak Kau Lim, Hamed Asasi, Jeffrey C.Y. Teo, Michael Mulligan, "Disentangling $(2+1)D$ topological sttes of matter with entanglement negativity", Phys. Rev. B 104, 115155 – Published 27 September 2021]

2.1 Introduction

2.1.1 Background

One of the defining characteristics of a topological phase of matter is the sensitivity of its ground state to the topology of the space on which it's placed [WN90] (see [OKS+07]

for a review). For instance, the Laughlin state at filling fraction $\nu = 1/m$ has ground state degeneracy m^g where g is the genus of space. Topological phases with robust ground state degeneracy, such as the Laughlin state at $m > 1$, are said to be *long-range entangled* [Wen13]. On the other hand, short-range entangled (topological) states [CGLW13, LV12], which occur in the integer quantum Hall effect, have a unique ground state when placed on any closed manifold, but share other defining topological characteristics such as protected gapless boundary modes [Wen91a].

The entanglement entropy is a useful diagnostic for these two classes of states. The entanglement entropy between subsystems A and B of a state $\rho \in \mathcal{H}_A \otimes \mathcal{H}_B$ equals the von Neumann entropy $S_A = -\operatorname{tr}_A \rho_A \ln \rho_A$ of its reduced density matrix $\rho_A = \operatorname{tr}_B \rho$. (Here we are denoting pure and mixed states by ρ.) In a topological phase, the entanglement entropy scales with the linear size $L \to \infty$ of region A as [HIZ05, LW06, KP06a]

$$S_A = \alpha L - \gamma. \tag{2.1}$$

The coefficient α is nonuniversal and UV divergent, while the topological entanglement entropy γ is a universal, geometry-dependent constant that characterizes the phase.[1]

For instance, if A is a disk, $\gamma = \frac{1}{2} \log \sum_a d_a^2$, where the sum is over all superselection sectors of the phase and $d_a \geq 1$ is the quantum dimension of quasiparticle a [KP06a, LW06].[2] Short-range entangled phases have a single superselection sector (corresponding to its unique

[1] For notational simplicity, we do not indicate the dependence of γ on A, B, and the state.

[2] d_a controls the Hilbert space dimension d_a^N of N quasiparticles a as $N \to \infty$. Abelian phases have $d_a = 1$ for all a; non-Abelian phases have at least one quasiparticle with $d_a > 1$.

ground state) with $d_0 = 1$; long-range entangled phases, which include both Abelian states like the toric code [Kit03] and non-Abelian states like the Moore-Read state [MR91a], have at least two superselection sectors and, consequently, $\gamma > 0$. There can be additional "boundary" contributions to γ due to interactions localized along the border of A in both short-range and long-range entangled states [CHM15, SCMH18] (see also [OT15, CKS14]). Importantly, for long-range entangled states *only* and when A is non-contractible, γ can receive "long-range" corrections that depend on the amplitude ψ_a to be in the sector a degenerate ground state [DFLN08b, ZGT+12]. For example, consider the ground state of a topological phase on the torus: $|\Psi\rangle = \sum_a \psi_a |\overline{\Psi}_a\rangle$, where ψ_a is the amplitude to be in the ground state $|\overline{\Psi}_a\rangle$ of sector a. If the torus is divided into two cylinders A and B, then the topological entanglement entropy of region A is $\gamma = \log \sum_a d_a^2 - \sum_a |\psi_a|^2 \log \frac{|\psi_a|^2}{d_a^2}$.

These different contributions to γ reflect distinct types of ground state entanglement, termed *boundary* and *long-range entanglement* in [LV13]. (We will use this terminology throughout this paper.) To better understand these different forms of entanglement, Lee and Vidal [LV13], Castelnovo [Cas13], and Wen, Matsuura, and Ryu [WMR16] employed the *entanglement negativity* [VW02]. Unlike the entanglement entropy, which only quantifies the quantum correlations between a subsystem and its complement when ρ is pure [PV05, GPW05], the entanglement negativity is a mixed state entanglement measure [Per96] that can thereby distinguish multipartite features of entanglement (e.g., [DVC00]), for instance if $\rho = \mathrm{tr}_C |\Psi_{ABC}\rangle\langle\Psi_{ABC}|$ obtains by tracing out degrees of freedom in a third subsystem C.

The entanglement negativity[3] is motivated by Peres' [Per96] necessary condition for a mixed state $\rho \in \mathcal{H}_A \otimes \mathcal{H}_B$ to be separable. This criterion says that a separable state ρ has positive partial transpose ρ^{T_A} with respect to subsystem A, where

$$\langle i_A j_B | \rho^{T_A} | k_A l_B \rangle = \langle k_A j_B | \rho | i_A l_B \rangle, \tag{2.2}$$

and $|i_A\rangle, |k_A\rangle$ ($|j_B\rangle, |l_B\rangle$) are basis states for $\mathcal{H}_A$ ($\mathcal{H}_B$). The negativity $\mathcal{N}_{A:B}(\rho) = (||\rho^{T_A}||_1 - 1)/2$ sums (the absolute value of) any negative eigenvalues of ρ^{T_A} and, thereby, measures the degree of nonseparability of ρ. Here, $||\rho||_1 \equiv \mathrm{tr}\sqrt{\rho^\dagger \rho}$ is the trace norm of ρ. The entanglement negativity $\mathcal{E}_{A:B}(\rho)$ is a closely related measure defined as

$$\mathcal{E}_{A:B}(\rho) = \log ||\rho^{T_A}||_1 = \log\big(1 + 2\mathcal{N}_{A:B}(\rho)\big). \tag{2.3}$$

In contrast to $\mathcal{N}_{A:B}(\rho)$, the entanglement negativity has an operational meaning as an upper bound to the amount of pure state entanglement contained in a general mixed state [VW02]. For pure states, $\mathcal{E}_{A:B}(\rho)$ reduces to the $q = 1/2$ Renyi entropy of ρ [LV13]. Other situations in which the entanglement negativity has been measured include conformal field theory [CCT12], holography [RR14, DQW21], thermal phase transitions [CCT14, KFNRT20, LG20], topological systems with symmetry [CGS18] or at nonzero temperature, [HC18, LHG20] non-equilibrium systems [CTC14, EZ14, HD15, WCR15, SLKFV21], and recently at measurement-driven phase transitions [SLZ+20, SDL20].

[3] This quantity is also known as the logarithmic negativity. See below for the definition of the negativity.

In this paper, we use the entanglement negativity to study how multipartite entanglement constrains the structure of the manybody wave function of a topological phase. In particular, we show how long-range entanglement, due to topological degeneracy, prevents the *disentanglement* [HV15] of a topological ground state.

In general, a state $\rho \in \mathcal{H}_A \otimes \mathcal{H}_B \otimes \mathcal{H}_C$ is said to satisfy the *disentangling condition*[4] with respect to $\mathcal{H}_A$ and $\mathcal{H}_C$ if

$$\mathcal{E}_{A:BC}(\rho) = \mathcal{E}_{A:B}(\rho_{AB}), \tag{2.4}$$

where $\rho_{AB} = \mathrm{tr}_C\, \rho$. To appreciate (2.4), we can heuristically view it as a special case of the monogamy-like relation,[5]

$$\mathcal{N}^2_{A:BC}(\rho) \geq \mathcal{N}^2_{A:B}(\rho_{AB}) + \mathcal{N}^2_{A:C}(\rho_{AC}), \tag{2.5}$$

which expresses how entanglement is shared between A, B, and C subsystems [CKW00, OV06]. Since the entanglement negativity is a monotonic function of the negativity (2.3), the disentangling condition obtains when $\mathcal{N}_{A:C}(\rho_{AC}) = \mathcal{E}_{A:C}(\rho_{AC}) = 0$, i.e., there are no quantum correlations between degrees of freedom in A and C. In three-qubit systems, for instance, only product states such as $|\Psi_{ABC}\rangle = |\Psi_{AB}\rangle \otimes |\Psi_C\rangle$ satisfy the disentangling condition [OF07]. When the Hilbert space of subsystem B factorizes as $\mathcal{H}_B = \mathcal{H}_{B_L} \otimes \mathcal{H}_{B_R}$,

[4] He and Vidal [HV15] introduced an equality like (2.5) in terms of the negativity $\mathcal{N}$ instead of $\mathcal{E}$. These two forms are equivalent when $\mathcal{N}_{A:C}(\rho_{AC}) = 0$.

[5] Monogamy-like relations such as these depend on the entanglement measure and aren't generally satisfied for all states in a given Hilbert space. For example, this inequality isn't satisfied generally if $\mathcal{N}^2$ is replaced by $\mathcal{N}$ [HV15].

pure states satisfying (2.4) can be disentangled as

$$|\Psi_{ABC}\rangle = |\Psi_{AB_L}\rangle \otimes |\Psi_{B_RC}\rangle\,, \tag{2.6}$$

a result known as the disentangling theorem [HV15]. A more general set of states that fulfill the disentangling condition are those that saturate the strong subadditivity of the entanglement entropy [GG18], i.e., $I_{A:BC} = I_{A:B}$, where the mutual information $I_{A:B} = S_A + S_B - S_{AB}$. For such states, Hayden et al. [HJPW04] showed there exists a decomposition of the Hilbert space as

$$\mathcal{H}_B = \bigoplus_j \mathcal{H}_{B_L^j} \otimes \mathcal{H}_{B_R^j} \tag{2.7}$$

such that ρ is separable:

$$\rho = \sum_j p_j \rho_{AB_L^j} \otimes \rho_{B_R^j C}. \tag{2.8}$$

Here $\{p_j\}$ are probabilities.

2.1.2 Summary of Results

We study the disentangling condition (2.4) for the (Abelian) Laughlin and (non-Abelian) Moore-Read states at filling fraction $\nu = 1/m$ and show explicitly how topological states satisfying this condition can be disentangled according to either Eqs. (2.6) or (2.8). To do this, we use the cut and glue construction of these states [EMSS89b, WEN92a, QKL12,

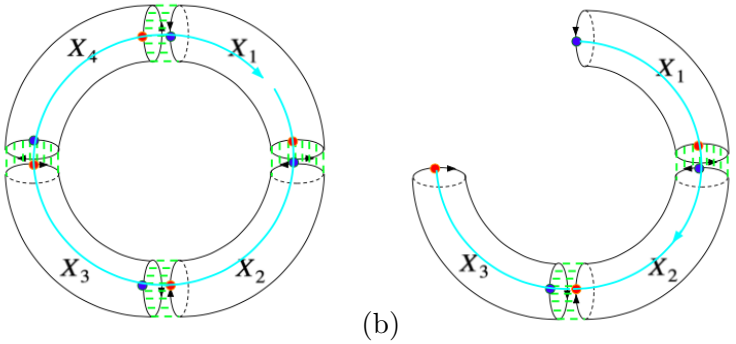

(a) (b)

Figure 2.1: (a) (*Torus geometry*) Decomposition of a torus X into $2M = 4$ cylinders X_1, X_2, X_3, X_4 with $X_{\text{odd}} = X_1 \cup X_3$ and $X_{\text{even}} = X_2 \cup X_4$; (b) (*Cylinder geometry*) Degrees of freedom in cylinder $\bar{Y} = X_4$ have been traced over; the remaining cylinders $Y = Y_{\text{odd}} \cup Y_{\text{even}}$ with $Y_{\text{odd}} = X_1 \cup X_3$ and $Y_{\text{even}} = X_2$ have $R = 2$ shared interfaces. Interactions between low-energy boundary modes at cylinder interfaces are indicated by dashed green lines. Superselection sector a is represented by the blue (quasiparticle) threading the center of the (solid) torus.

LFFO13, TK14b] to calculate the entanglement negativity in two related geometries (see Figure 2.1). (When there is overlap, our results agree with [LV13, Cas13, WMR16].) In the first, we partition a torus into $2M$ cylinders X_i ($i \in \{1, \ldots, 2M\}$) and perform partial transposition with respect to degrees of freedom on the "odd" cylinders $X_{\text{odd}} \equiv X_1 \cup X_3 \cup \cdots \cup X_{2M-1}$ (i.e., cylinders X_1 and X_3 in Figure 2.1a). We find that the entanglement negativity is

$$\mathcal{E}_{X_{\text{odd}}:X_{\text{even}}} = 2 \log \sum_a |\psi_a| \zeta_a^{2M}, \tag{2.9}$$

where $X_{\text{even}} \equiv X_2 \cup X_4 \cup \cdots \cup X_{2M}$ and ψ_a is the unit-normalized amplitude to be in the sector a torus ground state. ζ_a is a ratio of sector a edge state partition functions at inverse

"temperatures" $\beta = 1/2$ and $\beta = 1$:

$$\zeta_a = \frac{\operatorname{tr} e^{-H_a/2}}{\sqrt{\operatorname{tr} e^{-H_a}}} \tag{2.10}$$

with entanglement Hamiltonian H_a. This dependence of the entanglement negativity on the spectrum of the entanglement Hamiltonian is reminiscent of a similar dependence ($\rho_A \propto e^{-H_a}$) of the entanglement entropy, e.g., [LH08, RBH09, TSRB10, LBH10, PacBR11, CHRB11, HCRB11, RDSS13, PTBO10, Fid10, PHB10, FGB13]. In contrast to the entanglement entropy, the entanglement negativity measures the system at two different "temperatures" [RR14]. For the fully chiral topological phases that we study, i.e., when all the edge modes move in the same direction, H_a is proportional to the edge state Hamiltonian. In general, there can be a different H_a for each of the $2M$ interfaces [CHM15]; here we only consider torus states where the interactions are the same at each interface.

The second geometry that we consider is obtained by tracing over the degrees of freedom on $N \leq M$ cylinders $\bar{Y} \subset X$ (for example, X_4 in Figure 2.1b). We show that the entanglement negativity of the resulting state is

$$\mathcal{E}_{Y_{\text{odd}}:Y_{\text{even}}} = \log \sum_a \left(|\psi_a| \zeta_a^R \right)^2 , \tag{2.11}$$

where R is the number of shared interfaces between the remaining cylinders Y_{odd} and Y_{even} whose degrees of freedom have not been traced over (e.g., $R = 2$ in Figure 2.1b) and ζ_a is again given in (2.10).

Thus, the entanglement negativities (2.9) and (2.11) are determined by ratios of entanglement Hamiltonian partition functions. For the Laughlin and Moore-Read states, we show that the above entanglement negativities take the form:

$$\mathcal{E}_{X_{\text{odd}}:X_{\text{even}}} = M\alpha L - M\log\mathcal{D}^2 + 2\log\sum_a |\psi_a| d_a^M, \tag{2.12}$$

$$\mathcal{E}_{Y_{\text{odd}}:Y_{\text{even}}} = \frac{R}{2}\alpha L - \frac{R}{2}\log\mathcal{D}^2 + \log\sum_a |\psi_a|^2 d_a^R, \tag{2.13}$$

where α is nonuniversal, d_a is the quantum dimension of quasiparticle a, and $\mathcal{D} = \sqrt{\sum_a d_a^2}$ is the total quantum dimension of the phase. The Laughlin state has m Abelian anyons each with quantum dimension $d_a = 1$; the Moore-Read state has $2m$ Abelian anyons ($d_a = 1$) and m non-Abelian anyons with quantum dimensions $d_a = \sqrt{2}$, corresponding to the Majorana quasiparticle.

We use these entanglement negativities (2.12) and (2.13) to test the disentangling condition (2.4) for the geometries in Figure 2.1. For a general topological state on the torus, we find[6]

$$\mathcal{E}_{A:BC}(\rho) - \mathcal{E}_{A:B}(\rho_{AB}) = \log\frac{\left(\sum_a |\psi_a| d_a\right)^2}{\sum_a |\psi_a|^2 d_a^2}. \tag{2.14}$$

Thus, the disentangling condition is only satisfied when long-range entanglement is absent, i.e., the torus state lies in a specific topological sector with $\psi_a = 1$ for some a and all other amplitudes equal to zero. For topolotical states on the cylinder, the disentangling condition is always satisfied. Nevertheless, we find the disentangling condition is generally only a

[6] In (2.12) we set $M = 1$ for the two cylinders $A = X_2$ and $B \cup C = (X_1 \cup X_3) \cup X_4$; in (2.13) we set $R = 2$ for the two cylinders $A = X_2$ and $B = X_1 \cup X_3$; and we use $\mathcal{E}_{A:B} = \mathcal{E}_{B:A}$.

necessary condition to disentangle a topological state. Specifically, we show that Laughlin and untwisted sector Moore-Read states can be disentangled according to Eqs. (2.6) and (2.8); on the other hand, twisted sector Moore-Read states cannot be disentangled. (As we review later, the Moore-Read state decomposes into so-called untwisted and twisted sectors, associated to Abelian and non-Abelian bulk quasiparticles.) These results provide a precise illustration for how long-range entanglement and non-Abelian topological order constrain a manybody wave function.

2.2 Cut and Glue Approach to Torus Ground States

In this section we review the edge-state theories for the Laughlin and Moore-Read states and how topological states on the torus can be decomposed into states on the sub-cylinders using the corresponding edge states. In the next section we study the multipartite entanglement properties of these torus and cylinder states.

2.2.1 Laughlin Interface Ground State

We start by discussing the construction of the Laughlin state at filling fraction $\nu = 1/m$ on the torus. One approach is to "glue" together a collection of parallel 1d wires each hosting a single, nonchiral electron by suitable sine-Gordon inter-wire couplings [TK14b]. An equivalent approach [EMSS89b, WEN92a, QKL12, LFFO13, TK14b], which we follow here, is to construct the torus state by "glueing" together a collection of cylinder states

in the target phase of interest along their shared boundaries by appropriate edge-state interactions.

In the Laughlin phase, each cylinder X_i with $i \in \{1, \ldots, 2M\}$ hosts a pair of $U(1)_m$ chiral edge modes ϕ_i^σ with Lagrangian density,

$$\mathcal{L}_i^\sigma = \frac{m}{4\pi} \partial_x \phi_i^\sigma \left(\sigma \partial_t - v_c \partial_x \right) \phi_i^\sigma. \tag{2.15}$$

Here, $\phi_i^\sigma \sim \phi_i^\sigma + 2\pi\mathbb{Z}$ with $\sigma = L(R) = +1(-1)$ is a real, boson field that takes values on a circle of unit radius and $v_c > 0$ is the common[7] velocity of the edge modes. The charge density on each edge is $\rho_i^\sigma = \partial_x \phi_i^\sigma / (2\pi)$ in units where $e = 1$. The Lagrangian implies the equal-time commutation relations,

$$\left[\phi_i^\sigma(x), \partial_{x'} \phi_i^\sigma(x') \right] = \frac{2\pi i \sigma}{m} \delta(x - x'). \tag{2.16}$$

The primary fields of the theory are the vertex operators $e^{ia\phi_i^\sigma}$ for $a \in \{0, 1, \ldots, m-1\}$. They carry charge $\sigma a/m$ and spin[8] $a^2/2m$. For $a > 0$, these operators create/destroy for $\sigma = L/R$ fractionally-charged Laughlin quasiparticles on the edge. The monodromy braiding phase between bulk quasiparticles, corresponding to operators $e^{ir\phi}$ and $e^{ir'\phi}$, equals $e^{2\pi i r r'/m}$. Local quasiparticles correspond to products of the fundamental electronic operator $e^{im\phi_i^\sigma}$ carrying unit charge and integer (half-integer) spin when m is even (odd). The braiding phase between mutually local quasiparticles is trivial, i.e., equal to one. (For example, when m is odd, $e^{im\phi_i^\sigma}$ creates/destroys an electron on the edge.)

[7] This simplification does not affect our conclusions; it merely simplifies the presentation.

[8] The spin of an operator with left and right scaling dimensions (h_L, h_R) equals $|h_R - h_L|$.

Take the boundary circles on each cylinder to have circumference L. Then ϕ_i^σ has the mode expansion:

$$\begin{aligned}\phi_i^R &= \phi_{i,0}^R + 2\pi N^{RX_i}\frac{x}{L} \\ &\quad + \sum_{k>0}\sqrt{\frac{2\pi}{mL|k|}}\left(a_{i,k}e^{ikx} + (a_{i,k})^\dagger e^{-ikx}\right), \\ \phi_i^L &= \phi_{i,0}^L + 2\pi N^{LX_i}\frac{x}{L} \\ &\quad + \sum_{k<0}\sqrt{\frac{2\pi}{mL|k|}}\left(a_{i,k}e^{ikx} + (a_{i,k})^\dagger e^{-ikx}\right)\end{aligned} \tag{2.17}$$

with integer quantized momenta $k = 2\pi j/L$ and $j \in \mathbb{Z}\backslash\{0\}$. Here, $k > 0$ ($k < 0$) corresponds to a right (left) mover. The superscript "RX_i" ("LX_i") refers both to the right (left) edge and the right-moving (left-moving) edge mode of cylinder X_i. The equal-time commutation relations imply the mode operators in (2.17) satisfy the following commutation relations:

$$\begin{aligned}\left[a_{i,k}, (a_{i,k'})^\dagger\right] = \delta_{k,k'}, \quad \left[a_{i,k}, a_{i,k'}\right] = 0, \\ \left[\phi_{i,0}^R, N^{RX_i}\right] = -\left[\phi_{i,0}^L, N^{LX_i}\right] = -\frac{i}{m}.\end{aligned} \tag{2.18}$$

The winding number $N^{\sigma X_i}$ measures the total charge of the σX_i edge state since

$$N^{\sigma X_i} = \int_0^L \frac{\partial_x \phi_i^\sigma}{2\pi} dx. \tag{2.19}$$

The local operator $e^{im\phi_i^\sigma}$ obeys periodic boundary conditions (in the absence of any additional fields). For this requirement to be consistent with Eq. (2.19),

$$e^{im\phi_i^\sigma(x+L)} = e^{im\phi_i^\sigma(x)} e^{im2\pi N^{\sigma X_i}}, \tag{2.20}$$

the winding number must be quantized as $N^{\sigma X_i} - \sigma \frac{a}{m} \in \mathbb{Z}$ [SHST20]. Thus, $a = 0, 1, \ldots, m-1$ (mod m) specifies m inequivalent boundary conditions for ϕ_i^σ. As the notation suggests, these boundary conditions are in 1:1 correspondence with the different anyon types. In particular, boundary condition a can be viewed as resulting from threading the flux of anyon a through the cylinder (see Figure 2.2). Each of these boundary conditions corresponds to a Wilson line of type a connecting the two edges, obtained by the creation of an anyon of type a on, say, the left edge and its subsequent destruction on the right edge.

We are interested in "glueing" together the right edge states of cylinder X_{i-1} to the left edge states of cylinder X_i in order to form the torus state. (The subscripts are $2M$ periodic: $X_0 \equiv X_{2M}$ and therefore $X_{2M+1} \equiv X_1$.) This means we want to add a suitable interaction between edge modes on the right edge of cylinder X_{i-1} and the left edge of cylinder X_i that results in a gapped state along their shared interface i. According to (2.15), before the interaction is added, the relevant edge modes are controlled by the Hamiltonian,

$$H_i^{(0)} = \frac{mv_c}{4\pi} \int_0^L dx \left[(\partial_x \phi_{i-1}^R)^2 + (\partial_x \phi_i^L)^2 \right]. \tag{2.21}$$

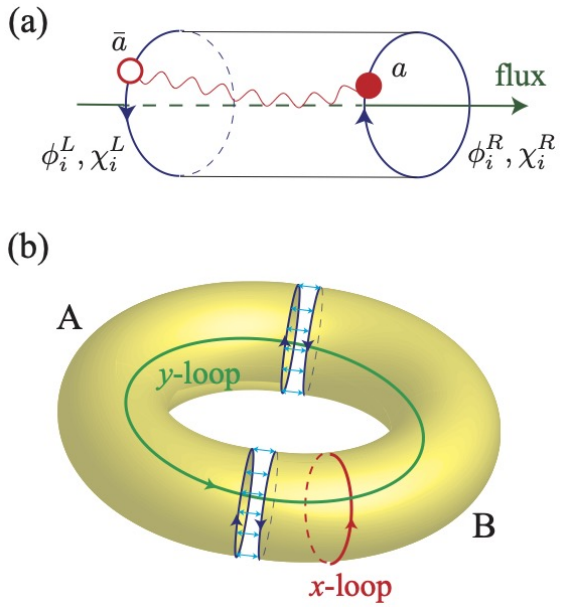

Figure 2.2: (a) Anyon flux threading continuously across a cylinder with no bulk excitation. $\phi_i^{L,R}$ refer to bosonic edge modes of the Laughlin and Moore-Read states; $\chi_i^{L,R}$ refer to fermionic edge modes that only in the Moore-Read state. (b) Wilson string operators in the x or y directions parallel or perpendicular to interfaces between cylinders A and B.

The edges are "glued" together by an interaction that tunnels a local boson or fermion between nearby edges. This is accomplished by the sine-Gordon interaction,

$$H_i^{(1)} = -\frac{2g}{\pi} \int_0^L dx \cos\left[m\left(\phi_{i-1}^R + \phi_i^L\right)\right]. \tag{2.22}$$

We take $g > 0$ to be independent of i. The total Hamiltonian at interface i is therefore

$$H_i = H_i^{(0)} + H_i^{(1)}. \tag{2.23}$$

The resulting torus Hamiltonian is then $H = \sum_i H_i$. Upon projecting each cylinder X_i into the same topological sector a, i.e., all edge modes obey the same boundary conditions around L, these decoupled H_i may be considered independently.

For large coupling $g \to \infty$, we approximate the sine-Gordon potential at quadratic order in an expansion in $(\phi^R_{i-1} + \phi^L_i)$ [LFFO13, TK14b]. This is a dramatic simplification that enables the following exact solution to the approximated H_i; it relies on the ability of the sine-Gordon potential to generate a gapped interface ground state. (We will denote and refer to the approximated Hamiltonian by H_i.) Using the mode expansion (2.17) for the bosons, the total Hamiltonian decouples into zero and oscillation (osc) mode sectors:

$$H_i = H^{\text{zero}}_{i,b} + H^{\text{osc}}_{i,b}. \tag{2.24}$$

Defining $X_i = m\left(N^{RX_{i-1}} - N^{LX_i}\right)/2$ and $P_i = \phi^R_{i-1,0} + \phi^L_{i,0}$ such that $[X_i, P_i] = i$, the zero mode Hamiltonian is

$$H^{\text{zero}}_{i,b} = \frac{2\pi v_c}{mL} X_i^2 + \frac{\pi \lambda v_c L}{2} P_i^2, \tag{2.25}$$

where $\lambda \equiv 2gm^2/\pi^2 v_c > 0$. This has the form of an harmonic oscillator Hamiltonian and a corresponding ground state,

$$|b^{\text{zero}}_{a,i}\rangle = \sum_{N_{a,i} \in \mathbb{Z} - \frac{a}{m}} e^{-\frac{v_e \pi m}{2L} N^2_{a,i}} |N^{RX_{i-1}} = N_{a,i}\rangle_{RX_{i-1}} \otimes |N^{LX_i} = -N_{a,i}\rangle_{LX_i}. \tag{2.26}$$

RX_{i-1} (LX_i) labels the Hilbert space of edge modes on the right (left) boundary of cylinder X_{i-1} (X_i) with $X_0 \equiv X_{2M}$ and $v_e = \frac{2}{\pi}\sqrt{\frac{m}{\lambda}}$ is the "entanglement velocity."

The oscillation mode Hamiltonian is

$$H_{i,b}^{\text{osc}} = v_c \sum_{k>0} \begin{bmatrix} (a_{i-1,k})^\dagger & a_{i,-k} \end{bmatrix} \begin{bmatrix} A_k & B_k \\ B_k & A_k \end{bmatrix} \begin{bmatrix} a_{i-1,k} \\ (a_{i,-k})^\dagger \end{bmatrix} \tag{2.27}$$

with $A_k \equiv |k| + \frac{2\lambda\pi^2}{m|k|}$ and $B_k \equiv \frac{2\lambda\pi^2}{m|k|}$. Using the Bogoliubov transformation,

$$\begin{bmatrix} \beta_{i,k} \\ (\gamma_{i,k})^\dagger \end{bmatrix} = \begin{bmatrix} \cosh\theta_k & \sinh\theta_k \\ \sinh\theta_k & \cosh\theta_k \end{bmatrix} \begin{bmatrix} a_{i-1,k} \\ (a_{i,-k})^\dagger \end{bmatrix}, \tag{2.28}$$

where $\cosh 2\theta_k = A_k/E_k$ and $\sinh 2\theta_k = B_k/E_k$ with $E_k = \sqrt{|k|^2 + 4\lambda\pi^2/m}$, the oscillation mode Hamiltonian is diagonal,

$$H_{i,b}^{\text{osc}} = v_c \sum_{k>0} E_k \left(\beta_{i,k}^\dagger \beta_{i,k} + \gamma_{i,k}^\dagger \gamma_{i,k} + 1 \right). \tag{2.29}$$

The ground state of the diagonalized Hamiltonian is given by the coherent state [SHST20]

$$|b_i^{\text{osc}}\rangle = \prod_{k>0} e^{-\Omega_k (a_{i-1,k})^\dagger (a_{i,-k})^\dagger} |0\rangle, \tag{2.30}$$

where $|0\rangle$ is the vacuum state annihilated by all $a_{i-1,k}$ and $a_{i,-k}$. $|b_i^{\text{osc}}\rangle$ satisfies $\beta_{i,k}|b_i^{\text{osc}}\rangle = \gamma_{i,k}|b_i^{\text{osc}}\rangle = 0$ for $k > 0$ with $\Omega_k = \tanh\theta_k$. In the limit $|k| \ll \lambda$, $\tanh\theta_k \approx v_e k/2$. Upon

expanding the exponential in (2.30), the oscillation ground state can be rewritten as

$$|b_i^{\text{osc}}\rangle = \sum_{\{n_{i,k}\in\mathbb{Z}^+\}} e^{-\sum_{k>0}\frac{v_e k}{2}(n_{i,k}+1/2)} |\{n_{b,k}^{RX_{i-1}} = n_{i,k}\}_{k>0}\rangle_{RX_{i-1}} \otimes |\{n_{b,-k}^{LX_i} = n_{i,k}\}_{k>0}\rangle_{LX_i}. \tag{2.31}$$

Here, $n_{b,k}^{RX_{i-1}}$ is the eigenvalue of the right-moving number operator $(a_{i-1,k})^\dagger a_{i-1,k}$ on cylinder X_{i-1} and $n_{b,k}^{LX_i}$ the eigenvalue of the left-moving number operator $(a_{i,-k})^\dagger a_{i,-k}$ on cylinder X_i. The coherent state form (2.30) for $|b_i^{\text{osc}}\rangle$ ensures these two eigenvalues coincide in each interface oscillator state.

Putting together these results, we find the unnormalized torus state in sector a equals

$$|\Psi_a\rangle = \bigotimes_i |b_{a,i}^{\text{zero}}\rangle \otimes |b_i^{\text{osc}}\rangle. \tag{2.32}$$

The topological sector label $a = 0, 1, \ldots, m-1$ coincides with the m-fold ground state degeneracy of the Laughlin phase on the torus. Notice that each cylinder is in the same topological sector a. This follows from our assumption that there are no bulk excitations inside any cylinder. Consequently, *all* cylinders are threaded by the same anyon flux a and $N^{RX_i} = -N^{LX_i} = a/m \mod 1$ for all X_i (see Figure 2.2). Using (2.26), $N_{a,i} = -N^{LX_i} = N^{RX_i} = N_{a,i+1} \mod 1$ and therefore $N_{a,i} \equiv a/m \mod 1$ for all cylinder i. A general (unnormalized) ground state on the torus is the linear combination of states $|\Psi_a\rangle$ with different anyon fluxes a.

2.2.2 Moore-Read Interface Ground State

The Moore-Read state at filling fraction $\nu = 1/m$ has $(U(1)_m \times \text{Ising})/\mathbb{Z}_2$ topological order. The $\mathbb{Z}_2$ symmetry couples together the $U(1)_m$ and Ising topological orders. The $U(1)_m$ sector edge states are described by the same bosonic fields ϕ_i^σ used in the construction in the Laughlin state. In particular, the commutation relations (2.16) and mode expansions (2.17) still hold. The Ising sector, which has electrically-neutral Majorana fermion edge states, supports bulk quasiparticles $1, \chi$, and ξ. Here, 1 labels the identity sector containing the vacuum; $\chi = \chi^\dagger$ is the neutral Majorana fermion; and ξ is the non-Abelian Ising twist field. The Ising anyon and the Majorana fermion have mutual semionic statistics, so that the monodromy braiding phase between χ and ξ is -1.

	1	$e^{1/2}$	e^1	$e^{3/2}$	$\dots$	e^r	$e^{r+1/2}$	$\dots$	e^{m-1}	$e^{m-1/2}$
1	0	$*$	$\frac{1}{2m}$	$*$	$\dots$	$\frac{r^2}{2m}$	$*$	$\dots$	$\frac{m^2+1}{2m}$	$*$
χ	0	$*$	$\frac{1}{2}+\frac{1}{2m}$	$*$	$\dots$	$\frac{1}{2}+\frac{r^2}{2m}$	$*$	$\dots$	$\frac{1}{2}+\frac{m^2+1}{2m}$	$*$
ξ	$*$	$\frac{1}{16}+\frac{1}{8m}$	$*$	$\frac{1}{16}+\frac{9}{8m}$	$\dots$	$*$	$\frac{1}{16}+\frac{(2r+1)^2}{8m}$	$\dots$	$*$	$\frac{1}{16}+\frac{(2m-1)^2}{8m}$

Table 2.1: The $3m$ anyon types of the Moore-Read topological order. Occupied entries are the spins (mod 1) of distinct (deconfined) anyons, $I^r = e^r \equiv e^{ir\phi}$, $\chi^r = \chi e^r$ and $\xi^{r+1/2} = \xi e^{r+1/2}$, for $r = 0, 1, \dots, m-1$. Empty entries $(*)$ are confined fields disallowed by electron locality.

We set the notion of locality in the Moore-Read theory by taking the fundamental electronic operator to be $\psi_{el} = \chi e^{im\phi}$. When m is even, ψ_{el} is a fermion; when m is odd, ψ_{el} is a boson. Integral combinations of the fundamental electronic operator, such as $e^{\pm 2im\phi}$, belong to the identity sector. They are mutually local in the sense that the corresponding bulk quasiparticles have trivial monodromy braiding phases with one another.

The remaining anyons in the Moore-Read theory correspond to the operators $I^r = e^{ir\phi}$, $\chi^r = \chi e^{ir\phi}$ and $\xi^{r+1/2} = \xi e^{i(r+1/2)\phi}$, where $r \in \{0, 1, \ldots, m-1\}$. The corresponding anyons have trivial braiding monodromy with linear combinations of ψ_{el}. The anyons obey the fusion rules:

$$\begin{aligned} &I^r \times I^{r'} = \chi^r \times \chi^{r'} = I^{r+r'}, \quad I^r \times \chi^{r'} = \chi^{r+r'} \\ &I^r \times \xi^{r'+1/2} = \chi^r \times \xi^{r'+1/2} = \xi^{r+r'+1/2}, \\ &\xi^{r+1/2} \times \xi^{r'+1/2} = I^{r+r'+1} + \chi^{r+r'+1}. \end{aligned} \tag{2.33}$$

The fusion rules imply the quantum dimensions $d_{I^r} = d_{\chi^r} = 1$ and $d_{\xi^{r+1/2}} = \sqrt{2}$. The locality of the electronic operator dictates that fields that differ by ψ_{el} belong in the same anyon class, $a \times \psi_{el} \equiv a$. Hence, the anyon types have a m-fold (i.e., charge e) periodicity

$$\chi^{r+m} \equiv I^r, \quad I^{r+m} \equiv \chi^r, \quad \xi^{r+m+1/2} \equiv \xi^{r+1/2}. \tag{2.34}$$

In total, there are $3m$ distinct anyon classes; they are listed in Table 2.1.

Bulk anyonic quasiparticles are non-local excitations that must come in conjugate pairs in real space, i.e., the total anyon charge contained in a region is conserved. Anyons in the physical Hilbert space are identified by equivalence classes of particles. Two anyons belong to the same class if they differ by a multiple of the electronic operator. Different topological sectors on the torus are obtained by imagining a process in which an anyon-anti-anyon pair is nucleated at a point and then each is dragged around the y-loop in Figure 2.2 in opposite directions until they meet again and annihilate. Decomposing the torus into cylinders, edges

of adjacent cylinders must therefore carry conjugate anyon charge (see Figure 2.1). This constraint was imposed implicitly when we considered the Laughlin state by requiring each cylinder to lie in sector a; in the present case, the presence of non-Abelian quasiparticles makes this more delicate, as we discuss.

The Moore-Read edge-states on cylinder X_i are described by the Lagrangian density [MR96],

$$\begin{aligned}\mathcal{L}_i^\sigma = &\frac{i}{2}\chi_i^\sigma\left(\partial_t - \sigma v_m \partial_x\right)\chi_i^\sigma \\ &+ \frac{m}{4\pi}\partial_x\phi_i^\sigma\left(\sigma\partial_t - v_c\partial_x\right)\phi_i^\sigma.\end{aligned} \tag{2.35}$$

As before, ϕ_i^σ is a real boson with unit compactification radius and $\sigma \in \{L, R\} = \{\pm 1\}$; χ_i^σ is a Majorana fermion; and v_c ($\tilde{v}_c$) is the velocity of the the boson (Majorana fermion). χ_i^σ satisfies the anti-commutation relations,

$$\{\chi_i^\sigma(x), \chi_i^\sigma(x')\} = \delta(x - x'). \tag{2.36}$$

The mode expansion [SHST20] of the Majorana fermion fields are

$$\chi_i^R = \frac{1}{\sqrt{L}}\sum_k e^{ikx}c_{i,k}^R, \quad \chi_i^L = \frac{1}{\sqrt{L}}\sum_k e^{ikx}c_{i,k}^L. \tag{2.37}$$

The fermionic mode operators $c_{i,k}^\sigma$ obey $(c_{i,k}^\sigma)^\dagger = c_{i,-k}^\sigma$ since χ_i^σ is real, and the anti-commutation relations

$$\{c_{i,k}^\sigma, c_{i',k'}^{\sigma'}\} = \delta_{k,-k'}\delta_{ii'}\delta^{\sigma\sigma'}. \tag{2.38}$$

The Moore-Read state is classified into untwisted and twisted sectors [SHST20]. In the untwisted sector, the Majorana fermions obey anti-periodic boundary conditions ($\chi_i^\sigma(x + L) = -\chi_i^\sigma(x)$). Consequently, the fermionic momenta are quantized in half-integers: $k = \frac{2\pi}{L}(j + 1/2)$ with $j \in \mathbb{Z}$. This sector consists of Abelian quasiparticles that correspond to vertex operators $\{e^{ir\phi_i^\sigma}, \chi_i^\sigma e^{ir\phi_i^\sigma}\}$. The boson winding number is quantized as $N^{\sigma X_i} - \sigma r/m \in \mathbb{Z}$.

In the twisted sector, the Majorana fermion is periodic ($\chi_i^\sigma(x + L) = \chi_i^\sigma(x)$) and the fermionic momenta are integrally quantized: $k = \frac{2\pi j}{L}, j \in \mathbb{Z}$. The change in boundary conditions is effected by inserting a π flux through the cylinder. In addition to the fermion oscillation modes with nonzero momenta ($k > 0$), there is an additional Majorana zero mode ($k = 0$) $c_{i,0}^\sigma$ due to the integral quantization of momenta in the twisted sector. The boson winding number also changes its quantization to $N^{\sigma X_i} - \sigma\frac{r+1/2}{m} \in \mathbb{Z}$ in response to the added π flux. The non-Abelian bulk quasiparticles are associated to the vertex operators $\{e^{i(r+1/2)\phi_i^\sigma}\}$.

While the boson and fermion modes are decoupled in the Lagrangian (2.35), physical states must be invariant under a $\mathbb{Z}_2$ internal symmetry. This neutrality requirement introduces correlations between the bosonic and fermionic components of a physical state. To see how this works, we first observe that the local electronic operator $(\psi_{el})_i^\sigma = \chi_i^\sigma e^{im\phi_i^\sigma}$ is neutral under the following $\mathbb{Z}_2$ transformation, which is local to a given cylinder X_i:

$$\mathbb{Z}_2(i): \quad \chi_{i'}^\sigma \to (-1)^{\delta_{ii'}}\chi_{i'}^\sigma, \quad \phi_{i'}^\sigma \to \phi_{i'}^\sigma + \frac{i\pi\sigma}{m}\delta_{ii'}. \tag{2.39}$$

Consequently, any integral combination of electron operators, such as a Wilson string that creates a conjugate pair of anyons on the two ends of X_i, must be even under the local $\mathbb{Z}_2$ symmetry. Assuming there are no bulk excitations inside any of the cylinders, the artifically extended Hilbert space in which the bosons and fermions are decoupled where (2.35) acts must be restricted to the physical Hilbert space that is invariant under all the $\mathbb{Z}_2(i)$ symmetries. The restriction can be achieved by the projection operator $\mathcal{P} = \prod_i \mathcal{P}_{X_i}$, where

$$\mathcal{P}_{X_i} = \frac{1}{2}\left(1 + (-1)^{N^{LX_i}+N^{RX_i}}(-1)^{F^{LX_i}+F^{RX_i}}\right) \tag{2.40}$$

is the projection operator for cylinder X_i that ensures the corresponding edge states are even under $\mathbb{Z}_2(i)$. Here $N^{\sigma X_i}$ is the winding number defined in (2.19) and $F^{\sigma X_i}$ measures the fermion parity of a state. In particular, $(-1)^{F^{\sigma X_i}}\chi_i^\sigma = -\chi_i^\sigma(-1)^{F^{\sigma X_i}}$.

Now consider "gluing" the right edge of cylinder X_{i-1} to the left edge of cylinder X_i. The strategy is similar to that of the Laughlin case. In the absence of any coupling, the edge modes are described by the free, decoupled Hamiltonians associated to (2.35). The cylinders can be pieced together at the interfaces by the electron tunneling terms,

$$\begin{aligned} H_i^{(1)} &= -\frac{2g}{2\pi}\int_0^L dx\left\{\left(\psi_i^L\right)^\dagger \psi_{i-1}^R + h.c.\right\} \\ &= -\frac{2g}{\pi}\int_0^L dx\Big\{i\chi_i^L\chi_{i-1}^R\cos\left[m\left(\phi_{i-1}^R+\phi_i^L\right)\right]\Big\}, \end{aligned} \tag{2.41}$$

where the coupling constant $g > 0$ is taken to be independent of the specific interface i. We treat the tunneling term in a mean-field approximation [SHST20] in which the corresponding

ground state expectation values (up to $\mathbb{Z}_2$ symmetry) of the bosonic and fermionic operators are

$$\begin{aligned} \langle m(\phi_i^L + \phi_{i-1}^R)\rangle = 0 \text{ mod } 2\pi \text{ and } \langle i\chi_i^L \chi_{i-1}^R\rangle > 0, \\ \text{or } \langle m(\phi_i^L + \phi_{i-1}^R)\rangle = \pi \text{ mod } 2\pi \text{ and } \langle i\chi_i^L \chi_{i-1}^R\rangle < 0. \end{aligned} \tag{2.42}$$

The overall scale of the expectation value of the fermion bilinear is absorbed into g. In the $g \to \infty$ limit, we once again employ the quadratic approximation to the sine-Gordon potential and pin the bosonic fields at the corresponding minima. This allows only neutral charge ($N^{RX_{i-1}} + N^{LX_i} = 0$) at the interfaces. With these approximations, the tunneling potential becomes

$$\begin{aligned} H_i^{(1)} = \int_0^L dx \Big[\frac{v_c \lambda \pi}{2} \big(\phi_{i-1}^R + \phi_i^L\big)^2 \\ + v_m \tilde{g} i \chi_i^L \chi_{i-1}^R + \text{const.} + \dots \Big], \end{aligned} \tag{2.43}$$

where $\tilde{g} = -\frac{2g}{v_m \pi} < 0$ and $\lambda > 0$. The ellipsis denotes higher-order terms which can be ignored as $g \to \infty$. It remains to construct torus ground state of this simplified model. We treat the untwisted and twisted sectors in turn.

Untwisted Sector

We construct the ground state of the quadratic Hamiltonian discussed in the previous section and then project the result to the physical Hilbert space. Since the bosonic zero and oscillation mode Hamiltonians are the same as in the Laughlin case, the bosonic parts

of the unprojected ground state are given in Eqs. (2.26) and (2.31). The Hamiltonian for the fermionic oscillation modes is

$$H_{i,f}^{\rm osc} = v_m \sum_{k>0} \begin{bmatrix} (c_{i-1,k}^R)^\dagger & c_{i,-k}^L \end{bmatrix} \begin{bmatrix} k & -i\tilde{g} \\ i\tilde{g} & -k \end{bmatrix} \begin{bmatrix} c_{i-1,k}^R \\ (c_{i,-k}^L)^\dagger \end{bmatrix} \tag{2.44}$$

where $k = 2\pi(j+1/2)/L$ with j a non-negative integer. For suitable φ_k, the following transformation,

$$\begin{bmatrix} \tilde{\beta}_{i,k} \\ (\tilde{\gamma}_{i,k})^\dagger \end{bmatrix} = \begin{bmatrix} \cos\varphi_k & -i\sin\varphi_k \\ \sin\varphi_k & i\cos\varphi_k \end{bmatrix} \begin{bmatrix} c_{i-1,k}^R \\ (c_{i,-k}^L)^\dagger, \end{bmatrix} \tag{2.45}$$

diagonalizes the Hamiltonian to

$$H_{i,f}^{\rm osc} = v_m \sum_{k>0} \left((\tilde{\beta}_{i,k})^\dagger \tilde{\beta}_{i,k} + (\tilde{\gamma}_{i,k})^\dagger \tilde{\gamma}_{i,k} - 1 \right). \tag{2.46}$$

We take $\cos 2\varphi_k = k/\epsilon_k$, $\sin 2\varphi_k = \tilde{g}/\epsilon_k$, and $\epsilon_k = \sqrt{k^2+\tilde{g}^2}$. The ground state is given by the BCS coherent state,

$$|f_i^{\rm osc}\rangle = \prod_{k>0} e^{-i\Xi_k (c_{i,-k}^L)^\dagger (c_{i-1,k}^R)^\dagger} |0\rangle, \tag{2.47}$$

where $\tilde{\beta}_{i,k}|f_i^{\rm osc}\rangle = \tilde{\gamma}_{i,k}|f_i^{\rm osc}\rangle = 0$, and $c_{i-1,-k}^L|0\rangle = c_{i,k}^R|0\rangle = 0$ for all $k > 0$. In the limit of $|k| \ll |\tilde{g}|$, $\Xi_k = \tan\varphi_k \approx \tilde{v}_e k/2$ with $\tilde{v}_e \equiv 2/|\tilde{g}|$ the "entanglement velocity" in the fermionic

sector. Similar to $|b_i^{\text{osc}}\rangle$ in (2.31), the ground state can be rewritten as

$$|f_i^{\text{osc}}\rangle = \sum_{\{\tilde{n}_{i,k}\in\{0,1\}\}} i^{\sum_{k>0}\tilde{n}_{i,k}} e^{-\sum_{k>0}\frac{\tilde{v}_e k}{2}(\tilde{n}_{i,k}+1/2)} \\ |\{n_{f,k}^{RX_{i-1}} = \tilde{n}_{i,k}\}_{k>0}\rangle_{RX_{i-1}} \otimes |\{n_{f,-k}^{LX_i} = \tilde{n}_{i,k}\}_{k>0}\rangle_{LX_i}. \tag{2.48}$$

where $n_{f,k}^{RX_{i-1}}$ and $n_{f,-k}^{LX_i}$ are the eigenvalues of the fermion number operators $(c_{i-1,k}^R)^\dagger c_{i-1,k}^R$ and $(c_{i,-k}^L)^\dagger c_{i,-k}^L$.

Because the zero mode and oscillation modes are decoupled (in the artificially extended Hilbert space), the torus ground state for the approximated Hamiltonian can be written as a tensor product of (2.26), (2.31), and (2.48):

$$\left|\hat{\Psi}_a\right\rangle = \bigotimes_i |b_{r,i}^{\text{zero}}\rangle \otimes |b_i^{\text{osc}}\rangle \otimes |f_i^{\text{osc}}\rangle. \tag{2.49}$$

The corresponding physical ground state that is invariant under the internal $\mathbb{Z}_2$ symmetry (2.39) is the projection:

$$|\Psi_a\rangle = \mathcal{P}\left|\hat{\Psi}_a\right\rangle \tag{2.50}$$
$$= \bigotimes_i P_{a,i}|b_{r,i}^{\text{zero}}\rangle \otimes |b_i^{\text{osc}}\rangle \otimes |f_i^{\text{osc}}\rangle,$$

where the projection operator $\mathcal{P}$ is given in (2.40). In the untwisted sector, the projection operator for each cylinder X_i decomposes into the product of left and right edge projection operators $P_{a,i}P_{a,i+1}$ given by

$$P_{a,i} = \frac{1}{2}\left(1 + (-1)^{N_{a,i} - r/m + \sum_{k>0}\tilde{n}_{i,k}}\right). \tag{2.51}$$

(Note that $\tilde{n}_{i,k}$ denotes one of the fermion number operators $(c_{i-1,k}^R)^\dagger c_{i-1,k}^R$ or $(c_{i,-k}^L)^\dagger c_{i,-k}^L$, whose eigenvalues coincide at interface i.) These operators restrict the winding number and fermion parity of the ground state at interface i between X_{i-1} and X_i.

Twisted Sector

In the twisted sector, we must include the Majorana zero mode excitations, which arise from the π flux that threads across all cylinders and results in fermionic momenta that is integrally quantized as $k = 2\pi j/L$. The contributions of the bosonic modes and fermion oscillator modes to the unprojected torus state have the same form as before and so we need only discuss the novelty presented by the Majorana zero modes.

The Majorana zero mode Hamiltonian is

$$H_f^{\text{zero}} = i\tilde{g}\sum_i c_{i-1,0}^R c_{i,0}^L = \tilde{g}\sum_i f_i^\dagger f_i, \tag{2.52}$$

where $\tilde{g} > 0$. This Hamiltonian is essentially the Kitaev chain [GSF21] with quantum states labeled by the eigenvalues $n_i' = 0, 1$ of the fermion number operators $f_i^\dagger f_i$ at the interface between cylinders X_{i-1} and X_i. Here, $f_i = (c_{i-1,0}^R + ic_{i,0}^L)/\sqrt{2}$ is an interface Dirac fermion. Suppose the torus is divided into four consecutive cylinders $X_1 \cup X_2 \cup X_3 \cup X_4$. Then the ground state of (2.52) is $|f^{\text{zero}}\rangle = |0'0'0'0'\rangle$, where the primes refer to the interface basis states.

Because the $\mathbb{Z}_2$ projection operator is not diagonal with respect to this interface basis, we need to change to an appropriate cylinder basis for the Majorana zero modes. To this end, we define the cylinder Dirac fermions $d_i = (c_{i,0}^R + ic_{i,0}^L)/\sqrt{2}$ on X_i and the corresponding occupation numbers $\gamma_i = 0, 1$ of the operators $d_i^\dagger d_i$. Notice that $f_i^\dagger f_i$ and $d_{i'}^\dagger d_{i'}$ do not commute when $i = i'$ or $i = i' + 1$. The F-symbols [Kia06] generate the basis transformation between cylinder and interface bases. This basis change is depicted in Figure 2.3. For Ising topological order, the relevant F-move transformation is given by the 2×2 matrix,

$$\left(F_\xi^{\xi\xi\xi}\right)_\mu^\nu = \frac{1}{\sqrt{2}}(-1)^{\mu\nu} \tag{2.53}$$

where $\mu, \nu \in \{0, 1\}$, corresponding to the two possible fusion channels of ξ. Thus, the F-moves transform $|0'0'0'0'\rangle$ to a basis written in terms of states labeled by the fusion channels

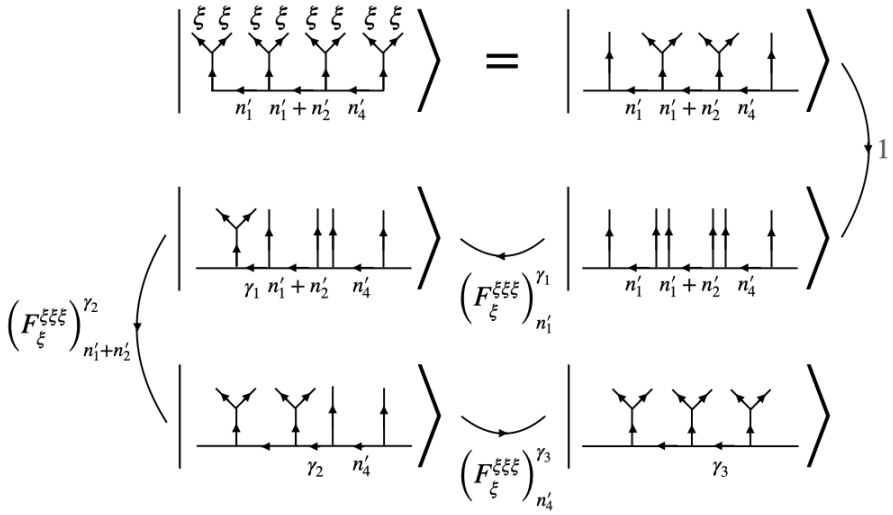

Figure 2.3: Basis Change. Three F-moves are used to transform from the interface to cylinder bases. Each $|n_i'=0\rangle$ in $|0'0'0'0'\rangle$ obtains by fusing two non-Abelian twist fields ξ into the vacuum channel; fusion into the χ channel is denoted by "1." The interface fermion numbers generally satisfy $n_1'+n_2'+n_3'+n_4'=0 \pmod 2$.

of pairs of ξ belonging to a particular cylinder. The index μ is the original internal channel and ν the new internal channel after the F-move. Thus, to transform the ground state $|n_1'=0, n_2'=0, n_3'=0, n_4'=0\rangle$, we use

$$\begin{aligned}
&|n_1'n_2'n_3'n_4'\rangle \\
&= \sum_{\gamma_1,\gamma_2,\gamma_3} \left(F_\xi^{\xi\xi\xi}\right)_{n_4'}^{\gamma_3} \left(F_\xi^{\xi\xi\xi}\right)_{n_1'+n_2'}^{\gamma_2} \left(F_\xi^{\xi\xi\xi}\right)_{n_1'}^{\gamma_1} \\
&\quad \times |\gamma_1\gamma_2\gamma_3\gamma_4\rangle, \qquad (2.54)
\end{aligned}$$

where $\gamma_4 = 1 + \gamma_1 + \gamma_2 + \gamma_3 \pmod 2$, with the result:

$$|f^{\text{zero}}\rangle = \frac{1}{\sqrt{8}}(|0001\rangle + |0010\rangle + |0100\rangle + |0111\rangle + |1000\rangle + |1011\rangle + |1101\rangle + |1110\rangle). \tag{2.55}$$

Each of the un-primed states in $|f^{\text{zero}}\rangle$ is an eigenstate of $d_i^\dagger d_i$. For example, $|\gamma_1\gamma_2\gamma_3\gamma_4\rangle$ has eigenvalue $(-1)^{\gamma_i}$ under $d_i^\dagger d_i$. Here, the total fermion parity in the cylinder basis, $\sum_i \gamma_i$, is odd, while the total parity in the interface basis, $\sum_i n_i'$, is even. This is because the two total parities are exactly opposite,

$$\begin{aligned}\prod_i (-1)^{f_i^\dagger f_i} &= (-1)^M 2^{2M} \prod_i c_{i-1,0}^R c_{i,0}^L \\ &= -(-1)^M 2^{2M} \prod_i c_{i,0}^R c_{i,0}^L \\ &= -\prod_i (-1)^{d_i^\dagger d_i}.\end{aligned} \tag{2.56}$$

For $2M$ cylinders, this result generalizes to

$$|f^{\text{zero}}\rangle = \frac{1}{\sqrt{2^{2M-1}}} \sum_{\vec{\gamma} \in \{0,1\}^{2M}|_C} |\gamma_1\gamma_2\cdots\gamma_{2M}\rangle. \tag{2.57}$$

Here, $\{0,1\}^{2M}|_C$ indicates that $\vec{\gamma}$ takes values in $\{0,1\}^{2M}$ subject to the constraint $\sum_{i=1}^{2M} \gamma_i \equiv 1 \pmod 2$; the overall normalization comes from the fact that there are 2^{2M-1} solutions to this constraint. Physically, this constraint on $\vec{\gamma}$ means the overall topological charge of the $2M$ Majorana fermions on the torus is in the vacuum channel. Similar to Eq. (2.54),

it will sometimes be convenient to take the sum in (2.57) to be over unconstrained γ_i for $i \in \{1, \ldots, 2M-1\}$ with γ_{2M} implicitly determined by the constraint.

Thus, the unprojected ground state for the twisted sector is

$$\left|\hat{\Psi}_a\right\rangle = \left(\bigotimes_i |b^{\text{zero}}_{r,i}\rangle \otimes |b^{\text{osc}}_i\rangle \otimes |f^{\text{osc}}_i\rangle\right) \otimes |f^{\text{zero}}\rangle. \tag{2.58}$$

Here a refers to the Ising twist field $\xi^{r+1/2} = \xi e^{i(r+1/2)\phi}$, for $r = 0, 1, \ldots, m-1$, and therefore the winding number $N_{r,i}$ of $|b^{\text{zero}}_{r,i}\rangle$ takes values in $(r+1/2)/m + \mathbb{Z}$. The physical ground state that is invariant under the internal $\mathbb{Z}_2$ symmetry (2.39) is the projection:

$$|\Psi_a\rangle = \mathcal{P}\left|\hat{\Psi}_a\right\rangle = \prod_i P_{a,X_i}\left|\hat{\Psi}_a\right\rangle \tag{2.59}$$

where the projection operator P_{a,X_i} on cylinder X_i is defined by

$$\begin{aligned} P_{a,X_i} &= \frac{1}{2}\left(1 + (-1)^{N_{a,X_i} + \sum_{k>0}(\tilde{n}_{X_i,k}) + d_i^\dagger d_i + u_i}\right), \\ N_{a,X_i} &\equiv -N_{a,i} + N_{a,i-1}, \quad \tilde{n}_{X_i,k} \equiv \tilde{n}_{i-1,k} + \tilde{n}_{i,k}, \\ u_i = \delta_{2M,i} &= \begin{cases} 0, & \text{if } i = 1, \ldots, 2M-1 \\ 1, & \text{if } i = 2M \end{cases}. \end{aligned} \tag{2.60}$$

Here, the additional u_{2M} accounts for the total odd parity $\prod_i (-1)^{d_i^\dagger d_i} = (-1)^{\sum_i u_i} = -1$ in the zero mode sector (see (2.56)).

2.3 Entanglement Negativity

We now study the entanglement negativity of the Laughlin and Moore-Read states at filling fraction $\nu = 1/m$ on the torus constructed in the previous section.

2.3.1 $\nu = 1/m$ Laughlin State

Torus Geometry

We begin with the Laughlin state at filling fraction $\nu = 1/m$ and the torus geometry (e.g., Figure 2.1a). The unnormalized torus ground state in sector $a \in \{0, \ldots, m-1\}$ factorizes as

$$|\Psi_a\rangle = \bigotimes_{i=1}^{2M} |\Psi_{a,i}\rangle, \tag{2.61}$$

where i refers to the interface between cylinders X_{i-1} and X_i and

$$|\Psi_{a,i}\rangle = |b_{a,i}^{\text{zero}}\rangle \otimes |b_i^{\text{osc}}\rangle. \tag{2.62}$$

The bosonic zero mode $|b_{a,i}^{\text{zero}}\rangle$ and oscillator $|b_i^{\text{osc}}\rangle$ states are given in Eqs. (2.26) and (2.31). Introducing the collective mode numbers,

$$\mathcal{N}^{LX_i} \equiv \big(- N^{LX_i}, \{n_{b,-k}^{LX_i}\}_{k>0}\big), \tag{2.63}$$

$$\mathcal{N}^{RX_i} \equiv \big(N^{RX_i}, \{n_{b,k}^{RX_i}\}_{k>0}\big), \tag{2.64}$$

$$\mathcal{N}_{a,i} \equiv \big(N_{a,i}, \{n_{i,k}\}_{k>0}\big), \tag{2.65}$$

with domains defined in Eqs. (2.26) and (2.31), we write

$$|\Psi_{a,i}\rangle = \sum_{\mathcal{N}_{a,i}} \lambda(\mathcal{N}_{a,i}) |\mathcal{N}^{RX_{i-1}} = \mathcal{N}_{a,i}\rangle_{RX_{i-1}} \otimes |\mathcal{N}^{LX_i} = \mathcal{N}_{a,i}\rangle_{LX_i}, \tag{2.66}$$

where

$$\lambda(\mathcal{N}_{a,i}) = \exp\left[-\frac{v_e \pi m}{2L} N_{a,i}^2 - \sum_{k>0} \frac{v_e k}{2} \left(n_{i,k} + \frac{1}{2} \right) \right]. \tag{2.67}$$

Assembling the preceding together, we have

$$|\Psi_a\rangle = \bigotimes_{i=1}^{2M} \sum_{\mathcal{N}_{a,i}} \lambda(\mathcal{N}_{a,i}) |\mathcal{N}_{a,i}\rangle_{RX_{i-1}} \otimes |\mathcal{N}_{a,i}\rangle_{LX_i}. \tag{2.68}$$

Eq. (2.68) shows how a product of cylinder states glue together to form the unnormalized torus state in sector a. The norm-squared of $|\Psi_a\rangle$ is

$$(Z_a)^{2M} = \left(\sum_{\mathcal{N}_a} \lambda^2(\mathcal{N}_a) \right)^{2M} \tag{2.69}$$

with mode number $\mathcal{N}_a$ defined as in (2.65). We identify Z_a as the partition function in sector a at inverse "temperature" $\beta = 1$ of the entanglement Hamiltonian H_a,

$$Z_a(\beta) = \operatorname{tr} e^{-\beta H_a}, \tag{2.70}$$

with entanglement spectrum equal to $-2 \log \lambda(\mathcal{N}_a)$.

We use Lemma 1 below to calculate the entanglement negativity of the general torus state $|\Psi\rangle = \sum_a \psi_a |\overline{\Psi}_a\rangle$ with respect to the torus partition (e.g., Figure 2.1a), where the normalized sector a state is

$$|\overline{\Psi}_a\rangle = Z_a^{-M} |\Psi_a\rangle. \tag{2.71}$$

While the details of the proof of the analogous lemma for the non-Abelian Moore-Read state differs slightly due to the presence of fermionic zero modes (in the twisted sector), it turns out that the result of Lemma 1 continues to apply. Readers uninterested in the details of the straightforward, but tedious proof of Lemma 1, may safely skip it and use the result.

Lemma 1. *The entanglement negativity of* $\rho = |\Psi\rangle\langle\Psi|$ *with respect to the torus partition* $X = X_{\text{odd}} \cup X_{\text{even}}$ *(e.g., Figure 2.1) and with partial transposition on "odd" cylinders* $X_{\text{odd}} = X_1 \cup X_3 \cup \cdots \cup X_{2M-1}$ *equals*

$$\mathcal{E}_{X_{\text{odd}}:X_{\text{even}}} = 2 \log \sum_a |\psi_a| \left(\frac{Z_a(1/2)}{\sqrt{Z_a(1)}} \right)^{2M}, \tag{2.72}$$

where $X_{\text{even}} = X_2 \cup X_4 \cup \cdots \cup X_{2M}$ *and* $Z_a(\beta)$ *is defined in* (2.70).

Proof. We directly evaluate $||\rho^{T_{\text{odd}}}||_1 = \text{tr}\sqrt{(\rho^{T_{\text{odd}}})^\dagger \rho^{T_{\text{odd}}}}$ in order to compute $\mathcal{E}_{X_{\text{odd}}:X_{\text{even}}} = \log||\rho^{T_{\text{odd}}}||_1$, where $\rho^{T_{\text{odd}}}$ denotes the partial transpose of ρ with respect to X_{odd}. Define $\{\vec{\mathcal{N}}_a\} \equiv \{(\mathcal{N}_{a,1}, \mathcal{N}_{a,2}, \ldots, \mathcal{N}_{a,2M})\}$ with $\mathcal{N}_{a,i}$ in (2.65) and $c_a(\vec{\mathcal{N}}_a) = \psi_a \prod_{i=1}^{2M} \lambda(\mathcal{N}_{a,i})/\sqrt{Z_a}$ (no sum over a) with $\lambda(\mathcal{N}_{a,i})$ given in (2.67); we will sometimes denote $c_a = c_a(\vec{\mathcal{N}}_a)$ for brevity. Then we may write

$$\begin{aligned}\rho = \sum_{a,a'} \sum_{\vec{\mathcal{N}}_a, \vec{\mathcal{N}}'_{a'}} & c_a^*(\vec{\mathcal{N}}_a) c_{a'}(\vec{\mathcal{N}}'_a) |\mathcal{N}'_{a',1}\mathcal{N}'_{a',2}\rangle\langle\mathcal{N}_{a,1}\mathcal{N}_{a,2}|_{X_1} \\ & \otimes \ldots \\ & \otimes |\mathcal{N}'_{a',2M-1}\mathcal{N}'_{a',2M}\rangle\langle\mathcal{N}_{a,2M-1}\mathcal{N}_{a,2M}|_{X_{2M-1}} \\ & \otimes |\mathcal{N}'_{a',2M}\mathcal{N}'_{a',1}\rangle\langle\mathcal{N}_{a,2M}\mathcal{N}_{a,1}|_{X_{2M}}.\end{aligned} \tag{2.73}$$

Note that $|\mathcal{N}'_{a',i}\mathcal{N}'_{a',i+1}\rangle\langle\mathcal{N}_{a,i}\mathcal{N}_{a,i+1}|_{X_i}$ denotes the outer product of states on the edges of cylinder X_i: the first entry of each ket refers to states on the left edge of X_i, while the second entry refers to states on the right edge of X_i. The partial transpose with X_{odd} is

$$\begin{aligned}\rho^{T_{\text{odd}}} = \sum_{a,a'} \sum_{\vec{\mathcal{N}}_a, \vec{\mathcal{N}}'_{a'}} & c_a^* c_{a'} |\mathcal{N}_{a,1}\mathcal{N}_{a,2}\rangle\langle\mathcal{N}'_{a',1}\mathcal{N}'_{a',2}|_{X_1} \\ & \otimes \ldots \\ & \otimes |\mathcal{N}'_{a',2M-2}\mathcal{N}'_{a',2M-1}\rangle\langle\mathcal{N}_{a,2M-2}\mathcal{N}_{a,2M-1}|_{X_{2M-2}} \\ & \otimes |\mathcal{N}_{a,2M-1}\mathcal{N}_{a,2M}\rangle\langle\mathcal{N}'_{a',2M-1}\mathcal{N}'_{a',2M}|_{X_{2M-1}} \\ & \otimes |\mathcal{N}'_{a',2M}\mathcal{N}'_{a',1}\rangle\langle\mathcal{N}_{a,2M}\mathcal{N}_{a,1}|_{X_{2M}}.\end{aligned} \tag{2.74}$$

Next we evaluate

$$(\rho^{T_{\rm odd}})^\dagger \rho^{T_{\rm odd}} \tag{2.75}$$

$$\begin{aligned}
&= \sum_{a,a',a'',a'''} \sum_{\vec{\mathcal{N}}_a,\vec{\mathcal{N}}'_{a'},\vec{\mathcal{N}}''_{a''},\vec{\mathcal{N}}'''_{a'''}} c^*_{a'''} c_{a''} c^*_a c_{a'} \\
&\quad \times |\mathcal{N}'''_{a''',1}\mathcal{N}'''_{a''',2}\rangle\langle\mathcal{N}''_{a'',1}\mathcal{N}''_{a'',2}|\mathcal{N}_{a,1}\mathcal{N}_{a,2}\rangle\langle\mathcal{N}'_{a',1}\mathcal{N}'_{a',2}|_{X_1} \\
&\quad \otimes \dots \\
&\quad \otimes |\mathcal{N}''_{a'',2M-2}\mathcal{N}''_{a'',2M-1}\rangle\langle\mathcal{N}'''_{a''',2M-2}\mathcal{N}'''_{a''',2M-1}|\mathcal{N}'_{a',2M-2}\mathcal{N}'_{a',2M-1}\rangle\langle\mathcal{N}_{a,2M-2}\mathcal{N}_{a,2M-1}|_{X_{2M-2}} \\
&\quad \otimes |\mathcal{N}'''_{a''',2M-1}\mathcal{N}'''_{a''',2M}\rangle\langle\mathcal{N}''_{a'',2M-1}\mathcal{N}''_{a'',2M}|\mathcal{N}_{a,2M-1}\mathcal{N}_{a,2M}\rangle\langle\mathcal{N}'_{a',2M-1}\mathcal{N}'_{a',2M}|_{X_{2M-1}} \\
&\quad \otimes |\mathcal{N}''_{a'',2M}\mathcal{N}''_{a'',1}\rangle\langle\mathcal{N}'''_{a''',2M}\mathcal{N}'''_{a''',1}|\mathcal{N}'_{a',2M}\mathcal{N}'_{a',1}\rangle\langle\mathcal{N}_{a,2M}\mathcal{N}_{a,1}|_{X_{2M}}.
\end{aligned} \tag{2.76}$$

Using the orthonormality of states with different quantum numbers in the above overlaps,

$$\begin{aligned}
a''' = a', \quad \mathcal{N}'''_{a''',i} = \mathcal{N}'_{a',i}, \\
a'' = a, \quad \mathcal{N}''_{a'',i} = \mathcal{N}_{a,i},
\end{aligned} \tag{2.77}$$

for all $1 \le i \le 2M$, we find that $(\rho^{T_{\rm odd}})^\dagger \rho^{T_{\rm odd}}$ is diagonal with entries given by

$$|c_{a'}(\vec{\mathcal{N}}'_{a'})|^2 |c_a(\vec{\mathcal{N}}_a)|^2. \tag{2.78}$$

Thus,

$$\begin{aligned}\sqrt{(\rho^{T_{\text{odd}}})^\dagger \rho^{T_{\text{odd}}}} = \sum_{a,a'} \sum_{\vec{\mathcal{N}}_a, \vec{\mathcal{N}}'_{a'}} & |c_{a'}||c_a| \\ & \times |\mathcal{N}'_{a',1}\mathcal{N}'_{a',2}\rangle\langle\mathcal{N}'_{a',1}\mathcal{N}'_{a',2}|_{X_1} \\ & \otimes |\mathcal{N}_{a,2}\mathcal{N}_{a,3}\rangle\langle\mathcal{N}_{a,2}\mathcal{N}_{a,3}|_{X_2} \\ & \otimes \cdots \\ & \otimes |\mathcal{N}_{a,2M}\mathcal{N}_{a,1}\rangle\langle\mathcal{N}_{a,2M}\mathcal{N}_{a,1}|_{X_{2M}}\end{aligned} \tag{2.79}$$

and $\text{tr}\sqrt{(\rho^{T_{\text{odd}}})^\dagger \rho^{T_{\text{odd}}}} = \sum_{a,a'} \sum_{\vec{\mathcal{N}}_a, \vec{\mathcal{N}}'_{a'}} |c_{a'}||c_a|$.

Tracing through our definitions, we find

$$\begin{aligned}||\rho^{T_{\text{odd}}}||_1 &= \Big(\sum_a \sum_{\vec{\mathcal{N}}_a} |c_a(\vec{\mathcal{N}}_a)|\Big)^2 \\ &= \left(\sum_a |\psi_a| \sum_{\vec{\mathcal{N}}_a} \prod_{i=1}^{2M} \frac{\lambda(\mathcal{N}_{a,i})}{\sqrt{Z_a}}\right)^2 \\ &= \left(\sum_a |\psi_a| \left(\frac{\sum_{\mathcal{N}_a} \lambda(\mathcal{N}_a)}{\sqrt{\sum_{\mathcal{N}_a} \lambda^2(\mathcal{N}_a)}}\right)^{2M}\right)^2 \\ &= \left(\sum_a |\psi_a| \left(\frac{Z_a(1/2)}{\sqrt{Z_a(1)}}\right)^{2M}\right)^2 .\end{aligned} \tag{2.80}$$

Taking the logarithm of $||\rho^{T_{\text{odd}}}||_1$, we obtain (2.72) and thereby complete the proof. □

It remains to calculate $Z_a(\beta)$. We are specifically interested in the $L \to \infty$ limit. The partition function of the Laughlin edge states in sector a can be written as

$$Z_a(\beta) = \frac{\theta_0^{-a/m}(m\tau)}{\eta(\tau)}, \quad \tau = i\tau_2 = \frac{i\beta v_e}{L}, \tag{2.81}$$

where the Jacobi θ and Dedekind η functions are

$$\theta_0^{-a/m}(m\tau) = \sum_{N_a \in \mathbb{Z} - \frac{a}{m}} e^{-\frac{\beta v_e \pi m}{L} N_a^2}, \tag{2.82}$$

$$= \sum_{n \in \mathbb{Z}} q^{\frac{1}{2}(n - \frac{a}{m})^2}, \tag{2.83}$$

$$\eta^{-1}(\tau) = \sum_{n_{i,k} \in \mathbb{Z}^+} e^{-\sum_{k>0} \beta v_e k (n_{i,k} + 1/2)} \tag{2.84}$$

$$= q^{-\frac{1}{24}} \prod_{n_{i,k} \in \mathbb{Z}^+} (1 - q^{n_{i,k}})^{-1}, \tag{2.85}$$

and $q = e^{2\pi i \tau}$. These functions have a useful transformation under the modular transformation $\tau \mapsto -1/\tau$ that allows us to easily extract the scaling behavior of the entanglement negativity as $L \to \infty$. Specifically,

$$\theta_0^{-a/m}(m\tau) = \frac{\theta^0_{-a/m}(-1/m\tau)}{\sqrt{-im\tau}}, \tag{2.86}$$

$$\eta(\tau) = \frac{\eta(-1/\tau)}{\sqrt{-i\tau}}. \tag{2.87}$$

Thus, $Z_a(\beta) = \frac{1}{\sqrt{m}} \exp\left[\frac{\pi L}{12\beta v_e}\right]$ and so

$$\frac{Z_a(1/2)}{\sqrt{Z_a(1)}} = \frac{1}{\sqrt[4]{m}} e^{\frac{\pi L}{8 v_e}}. \tag{2.88}$$

Inserting this expression into (2.72) and taking the $L \to \infty$ limit, we find the topological entanglement negativity

$$\mathcal{E}_{X_{\text{odd}}:X_{\text{even}}} = M\left(\frac{\pi}{2v_e}\right) L - M \log m + 2 \log \sum_a |\psi_a|. \tag{2.89}$$

We see that $\mathcal{E}_{X_{\text{odd}}:X_{\text{even}}}$ receives $2M$ boundary entanglement contributions, proportional to $\log \sqrt{m}$, and a single long-range entanglement contribution, equal to $2 \log \sum_a |\psi_a|$. Since the Laughlin phase has only Abelian quasiparticles ($d_a = 1$), $\mathcal{E}_{X_{\text{odd}}:X_{\text{even}}}$ takes the form given in (2.12) with $\alpha = \frac{\pi}{2v_e}$ and $\mathcal{D} = \sqrt{m}$.

Cylinder Geometry

Next we consider the entanglement negativity between subsets of X_{even} and X_{odd} when the degrees of freedom on $N \leq M$ cylinders $\bar{Y} \subset X$ have been traced over. We denote the remaining $(2M - N)$ cylinders by Y and their decomposition into "odd" and "even" cylinders as Y_{odd} and Y_{even}. The resulting entanglement negativity will depend on the number R of shared interfaces between the remaining cylinders in $Y_{\text{odd}} \cup Y_{\text{even}}$. As an example, Figure 2.1b represents $\text{Tr}_{X_4} |\Psi\rangle\langle\Psi|$, i.e., the $X_1 \cup X_2 \cup X_3$ cylinder state when the degrees of freedom on $\bar{Y} = X_4$ have been traced over; we then consider the entanglement negativity of $\text{Tr}_{X_4} |\Psi\rangle\langle\Psi|$ between degrees of freedom on $Y_{\text{odd}} = X_1 \cup X_3$ and $Y_{\text{even}} = X_2$ with a result that depends on $R = 2$.

Our calculation of the entanglement negativity will apply Lemma 2 below to the torus ground state from the previous section. This lemma applies to both the Abelian Laughlin

and non-Abelian Moore-Read states. We will summarize the appropriate generalization of its proof in the non-Abelian case in a later section.

Lemma 2. *Consider the reduced density matrix* $\rho_Y = \mathrm{Tr}_{\bar{Y}} |\Psi\rangle\langle\Psi|$, *where* $|\Psi\rangle = \sum_a \psi_a |\overline{\Psi}_a\rangle$ *is a general state on the torus* $X = Y \cup \bar{Y}$. *Then the entanglement negativity of* ρ_Y *equals*

$$\mathcal{E}_{Y_{\mathrm{odd}}:Y_{\mathrm{even}}} = \log \sum_a \left(|\psi_a| \left(\frac{Z_a(1/2)}{\sqrt{Z_a(1)}} \right)^R \right)^2 , \tag{2.90}$$

where R *equals the number of interfaces shared between the remaining cylinders* $Y = Y_{\mathrm{odd}} \cup Y_{\mathrm{even}}$ *and* $Z_a(\beta)$ *is defined in* (2.70).

Proof. We use notation introduced in Lemma 1. There are four cases to consider.

(Case I) We remove cylinder $\bar{Y} = X_{2k}$ where $1 < 2k \leq 2M$ by tracing over its left and right edge states. Thus, $Y_{\mathrm{odd}} = X_{\mathrm{odd}}$, $Y_{\mathrm{even}} = X_2 \cup \cdots \cup X_{2k-2} \cup X_{2k+2} \cdots X_{2M}$, and $R = 2M - 2$.

We begin with the torus ground state $|\Psi\rangle\langle\Psi|$:

$$\begin{aligned}\rho = \sum_{a,a'} \sum_{\vec{\mathcal{N}}_a, \vec{\mathcal{N}}'_{a'}} & c_a(\vec{\mathcal{N}}_a) c^*_{a'}(\vec{\mathcal{N}}'_{a'}) \times \cdots \\ & \otimes |\mathcal{N}_{a,2k-2}\mathcal{N}_{a,2k-1}\rangle\langle\mathcal{N}'_{a',2k-2}\mathcal{N}'_{a',2k-1}|_{X_{2k-2}} \\ & \otimes |\mathcal{N}_{a,2k-1}\mathcal{N}_{a,2k}\rangle\langle\mathcal{N}'_{a',2k-1}\mathcal{N}'_{a',2k}|_{X_{2k-1}} \\ & \otimes |\mathcal{N}_{a,2k}\mathcal{N}_{a,2k+1}\rangle\langle\mathcal{N}'_{a',2k}\mathcal{N}'_{a',2k+1}|_{X_{2k}} \\ & \otimes |\mathcal{N}_{a,2k+1}\mathcal{N}_{a,2k+2}\rangle\langle\mathcal{N}'_{a',2k+1}\mathcal{N}'_{a',2k+2}|_{X_{2k+1}} \\ & \otimes |\mathcal{N}_{a,2k+2}\mathcal{N}_{a,2k+3}\rangle\langle\mathcal{N}'_{a',2k+2}\mathcal{N}'_{a',2k+3}|_{X_{2k+2}} \\ & \otimes \cdots .\end{aligned} \tag{2.91}$$

Tracing over degrees of freedom on X_{2k} sets

$$a' = a, \quad \mathcal{N}'_{a',2k} = \mathcal{N}_{a,2k}, \quad \mathcal{N}'_{a',2k+1} = \mathcal{N}_{a,2k+1}, \tag{2.92}$$

and removes the corresponding outer products involving states on X_{2k}. The first condition above ($a = a'$) removes any "interference" in $\mathrm{Tr}_{X_{2k}}(\rho)$ between states in different topological sectors.

Using (2.92) and the definition of $c_a(\vec{\mathcal{N}}_a)$, the partial transpose of $\mathrm{Tr}_{X_{2k}}(\rho)$ with respect to Y_{odd} is

$$\begin{aligned}\rho_Y^{T_{\mathrm{odd}}} = \sum_a \sum_{\vec{\mathcal{N}}_a, \vec{\mathcal{N}}'_a} & c_a(\vec{\mathcal{N}}_a) c_a^*(\vec{\mathcal{N}}'_a) \times \cdots \\ & \otimes |\mathcal{N}_{a,2k-2}\mathcal{N}_{a,2k-1}\rangle\langle \mathcal{N}'_{a,2k-2}\mathcal{N}'_{a,2k-1}|_{X_{2k-2}} \\ & \otimes |\mathcal{N}'_{a,2k-1}\mathcal{N}_{a,2k}\rangle\langle \mathcal{N}_{a,2k-1}\mathcal{N}_{a,2k}|_{X_{2k-1}} \\ & \otimes |\mathcal{N}_{a,2k+1}\mathcal{N}'_{a,2k+2}\rangle\langle \mathcal{N}_{a,2k+1}\mathcal{N}_{a,2k+2}|_{X_{2k+1}} \\ & \otimes |\mathcal{N}_{a,2k+2}\mathcal{N}_{a,2k+3}\rangle\langle \mathcal{N}'_{a,2k+2}\mathcal{N}'_{a,2k+3}|_{X_{2k+2}} \\ & \otimes \cdots,\end{aligned} \tag{2.93}$$

where

$$\begin{aligned} c_a(\vec{\mathcal{N}}_a) c_a^*(\vec{\mathcal{N}}'_a) = \frac{|\psi_a|^2}{Z_a^{2M}} & \lambda(\mathcal{N}_{a,1})\lambda(\mathcal{N}'_{a,1}) \times \ldots \\ & \times \lambda(\mathcal{N}_{a,2k-1})\lambda(\mathcal{N}'_{a,2k-1}) \\ & \times \lambda^2(\mathcal{N}_{a,2k})\lambda^2(\mathcal{N}_{a,2k+1}) \\ & \times \lambda(\mathcal{N}_{a,2k+2})\lambda(\mathcal{N}'_{a,2k+2}) \times \ldots \\ & \times \lambda(\mathcal{N}_{a,2M})\lambda(\mathcal{N}'_{a,2M}). \end{aligned} \tag{2.94}$$

There is no dependence on $\mathcal{N}'_{a,2k}$ or $\mathcal{N}'_{a,2k+1}$ above because of (2.92). In what follows, it will be implicitly understood that $\mathcal{N}'_{a,2k}, \mathcal{N}'_{a,2k+1}$ are removed in sums over $\vec{\mathcal{N}}'_a$. The remainder

of the proof follows that of Lemma 1. Specifically, we compute

$$
\begin{aligned}
(\rho_Y^{T_{\rm odd}})^\dagger \rho_Y^{T_{\rm odd}} = \sum_{a,a'} \sum_{\vec{\mathcal{N}}_a, \vec{\mathcal{N}}'_a, \vec{\mathcal{N}}''_{a'}, \vec{\mathcal{N}}'''_{a'}} & c^*_{a'}(\vec{\mathcal{N}}''_{a'}) c_{a'}(\vec{\mathcal{N}}'''_{a'}) c_a(\vec{\mathcal{N}}_a) c^*_a(\vec{\mathcal{N}}'_a) \times \cdots \\
& \otimes |\mathcal{N}'''_{a',2k-2} \mathcal{N}'''_{a',2k-1}\rangle\langle \mathcal{N}''_{a',2k-2} \mathcal{N}''_{a',2k-1} | \mathcal{N}_{a,2k-2} \mathcal{N}_{a,2k-1}\rangle\langle \mathcal{N}'_{a,2k-2} \mathcal{N}'_{a,2k-1}|_{X_{2k-2}} \\
& \otimes |\mathcal{N}''_{a',2k-1} \mathcal{N}''_{a',2k}\rangle\langle \mathcal{N}'''_{a',2k-1} \mathcal{N}''_{a',2k} | \mathcal{N}'_{a,2k-1} \mathcal{N}_{a,2k}\rangle\langle \mathcal{N}_{a,2k-1} \mathcal{N}_{a,2k}|_{X_{2k-1}} \\
& \otimes |\mathcal{N}''_{a',2k+1} \mathcal{N}''_{a',2k+2}\rangle\langle \mathcal{N}''_{a',2k+1} \mathcal{N}'''_{a',2k+2} | \mathcal{N}_{a,2k+1} \mathcal{N}'_{a,2k+2}\rangle\langle \mathcal{N}_{a,2k+1} \mathcal{N}_{a,2k+2}|_{X_{2k+1}} \\
& \otimes |\mathcal{N}'''_{a',2k+2} \mathcal{N}'''_{a',2k+3}\rangle\langle \mathcal{N}''_{a',2k+2} \mathcal{N}''_{a',2k+3} | \mathcal{N}_{a,2k+2} \mathcal{N}_{a,2k+3}\rangle\langle \mathcal{N}'_{a,2k+2} \mathcal{N}'_{a,2k+3}|_{X_{2k+2}} \\
& \otimes \cdots .
\end{aligned}
\tag{2.95}
$$

Note that $\mathcal{N}'_{a,2k}, \mathcal{N}'_{a,2k+1}$ and $\mathcal{N}'''_{a,2k}, \mathcal{N}'''_{a,2k+1}$ are absent in the sums over $\vec{\mathcal{N}}'_a$ and $\vec{\mathcal{N}}'''_a$. The above overlaps fix $a = a'$ and

$$
\mathcal{N}'''_{a',i} = \mathcal{N}'_{a,i}, \quad \mathcal{N}''_{a',i} = \mathcal{N}'_{a,i}, \tag{2.96}
$$

for $1 \leq i \leq 2M$. Analogous to (2.79), we may now read off $||\rho_Y^{T_{\rm odd}}||_1 = \mathrm{tr}\sqrt{(\rho_Y^{T_{\rm odd}})^\dagger \rho_Y^{T_{\rm odd}}}$ to find

$$
\begin{aligned}
||\rho_Y^{T_{\rm odd}}||_1 &= \sum_a \sum_{\vec{\mathcal{N}}_a, \vec{\mathcal{N}}'_a} |c_a(\vec{\mathcal{N}}_a)||c_a(\vec{\mathcal{N}}'_a)| \\
&= \sum_a |\psi_a|^2 \left| \frac{Z_a^{2M-2}(1/2)}{Z_a^{M-2}(1)} \right| \left| \frac{Z_a^{2M-2}(1/2)}{Z_a^{M}(1)} \right| \\
&= \sum_a \left(|\psi_a| \left(\frac{Z_a(1/2)}{\sqrt{Z_a(1)}} \right)^{2M-2} \right)^2 .
\end{aligned}
\tag{2.97}
$$

The second equality follows from (2.94) and the definition of the $c_a(\vec{\mathcal{N}}_a)$. Taking the logarithm of $||\rho_Y^{T_{\rm odd}}||_1$, we obtain (2.90) and thereby complete the proof of the lemma when $\bar{Y} = X_{2k}$, i.e., a single "even" cylinder has been removed.

This dependence of the entanglement negativity on the number R of shared interfaces of the remaining cylinders Y not traced over continues in the other cases.

(Case II) If X_{2k} and an additional "even" cylinder $X_{2k'}$ are traced out, then the generalization of (2.92) will also remove any dependence on $\mathcal{N}'_{a,2k'}$ and $\mathcal{N}'_{a,2k'+1}$. Proceeding with the remaining steps outlined for Case 1, we find $R = 2M - 4$, reflective of the number of remaining shared interfaces. In the special case when $k' = k + 1$, degrees of freedom on X_{2k+1} become disconnected from those on the remaining cylinders; because X_{2k+1} has no shared interface with the remaining cylinders, we conclude that it effectively makes no contribution to the entanglement negativity.

(Case III) The proof proceeds identically if instead $\bar{Y} = X_{2k-1}$. Then (2.92) removes the dependence on $\mathcal{N}'_{a,2k'-1}$ and $\mathcal{N}'_{a,2k'}$, and the remainder of the proof proceeds as before, obtaining $R = 2M - 2$ in this case.

It is straightforward to generalize the above reasoning to the situation when more than two nonconsecutive cylinders, e.g., a subset of the "even" cylinders, are removed. In this situation, the generalization of the above arguments gives $R = 2M - 2Q$, where Q equals the number of cylinders removed.

(Case IV) The remaining case to discuss involves the removal (by trace) of two consecutive cylinders, say, X_{2k-1} and X_{2k}. In this case, (2.92) removes the dependence on $\mathcal{N}'_{a,2k-1}, \mathcal{N}'_{a,2k}$, and $\mathcal{N}'_{a,2k+1}$. There are only three mode numbers in this case because states at the interface between X_{2k-1} and X_{2k} share $\mathcal{N}'_{a,2k}$. Proceeding then as above we obtain $R = 2M - 3$.

The above reasoning can then be suitably generalized, as needed, to show (2.90) with R equal to the number of shared interfaces in Y. This completes our proof of Lemma 2. □

By Lemma 2, the calculation of the entanglement negativity between Y_{odd} and Y_{even} reduces to the calculation of the ratio of entanglement Hamiltonian partition functions. Making use of the partition function results from the previous section, we find

$$\begin{aligned}\mathcal{E}_{Y_{\text{odd}}:Y_{\text{even}}} &= \frac{R}{2}\left(\frac{\pi}{2v_e}\right)L - \frac{R}{2}\log m + \log\sum_a |\psi_a|^2 \\ &= \frac{R}{2}\left(\frac{\pi}{2v_e}\right)L - \frac{R}{2}\log m,\end{aligned} \tag{2.98}$$

where in the last line we used $\sum_a |\psi_a|^2 = 1$. This verifies (2.13) with $\alpha = \pi/2v_e$ and $\mathcal{D} = \sqrt{m}$. Similar to the torus geometry, there are R boundary entanglement contributions, equal to $\log\sqrt{m}$. However, the long-range entanglement contribution is absent: the trace that is used to construct the cylinder state removes the correlations between different topological sectors when the state is Abelian ($d_a = 1$). We show in the next section that a long-range entanglement term is present for the Moore-Read state.

2.3.2 $\nu = 1/m$ Moore-Read State

Torus Geometry

We now consider the entanglement negativity of the Moore-Read state on the torus geometry (e.g., Figure 2.1a). At filling fraction $\nu = 1/m$, there are $2m$ untwisted anyon sectors $a = I^r = e^r$ or $\chi^r = \chi e^r$ and m twisted anyon sectors $a = \xi^{r+1/2} = \xi e^{r+1/2}$ topological sectors, for $r = 0, 1, \ldots, m$ (see table 2.1). For the untwisted sector, much of our presentation will mirror that of the Laughlin state; in the twisted sector, there are some differences associated to Majorana fermion zero modes that we will highlight and discuss as they arise.

We begin with the untwisted sectors. The un-normalized torus ground state in sector a can be factorized as (see (2.50))

$$|\Psi_a\rangle = P_a|\hat{\Psi}_a\rangle = \bigotimes_{i=1}^{2M} P_{a,i}|\hat{\Psi}_{a,i}\rangle, \tag{2.99}$$

where i labels the interface between cylinders X_i and X_{i+1}, $P_a = \otimes_i P_{a,i}$ is the decomposition of the sector a projection operator into projection operators local to each interface, and the unprojected state:

$$|\hat{\Psi}_{a,i}\rangle = |b_{r,i}^{\text{zero}}\rangle \otimes |b_i^{\text{osc}}\rangle \otimes |f_i^{\text{osc}}\rangle. \tag{2.100}$$

The bosonic zero mode and oscillator states are given in Eqs. (2.26) and (2.31); the fermionic oscillator states are given in Eq. (2.48). The collective mode numbers are now

$$\mathcal{N}^{LX_i} \equiv \big(- N^{LX_i}, \{n^{LX_i}_{b,-k}\}_{k>0}, \{n^{LX_i}_{f,-k}\}_{k>0}\big), \tag{2.101}$$

$$\mathcal{N}^{RX_i} \equiv \big(N^{RX_i}, \{n^{RX_j}_{b,k}\}_{k>0}, \{n^{RX_i}_{f,k}\}_{k>0}\big), \tag{2.102}$$

$$\mathcal{N}_{a,i} \equiv \big(N_{a,i}, \{n_{i,k}\}_{k>0}, \{\tilde{n}_{i,k}\}_{k>0}\big), \tag{2.103}$$

with domains defined in Eqs. (2.26), (2.31), (2.48). When acting on $|\hat{\Psi}_{a,i}\rangle$, we may replace $P_{a,i}$ with its eigenvalue $P_a(\mathcal{N}_{a,i})$ using

$$\begin{aligned} P_{a,i}\left(|\mathcal{N}_{a,i}\rangle_{RX_{i-1}} \otimes |\mathcal{N}_{a,i}\rangle_{LX_i}\right) &= \frac{1}{2}\left(1 + (-1)^{N_{a,i} - \frac{r}{m} + \sum_{k>0}\tilde{n}_{i,k}}\right)|\mathcal{N}_{a,i}\rangle_{RX_{i-1}} \otimes |\mathcal{N}_{a,i}\rangle_{LX_i} \\ &\equiv P_a(\mathcal{N}_{a,i})|\mathcal{N}_{a,i}\rangle_{RX_{i-1}} \otimes |\mathcal{N}_{a,i}\rangle_{LX_i}. \end{aligned} \tag{2.104}$$

Putting this all together, we have

$$|\Psi_a\rangle = \bigotimes_{i=1}^{2M} \sum_{\mathcal{N}_{a,i}} P_a(\mathcal{N}_{a,i})\lambda(\mathcal{N}_{a,i})|\mathcal{N}_{a,i}\rangle_{RX_{i-1}} \otimes |\mathcal{N}_{a,i}\rangle_{LX_i}, \tag{2.105}$$

where

$$\lambda(\mathcal{N}_{a,i}) = \exp\left[-\frac{v_e \pi m}{2L} N_{a,i}^2 - \sum_{k>0}\frac{v_e k}{2}\left(n_{i,k} + \frac{1}{2}\right) - \sum_{k>0}\frac{\tilde{v}_e k}{2}\left(\tilde{n}_{i,k} + \frac{1}{2}\right)\right]. \tag{2.106}$$

The norm-squared of $|\Psi_a\rangle$ is

$$\left(Z_a^{\text{untwisted}}\right)^{2M} = \left(\sum_{\mathcal{N}_a} P(\mathcal{N}_a)\lambda^2(\mathcal{N}_a)\right)^{2M}. \tag{2.107}$$

Similar to the Laughlin case, $Z_a^{\text{untwisted}}$ defines the untwisted sector a partition function at inverse "temperature" $\beta = 1$ of the Moore-Read entanglement Hamiltonian H_a:

$$Z_a^{\text{untwisted}}(\beta) = \text{tr}\, e^{-\beta H_a} \tag{2.108}$$

with untwisted entanglement spectrum equal to $-2\log\lambda(\mathcal{N}_a)$, subject to the condition on allowed states imposed by the projection operator eigenvalues in (2.104). (As we have already done above, we will continue to abuse notation below; however, we will make sure to specify whether we are dealing with the untwisted or twisted topological sectors.)

We next turn to the twisted sectors. The unprojected sector a torus state is

$$|\hat{\Psi}_a\rangle = \Big(\bigotimes_{i=1}^{2M} |\hat{\Psi}_{a,i}\rangle\Big) \otimes |f^{\text{zero}}\rangle, \tag{2.109}$$

where $|\hat{\Psi}_{a,i}\rangle$ takes the form in (2.100) and the Majorana zero mode state $|f^{\text{zero}}\rangle$ is given in (2.57). Note that the domain of $N_{a,i} \in \mathbb{Z} + (r+1/2)/m$ and oscillator fermion momenta are shifted by an half-integer.

The presence of Majorana zero modes makes the decomposition of the torus ground states into cylinder states more delicate. In particular, the twisted sector a projection operator P_a does not factorize in terms of independent projection operators local to each interface (as

in, e.g., (2.99)); instead, we can at most decompose $P_a = \otimes_{i=1}^{2M} P_{a,X_i}$, where P_{a,X_i} is the projection operator for cylinder X_i. When acting on a cylinder state $|\hat{\Psi}_{a,i}\rangle \otimes |\gamma_i\rangle \in (\otimes_i |\hat{\Psi}_{a,i}\rangle) \otimes |f^{\text{zero}}\rangle$ we may replace the projection operator P_{a,X_i} with its eigenvalue $P_a(\mathcal{N}_{a,i}, \mathcal{N}_{a,i+1}, \gamma_i)$ using

$$\begin{aligned} P_{a,X_i}|\mathcal{N}_{a,i}, \mathcal{N}_{a,i+1}, \gamma_i\rangle|_{X_i} &= \frac{1}{2}\Big(1 + (-1)^{-N_{a,i}+N_{a,i+1}+\sum_{k>0}\left(\tilde{n}_{i,k}+\tilde{n}_{i+1,k}\right)+\gamma_i}\Big)|\mathcal{N}_{a,i}, \mathcal{N}_{a,i+1}, \gamma_i\rangle|_{X_i} \\ &\equiv P_a(\mathcal{N}_{a,i}, \mathcal{N}_{a,i+1}, \gamma_i)|\mathcal{N}_{a,i}, \mathcal{N}_{a,i+1}, \gamma_i\rangle|_{X_i}. \end{aligned} \tag{2.110}$$

Using these eigenvalues, the product of $2M$ projection operators can be reduced to a product of $(2M-1)$ operators, e.g.,

$$\prod_{i=1}^{2M} P_{a,X_i}|\hat{\Psi}_a\rangle = \prod_{i=1}^{2M-1} P_{a,X_i}|\hat{\Psi}_a\rangle. \tag{2.111}$$

Thus, the norm-squared of twisted sector a state $|\Psi_a\rangle = P_a|\hat{\Psi}_a\rangle$ (see (2.59)) equals

$$\begin{aligned} \left(Z_a^{\text{twisted}}\right)^{2M} &= \frac{1}{2^{2M-1}} \sum_{\vec{\mathcal{N}}_a} \lambda^2(\mathcal{N}_{a,2M}) \sum_{\gamma_1,\ldots,\gamma_{2M-1}\in\{0,1\}} \prod_{i=1}^{2M-1} P_a(\mathcal{N}_{a,i}, \mathcal{N}_{a,i+1}, \gamma_i)\lambda^2(\mathcal{N}_{a,i}) \\ &= \frac{1}{2^{2M-1}} \left(\sum_{\mathcal{N}_a} \lambda^2(\mathcal{N}_a)\right)^{2M}, \end{aligned} \tag{2.112}$$

where $\lambda(\mathcal{N}_{a,i})$ is given in (2.106) and we have used $\sum_{\gamma_i\in\{0,1\}} P_a(\mathcal{N}_{a,i}, \mathcal{N}_{a,i+1}, \gamma_i) = 1$. As before, we may interpret Z_a^{twisted} in terms of a twisted sector partition function $Z_a^{\text{twisted}}(\beta)$ of a Hamiltonian H_a with spectrum $-2\log\lambda(\mathcal{N}_a)$ at inverse "temperature" equal to one. In

contrast to the untwisted sector, the projection operator eigenvalues do not appear in the norm-squared of the twisted sector state $|\Psi_a\rangle$ or the corresponding partition function.

To calculate the entanglement negativity of $|\Psi\rangle = \sum_a \psi_a |\overline{\Psi}_a\rangle$, where the sum is over all topological sectors and the normalized sector a state is

$$|\overline{\Psi}_a\rangle = Z_a^{-M} |\Psi_a\rangle. \tag{2.113}$$

We will again use Lemma 1. (Here and in the generalized proof below we drop the untwisted/twisted superscripts for the normalization factors in (2.107) and (2.112).) The proof that we previously gave of this lemma was special to the Laughlin state; below we will sketch how the proof generalizes for the Moore-Read state.

Generalized Proof of Lemma 1. As before, we will directly evaluate

$$||\rho^{T_{\text{odd}}}||_1 = \text{tr}\sqrt{(\rho^{T_{\text{odd}}})^\dagger \rho^{T_{\text{odd}}}}. \tag{2.114}$$

We begin by writing the torus state as

$$|\Psi\rangle = \sum_a \sum_{\vec{\mathcal{X}}_a} c_a(\vec{\mathcal{N}}_a) P_a(\vec{\mathcal{X}}_a) \bigotimes_{i=1}^{2M} |\mathcal{X}_{a,i}\rangle, \tag{2.115}$$

$$\mathcal{X}_{a,i} \equiv (\mathcal{N}_{a,i}, \mathcal{N}_{a,i+1}, s_a \gamma_i), \tag{2.116}$$

$$c_a(\vec{\mathcal{N}}_a) \equiv \psi_a \prod_{i=1}^{2M} \frac{\lambda(\mathcal{N}_{a,i})}{\sqrt{Z_a}}, \tag{2.117}$$

$$P_a(\vec{\mathcal{X}}_a) \equiv \prod_{i=1}^{2M} P_a(\mathcal{X}_{a,i}) \tag{2.118}$$

where $s_a = 0$ if a belongs to an untwisted sector and $s_a = 1$ if a belongs to a twisted sector. The sum over $\vec{\mathcal{X}}_a$ is understood to be a sum over $\vec{\mathcal{N}}_a$ and, when $s_a = 1$, the Majorana fermion parity eigenvalues $\vec{\gamma}$, (i.e., $\sum_{\vec{\mathcal{X}}_a} = \sum_{\vec{\mathcal{N}}_a, s_a\vec{\gamma}}$). $P_a(\mathcal{X}_{a,i}) = P_a(\mathcal{N}_{a,i}, \mathcal{N}_{a,i+1}, s_a\gamma_i)$ is defined in (2.110) for twisted sector a where $s_a = 1$, this eigenvalue is also valid for untwisted a, in which case $s_a = 0$.

The density matrix $\rho = |\Psi\rangle\langle\Psi|$ and its partial transpose with respect to X_{odd} are then

$$\begin{aligned}
\rho = &\sum_{a,a'} \sum_{\vec{\mathcal{X}}_a, \vec{\mathcal{X}}'_{a'}} c_a(\vec{\mathcal{N}}_a) c^*_{a'}(\vec{\mathcal{N}}'_{a'}) \\
&\times P_a(\mathcal{X}_{a,1}) |\mathcal{X}_{a,1}\rangle\langle\mathcal{X}'_{a',1}| P_{a'}(\mathcal{X}'_{a',1}) \\
&\otimes P_a(\mathcal{X}_{a,2}) |\mathcal{X}_{a,2}\rangle\langle\mathcal{X}'_{a',2}| P_{a'}(\mathcal{X}'_{a',2}) \\
&\otimes \cdots \\
&\otimes P_a(\mathcal{X}_{a,2M}) |\mathcal{X}_{a,2M}\rangle\langle\mathcal{X}'_{a',2M}| P_{a'}(\mathcal{X}'_{a',2M}),
\end{aligned} \tag{2.119}$$

$$\begin{aligned}
\rho^{T_{\text{odd}}} = &\sum_{a,a'} \sum_{\vec{\mathcal{X}}_a, \vec{\mathcal{X}}'_{a'}} c_a(\vec{\mathcal{N}}_a) c^*_{a'}(\vec{\mathcal{N}}'_{a'}) \\
&\times P_{a'}(\mathcal{X}'_{a',1}) |\mathcal{X}'_{a',1}\rangle\langle\mathcal{X}_{a,1}| P_a(\mathcal{X}_{a,1}) \\
&\otimes P_a(\mathcal{X}_{a,2}) |\mathcal{X}_{a,2}\rangle\langle\mathcal{X}'_{a',2}| P_{a'}(\mathcal{X}'_{a',2}) \\
&\otimes \cdots \\
&\otimes P_a(\mathcal{X}_{a,2M}) |\mathcal{X}_{a,2M}\rangle\langle\mathcal{X}'_{a',2M}| P_{a'}(\mathcal{X}'_{a',2M}).
\end{aligned} \tag{2.120}$$

Thus,

$$
\begin{aligned}
&(\rho^{T_{\text{odd}}})^\dagger \rho^{T_{\text{odd}}} \\
&= \sum_{a,a',a'',a'''} \sum_{\vec{\mathcal{X}}_a} \sum_{\vec{\mathcal{X}}'_{a'}} \sum_{\vec{\mathcal{X}}''_{a''}} \sum_{\vec{\mathcal{X}}'''_{a'''}} c_a(\vec{\mathcal{N}}_a) c^*_{a'}(\vec{\mathcal{N}}'_{a'}) c_{a'''}(\vec{\mathcal{N}}'''_{a'''}) c^*_{a''}(\vec{\mathcal{N}}'''_{a''}) \\
&\quad \times P_{a'''}(\mathcal{X}'''_{a''',1}) P_{a''}(\mathcal{X}''_{a'',1}) |\mathcal{X}''_{a'',1}\rangle\langle \mathcal{X}'''_{a''',1}| \mathcal{X}'_{a',1}\rangle\langle \mathcal{X}_{a,1}| P_a(\mathcal{X}_{a,1}) P_{a'}(\mathcal{X}'_{a',1}) \\
&\quad \otimes P_{a''}(\mathcal{X}''_{a'',2}) P_{a'''}(\mathcal{X}'''_{a''',2}) |\mathcal{X}'''_{a''',2}\rangle\langle \mathcal{X}''_{a'',2}| \mathcal{X}_{a,2}\rangle\langle \mathcal{X}'_{a',2}| P_{a'}(\mathcal{X}'_{a',2}) P_a(\mathcal{X}_{a,2}) \\
&\quad \otimes P_{a'''}(\mathcal{X}'''_{a''',3}) P_{a''}(\mathcal{X}''_{a'',3}) |\mathcal{X}''_{a'',3}\rangle\langle \mathcal{X}'''_{a''',3}| \mathcal{X}'_{a',3}\rangle\langle \mathcal{X}_{a,3}| P_a(\mathcal{X}_{a,3}) P_{a'}(\mathcal{X}'_{a',3}) \\
&\quad \otimes \dots \\
&\quad \otimes P_{a''}(\mathcal{X}''_{a'',2M}) P_{a'''}(\mathcal{X}'''_{a''',2M}) |\mathcal{X}'''_{a''',2M}\rangle\langle \mathcal{X}''_{a'',2M}| \mathcal{X}_{a,2M}\rangle\langle \mathcal{X}'_{a',2M}| P_{a'}(\mathcal{X}'_{a',2M}) P_a(\mathcal{X}_{a,2M}).
\end{aligned}
\tag{2.121}
$$

The inner products identify:

$$
\begin{aligned}
&a''' = a', \quad \mathcal{X}'''_{a''',2k-1} = \mathcal{X}'_{a',2k-1}, \quad P_{a'''}(\mathcal{X}'''_{a''',2k-1}) = P_{a'}(\mathcal{X}'_{a',2k-1}), \\
&a'' = a, \qquad \mathcal{X}''_{a'',2k} = \mathcal{X}_{a,2k}, \qquad\quad P_{a''}(\mathcal{X}''_{a'',2k}) = P_a(\mathcal{X}_{a,2k}),
\end{aligned}
\tag{2.122}
$$

for $k \in \{1, \dots, M\}$. From (2.116), we see that $\mathcal{X}'''_{a''',2k-1} = \mathcal{X}'_{a',2k-1}$ means that $\mathcal{N}'''_{a''',i} = \mathcal{N}'_{a',i}$ for all $i = 1, 2, \dots, 2M$ and $s_{a'''}\gamma'''_{2k-1} = s_{a'}\gamma'_{2k-1}$ for $k = 1, 2, \dots, M$. If the projection operators $P_{a'''}(\mathcal{X}'''_{a''',2k})$ and $P_{a'}(\mathcal{X}'_{a',2k})$ are to be nonzero simultaneously for fixed $\vec{\mathcal{N}}'''_{a'''} = \vec{\mathcal{N}}'_{a'}$, then $s_{a'''}\gamma'''_{2k} = s_{a'}\gamma'_{2k}$ for $k = 1, 2, \dots, M$. We conclude the above inner products identify $P_{a'''}(\mathcal{X}'''_{a''',i}) = P_{a'}(\mathcal{X}'_{a',i})$ and $\mathcal{X}'''_{a''',i} = \mathcal{X}'_{a',i}$ for *all* i. Using similar logic, we likewise find

$\mathcal{X}''_{a'',i} = \mathcal{X}_{a,i}$ and $P_{a''}(\mathcal{X}''_{a'',i}) = P_a(\mathcal{X}_{a,i})$ for all i. Thus, $(\rho^{T_{\rm odd}})^\dagger \rho^{T_{\rm odd}}$ is again diagonal and

$$\begin{aligned}\sqrt{(\rho^{T_{\rm odd}})^\dagger\,\rho^{T_{\rm odd}}} = \sum_{a,a'}\sum_{\vec{\mathcal{X}}_a}\sum_{\vec{\mathcal{X}}'_{a'}} P_a(\vec{\mathcal{X}}_a)P_{a'}(\vec{\mathcal{X}}'_{a'})|c_a(\vec{\mathcal{N}}_a)||c_{a'}(\vec{\mathcal{N}}'_{a'})| \\ \times \quad |\mathcal{X}_{a,1}\rangle\langle\mathcal{X}_{a,1}| \otimes |\mathcal{X}'_{a',2}\rangle\langle\mathcal{X}'_{a',2}| \otimes \cdots \otimes |\mathcal{X}'_{a',2M}\rangle\langle\mathcal{X}'_{a',2M}|.\end{aligned} \tag{2.123}$$

Consequently,

$$\begin{aligned}{\rm tr}\sqrt{(\rho^{T_{\rm odd}})^\dagger\,\rho^{T_{\rm odd}}} &= \sum_{a,a'}\sum_{\vec{\mathcal{X}}_a}\sum_{\vec{\mathcal{X}}'_{a'}} P_a(\vec{\mathcal{X}}_a)P_{a'}(\vec{\mathcal{X}}'_{a'})|c_a(\vec{\mathcal{N}}_a)||c_{a'}(\vec{\mathcal{N}}'_{a'})| \\ &= \left(\sum_a\sum_{\vec{\mathcal{X}}_a} P_a(\vec{\mathcal{X}}_a)|c_a(\vec{\mathcal{N}}_a)|\right)^2.\end{aligned} \tag{2.124}$$

Following the same logic as in (2.80)) and using the definitions in Eqs. (2.107) and (2.112) as well as the identity $\sum_{\gamma_i\in\{0,1\}} P(\mathcal{X}_{a,i}) = 1$ when $s_a = 1$, we find

$$||\rho^{T_{\rm odd}}||_1 = \left(\sum_{a\in{\rm untwisted}} |\psi_a| \left(\frac{Z_a^{\rm untwisted}(1/2)}{\sqrt{Z_a^{\rm untwisted}(1)}}\right)^{2M} + \sum_{a\in{\rm twisted}} |\psi_a| \left(\frac{Z_a^{\rm twisted}(1/2)}{\sqrt{Z_a^{\rm twisted}(1)}}\right)^{2M}\right)^2. \tag{2.125}$$

We obtain Lemma 1 upon taking the logarithm of $||\rho^{T_{\rm odd}}||_1$. □

To finish the computation of the entanglement negativity, we need to evaluate the untwisted and twisted partition functions in the $L \to \infty$ limit. The untwisted sector a partition

function at inverse "temperature" β can be written as [SHST20]

$$\begin{aligned} Z_a^{\text{untwisted}}(\beta) = &\frac{1}{2}\chi_0^{\text{Ising}}(\tilde{q})[\chi_{r/m}^{+}(q) + \chi_{r/m}^{-}(q)] \\ &+ \frac{1}{2}\chi_{1/2}^{\text{Ising}}(\tilde{q})[\chi_{r/m}^{+}(q) - \chi_{r/m}^{-}(q)], \end{aligned} \tag{2.126}$$

where the characters χ are

$$\begin{aligned} \chi_0^{\text{Ising}}(\tilde{q}) &= \frac{1}{2}\tilde{q}^{-\frac{1}{48}}\left[\prod_{j>0}\left(1+\tilde{q}^{j+\frac{1}{2}}\right) + \prod_{j>0}\left(1-\tilde{q}^{j+\frac{1}{2}}\right)\right] \\ \chi_{1/2}^{\text{Ising}}(\tilde{q}) &= \frac{1}{2}\tilde{q}^{-\frac{1}{48}}\left[\prod_{j>0}\left(1+\tilde{q}^{j+\frac{1}{2}}\right) - \prod_{j>0}\left(1-\tilde{q}^{j+\frac{1}{2}}\right)\right] \\ \chi_{r/m}^{\pm}(q) &= \left(\sum_{n\in\mathbb{Z}}(\pm 1)^n q^{m\left(n-\frac{r}{m}\right)^2/2}\right) \\ &\quad \times q^{-\frac{1}{24}}\prod_{j>0}(1-q^j)^{-1}. \end{aligned} \tag{2.127}$$

Recall that $q = e^{2\pi i\tau}$ and τ is defined in (2.81). In addition, we have a new pair of modular parameters $\tilde{\tau}$ and $\tilde{q}$ defined by $\tilde{\tau} = \tau/2 = i\tilde{\tau}_2$ and $\tilde{q} = e^{2\pi i\tilde{\tau}}$. The characters can be rewritten in terms of modular functions as

$$\begin{aligned} \chi_0^{\text{Ising}}(\tilde{q}) &= \frac{1}{2}\sqrt{\frac{\theta_0^0(\tilde{\tau})}{\eta(\tilde{\tau})}} + \frac{1}{2}\sqrt{\frac{\theta_{1/2}^0(\tilde{\tau})}{\eta(\tilde{\tau})}}, \\ \chi_{1/2}^{\text{Ising}}(\tilde{q}) &= \frac{1}{2}\sqrt{\frac{\theta_0^0(\tilde{\tau})}{\eta(\tilde{\tau})}} - \frac{1}{2}\sqrt{\frac{\theta_{1/2}^0(\tilde{\tau})}{\eta(\tilde{\tau})}}, \\ \chi_{r/m}^{\pm}(q) &= \frac{\theta_0^{-r/m}(m\tau)}{\eta(\tau)}, \quad \text{or} \quad \frac{e^{\frac{i\pi r}{m}}\theta_{1/2}^{-r/m}(m\tau)}{\eta(\tau)}. \end{aligned} \tag{2.128}$$

$\theta^0_{1/2}(\tilde{\tau})$ goes to zero in the $L \to \infty$ limit. Therefore, the untwisted 1 and χ sector partition functions both reduce to

$$Z_a^{\text{untwisted}}(\beta) = \frac{1}{2}\sqrt{\frac{\theta_0^0(\tilde{\tau})}{\eta(\tilde{\tau})}}\frac{\theta_0^{-r/m}(m\tau)}{\eta(\tau)}. \tag{2.129}$$

In the $L \to \infty$ limit,

$$\frac{Z_a^{\text{untwisted}}(1/2)}{\sqrt{Z_a^{\text{untwisted}}(1)}} = \frac{1}{\sqrt{2\sqrt{m}}}\exp\left[\frac{\pi L}{8}\left(\frac{1}{v_e}+\frac{1}{2\tilde{v}_e}\right)\right]. \tag{2.130}$$

The twisted sector a partition function is

$$Z_a^{\text{twisted}} = \chi^{\text{Ising}}_{1/16}(\tilde{q})\chi^{+}_{(r+1/2)/m}(q), \tag{2.131}$$

where the characters are

$$\begin{aligned}
\chi^{\text{Ising}}_{1/16}(\tilde{q}) &= \sum_{n_{i,k}\in\mathbb{Z}^+} e^{-\sum_{k>0}\beta\tilde{v}_e k(n_{i,k}+\frac{1}{2})} \\
&= \tilde{q}^{\frac{1}{24}}\prod_{j=1}^{\infty}(1+\tilde{q}^j), \quad k=\frac{2\pi j}{L}, j\in\mathbb{Z}^+ \\
\chi_{(r+1/2)/m}(q) &= q^{-\frac{1}{24}}\prod_{j=1}^{\infty}(1-q^j)^{-1} \\
&\quad\times\left(\sum_{n\in\mathbb{Z}} q^{m\left(n-\frac{r+1/2}{m}\right)^2/2}\right).
\end{aligned} \tag{2.132}$$

$\chi^{\text{Ising}}_{1/16}$ produces the $d_a = \sqrt{2}$ quantum dimension associated to the Majorana quasiparticle of the Moore-Read state. In terms of modular functions, the characters are

$$\begin{aligned} \chi^{\text{Ising}}_{1/16}(\tilde{q}) &= \sqrt{\frac{\theta_0^{1/2}(\tilde{\tau})}{2\eta(\tilde{\tau})}}, \\ \chi_{(r+1/2)/m}(q) &= \frac{\theta_0^{-(r+1/2)/m}(m\tau)}{\eta(\tau)}. \end{aligned} \tag{2.133}$$

Thus,

$$Z_a^{\text{twisted}} = \sqrt{\frac{\theta_0^{1/2}(\tilde{\tau})}{2\eta(\tilde{\tau})}} \frac{\theta_0^{-(r+1/2)/m}(m\tau)}{\eta(\tau)}, \tag{2.134}$$

and for $L \to \infty$,

$$\frac{Z_a^{\text{twisted}}(1/2)}{\sqrt{Z_a^{\text{twisted}}(1)}} = \frac{1}{\sqrt[4]{2m}} \exp\left[\frac{\pi L}{8}\left(\frac{1}{v_e} + \frac{1}{2\tilde{v}_e}\right)\right]. \tag{2.135}$$

Plugging these untwisted and twisted partition function ratios (2.130) and (2.135) into Lemma 1, we find

$$\begin{aligned} ||\rho^{T_{\text{odd}}}||_1 &= \left(\sum_{a \in \text{untwisted}} |\psi_a| \left[\frac{Z_a^{\text{untwisted}}(1/2)}{\sqrt{Z_a^{\text{untwisted}}(1)}}\right]^{2M} + \sum_{a \in \text{twisted}} |\psi_a| \left[\frac{Z_a^{\text{twisted}}(1/2)}{\sqrt{Z_a^{\text{twisted}}(1)}}\right]^{2M} \right)^2 \\ &= \left(\left(\frac{1}{2\sqrt{m}}\right)^M \exp\left[\frac{M\pi L}{4}\left(\frac{1}{v_e} + \frac{1}{2\tilde{v}_e}\right)\right] \sum_a |\psi_a| (d_a)^M \right)^2; \end{aligned} \tag{2.136}$$

$$\mathcal{E}_{X_{\text{odd}}:X_{\text{even}}} = M\left[\frac{\pi}{2}\left(\frac{1}{v_e} + \frac{1}{2\tilde{v}_e}\right)\right] L - 2M \log\sqrt{4m} + 2\log \sum_a |\psi_a| (d_a)^M. \tag{2.137}$$

In the second identity above, we recovered the quantum dimensions of the quasiparticles associated to each sector: for the $\{1, \chi\}$ untwisted sectors, $d_a = 1$; while for the ξ twisted sectors, $d_a = \sqrt{2}$. In addition to the $2M$ boundary entanglement contributions, proportional to $\log \sqrt{4m}$, in the entanglement negativity, there is a long-range entanglement contribution is equal to $2 \log \sum_a |\psi_a| (d_a)^M$. This recovers (2.12) with the non-universal constant given by $\alpha = \frac{\pi}{2} \left(\frac{1}{v_e} + \frac{1}{2\tilde{v}_e} \right)$ and the total quantum dimension equal to $\mathcal{D} = \sqrt{4m}$.

Cylinder Geometry

Next we calculate the entanglement negativity between subsets of X_{even} and X_{odd} when the degrees of freedom on $N \leq M$ cylinders $\bar{Y} \subset X$ of the Moore-Read state (constructed in the previous section) have been traced over (e.g., Figure 2.1b). As in §2.3.1, we denote the remaining $(2M - N)$ cylinders by Y and their decomposition into "odd" and "even" cylinders as Y_{odd} and Y_{even}. The resulting entanglement negativity will depend on the number R of shared interfaces between the remaining cylinders in $Y_{\text{odd}} \cup Y_{\text{even}}$.

To find the entanglement negativity in this cylinder geometry, we will apply Lemma 2. Before doing so, we describe how the proof of this lemma generalizes to the Moore-Read state.

Generalized Proof of Lemma 2. The argument follows almost exactly the proof for the Laughlin case upon updating the notation to the Moore-Read state with the replacements: $c_a(\vec{\mathcal{N}}_a) \to P_a(\vec{\mathcal{X}}_a) c_a(\vec{\mathcal{N}}_a)$ and $|\mathcal{N}_{a,i}, \mathcal{N}_{a,i+1}\rangle \to |\mathcal{X}_{a,i}\rangle$. Because of this, we will only discuss one case (Case I) below; the remaining cases (Case II - Case IV) follow straightforwardly using the

same logic as in the Laughlin case and the manipulations outlined for the generalized proof of Lemma 1. We will suppress the untwisted/twisted superscripts on Z_a when convenient.

(Case I) We remove cylinder $\bar{Y} = X_{2k}$ where $1 < 2k \leq 2M$ by tracing over its left and right edge states. Thus, $Y_{\text{odd}} = X_{\text{odd}}$, $Y_{\text{even}} = X_2 \cup \cdots \cup X_{2k-2} \cup X_{2k+2} \cdots X_{2M}$, and $R = 2M - 2$.

The density matrix of the Moore-Read torus state in (2.115) is

$$\begin{aligned}\rho = \sum_{a,a'} \sum_{\vec{\mathcal{X}}_a, \vec{\mathcal{X}}'_{a'}} & c_a(\vec{\mathcal{N}}_a) c^*_{a'}(\vec{\mathcal{N}}'_{a'}) \times \cdots \\ & \times P_a(\mathcal{X}_{a,2k-1}) |\mathcal{X}_{a,2k-1}\rangle \langle \mathcal{X}'_{a',2k-1}| P_{a'}(\mathcal{X}'_{a',2k-1}) \\ & \otimes P_a(\mathcal{X}_{a,2k}) |\mathcal{X}_{a,2k}\rangle \langle \mathcal{X}'_{a',2k}| P_{a'}(\mathcal{X}'_{a',2k}) \\ & \otimes P_a(\mathcal{X}_{a,2k+1}) |\mathcal{X}_{a,2k+1}\rangle \langle \mathcal{X}'_{a',2k+1}| P_{a'}(\mathcal{X}'_{a',2k+1}) \\ & \otimes \cdots .\end{aligned} \tag{2.138}$$

The trace over degrees of freedom on cylinder $\bar{Y} = X_{2k}$ sets

$$a' = a, \quad \mathcal{X}'_{a',2k} = \mathcal{X}_{a,2k}, \quad P_{a'}(\mathcal{X}'_{a',2k}) = P_a(\mathcal{X}_{a,2k}) \tag{2.139}$$

and removes the corresponding outer products involving states on X_{2k} In particular, $\text{Tr}_{\bar{Y}}(\rho)$ is a direct sum over untwisted and twisted topological sectors. The partial transpose of

$\rho_Y = \mathrm{Tr}_{\bar{Y}}(\rho)$ with respect to Y_{odd} is

$$\begin{aligned}
\rho_Y^{T_{\mathrm{odd}}} = \sum_a \sum_{\vec{\mathcal{X}}_a, \vec{\mathcal{X}}'_a} & c_a(\vec{\mathcal{N}}_a) c_a^*(\vec{\mathcal{N}}'_a) P_a^2(\mathcal{X}_{a,2k}) \times \cdots \\
& \times P_a(\mathcal{X}_{a,2k-2}) |\mathcal{X}_{a,2k-2}\rangle\langle \mathcal{X}'_{a,2k-2}| P_a(\mathcal{X}'_{a,2k-2}) \\
& \otimes P_a(\mathcal{X}_{a,2k-1}) |\mathcal{N}'_{a,2k-1}, \mathcal{N}_{a,2k}, s_a\gamma'_{i-1}\rangle\langle \mathcal{X}_{a,2k-1}| P_a(\mathcal{N}'_{a,2k-1}, \mathcal{N}_{a,2k}, s_a\gamma'_{i-1}) \\
& \otimes P_a(\mathcal{X}_{a,2k+1}) |\mathcal{N}_{a,2k+1}, \mathcal{N}'_{a,2k+2}, s_a\gamma'_{2k+1}\rangle\langle \mathcal{X}_{a,2k+1}| P_a(\mathcal{N}_{a,2k+1}, \mathcal{N}'_{a,2k+2}, s_a\gamma'_{2k+1}) \\
& \otimes P_a(\mathcal{X}_{a,2k+2}) |\mathcal{X}_{a,2k+2}\rangle\langle \mathcal{X}'_{a,2k+2}| P_a(\mathcal{X}'_{a,2k+2}) \\
& \otimes \cdots ,
\end{aligned} \tag{2.140}$$

where $c_a(\vec{\mathcal{N}}_a) c_a^*(\vec{\mathcal{N}}'_a)$ takes the same form as in (2.94). There is no dependence on $\mathcal{X}'_{a,2k}$ above because of (2.139). In (2.140), we have expanded out the arguments of two of the projection operator eigenvalues and kets involved in the outerproducts associated to cylinders X_{2k-1}

and X_{2k+1} to make the identifications (2.139) manifest. Next, we compute

$$
\begin{aligned}
&(\rho_Y^{T_{\rm odd}})^\dagger \rho_Y^{T_{\rm odd}} \\
&= \sum_{a,a'} \sum_{\vec{\mathcal{X}}_a, \vec{\mathcal{X}}'_a, \vec{\mathcal{X}}''_{a'}, \vec{\mathcal{X}}'''_{a'}} c^*_{a'}(\vec{\mathcal{N}}''_{a'}) c_{a'}(\vec{\mathcal{N}}'''_{a'}) c_a(\vec{\mathcal{N}}_a) c^*_a(\vec{\mathcal{N}}'_a) P^2_a(\mathcal{X}_{a,2k}) P^2_{a'}(\mathcal{X}''_{a,2k}) \times \cdots \\
&\quad \otimes P_{a'}(\mathcal{X}'''_{a,2k-2}) P_{a'}(\mathcal{X}''_{a,2k-2}) P_a(\mathcal{X}_{a,2k-2}) P_a(\mathcal{X}'_{a,2k-2}) |\mathcal{X}'''_{a',2k-2}\rangle\langle \mathcal{X}''_{a',2k-2}|\mathcal{X}_{a,2k-2}\rangle\langle \mathcal{X}'_{a,2k-2}| \\
&\quad \otimes P_{a'}(\mathcal{X}'''_{a,2k-1}) P_{a'}(\mathcal{X}''_{a,2k-1}) P_a(\mathcal{X}_{a,2k-1}) P_a(\mathcal{X}'_{a,2k-1}) |\mathcal{X}''_{a',2k-1}\rangle\langle \mathcal{X}'''_{a',2k-1}|\mathcal{X}'_{a,2k-1}\rangle\langle \mathcal{X}_{a,2k-1}| \\
&\quad \otimes P_{a'}(\mathcal{X}'''_{a,2k+1}) P_{a'}(\mathcal{X}''_{a,2k+1}) P_a(\mathcal{X}_{a,2k+1}) P_a(\mathcal{X}'_{a,2k+1}) |\mathcal{X}''_{a',2k+1}\rangle\langle \mathcal{X}''_{a',2k+1}|\mathcal{X}_{a,2k+1}\rangle\langle \mathcal{X}_{a,2k+1}| \\
&\quad \otimes P_{a'}(\mathcal{X}'''_{a,2k+2}) P_{a'}(\mathcal{X}''_{a,2k+2}) P_a(\mathcal{X}_{a,2k+2}) P_a(\mathcal{X}'_{a,2k+2}) |\mathcal{X}'''_{a',2k+2}\rangle\langle \mathcal{X}''_{a',2k+2}|\mathcal{X}_{a,2k+2}\rangle\langle \mathcal{X}'_{a,2k+2}| \\
&\quad \otimes \cdots .
\end{aligned}
\tag{2.141}
$$

Note that $\mathcal{X}'_{a,2k}$ and $\mathcal{X}'''_{a,2k}$ are absent in the sums over $\vec{\mathcal{X}}'_a$ and $\vec{\mathcal{X}}'''_a$ and it is to be understood that we have imposed (2.139) and the analogous constraints for $\mathcal{X}'''_{a,2k}$ above. The above overlaps fix $a' = a$ and identify

$$
\begin{aligned}
\mathcal{X}'''_{a',2i-1} = \mathcal{X}'_{a,2i-1}, \quad \mathcal{X}''_{a',2i} = \mathcal{X}_{a,2i}, \\
P_{a'}(\mathcal{X}'''_{2i-1}) = P_a(\mathcal{X}'_{2i-1}), \quad P_{a'}(\mathcal{X}''_{2i}) = P_a(\mathcal{X}_{2i}),
\end{aligned}
\tag{2.142}
$$

for $1 < 2i \leq 2M$. (Recall that $2M + 1 \equiv 1$.) As in the generalized proof of Lemma 1, these identifications imply $\mathcal{X}'''_{a',i} = \mathcal{X}'_{a,i}$, $\mathcal{X}'_{a',i} = \mathcal{X}_{a,i}$, and equate corresponding projection operators for all i. Thus, $(\rho_Y^{T_{\rm odd}})^\dagger \rho_Y^{T_{\rm odd}}$ is again diagonal and, analogous to (2.123), we may

read off $\mathrm{tr}\sqrt{(\rho_Y^{T_{\rm odd}})^\dagger \rho_Y^{T_{\rm odd}}}$ to find

$$
\begin{aligned}
||\rho_Y^{T_{\rm odd}}||_1 &= \sum_a \sum_{\vec{\mathcal{X}}_a, \vec{\mathcal{X}}'_a} P_a(\vec{\mathcal{X}}_a)|c_a(\vec{\mathcal{N}}_a)|P_a(\vec{\mathcal{X}}'_a)|c_a(\vec{\mathcal{N}}'_a)| \\
&= \sum_a \left(|\psi_a| \left(\frac{Z_a(1/2)}{\sqrt{Z_a(1)}} \right)^{2M-2} \right)^2 ,
\end{aligned} \tag{2.143}
$$

where the sum is over all topological sectors and the identifications in (2.139) are understood and the corresponding sums are removed. Taking the logarithm of $||\rho_Y^{T_{\rm odd}}||_1$, we complete the proof of Lemma 2 for the Moore-Read state when $X'' = X_{2k}$. As remarked above, the remaining cases follow similarly. □

By Lemma 2, the entanglement negativity between $Y_{\rm odd}$ and $Y_{\rm even}$ reduces to the calculation of entanglement Hamiltonian partition functions for the Moore-Read state. Using the partition functions calculated in the previous section, we find

$$
\begin{aligned}
\mathcal{E}_{Y_{\rm odd}:Y_{\rm even}} &= \frac{R}{2}\left(\frac{\pi}{2}\left(\frac{1}{v_e}+\frac{1}{2\tilde{v}_e}\right)\right) L - R\log\sqrt{4m} \\
&\quad + \log\sum_a |\psi_a|^2 d_a^R,
\end{aligned} \tag{2.144}
$$

where the sum is over a in the last term is over all topological sectors and the quantum dimensions $d_a = 1$ for the $\{1, \chi\}$ untwisted sectors and $d_a = \sqrt{2}$ for the ξ twisted sectors. This verifies (2.13) with $\alpha = \frac{\pi}{2}\left(\frac{1}{v_e} + \frac{1}{2\tilde{v}_e}\right)$ and $\mathcal{D} = \sqrt{4m}$. Similar to the torus geometry, there are R boundary entanglement terms each proportional to $\log \mathcal{D}$. In addition and in

contrast to the Abelian case (where $d_a = 1$), there is a long-range entanglement contribution equal to $\log |\psi_a|^2 d_a^R$.

The disentangling condition to $2M$ cylinders can be calculated by tracing out degrees of freedom on non-transposed cylinders. Setting $R = 2M$ and subtracting (2.144) from (2.137), we obtain

$$\mathcal{E}_{X_{\text{odd}}:X_{\text{even}}} - \mathcal{E}_{Y_{\text{odd}}:Y_{\text{even}}} = \log \frac{\left(\sum_a |\psi_a| d_a^M\right)^2}{\sum_a |\psi_a|^2 d_a^{2M}}. \tag{2.145}$$

2.4 Disentangling

In this section, we discuss how long-range entanglement affects the structure of the Laughlin and Moore-Read manybody wavefunctions. Specifically, we determine when the disentangling condition,

$$\mathcal{E}_{A:BC}(\rho) = \mathcal{E}_{A:B}(\rho_{AB}), \tag{2.146}$$

holds, for suitable choices of cylinder subsets A, B, and C of the torus, and the implication of (2.146) for the manybody wavefunction. We focus on two decompositions of the torus:

1. AB_1CB_2 geometry: the torus is divided into four consecutive cylinders A, B_1, C, and B_2 with disjoint $B = B_1 \cup B_2$. In this case, $\rho_{ABC} = |\Psi_{ABC}\rangle\langle\Psi_{ABC}|$ with $|\Psi_{ABC}\rangle$ a pure ground state on the torus.

2. $ABCD$ geometry: the torus is divided into four consecutive cylinders A, B, C, and D. In this case, $\rho_{ABC} = \mathrm{tr}_D\, |\Psi_{ABCD}\rangle\langle\Psi_{ABCD}|$ is a mixed state on cylinder $A \cup B \cup C$ and $|\Psi_{ABCD}\rangle$ is a pure torus ground state.

The entanglement negativity results in the previous section can be used to determine when the disentangling condition (2.146) is satisfied. Applying Eqs. (2.12) with $M = 1$ and (2.13) with $R = 2$ to the AB_1CB_2 geometry, we find

$$\mathcal{E}_{A:BC}(\rho_{ABC}) - \mathcal{E}_{A:B}(\rho_{AB}) = \log \frac{\left(\sum_a |\psi_a| d_a\right)^2}{\sum_a |\psi_a|^2 d_a^2} \tag{2.147}$$

(c.f. (2.145)). Consequently, only torus states in a specific topological sector, i.e., $\psi_a = 1$ for a single a with all other amplitudes vanishing, satisfy the disentangling condition. For the $ABCD$ geometry, (2.13) with $R = 1$ implies any mixed cylinder state on $A \cup B \cup C$ satisfies (2.146).

Generally, for a tripartite Hilbert space $\mathcal{H}_A \otimes \mathcal{H}_B \otimes \mathcal{H}_C$, the degrees of freedom in subsystems A and C have no quantum correlations in states that satisfy the disentangling condition. This allows their corresponding wavefunctions to be disentangled in the following sense. For pure states $|\Psi_{ABC}\rangle$, He and Vidal [HV15] showed that (2.146) implies that there exists a decomposition of the Hilbert space of region B as $\mathcal{H}_B = \mathcal{H}_{B_L} \otimes \mathcal{H}_{B_R}$ such that the state can be factorized as

$$|\Psi_{ABC}\rangle = |\Psi_{AB_L}\rangle \otimes |\Psi_{B_RC}\rangle\,. \tag{2.148}$$

The reverse statement is also valid: the disentangling condition (2.146) is implied by states satsifying (2.148). For mixed states, Gour and Guo [GG18] demonstrated that the disentangling condition (2.146) is satisfied for all states that saturate the strong subadditivity of the entanglement entropy. The structure of these states follows

$$\rho_{ABC} = \sum_j p_j \rho_{AB_L^j} \otimes \rho_{B_R^j C}, \tag{2.149}$$

where the Hilbert space of B decomposes into $\mathcal{H}_B = \bigoplus_j \mathcal{H}_{B_L^j} \otimes \mathcal{H}_{B_R^j}$ and $\{p_j\}$ are probabilities. The reverse statement of this case is not necessarily true: not all mixed states that satisfy the disentangling condition have the structure of (2.149).

To what extent does (2.146) relates to (2.148) and (2.149) for topological ground states? Because the relevant ground state of a topological phase is generally a direct sum over distinct topological sectors, $|\Psi\rangle = \sum_a \psi_a |\Psi_a\rangle$, the applicability of the above results is less clear. For example, the degenerate ground state Hilbert space $\mathcal{H} = \bigoplus_a \mathcal{H}_a$ does not decompose into tensor product $\mathcal{H}_A \otimes \mathcal{H}_B \otimes \mathcal{H}_C$ of local cylinder spaces. (See Ref. [CHR14] for a related discussion in the context of entanglement entropy in gauge theory.) This provides an a priori explanation for the necessity of restriction to a single topological sector a to disentangle a ground state.

In this section, we will show that the Abelian Laughlin and untwisted sector Moore-Read states can be decomposed according to Eqs. (2.148) in the AB_1CB_2 geometry and (2.149) in the $ABCD$ geometry. On the other hand, the twisted sector Moore-Read states fails to decompose according to (2.148) or (2.149). In other words, even when the disentangling

condition (2.146) is satisfied, the ground state $|\Psi_a\rangle$ cannot be disentangled, if $a = \xi^{r+1/2}$ is an Ising twist field.

The failure to disentangle stems from the non-Abelian nature of the twisted sectors. The Ising twist field carries the non-trivial quantum dimension $d_a = \sqrt{2} > 1$, associated to each Majorana zero mode $c^{\sigma}_{i,0}$. The ground state fixes the fermion parity $(-1)^{n'_i} = ic^R_{i-1,0}c^L_{i,0}$ of the pair of zero modes to be even at any given interface. However, the two zero modes do not belong to the same cylinder. When decomposing the ground state in a tensor product of local cylinder states, the ground state becomes a superposition of states with different cylinder fermion parities $(-1)^{\gamma_i} = ic^R_{i,0}c^L_{i,0}$. Since $(-1)^{n'_i}$ and $(-1)^{\gamma_i}$ do not commute, they do not share simultaneous eigenstates and the basis transformations between the two basis are generated by the non-diagonal F-symbol in (2.53). Consequently, the zero mode part of the ground state, $|f^{\text{zero}}\rangle$ in (2.57), is a maximally entangled state where the cylinder fermion parities $(-1)^{\gamma_i}$ are scrambled. This state $|f^{\text{zero}}\rangle$ does not decompose because the total fermion parity $\sum_i \gamma_i$ has a fixed value (see (2.56)).

The main results of this section are summarized as the follows. The ground state of a fixed Abelian (Laughlin or untwisted Moore-Read) sector $|\Psi_a\rangle$ admits the factorization (2.152) in the AB_1CB_2 geometry. The reduced density matrix $\text{Tr}_D\,|\Psi_a\rangle\langle\Psi_a|$ in the $ABCD$ geometry also factorizes according to (2.173). These results are in agreement with the factorizability (2.148) and (2.149) (from [HV15] and [GG18]) as the ground state $|\Psi_a\rangle$ obeys the disentangling condition (2.146). On the other hand, we show that the ground state $|\Psi_a\rangle$ (see (2.165)) of a non-Abelian twisted sector $a = \xi^{r+1/2}$ of the Moore-Read state fails to decompose. We demonstrate this by focusing on the zero mode sector and seeing that (i)

the (partially traced) reduced density matrix (2.166) is a mixed state and therefore the ground state must be entangled and (ii) the (partially transposed) density matrix (2.167) in the AB_1CB_2 geometry does not factorize. Furthermore, we show that (iii) the reduced density matrix (2.174) in the $ABCD$ geometry also fails to disentangle. These results serve as concrete examples where (2.148) and (2.149) both fail to hold despite the disentangling condition (2.146) being satisfied.

2.4.1 AB_1CB_2 Geometry

We first consider the AB_1CB_2 torus geometry with $X_1 = A$, $X_2 = B_1$, $X_3 = C$, and $X_4 = B_2$. Our discussion below will apply to both the Laughlin and Moore-Read states, with the understanding that Majorana fermion labels and projection operators are dropped for the Laughlin and untwisted Moore-Read states.

Since we are interested in measuring the entanglement $\mathcal{E}_{A:BC}(\rho_{ABC})$ between A and its complement in (2.146), we first show how the corresponding four-cylinder state can be viewed as a two-cylinder state on cylinders A and $\bar{A} = B_1 \cup C \cup B_2$. The torus state is given by

$$\begin{aligned} |\Psi\rangle = \sum_a P_a \psi_a \sum_{\mathcal{N}_{a,1},\mathcal{N}_{a,2}} & \frac{\lambda(\mathcal{N}_{a,1})\lambda(\mathcal{N}_{a,2})}{\sqrt{Z_{a,1}Z_{a,2}}} \\ & \times |0_1\rangle'_{s_a} \otimes |\mathcal{N}_{a,1}\mathcal{N}_{a,2}\rangle_{X_1} \otimes |0_2\rangle'_{s_a} \\ & \otimes |\mathcal{N}_{a,2}\rangle_{LX_2} \otimes |\hat{\Psi}_{\text{bulk}}\rangle \otimes |\mathcal{N}_{a,1}\rangle_{RX_4}. \end{aligned} \tag{2.150}$$

The partition functions $Z_{a,i} = Z_a$ for all i with Z_a defined in (2.70) for the Laughlin state and in (2.108) and (2.112) for the untwisted and twisted sectors of the Moore-Read state; the additional i indices are bookkeeping devices that associate these factors to their corresponding cylinders X_i. The (unprojected) "bulk" state is

$$|\hat{\Psi}_{\text{bulk}}\rangle = \sum_{\mathcal{N}_{a,3},\mathcal{N}_{a,4}} \prod_{i=3,4} \frac{\lambda(\mathcal{N}_{a,i})}{\sqrt{Z_{a,i}}} |\mathcal{N}_{a,3}\rangle_{RX_2} \otimes |0_3\rangle'_{s_a} \\ \otimes |\mathcal{N}_{a,3}\mathcal{N}_{a,4}\rangle_{X_3} \otimes |0_4\rangle'_{s_a} \otimes |\mathcal{N}_{a,4}\rangle_{LX_4}. \tag{2.151}$$

It is normalized: $\langle\hat{\Psi}_{\text{bulk}}|\hat{\Psi}_{\text{bulk}}\rangle = 1$. Because of summing over all the internal indexes labeled by $\mathcal{N}_{a,3}$, $\mathcal{N}_{a,4}$, $|0_1\rangle'_{s_a}$, and $|0_4\rangle'_{s_a}$ in (2.151), $|\hat{\Psi}_{\text{bulk}}\rangle\langle\hat{\Psi}_{\text{bulk}}|$ acts as an identity operator when computing $\rho = |\Psi\rangle\langle\Psi|$. Therefore $|\hat{\Psi}_{\text{bulk}}\rangle$ makes no contribution to the measured entanglement. This is the key observation for relating the four-cylinder and two-cylinder states. Note that $|0_i\rangle'_{s_a} = |0_i\rangle'$ when $s_a = 1$ in the twisted sector where $|0_i\rangle'$ denotes the parity of the Majorana zero mode states at the interfaces between cylinders. These states appear before the F-symbol basis change to states labeled by the parity of Majorana zero mode states on a given cylinder. $|0_i\rangle'_{s_a} = 1$ when $s_a = 0$ in an Abelian or untwisted sector. One can then perform a basis transformation using the F-symbols and shift the labeling of Majorana fermion parity from the interfaces to the cylinders. The second identity in (2.150) shows that the above four-cylinder torus state is equivalent to the the two-cylinder torus state. Thus, we may safely apply the results of the previous section for the entanglement negativity to conclude that only pure states is a specific topological sector, i.e., those states without long-range entanglement, satisfy the disentangling condition (2.146).

In a specific sector a, the unprojected state $|\hat{\Psi}_a\rangle$ can be factorized as

$$|\hat{\Psi}_a\rangle = |\hat{\Psi}_{X_1(LX_2RX_4),a}\rangle \otimes |\hat{\Psi}_{(RX_2LX_4)X_3,a}\rangle, \tag{2.152}$$

where

$$\begin{aligned}
&|\hat{\Psi}_{X_1(LX_2RX_4),a}\rangle = \\
&\quad \sum_{\mathcal{N}_{a,1},\mathcal{N}_{a,2}} \frac{\lambda(\mathcal{N}_{a,1})}{\sqrt{Z_{a,1}}} \frac{\lambda(\mathcal{N}_{a,2})}{\sqrt{Z_{a,2}}} \hat{\Psi}_{X_1,a}^{(\mathcal{N}_{a,1}\mathcal{N}_{a,2})} \hat{\Psi}_{LX_2RX_4}^{\mathcal{N}_{a,2}\mathcal{N}_{a,1}}, \\
&|\hat{\Psi}_{(RX_2LX_4)X_3,a}\rangle = \\
&\quad \sum_{\mathcal{N}_{a,3},\mathcal{N}_{a,4}} \frac{\lambda(\mathcal{N}_{a,3})}{\sqrt{Z_{a,3}}} \frac{\lambda(\mathcal{N}_{a,4})}{\sqrt{Z_{a,4}}} \hat{\Psi}_{X_3,a}^{(\mathcal{N}_{a,3}\mathcal{N}_{a,4})} \hat{\Psi}_{RX_2LX_4}^{\mathcal{N}_{a,3}\mathcal{N}_{a,4}},
\end{aligned} \tag{2.153}$$

and

$$\begin{aligned}
\hat{\Psi}_{X_1,a}^{(\mathcal{N}_{a,1}\mathcal{N}_{a,2})} &= |0_1\rangle'_{s_a} \otimes |\mathcal{N}_{a,1}\mathcal{N}_{a,2}\rangle_{X_1} \otimes |0_2\rangle'_{s_a}, \\
\hat{\Psi}_{X_3,a}^{(\mathcal{N}_{a,3}\mathcal{N}_{a,4})} &= |0_3\rangle'_{s_a} \otimes |\mathcal{N}_{a,3}\mathcal{N}_{a,4}\rangle_{X_3} \otimes |0_4\rangle'_{s_a}, \\
\hat{\Psi}_{LX_2RX_4}^{\mathcal{N}_{a,2}\mathcal{N}_{a,1}} &= |\mathcal{N}_{a,1}\rangle_{RX_4} \otimes |\mathcal{N}_{a,2}\rangle_{LX_2}, \\
\hat{\Psi}_{RX_2LX_4}^{\mathcal{N}_{a,3}\mathcal{N}_{a,4}} &= |\mathcal{N}_{a,3}\rangle_{RX_2} \otimes |\mathcal{N}_{a,4}\rangle_{LX_4}.
\end{aligned} \tag{2.154}$$

Here, $|\hat{\Psi}_{X_1(LX_2RX_4),a}\rangle$ and $|\hat{\Psi}_{(RX_2LX_4)X_3,a}\rangle$ are normalized. (2.152) is the desired factorization for the Laughlin state, where there is no projection operator. For a untwisted sector Moore-Read state, the projection operator P_a can be decomposed into cylinder state projection operators P_{a,X_i}, which in turn decompose into left and right edge projection operators

as $P_{a,X_i} = P_{a,i}P_{a,i+1}$. Including these factorized projection operators, we find the untwisted Moore-Read ground state wavefunction in a specific sector a can be disentangled.

In the twisted sector of the Moore-Read phase, the projection operator P_{X_i} does not factorize into left and right edge components. Further division of a given cylinder into sub-cylinders does not appear to help, as the resulting Hilbert space is not a simple tensor product. Thus, the corresponding manybody wavefunction does not factorize as (2.148). Although the corresponding pure state density matrix can be written in a form similar to (2.149), we will show in the following that the factorization of $\mathcal{H}_B = \mathcal{H}_{B_L} \otimes \mathcal{H}_{B_R}$ fails.

By splitting cylinder B_1 into sub-cylinders X_2, X_3 and B_2 into sub-cylinders X_5, X_6 (see Figure 2.4), the torus ground state of a fixed twisted sector $a = \xi^{r+1/2}$ is

$$|\Psi_a\rangle = \sum_{\vec{\mathcal{N}}_a, \vec{\gamma}} c_a(\vec{\mathcal{N}}_a) P_a(\vec{\mathcal{N}}_a, \vec{\gamma}) \bigotimes_{i=1}^{6} |\mathcal{N}_{a,i}\mathcal{N}_{a,i+1}\gamma_i\rangle_{X_i}, \tag{2.155}$$

where $c_a(\vec{\mathcal{N}}_a) \equiv \prod_{i=1}^{6} \frac{\lambda(\mathcal{N}_{a,i})}{\sqrt{Z_a}}$ and the projection operator eigenvalues

$$P_a(\vec{\mathcal{N}}_a, \vec{\gamma}) = \prod_{i=1}^{6} P_a(\mathcal{N}_{a,i}, \gamma_i) \tag{2.156}$$

are defined in (2.60). We find that under the restricted sum $\sum_{i=1}^{6} \gamma_i = 1 \bmod 2$ (see (2.56)), we can split and restrict the sum over $\gamma_1, \gamma_2, \gamma_6$ and the sum over $\gamma_3, \gamma_4, \gamma_5$ according to the parity

$$s = -(-1)^{\gamma_1+\gamma_2+\gamma_6} = (-1)^{\gamma_3+\gamma_4+\gamma_5} = \pm. \tag{2.157}$$

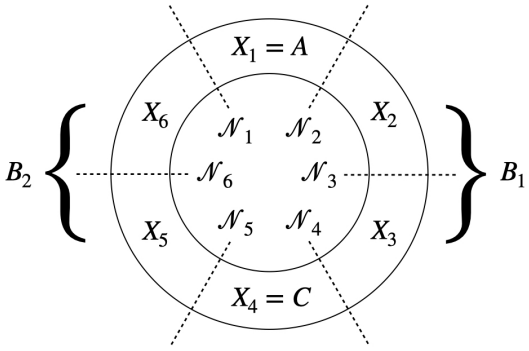

Figure 2.4: A torus is divided by the dashed lines into the AB_1CB_2 geometry: region A is the X_1 cylinder while region C the X_4 cylinder. Region B_1 is the union of X_2 and X_3; and B_2 the union of X_5 and X_6. The collective mode $\mathcal{N}_i$ are defined on the i^{th} interface as in (2.65) or (2.103).

The projections $P_{a,X_1}P_{a,X_2}P_{a,X_6}$ and $P_{a,X_3}P_{a,X_4}P_{a,X_5}$ from (2.60) both require

$$s(-1)^{\mathcal{N}_{a,3}+\mathcal{N}_{a,6}} \tag{2.158}$$

.

The density matrix $\rho^{\text{twist}} = |\Psi_a\rangle\langle\Psi_a|$ from the twisted sector $a = \xi^{r+1/2}$ can now be factorized as

$$\rho^{\text{twist}} = \sum_j p_j \rho^j_{X_1(X_2X_6)} \otimes \rho^j_{(X_3X_5)X4}. \tag{2.159}$$

Here the summation index j is an abbreviation for the collection of quantities

$$j = \left\{ \begin{array}{l|l} \mathcal{N}_{a,3}, \mathcal{N}_{a,6}, s & s = (-1)^{\mathcal{N}_{a,3},\mathcal{N}_{a,6}} \\ \mathcal{N}'_{a,3}, \mathcal{N}'_{a,6}, s' & s' = (-1)^{\mathcal{N}'_{a,3},\mathcal{N}'_{a,6}} \end{array} \right\}. \tag{2.160}$$

The probabilities in the density matrix are

$$p_j \equiv \prod_{i=3,6} \frac{\lambda(\mathcal{N}_{a,i})\lambda(\mathcal{N'}_{a',i})}{\sqrt{Z_{a,i}Z_{a,i}}} \tag{2.161}$$

so that $\sum_j p_j = 1$. The density matrix components are

$$\begin{aligned}\rho^j_{X_1(X_2X_6)} = \sum_{\{h\}} \prod_{i=1,2} \frac{\lambda(\mathcal{N}_{a,i})\lambda(\mathcal{N'}_{a,i})}{\sqrt{Z_{a,i}Z_{a,i}}} \sum_{\substack{\gamma_1,\gamma_2,\gamma_6 \\ s=-(-1)^{\gamma_1+\gamma_2+\gamma_6}}} \sum_{\substack{\gamma'_1,\gamma'_2,\gamma'_6 \\ s'=-(-1)^{\gamma'_1+\gamma'_2+\gamma'_6}}} \\ \times P_{a,X_6}|\mathcal{N}_{a,6}\mathcal{N}_{a,1}\gamma_6\rangle\langle\mathcal{N}'_{a,6},\mathcal{N}'_{a,1},\gamma'_6|P_{a,X_6} \\ \otimes P_{a,X_1}|\mathcal{N}_{a,1}\mathcal{N}_{a,2}\gamma_1\rangle\langle\mathcal{N}'_{a,1}\mathcal{N}'_{a,2}\gamma'_1|_{X_1}P_{a,X_1} \\ \otimes P_{a,X_2}|\mathcal{N}_{a,2}\mathcal{N}_{a,3}\gamma_2\rangle\langle\mathcal{N}'_{a,2},\mathcal{N}'_{a,3},\gamma'_2|P_{a,X_2}\end{aligned} \tag{2.162}$$

with $\{h\} \equiv \{\mathcal{N}_{a,1}\mathcal{N}'_{a,1}, \mathcal{N}_{a,2}, \mathcal{N}'_{a,2}\}$, and

$$\begin{aligned}\rho^j_{(X_3X_5)X_4} = \sum_{\{e\}} \prod_{i=4,5} \frac{\lambda(\mathcal{N}_{a,i})\lambda(\mathcal{N'}_{a,i})}{\sqrt{Z_{a,i}Z_{a,i}}} \sum_{\substack{\gamma_3,\gamma_4,\gamma_5 \\ s=(-1)^{\gamma_3+\gamma_4+\gamma_5}}} \sum_{\substack{\gamma'_3,\gamma'_4,\gamma'_5 \\ s'=(-1)^{\gamma'_3+\gamma'_4+\gamma'_5}}} \\ \times P_{a,X_3}|\mathcal{N}_{a,3}\mathcal{N}_{a,4}\gamma_3\rangle\langle\mathcal{N}'_{a,3},\mathcal{N}'_{a,4},\gamma'_3|P_{a,X_3} \\ \otimes P_{a,X_4}|\mathcal{N}_{a,4}\mathcal{N}_{a,5}\gamma_4\rangle\langle\mathcal{N}'_{a,4}\mathcal{N}'_{a,5}\gamma'_4|P_{a,X_4} \\ \otimes P_{a,X_5}|\mathcal{N}_{a,5}\mathcal{N}_{a,6}\gamma_5\rangle\langle\mathcal{N}'_{a,6},\mathcal{N}'_{a,6},\gamma'_5|P_{a,X_5},\end{aligned} \tag{2.163}$$

with $\{e\} \equiv \{\mathcal{N}_{a,4}\mathcal{N}'_{a,4}, \mathcal{N}_{a,5}, \mathcal{N}'_{a,5}\}$. All density matrix components ρ's are Hermitian and have unit trace.

We notice that the ground state (2.155) and the density matrix (2.159) of any of the twisted sectors are *not* factorizable and cannot be expressed in (2.148) and (2.149). This is because

the summation index j involves the parities s, s', which specify the fermion parity of half of the torus $AB_{\text{top}} = X_1(X_2X_6)$ and $B_{\text{bottom}}C = (X_3X_5)X_4$. These parity indices cannot be absorbed entirely into B_{top} and B_{bottom}, and therefore the Hilbert space decomposition $\mathcal{H}_B = \bigoplus_j \mathcal{H}_{B^j_{\text{top}}} \otimes \mathcal{H}_{B^j_{\text{bottom}}}$ is *not* satisfied. We show this failure of decomposition of the ground state below by focusing on the zero mode sector

$$|GS\rangle = \frac{1}{4\sqrt{2}} \sum_{\{\gamma_i\}|_C} |\gamma_1\gamma_2\gamma_3\gamma_4\gamma_5\gamma_6\rangle \tag{2.164}$$

where the constraint C requires that $\sum_{i=1}^6 \gamma_i = 1 \bmod 2$.

Proof. We first see that the ground state can be re-expressed as

$$|GS\rangle = \frac{1}{\sqrt{2}} \sum_{s=\pm} \left(\frac{1}{2} \sum_{\substack{\gamma_1,\gamma_2,\gamma_6 \\ s=-(-1)^{\gamma_1+\gamma_2+\gamma_6}}} |\gamma_1\gamma_2\gamma_6\rangle \right) \otimes \left(\frac{1}{2} \sum_{\substack{\gamma_3,\gamma_4,\gamma_5 \\ s=(-1)^{\gamma_3+\gamma_4+\gamma_5}}} |\gamma_3\gamma_4\gamma_5\rangle \right). \tag{2.165}$$

To show that the above ground state does not decompose according to (2.148), we assume the contrary that $|GS\rangle = |GS\rangle_{AB_{\text{top}}} \otimes |GS\rangle_{B_{\text{bottom}}C}$. This would imply the reduced density matrix $\rho_{AB_{\text{top}}} = \text{Tr}_{B_{\text{bottom}}C}(\rho)$ is a pure state, where $\rho = |GS\rangle\langle GS|$. However, from (2.165),

$$\text{Tr}_{B_{\text{bottom}}C} |GS\rangle\langle GS| = \frac{1}{8} \sum_{\substack{(-1)^{\gamma_1+\gamma_2+\gamma_6} \\ =(-1)^{\gamma_1'+\gamma_2'+\gamma_6'}}} |\gamma_1\gamma_2\gamma_6\rangle\langle\gamma_1'\gamma_2'\gamma_6'| \tag{2.166}$$

has spectrum $\{1/2, 1/2, 0, 0, 0, 0, 0, 0\}$ and is a mixed state. Therefore the assumption $|GS\rangle = |GS\rangle_{AB_{\text{top}}} \otimes |GS\rangle_{B_{\text{bottom}}C}$ must be false, and the ground state does not disentangle according to (2.148).

Furthermore, we consider the density matrix $\rho = |GS\rangle\langle GS|$,

$$\begin{aligned}\rho &= \frac{1}{32}\sum_{\vec{\gamma}|_C}\sum_{\vec{\gamma}'|_C}|\gamma_1\gamma_2\gamma_6\rangle\langle\gamma_1'\gamma_2'\gamma_6'|\otimes|\gamma_3\gamma_4\gamma_5\rangle\langle\gamma_3'\gamma_4'\gamma_5'| \\ &= \frac{1}{32}\sum_{s,s'=\pm}\left(\sum_{\substack{s=-(-1)^{\gamma_1+\gamma_2+\gamma_6}\\ s'=-(-1)^{\gamma_1'+\gamma_2'+\gamma_6'}}}|\gamma_1\gamma_2\gamma_6\rangle\langle\gamma_1'\gamma_2'\gamma_6'|\right)\otimes\left(\sum_{\substack{s=(-1)^{\gamma_3+\gamma_4+\gamma_5}\\ s'=(-1)^{\gamma_3'+\gamma_4'+\gamma_5'}}}|\gamma_3\gamma_4\gamma_5\rangle\langle\gamma_3'\gamma_4'\gamma_5'|\right).\end{aligned} \tag{2.167}$$

We define the density matrix components

$$\begin{aligned}\rho^{ss'}_{AB_{\text{top}}} &= \frac{1}{4}\sum_{\substack{s=-(-1)^{\gamma_1+\gamma_2+\gamma_6}\\ s'=-(-1)^{\gamma_1'+\gamma_2'+\gamma_6'}}}|\gamma_1\gamma_2\gamma_6\rangle\langle\gamma_1'\gamma_2'\gamma_6'|, \\ \rho^{ss'}_{B_{\text{bottom}}C} &= \frac{1}{4}\sum_{\substack{s=(-1)^{\gamma_3+\gamma_4+\gamma_5}\\ s'=(-1)^{\gamma_3'+\gamma_4'+\gamma_5'}}}|\gamma_3\gamma_4\gamma_5\rangle\langle\gamma_3'\gamma_4'\gamma_5'|.\end{aligned} \tag{2.168}$$

These components have unit trace only when $s = s'$, and have vanishing trace when $s \neq s'$. Therefore (2.167) does *not* admit a density matrix decomposition (2.149). Moreover, even when $s = s'$, the parity index cannot be absorbed entirely in B_{top} and B_{bottom}. To see this, we assume the contrary that the density matrix components decompose, $\rho^s_{AB_{\text{top}}} = \rho_A \otimes \rho^s_{B_{\text{top}}}$, where ρ_A and $\rho_{B_{\text{top}}}$ have unit trace. This implies $\rho_A = \text{Tr}_{B_{\text{top}}}(\rho^s_{AB_{\text{top}}})$ and

$\rho^s_{B_{\text{top}}} = \text{Tr}_A(\rho^s_{AB_{\text{top}}})$. By taking the partial traces in (2.168),

$$\begin{aligned}\rho_A = \text{Tr}_{B_{\text{top}}}(\rho^s_{AB_{\text{top}}}) &= \frac{1}{2}\sum_{\gamma_1=0,1} |\gamma_1\rangle\langle\gamma_1| \\ \rho^s_{B_{\text{top}}} = \text{Tr}_A(\rho^s_{AB_{\text{top}}}) &= \frac{1}{4}\sum_{\substack{(-1)^{\gamma_2+\gamma_6} \\ =(-1)^{\gamma_2'+\gamma_6'}}} |\gamma_2\gamma_6\rangle\langle\gamma_2'\gamma_6'|.\end{aligned} \tag{2.169}$$

The product $\rho_A \otimes \rho^s_{B_{\text{top}}} = \text{Tr}_{B_{\text{top}}}(\rho^s_{AB_{\text{top}}}) \otimes \text{Tr}_A(\rho^s_{AB_{\text{top}}})$ is

$$\frac{1}{8}\sum_{\gamma_1=0,1}\sum_{\substack{(-1)^{\gamma_2+\gamma_6} \\ =(-1)^{\gamma_2'+\gamma_6'}}} |\gamma_1\gamma_2\gamma_6\rangle\langle\gamma_1'\gamma_2'\gamma_6'|, \tag{2.170}$$

which contradicts (2.168). Therefore, the assumption $\rho^s_{AB_{\text{top}}} = \rho_A \otimes \rho^s_{B_{\text{top}}}$ must be false. Similarly, $\rho^s_{B_{\text{bottom}}C}$ is also not factorizable.

□

2.4.2 $ABCD$ Geometry

.

As we found in the proof of Lemma 2, the trace over degrees of freedom in cylinder D results in a reduced density matrix ρ_{ABC} that is a direct sum over each of the topological sectors. We may therefore consider the decomposition (2.149) for the Laughlin and untwisted Moore-Read states separately from that of the twisted Moore-Read states. We will show how the latter set of states admits a refinement of the decomposition (2.149). In both

cases, the reduced density matrices ρ_{ABC} saturate the strong subadditivity relation of the entanglement entropy.

Laughlin and Untwisted Sector Moore-Read States

We begin with a fixed pure torus state with anyon flux a,

$$|\Psi\rangle = \sum_{\vec{\mathcal{N}}_a} P_a(\vec{\mathcal{N}}_a) \prod_{i=1}^{4} \frac{\lambda(\mathcal{N}_{a,i})}{\sqrt{Z_{a,i}}} \times |\mathcal{N}_{a,1}\mathcal{N}_{a,2}\rangle_{X_1} \otimes |\mathcal{N}_{a,2}\mathcal{N}_{a,3}\rangle_{X_2} \otimes |\mathcal{N}_{a,3}\mathcal{N}_{a,4}\rangle_{X_3} \otimes |\mathcal{N}_{a,4}\mathcal{N}_{a,1}\rangle_{X_4}. \tag{2.171}$$

Here we are taking $X_1 = A$, $X_2 = B$, $X_3 = C$, and $X_4 = D$. $P_a(\vec{\mathcal{N}}_a)$ is the product of projection operator eigenvalue for the four cylinders. For the Laughlin state, $P_a(\vec{\mathcal{N}}_a) = 1$. For the untwisted sectors of the Moore-Read state, a cylinder projection operator eigenvalue can be factorized into a product of left and right edge projection operator eigenvalues for each cylinder, i.e., $P_{a,X_i}(\mathcal{N}_{a,i}, \mathcal{N}_{a,i+1}) = P_{a,i}(\mathcal{N}_{a,i}) P_{a,i+1}(\mathcal{N}_{a,i+1})$ with $P_{a,i}(\mathcal{N}_{a,i})$ given in

(2.104). The density matrix $\rho_{ABC} = \mathrm{tr}_{X_4} |\Psi\rangle\langle\Psi|$ obtained by tracing out X_4 is

$$\begin{aligned}
\rho_{ABC} = & \sum_{\mathcal{N}_{a,1},\mathcal{N}_{a,2},\mathcal{N}'_{a,2}} \frac{\lambda^2(\mathcal{N}_{a,1})}{Z_{a,1}} \frac{\lambda(\mathcal{N}_{a,2})}{\sqrt{Z_{a,2}}} \frac{\lambda(\mathcal{N}'_{a,2})}{\sqrt{Z_{a,2}}} \\
& \times P_{a,X_1} |\mathcal{N}_{a,1}\mathcal{N}_{a,2}\rangle\langle\mathcal{N}_{a,1}\mathcal{N}'_{a,2}|_{X_1} P_{a,X_1} \\
& \otimes P_{a,2} |\mathcal{N}_{a,2}\rangle\langle\mathcal{N}'_{a,2}|_{LX_2} P_{a,2} \\
& \otimes \sum_{\mathcal{N}_{a,3},\mathcal{N}'_{a,3},\mathcal{N}_{a,4}} \frac{\lambda^2(\mathcal{N}_{a,4})}{Z_{a,4}} \frac{\lambda(\mathcal{N}_{a,3})}{\sqrt{Z_{a,3}}} \frac{\lambda(\mathcal{N}'_{a,3})}{\sqrt{Z_{a,3}}} \\
& \times P_{a,3} |\mathcal{N}_{a,3}\rangle\langle\mathcal{N}'_{a,3}|_{RX_2} P_{a,3} \\
& \otimes P_{a,X_3} |\mathcal{N}_{a,3}\mathcal{N}_{a,4}\rangle\langle\mathcal{N}_{a,3}\mathcal{N}'_{a,4}|_{X_1} P_{a,X_3},
\end{aligned} \tag{2.172}$$

where the partition functions $Z_{a,i} = Z_a$ for all i (for the uniform states we consider) with Z_a defined in (2.70) for the Laughlin state and in (2.108) for the untwisted sectors of the Moore-Read state. By inspection this admits the decomposition (2.149):

$$\rho_{ABC} = \rho^a_{A(LB)} \otimes \rho^a_{(RB)C} \tag{2.173}$$

The density matrices associate with (2.173) are,

$$\rho^a_{A(LB)} = \sum_{\mathcal{N}_{a,2},\mathcal{N}'_{a,2}} \frac{\lambda(\mathcal{N}_{a,2})\lambda(\mathcal{N}'_{a,2})}{Z_{a,2}} \rho_{A,a}^{\mathcal{N}_{a,2}\mathcal{N}'_{a,2}} \rho_{LB,a}^{\mathcal{N}_{a,2}\mathcal{N}'_{a,2}} \tag{2.174}$$

where

$$\rho_{A,a}^{\mathcal{N}_{a,2}\mathcal{N}'_{a,2}} = \sum_{\mathcal{N}_{a,1}} \frac{\lambda^2(\mathcal{N}_{a,1})}{Z_{a,1}} P_{a,X_1} |\mathcal{N}_{a,1}\mathcal{N}_{a,2}\rangle\langle\mathcal{N}_{a,1}\mathcal{N}'_{a,2}|_{X_1} P_{a,X_1},$$
$$\rho_{LB,a}^{\mathcal{N}_{a,2}\mathcal{N}'_{a,2}} = P_{a,2} |\mathcal{N}_{a,2}\rangle\langle\mathcal{N}'_{a,2}|_{LX_2} P_{a,2}. \tag{2.175}$$

$\rho_{(RB)C,a}$ has a similar decomposition,

$$\rho^a_{(RB)C} = \sum_{\mathcal{N}_{a,3},\mathcal{N}'_{a,3}} \frac{\lambda(\mathcal{N}_{a,3})\lambda(\mathcal{N}'_{a,3})}{Z_{a,3}} \rho_{RB,a}^{\mathcal{N}_{a,3}\mathcal{N}'_{a,3}} \rho_{C,a}^{\mathcal{N}_{a,3}\mathcal{N}'_{a,3}}. \tag{2.176}$$

Twisted Sector Moore-Read States

For the twisted sectors of the Moore-Read state, we need to split B into two consecutive cylinders B_I and B_{II}. Specifically, we take $X_1 = A$, $X_2 = B_I$, $X_3 = B_{II}$, $X_4 = C$, $X_5 = D_1$ and $X_6 = D_2$ (see Figure 2.5) and begin with the generic twisted sector pure state,

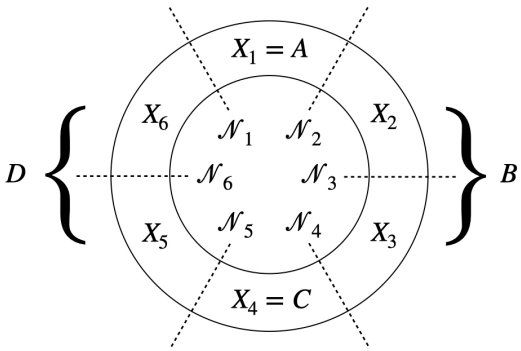

Figure 2.5: A torus is divided by the dashed lines into the $ABCD_1D_2$ geometry: region A is the X_1 cylinder while region C the X_4 cylinder. Region B is the union of X_2 and X_3; and D the union of X_5 and X_6.

The ground state of a fixed twisted sector $a = \xi^{r+1/2}$ is again described by (2.155). We will show the reduced density matrix $\rho^{\text{twist}}_{ABC}$, after tracing out subsystem D, cannot factorize according (2.149). Similar to the previous AB_1CB_2 geometry in the last subsection, it suffice to focus on the zero mode sector. The ground state in the zero mode sector is $|GS\rangle = \sum_{\{\gamma_i\}|_C} |\gamma_1 \dots \gamma_6\rangle/(4\sqrt{2})$, where the sum is restricted by $\sum_{i=1}^{6} \gamma_i = 1 \bmod 2$.

The reduced density matrix is

$$\rho^{\text{twist}}_{ABC} = \text{Tr}_D \left(|GS\rangle\langle GS|\right) = \frac{1}{16} \sum_{\substack{\gamma_1+\ldots+\gamma_4 \\ =\gamma_1'+\ldots+\gamma_4'}} |\gamma_1 \dots \gamma_4\rangle\langle\gamma_1' \dots \gamma_4'|. \tag{2.177}$$

To show that it does not decompose, we follow a similar procedure to before and assume the contrary that $\rho^{\text{twist}}_{ABC} = \sum_j p_j \rho_{AB^j_I} \otimes \rho_{B^j_{II}C}$, where p_j are probabilities satisfying $\sum_j p_j = 1$. Tracing over subsystem B, the factorization would imply $\text{Tr}_B(\rho^{\text{twist}}_{ABC}) = \rho_A \otimes \rho_C$. At the same time, from (2.177),

$$\begin{aligned}
\text{Tr}_B(\rho^{\text{twist}}_{ABC}) &= \frac{1}{4} \sum_{\substack{\gamma_1+\gamma_4 \\ =\gamma_1'+\gamma_4'}} |\gamma_1\gamma_4\rangle\langle\gamma_1'\gamma_4'|, \\
\rho_A = \text{Tr}_{BC}\left(\rho^{\text{twist}}_{ABC}\right) &= \frac{1}{2} \sum_{\gamma_1=0,1} |\gamma_1\rangle\langle\gamma_1|, \\
\rho_C = \text{Tr}_{AB}\left(\rho^{\text{twist}}_{ABC}\right) &= \frac{1}{2} \sum_{\gamma_4=0,1} |\gamma_4\rangle\langle\gamma_4|.
\end{aligned} \tag{2.178}$$

However, this would lead to a contradiction because $\rho_A \otimes \rho_C = \frac{1}{4} \sum_{\gamma_1\gamma_4} |\gamma_1\gamma_4\rangle\langle\gamma_1\gamma_4|$, which disagrees with $\text{Tr}_B(\rho^{\text{twist}}_{ABC})$ in the equation above. Therefore, the assumption that the reduced density matrix decomposes, $\rho^{\text{twist}}_{ABC} = \sum_j p_j \rho_{AB^j_I} \otimes \rho_{B^j_{II}C}$, must be false.

2.5 Discussion and Conclusion

In this paper, we studied multipartite entanglement in the Laughlin and Moore-Read ground states at filling fraction $\nu = 1/m$ using the entanglement negativity. Our main results for the entanglement negativity of these states are summarized in Eqs. (2.12) and (2.13). We then showed how the disentangling condition (2.4) (expressed in terms of the entanglement negativity) can be used to isolate the long-range entanglement (as defined by Lee and Vidal [LV13]) in these topological ground states. In particular, only states in a definite topological sector satisfy the disentangling condition. We then studied the implication of these results for the structure of the manybody ground state wavefunctions, showing explicitly how the Laughlin and Moore-Read states can be factorized according to Eqs. (2.6) and (2.8). This shows how (topological) long-range entanglement can constrain the structure of a manybody wavefunction.

Despite satisfying the disentangling condition, a twisted sector Moore-Read ground state wavefunction on the torus cannot be disentangled (i.e., decompose into an appropriate tensor product). (The Laughlin and untwisted sector Moore-Read ground state wavefunctions can be disentangled.) The obstruction is due to the lack of a tensor product decomposition of the twisted sector torus Hilbert space into appropriate subspaces. It would be interesting to find a generalization of the disentangling condition, perhaps one that involves the partial time-reversal [SSR17] or anyonic partial transpose [SRRC19], that is sensitive to this particular obstruction to wavefunction disentanglement.

Our results rely on the cut and glue construction of topological ground states. In this approach, the correlation length is zero. With finite correlation length, we expect exponentially suppressed corrections to appear in the disentangling condition. It would also be interesting to consider the disentangling condition at phase transitions where the correlation length is infinite.

We focused on the Laughlin and Moore-Read topological states. We expect that our entanglement negativity results hold for more general topological states in $2+1$ dimensions, such as those phases hosting metaplectic anyons [HNW13] and Fibonacci anyons [NSS+08a]. It is unclear to us whether the corresponding wavefunctions for such states might disentangle, as the fusion rule structure of general states is more intricate than the Laughlin and Moore-Read states. Fracton orders in $3+1$ dimensions [NH19] have similar entanglement signatures as their lower-dimensional "conventional" topologically ordered counterparts [SSC19]. Recent work has shown how certain types of fracton order obtain from coupled-wire constructions [SDC21, SIW21] or from infinite-component (2+1)-dimensional Chern-Simons gauge theory [MSC+22]. The multipartite entanglement characteristics of this order are yet to be understood.

Chapter 3

BOSONIC FRACTIONAL QUANTUM HALL STATES

This chapter was previous published as [Pak Kau Lim, Michael Mulligan, Jeffrey C.Y. Teo, "Partial fillings of the bosonic E8 quantum Hall state", Phys. Rev. B 108, 035136 – Published 18 July 2023]

3.1 Introduction

Of all the topological phases of matter in two spatial dimensions, the integer quantum Hall effect (IQHE) of electrons is particularly special [PG90, SP08]. The IQHE was the first topological phase to be recognized experimentally; it furthermore provides a basis for understanding more general topological states, such as the fractional quantum Hall effect

(FQHE). The IQHE is observed when all single-electron states of an integer number of Landau levels are occupied; the fractional effect occurs when a Landau level is partially filled. Due to the extensive degeneracy of a partially-filled Landau level, the FQHE ground state is determined by the underlying microscopic electron interactions (and disorder in realistic systems). Empirically, the most "attractive" states are found in the lowest Landau level at filling fractions $\nu = p/(2p+1)$ (with integer p) and the particle-hole conjugate filling fractions $1-\nu$. Both the IQHE and FQHE are stable against weak external perturbations.

To what extent is this picture unique to electron systems? In particular, what are the analogous families of states composed out of fundamental bosons? In this paper, we report progress on answering these questions.

To begin, we first need to understand what it means for a bosonic system to exhibit an integer quantum Hall effect. The IQHE of electrons is characterized by the absence of any topological order, i.e., there are no anyonic quasiparticle excitations [Wil90] and the topological entanglement entropy [KP06b] vanishes. Furthermore, the IQHE of electrons has robust gapless edge modes that do not require symmetry for their stabilization. These properties can only be reproduced by bosonic states with $8k$ chiral edge modes (k is a non-negative integer) [Kit, LV12], the simplest example occurring when $k = 1$—the so-called E_8 state. We will therefore identify the E_8 state as the bosonic analog of the $\nu = 1$ IQHE of electrons. (The primary distinction between the E_8 state and the bosonic QH state proposed in [SL13] is that the edge modes of the E_8 state do not require symmetry for their stability.) As its name suggests, the E_8 state is based on the E_8 Lie algebra; for instance, the K-matrix in its Chern-Simons [WZ92] field theory description is the E_8 Cartan matrix.

Unlike the IQHE of electrons, the E_8 state does not have a single-particle interpretation. The bosonic state is inherently interacting. For example, the primitive low-energy excitations, the E_8 bosons, are all even combinations of electrons. This makes the general description, let alone a specific construction, of a bosonic analog of the FQHE of electrons less clear. We attack this problem following the earlier work of Lopes et al. [LQHT19], where it was shown: (1) how the E_8 state can be constructed from interacting electrons in a coupled-wire model (an anisotropic 2d array of coupled Luttinger liquids that serves as the normal state for a large variety of distinct topological phases, e.g., [KML02, TK14a], among many others); and (2) within this construction, the E_8 state is the parent state of states with G_2 or F_4 Fibonacci topological order. (Other constructions of a state with Fibonacci topological order are given in [MCA+14, SCMA15, GSF21].) These and the other phases considered in this paper are bosonic in the sense that there is a fermion energy gap, which can be made arbitrarily large, below which all local excitations in the bulk and on the edge are even combinations of electrons.

Within this construction [LQHT19], the G_2 and F_4 symmetries arise from the Lie algebraic factorization $G_2 \times F_4 \subset E_8$. The theory of conformal embeddings [FMS12] allows this symmetry factorization to be realized within the E_8 edge-state theory. This factorization allows the E_8 quasiparticle excitations (created, for instance, along any boundary by operators in the edge-state theory) to be decomposed into G_2 and F_4 Fibonacci components, in such a way that the product is a boson. This is a generalization of spin-charge separation in the theory of a 1D spin-1/2 electron [Gia03].

The bulk-boundary correspondence [EMSS89a, Wen92b] implies this edge-state symmetry factorization can be used to construct states with either G_2 or F_4 topological order as follows. The E_8 state is equivalent to a collection of wires—each hosting nonchiral conformal field theories with E_8 symmetry—that are glued together via interactions that gap out nearby counter-propagating modes. The $G_2 \times F_4 \subset E_8$ conformal embedding allows for an alternative set of interactions that gap out the nonchiral E_8 wires in such a way that at low energies only chiral G_2 or F_4 edge states remain. The relative dominance of the different sets of interactions can be tuned by an external magnetic field (proportional to ν^{-1}) transverse to the plane of the wires and/or short-ranged density-density interactions between modes on a finite number of nearby wires. Importantly, the various gap-generating interactions are local, being constructed from products of the fundamental E_8 boson creation/annihilation operators.

Here, we show how this picture can be generalized to a large class of conformal embeddings $\mathcal{G}_A \times \mathcal{G}_B \subset E_8$ [BB87, SW86]:

$$\mathcal{G}_A \times \mathcal{G}_B = \begin{cases} SU(3) \times E_6 \\ SU(2) \times E_7 \\ SU(5) \times SU(5) \\ SO(M) \times SO(16-M) \\ G_2 \times F_4 \\ U(1)_8 \times SU(8) \\ SU(2)_4 \times Sp(8) \end{cases} \tag{3.1}$$

for $M = 1, \ldots, 8$. Above, $SO(1)$ refers to a state—described in detail in the main text—with Ising topological order. The levels of the Wess-Zumino-Witten (WZW) [WZ71, Wit83, Wit84] theories are $k = 1$ unless specified otherwise. By the mechanism outlined in the previous paragraph, we show how the above embeddings give rise to states with either $\mathcal{G}_A$ or $\mathcal{G}_B$ topological order. We refer to the $\mathcal{G}_A$ or $\mathcal{G}_B$ topological states as bosonic fractional E_8 states.

We catalog the possible bosonic fractional E_8 states in Fig. 3.1 according to their filling number ν and chiral central charge c. Recall that ν and c determine the electrical (σ_{xy})

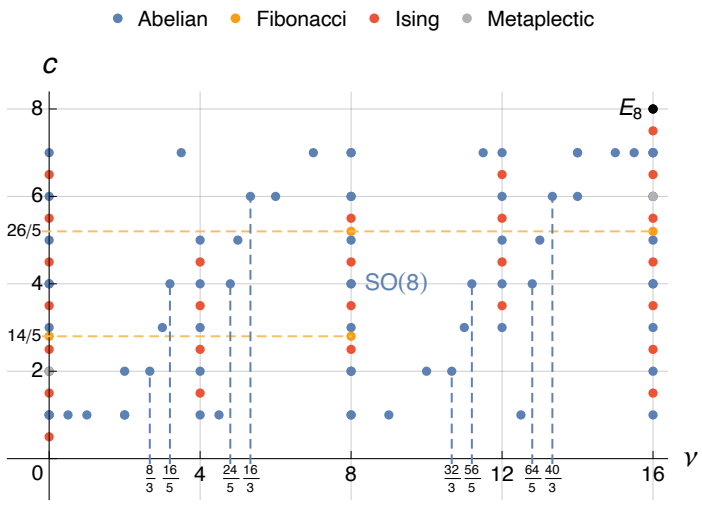

Figure 3.1: Bosonic fractional quantum Hall (bFQH) states with filling number ν and chiral central charge c. Particle-hole conjugation flips $(\nu, c) \leftrightarrow (16-\nu, 8-c)$. The particle-hole symmetric point lies at $(\nu, c) = (8, 4)$. The metaplectic states and the Abelian states are overlapping at $(\nu, c) = (0, 2), (16, 6)$.

and thermal (κ_{xy}) [KF97, CHZ02] Hall conductance via the relations:

$$\sigma_{xy} = \nu \frac{e^2}{h}, \quad \kappa_{xy} = c \frac{\pi^2 k_B^2}{3h} T, \tag{3.2}$$

where T is the temperature. In general, the chiral central charges c_A and c_B of the $\mathcal{G}_A$ and $\mathcal{G}_B$ states are not integers; this is the case for the G_2 and F_4 states, for instance. When this occurs, the $\mathcal{G}_A$ and $\mathcal{G}_B$ states have non-Abelian topological order.

The filling numbers of the $\mathcal{G}_A$ and $\mathcal{G}_B$ states associated with the conformal embedding $\mathcal{G}_A \times \mathcal{G}_B \subset E_8$ satisfy $\nu_A + \nu_B = \nu_{E_8} = 16$. Similarly, the chiral central charges $c_A + c_B = c_{E_8} = 8$. These constraints are reminiscent to the relations between the filling numbers and chiral central charges of particle-hole conjugate states in the lowest Landau level, upon the replacements $16 \to 1$ and $8 \to 1$. (The relative factor of 2 between ν_{E_8} and c_{E_8} arises from

the construction of the E_8 state from a collection of electron wires, in which the E_8 bosons are formed from electrons of unit charge.) To emphasize this analogy, we refer to $\mathcal{G}_A$ and $\mathcal{G}_B$ topological states—associated with a particular embedding $\mathcal{G}_A \times \mathcal{G}_B \subset E_8$—as particle-hole conjugates. Indeed, this identification can be made precise with the particle-hole symmetry operation given in [LQHT19].

It is worth noting that, for a fixed conjugate pair $\mathcal{G}_A$ and $\mathcal{G}_B$, there are, in general, multiple inequivalent ways they can be embedded in E_8, with distinct electrical responses. In other words, a bosonic fractional quantum state with $\mathcal{G}_{A/B}$ topological order can occur at different filling numbers (see Fig. 3.1) and have distinct quasiparticle charge assignments. In this paper, we exhaust these charged phases with topological orders appearing in (3.1) (perhaps except the metaplectic phases $SU(2)_4$ and $Sp(8)_1$). The various bosonic fractional quantum Hall phases encountered in this paper can be summarized by the family tree in Fig 3.2.

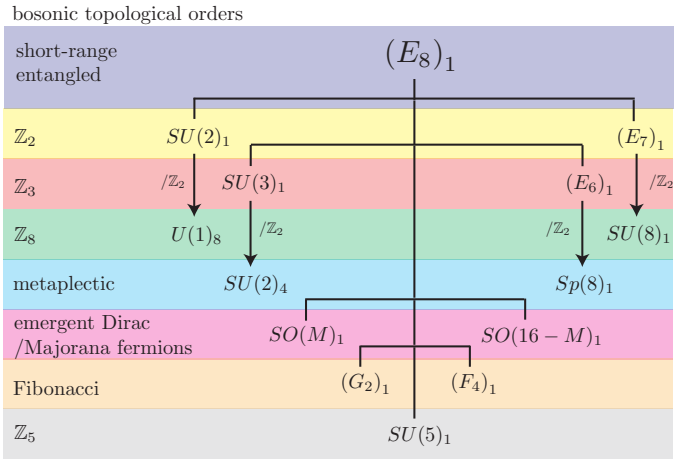

Figure 3.2: Family tree of bosonic fractional quantum Hall states that descend from the E_8 state, and their topological orders. States on the same line are pairwise related by particle-hole conjugation. Vertical down arrows represent $\mathbb{Z}_2$ gauging (or orbifolding).

3.2 The bosonic E_8 quantum Hall state

In this section, we review [LQHT19] the coupled-wire construction of the E_8 quantum Hall state at filling fraction $\nu = 16$.

3.2.1 Review of the E_8tate

The E_8 state is a bosonic topological state of matter. "Bosonic" means that its fundamental excitations have bosonic self and mutual statistics. The state is insulating, possessing a finite bulk excitation gap $E_g^{(0)} > 0$. The topological order of the E_8 state is trivial: All bulk and boundary excitations are local integral combination of the fundamental bosons. One consequence of this is that the ground state is non-degenerate. These properties are summarized by saying that the E_8 state is a short-range entangled bosonic topological state. The state supports eight gapless, chiral edge modes. These edge states are responsible for the quantized (in appropriate units) electric σ_{xy} and thermal κ_{xy} Hall conductivities $\sigma_{xy} = \nu_{E_8} \frac{e^2}{h}$ and $\kappa_{xy} = c_{E_8} \frac{\pi^2 k_B^2}{3h} T$, where $\nu_{E_8} = 16$ and $c_{E_8} = 8$. These conductivities distinguish the E_8 state from the topologically trivial insulator, for which both σ_{xy} and κ_{xy} vanish. In contrast to the IQHE of electrons, for which both the filling number and the chiral central charge equal one, the E_8 state has an unconventional Wiedemann-Franz law [FW53] since $c_{E_8} \neq \nu_{E_8}$. The E_8 state is adiabaticlly connected by stable equivalence to eight copies of the IQHE of electrons [PMN13, CCM+14].

In general, the chiral central charge c of a bosonic topological phase is related to its anyon quasiparticle content through the Gauss-Milgram formula [Kit06],

$$e^{2\pi ic/8} = \frac{1}{\mathcal{D}} \sum_x d_x^2 e^{2\pi i h_x}. \tag{3.3}$$

Here, the sum is over anyon classes x, with quantum dimensions d_x and spins h_x, and is normalized by the total quantum dimension $\mathcal{D} = \sqrt{\sum_x d_x^2}$. For trivial topological order, the chiral central charge of a bosonic short-range entangled state must be $c \equiv 0$ modulo 8. Up to the addition of unprotected nonchiral edge modes, the E_8 state is therefore the simplest fully-chiral short-range entangled topological state.

The Chern-Simons theory for the E_8 state is [LV12]

$$S_{\text{bulk}} = \frac{1}{4\pi} \int_{2+1} (K_{E_8})_{IJ} a^I \wedge da^J + \frac{e}{2\pi} \int_{2+1} t_I A \wedge da^I. \tag{3.4}$$

Here, a_I $(I = 1, \ldots, 8)$ are dynamical $U(1)$ gauge fields; A is the external electromagnetic gauge potential; $(K_{E_8})_{IJ}$ is the Cartan matrix of the E_8 Lie algebra:

$$K_{E_8} = \begin{pmatrix} 2 & -1 & & & & & & \\ -1 & 2 & -1 & & & & & \\ & -1 & 2 & -1 & & & & \\ & & -1 & 2 & -1 & & & \\ & & & -1 & 2 & -1 & & -1 \\ & & & & -1 & 2 & -1 & \\ & & & & & -1 & 2 & \\ & & & & -1 & & & 2 \end{pmatrix}, \tag{3.5}$$

with elements not shown equal to zero; t_I is the charge vector (in the electron basis); repeated indices are summed over. The wedge product $a^I \wedge da^J = \epsilon^{\mu\nu\rho} a^I_\mu \partial_\nu a^J_\rho$, where $\epsilon^{\mu\nu\rho}$ is the totally antisymmetric symbol and $\mu, \nu, \rho \in \{0, 1, 2\} = \{t, x, y\}$.

Positive-definiteness of K_{E_8} implies the topological state is fully chiral, i.e., all 8 edge modes move in the same direction. The state is bosonic since there are only even entries along the diagonal. Excitations are defined by 8-dimensional integer vectors l_I, l'_I: the self and mutual statistics, $\pi l_I (K^{-1}_{E_8})^{IJ} l_I$ and $2\pi l_I (K^{-1}_{E_8})^{IJ} l'_I$, are integer multiples of 2π. Unimodularity of K_{E_8}, i.e., $|\det K_{E_8}| = 1$, ensures E_8 is short-range entangled. K_{E_8} is the unique 8-dimensional matrix (up to equivalence by $GL(8, \mathbb{Z})$ similarity transformation) with these properties. All excitations of the E_8 state are even combinations of electrons and therefore carry even electric charge. Given an 8-dimensional integral vector l_I, representing

an E_8 excitation, its charge is $l_I \tilde{q}^I \equiv l_I (K_{E_8}^{-1})^{IJ} t_J$ (in units of e). The charge vector and K-matrix together determine the filling fraction $\nu = \tilde{q}^I (K_{E_8}^{-1})_{IJ} \tilde{q}^J$. These considerations imply that ν must be an integral multiple of 8.

3.2.2 Coupled-wire construction of the E_8 state

The coupled-wire construction of the E_8 state given in Ref. [LQHT19] begins with a 2d array of metallic wires, each consisting of 11 channels of nonrelativistic fermions (electrons). Near the Fermi level, the electron operator $c_{ya}^{\sigma}(\mathsf{x})$ decomposes in terms of left (L) and right (R) propagating chiral Dirac electrons that can be represented by vertex operators of bosonized variables $\Phi_{ya}^{\sigma}(\mathsf{x})$ [Gia03]:

$$c_{ya}^{\sigma}(\mathsf{x}) \sim \exp\left[i\left(\Phi_{ya}^{\sigma}(\mathsf{x}) + k_{ya}^{\sigma}\mathsf{x}\right)\right], \tag{3.6}$$

where $a = 1, \ldots, 11$; y is an integer that labels a given wire; x is the continuous spatial coordinate along the wire; $\sigma = R, L = +1, -1$ signifies the direction of propagation. A dimensionful factor $1/\sqrt{l_0}$ (where l_0 is a microscopic length scale) that ensures the electron operators have the correct engineering dimensions is suppressed under the proportionality sign $\sim$ in (3.6). The Fermi momentum in the x-direction is

$$k_{ya}^{\sigma} = \frac{eB}{\hbar c}\mathsf{y} + \sigma k_{F,a}, \tag{3.7}$$

where $\mathsf{y} = yd$ is the vertical location of the y^{th} wire and d is the separation between adjacent wires. The first term in (3.7) shifts the electron momentum in the presence of

an out-of-plane magnetic field $\mathbf{B} = B\hat{\mathbf{z}}$, written in Landau gauge $A_x = -B\mathsf{y}$. The bare momentum $k_{F,a}$ is model dependent and will be determined by momentum conservation of backscattering interactions presented below. The filling number, which counts the electron number per magnetic flux quantum $\phi_0 = hc/e$, is

$$\nu = \frac{N_e}{N_B} = \frac{\frac{l}{2\pi}\sum_a 2k_{F,a}}{Bdl/\phi_0} = \frac{\hbar c}{eBd}\sum_a 2k_{F,a}, \tag{3.8}$$

where l is the length of each wire.

The bosonized variables Φ^σ_{ya} are described by the Luttinger liquid Lagrangian density,

$$\mathcal{L} = \sum_y \sum_{a=1}^{11} \sum_{\sigma=\pm} \frac{1}{4\pi}\sigma\partial_\mathsf{x}\Phi^\sigma_{ya}\partial_\mathsf{t}\Phi^\sigma_{ya} - \mathcal{H}, \tag{3.9}$$

and obey the equal-time commutation relations,

$$\left[\Phi^\sigma_{ya}(\mathsf{x}), \partial_{\mathsf{x}'}\Phi^{\sigma'}_{y'a'}(\mathsf{x}')\right] = 2\pi i\sigma\delta^{\sigma\sigma'}\delta_{yy'}\delta_{aa'}\delta(\mathsf{x}-\mathsf{x}'). \tag{3.10}$$

Before introducing any backscattering interactions, the Hamiltonian $\mathcal{H}$ equals the bare Hamiltonian density,

$$\mathcal{H}_0 = \sum_y \sum_{a,a'=1}^{11} \sum_{\sigma,\sigma'=\pm} v^{aa'}_{\sigma\sigma'}\partial_\mathsf{x}\Phi^\sigma_{ya}\partial_\mathsf{x}\Phi^{\sigma'}_{ya'}. \tag{3.11}$$

$\mathcal{H}_0$ includes the single-body massless Dirac Hamiltonian

$$\mathcal{H}_{\text{Dirac}} = iv\sigma {c_{ya}^{\sigma}}^{\dagger}\partial_{\text{x}} c_{ya}^{\sigma} = \frac{v}{4\pi}\left(\partial_{\text{x}}\Phi_{ya}^{\sigma}\right)^2, \tag{3.12}$$

as well as the intra-wire density-density interactions

$$\mathcal{H}_{\text{int}} = u_{\sigma\sigma'}^{aa'} n_{ya}^{\sigma} n_{ya'}^{\sigma'}, \tag{3.13}$$

where $n_{ya}^{\sigma} = {c_{ya}^{\sigma}}^{\dagger} c_{ya}^{\sigma} = \sigma\partial_{\text{x}}\Phi_{ya}^{\sigma}/(2\pi)$ is the electron number density for given y, a, σ.

On each wire, a non-chiral bosonic E_8 Wess-Zumino-Witten (WZW) conformal field theory (CFT) [FMS12] can be singled out by introducing a set of many-body backscattering interactions within the wire that gaps out all fermionic excitations with odd fermion parity. To do this, we first perform a basis transformation that decomposes the 11 counter-propagating pairs of Dirac electrons into E_8 bosons and three decoupled "integrated" Dirac fermions f_{yn}^{σ}, for $n = 1, 2, 3$. This corresponds to the symmetry decomposition:

$$U(11)_1 = (E_8)_1 \otimes U(3)_1. \tag{3.14}$$

The basis transformation from the electron to the "Chevalley" basis,

$$\tilde{\Phi}_{yI}^{\sigma} = \sum_{a,\sigma'} U_{Ia}^{\sigma\sigma'} \Phi_{ya}^{\sigma'}, \quad \tilde{k}_{yI}^{\sigma} = \sum_{a,\sigma'} U_{Ia}^{\sigma\sigma'} k_{ya}^{\sigma'}, \tag{3.15}$$

uses the integral unimodular U matrix,

$$U = \begin{pmatrix} U^{++} & U^{+-} \\ U^{-+} & U^{--} \end{pmatrix}, \tag{3.16}$$

$$(U^{++}|U^{+-}) = (U^{--}|U^{-+}) =$$

$$\left(\begin{array}{cccccccccccc|cccccccccc}
-1 & -1 & -1 & & & & & & & & & & & & & & & & & & & -1 \\
 & 1 & 1 & & & & & & & & & & & & & & & & & & & \\
 & & -1 & 1 & & & & & & & & & & & & & & & & & & \\
 & & & -1 & 1 & & & & & & & & & & & & & & & & & \\
 & & & & -1 & -1 & & & & & & & & & & & & & & & & \\
 & & & & & 1 & 1 & & & & & & & & & & & & & & & \\
 & & & & & & -1 & 1 & & & & & & & & & & & & & & \\
 & -1 & 1 & 1 & 1 & & & & & & & & & & & & & & & & 1 & -1 \\
 & & & & & & & & 1 & 1 & 1 & & & & & & & & & & & \\
 & & & & & & & & 3 & -5 & -2 & -1 & -2 & 2 & 2 & 2 & -2 & 2 & 2 & & & \\
2 & & 1 & -1 & -1 & -1 & 1 & -1 & -1 & & & & & & & & & & & & -1 & 3
\end{array}\right), \tag{3.17}$$

where the rows and columns of $U^{\sigma\sigma'}$ are labeled by $I, a = 1, \ldots, 11$. The Lagrangian density (3.9) in the "Chevalley" basis is

$$\mathcal{L} = \sum_y \left(\sum_{I,J=1}^{8} \sum_{\sigma=\pm} \frac{1}{4\pi} \sigma \left(K_{E_8}^{-1}\right)^{IJ} \partial_{\mathsf{x}} \tilde{\Phi}^{\sigma}_{yI} \partial_{\mathsf{t}} \tilde{\Phi}^{\sigma}_{yJ} + \sum_{n=1}^{3} \sum_{\sigma=\pm} \frac{1}{4\pi} \sigma \partial_{\mathsf{x}} \tilde{\Phi}^{\sigma}_{y,n+8} \partial_{\mathsf{t}} \tilde{\Phi}^{\sigma}_{y,n+8} \right) - \mathcal{H},$$

where K_{E_8} is the Cartan matrix defined in (3.5). Since K_{E_8} has unit determinant, its inverse $K_{E_8}^{-1}$ is also integral.

For each chiral sector $\sigma = R, L = +, -$, the first eight bosonized variables $\tilde{\Phi}^{\sigma}_{yI}$, $I = 1, \ldots, 8$, generate the E_8 WZW CFT at level 1. The vertex operators,

$$[\mathtt{E}_{E_8}(\mathsf{x})]^{\sigma}_{yI} = \exp\left[i(\tilde{\Phi}^{\sigma}_{yI}(\mathsf{x}) + \tilde{k}^{\sigma}_{yI}\mathsf{x})\right], \tag{3.18}$$

correspond to the simple roots of the E_8 algebra. These operators all have spin $|h| = 1$ and are (each the exponential of) integral linear combinations of the bosonized electrons (3.6). The electric charges $\tilde{q}_J$ (in units of e) of the simple roots $[\mathtt{E}_{E_8}(\mathsf{x})]^{\sigma}_{yI}$ can be read off by summing over the entries in each of the first 8 rows of the U matrix:

$$\tilde{q}_{J=1,\ldots,8} = \sum_{a=1}^{11} \left(U^{++}_{Ja} + U^{+-}_{Ja}\right) = (-4, 2, 0, 0, -2, 2, 0, 2). \tag{3.19}$$

The last three elements of $\tilde{\Phi}^{\sigma}_{y,I+8+n}$ define the "integrated" Dirac fermions:

$$f^{\sigma}_{yn} = \exp\left[i(\tilde{\Phi}^{\sigma}_{y,8+n} + \tilde{k}^{\sigma}_{y,n+8}\mathsf{x})\right] \tag{3.20}$$

, for $n = 1, 2, 3$. These bosons generate the $U(3)_1$ symmetry, which is decoupled from the $(E_8)_1$ symmetry. The "integrated" Dirac fermions have spin $|h| = 1/2$ and carry electric charges $\tilde{q}_{n=1,2,3} = (3, 1, 1)$.

The electron density-density interactions $u^{aa'}_{\sigma\sigma'}$— equivalently, the velocity matrix $v^{aa'}_{\sigma\sigma'}$ in (3.11)—can be tuned so that the bare Hamiltonian density in the "Chevalley" basis is

$$\mathcal{H}_0 = \frac{\tilde{v}}{4\pi} \sum_y \sum_{\sigma=\pm} \left[\sum_{I,J=1}^{8} \left(K^{-1}_{E_8}\right)^{IJ} \partial_{\mathsf{x}} \tilde{\Phi}^{\sigma}_{yI} \partial_{\mathsf{x}} \tilde{\Phi}^{\sigma}_{yJ} + \sum_{n=1}^{3} \left(\partial_{\mathsf{x}} \tilde{\Phi}^{\sigma}_{y,n+8}\right)^2 \right]. \tag{3.21}$$

At this fixed point, the E_8 bosons and the three integrated Dirac fermions are completely decoupled and their theories are conformally symmetric. The fine tuning of the density interactions can be relaxed after a bulk excitation energy gap is established by backscattering terms. The 2D topological phase thus constructed is robust against all gap preserving perturbations, including small deviations of the density interactions away from their fine-tuned values.

The three integrated Dirac fermions can be gapped out by the intra-wire backscattering interactions

$$\begin{aligned}\mathcal{H}^f_{\text{intra}} &= u_{\text{intra}} \sum_y \sum_{n=1}^{3} f^{R\,\dagger}_{yn} f^L_{yn} + h.c. \\ &= 2u_{\text{intra}} \sum_y \sum_{n=1}^{3} \cos\left(\tilde{\Phi}^L_{y,n+8} - \tilde{\Phi}^R_{y,n+8}\right).\end{aligned} \tag{3.22}$$

These interactions conserve charge because f^R_{yn} and f^L_{yn} carry the same charge. In addition, if the L and R "integrated" Dirac fermions have equal momentum, $\tilde{k}^R_{y,8+n} = \tilde{k}^L_{y,8+n}$, then the x-dependent oscillation factors $e^{ik\mathsf{x}}$ in (3.22) cancel. The intra-wire interaction strength sets the fermion gap energy scale $E^1_g \sim u_{\text{intra}}$. We take this to be the largest energy scale for all of the bosonic topological states constructed using the coupled-wire models in this paper.

The $(E_8)_1$ Kac-Moody (KM) [Kac68, Moo68] current algebra is spanned by the eight Cartan generators $[\mathtt{H}_{E_8}]_I$ and 240 roots $[\mathtt{E}_{E_8}]_{\boldsymbol{\alpha}}$ (eight of which have already been given in (3.18)).

On any given wire y and in chiral sector $\sigma = R, L$, the Cartan generators are

$$[\mathtt{H}_{E_8}(\mathsf{x})]^{\sigma}_{yI} = \partial_{\mathsf{x}} \tilde{\Phi}^{\sigma}_{yI}(\mathsf{x}), \tag{3.23}$$

where $I = 1, \ldots, 8$. These operators, which are proportional to the normal ordered product $[\mathtt{E}_{E_8}]^{\dagger}_{I} [\mathtt{E}_{E_8}]_{I}$, are bosonic combination of electrons. The roots are spin-1 vertex operators of integral combinations of $\tilde{\Phi}_I$:

$$[\mathtt{E}_{E_8}(\mathsf{x})]^{\sigma}_{y,\boldsymbol{\alpha}} = \exp\left[i\tilde{\alpha}^I (\tilde{\Phi}^{\sigma}_{yI}(\mathsf{x}) + \tilde{k}^{\sigma}_{yI}\mathsf{x}) \right], \tag{3.24}$$

where the root vector $\tilde{\boldsymbol{\alpha}} = (\tilde{\alpha}^1, \ldots, \tilde{\alpha}^8)$ (in the "Chevalley" basis) has integral entries and length $|\boldsymbol{\alpha}| = \sqrt{K_{IJ}\tilde{\alpha}^I\tilde{\alpha}^J} = \sqrt{2}$. It will become clear below that there are 240 root vectors. Since the eight simple roots in (3.18) are bosonic combinations of electrons, so are all the 240 roots.

Introducing the complex Euclidean spacetime parameters $z = e^{2\pi(\tilde{v}\tau + i\mathsf{x})/l}$ and $\bar{z} = e^{2\pi(\tilde{v}\tau - i\mathsf{x})/l}$ (i.e., mapping spacetime to the cylinder), where $\tau = i\mathtt{t}$ is the Wick rotated time and l is the length of a wire, the chiral operators evolve as holomorphic and anti-holomorphic fields $\tilde{\Phi}^L(x,\tau) = \tilde{\Phi}^L(z)$ and $\tilde{\Phi}^R(x,\tau) = \tilde{\Phi}^R(\bar{z})$ at the conformal fixed point $\mathcal{H}_0 + \mathcal{H}^f_{\text{intra}}$. Focusing on the L sector on any given wire, the Chevalley bosonized operators obey the operator product expansion (OPE):

$$\left\langle \tilde{\Phi}_I(z)\tilde{\Phi}_J(w) \right\rangle = -(K_{E_8})_{IJ} \log(z-w) + \ldots, \tag{3.25}$$

up to finite non-singular factors, including those that are responsible for the anticommutation between electron operators of different channels. The $(E_8)_1$ KM currents obey the OPEs (up to finite non-singular terms):

$$\begin{aligned}
[\mathtt{H}(z)]_I\,[\mathtt{H}(w)]_J &= \frac{(K_{E_8})_{IJ}}{(z-w)^2}+\ldots,\\
[\mathtt{H}(z)]_I\,[\mathtt{E}(w)]_{\boldsymbol{\alpha}} &= \frac{(K_{E_8})_{IJ}\tilde{\alpha}^J}{z-w}\,[\mathtt{E}(w)]_{\boldsymbol{\alpha}}+\ldots,\\
[\mathtt{E}(z)]_{\boldsymbol{\alpha}}\,[\mathtt{E}(w)]_{-\boldsymbol{\alpha}} &= \frac{1}{(z-w)^2}+\frac{\tilde{\alpha}^I}{z-w}\,[\mathtt{H}(w)]_I+\ldots,\\
[\mathtt{E}(z)]_{\boldsymbol{\alpha}}\,[\mathtt{E}(w)]_{\boldsymbol{\beta}} &= \frac{Z_{\boldsymbol{\alpha}\boldsymbol{\beta}}}{z-w}\,[\mathtt{E}(w)]_{\boldsymbol{\alpha}+\boldsymbol{\beta}}+\ldots,
\end{aligned} \tag{3.26}$$

if $(K_{E_8})_{IJ}\alpha^I\beta^J=-1$. The cocycle coefficients $Z_{\boldsymbol{\alpha}\boldsymbol{\beta}}$ ensure the last equality is unchanged under the exchange $z\leftrightarrow w$ and $\boldsymbol{\alpha}\leftrightarrow\boldsymbol{\beta}$. They can be determined from the non-singular pieces in (3.25) that guarantee electron mutual anticommutation. The exact form of $Z_{\boldsymbol{\alpha}\boldsymbol{\beta}}$ is inconsequential to this paper and will not be presented.

The E_8 current algebra, as well as its subalgebras discussed in the following sections, is sometimes more conveniently presented using a *non-local* Dirac fermion basis

$$d^\sigma_{yj}(\mathsf{x})=\frac{\psi_{2j-1}(\mathsf{x})+i\psi_{2j}(\mathsf{x})}{\sqrt{2}}\sim e^{i\phi^\sigma_{yj}(\mathsf{x})+ik^\sigma_{yj}\mathsf{x}}, \tag{3.27}$$

for $j=1,\ldots,8$, where the "Cartan-Weyl" bosons ϕ^σ_{yj} and Fermi momenta k^σ_{yj} are defined by the (non-unimodular) basis transformation:

$$\tilde{\Phi}^\sigma_{yI}=R^j_I\phi^\sigma_{yj},\quad \tilde{k}_I=R^j_Ik_j. \tag{3.28}$$

The electric charge q_j carried by d_j is related to the charge $\tilde{q}_I$ of the E_8 simple roots in (3.19) using the same transformation: $\tilde{q}_I = R_I^j q_j$. The R-transformation obeys $R_I^j R_J^l \delta_{jl} = (K_{E_8})_{IJ}$. The vectors $\boldsymbol{\alpha}_I = (R_I^1, \ldots, R_I^8)$ represent the 8 simple roots of E_8 in Euclidean space, and their entries R_I^j are integers or half-integers. It can be shown that, depending on the choice of the R-matrix, the electric charge vector $\mathbf{q} = (q_1, \ldots, q_8)$ of the non-local Dirac fermions are entry-wise permutations of one of the following vectors:

(i) $(\pm 4, 0, 0, 0, 0, 0, 0, 0)$,

(ii) $(2s_1, 2s_2, 2s_3, 2s_4, 0, 0, 0, 0)$ for $s_{1,2,3,4} = \pm 1$,

(iii) $(3s_1, s_2, s_3, s_4, s_5, s_6, s_7, s_8)$ for $s_{1,\ldots,8} = \pm 1$ and $\prod_{j=1}^8 s_j = -1$.

The possible $\mathbf{q}$ have the same length squared:

$$\nu_{E_8} = |\mathbf{q}|^2 = \sum_{J,J'=1}^{8} \tilde{q}_J \left(K_{E_8}^{-1}\right)^{JJ'} \tilde{q}_{J'} = 16. \tag{3.29}$$

In cases (i) and (ii), the non-local Dirac fermions all have even electric charges, and in case (iii), the fermions all have odd charges. The condition on the product of the s_j in case (iii) ensures the E_8 current operators, which are even combinations of electrons, have even charge. Ignoring the integrated fermions that are gapped out by $\mathcal{H}^f_{\text{intra}}$ (3.22), the low-energy parts of the Lagrangian (3.17) and bare Hamiltonian (3.21) densities, which only

retain the E_8 degrees of freedom, become in the "Cartan-Weyl" basis:

$$\begin{aligned}\mathcal{L}^{E_8} &= \sum_y \sum_{j=1}^{8} \sum_{\sigma=\pm} \frac{1}{4\pi} \sigma \partial_{\mathsf{x}} \phi^{\sigma}_{yj} \partial_{\mathsf{t}} \phi^{\sigma}_{yj} - \mathcal{H}, \\ \mathcal{H}_0^{E_8} &= \frac{\tilde{v}}{4\pi} \sum_y \sum_{j=1}^{8} \sum_{\sigma=\pm} \left(\partial_{\mathsf{x}} \phi^{\sigma}_{yj}\right)^2 .\end{aligned} \tag{3.30}$$

(Recall the full Hamiltonian $\mathcal{H}$ includes $\mathcal{H}_0^{E_8}$ and various to-be-discussed backscattering interactions.) Although this looks identical to the theory of 8 free Dirac fermions, the fermion non-locality dictates that the Hilbert space must be changed so that only the bosonic E_8 current operators (and their combinations) are integral and local. Below we express the 248 E_8 currents $\mathbf{J}_{E_8}$ as fermion bilinears or spinor combinations.

On each wire y and in chiral sector $\sigma = R, L$, the 8 Cartan generators of $(E_8)_1$ in (3.23) are equal to the fermion densities,

$$[\mathtt{H}_{E_8}]_j = \partial_{\mathsf{x}} \phi_j \sim d_j^\dagger d_j, \quad j = 1, \ldots, 8. \tag{3.31}$$

Each one of these is a linear combination of Cartan generators in (3.23). The 240 $(E_8)_1$ roots in (3.24) can be expressed in the Cartan-Weyl basis as

$$[\mathtt{E}_{E_8}(\mathsf{x})]_{\boldsymbol{\alpha}} = e^{i\tilde{\alpha}^I(\tilde{\Phi}_I(\mathsf{x}) + \tilde{k}_I \mathsf{x})} = e^{i\alpha^j(\phi_j(\mathsf{x}) + k_j \mathsf{x})}, \tag{3.32}$$

where the Chevalley and Cartan-Weyl root vectors and momenta are related by $\alpha^j = \tilde{\alpha}^I R_I^j$ and $\tilde{k}_I = R_I^j k_j$. The roots consist of (i) the 112 $SO(16)_1$ roots and (ii) the 128 $SO(16)_1$ even spinors. The $SO(16)_1$ roots are the fermion bilinears $d_{j_1} d_{j_2}$, $d_{j_1}^\dagger d_{j_2}$, $d_{j_1} d_{j_2}^\dagger$, or $d_{j_1}^\dagger d_{j_2}^\dagger$,

for $1 \le j_1 < j_2 \le 8$:

$$[\mathtt{E}_{E_8}(\mathsf{x})]_{\boldsymbol{\alpha}} = e^{i(\pm\phi_{j_1}(\mathsf{x})\pm\phi_{j_2}(\mathsf{x}))+i\alpha^j k_j \mathsf{x}}, \tag{3.33}$$

where the $SO(16)$ root vectors in the Cartan-Weyl basis are the integral vectors $\boldsymbol{\alpha} = \pm\mathbf{e}_{j_1} \pm \mathbf{e}_{j_2}$. Here, $\mathbf{e}_j$ is the unit 8-vector with a 1 in the j-th entry and 0 elsewhere. Together with the Cartan generators, they form the $SO(16)_1$ WZW subalgebra, whose current operators are $J_{pq} = i\psi_p\psi_q$, $1 \le p < q \le 16$ (see (3.27)). The $(E_8)_1$ theory extends $SO(16)_1$ by including its even spinors,

$$[\mathtt{E}_{E_8}(\mathsf{x})]_{\boldsymbol{\alpha}} = e^{i\varepsilon^j(\phi_j(\mathsf{x})+k_j\mathsf{x})/2}. \tag{3.34}$$

The E_8 root vectors $\boldsymbol{\alpha} = \boldsymbol{\varepsilon}/2$ here have half-integer entries $\varepsilon^j/2 = \pm 1/2$, where $\prod_{j=1}^8 \varepsilon^j = +1$. Since the root vectors in (3.33) and (3.34) both have length $|\boldsymbol{\alpha}| = \sqrt{2}$, they all correspond to bosonic vertex operators $e^{i\alpha^j\phi_j}$ with spin $|h| = 1$. Moreover, (3.33) and (3.34) are both local integral operators by construction since they both originate from (3.18) and (3.24), which are even combinations of electrons. The distinction of $SO(16)$ roots and even spinors is artificial and depends on the choice of the Cartan-Weyl basis R_I^a. The $SO(16)$ embedding in E_8 is not unique. In the physical theory, all E_8 bosons, including both $SO(16)$ roots and even spinors, can be rotated into one another by the E_8 symmetry and should be treated impartially.

The "Chevalley" bosons $\tilde{\boldsymbol{\Phi}} = (\tilde{\Phi}_1, \ldots, \tilde{\Phi}_8)$ take values in the torus $\mathbb{R}^8/2\pi\mathbb{Z}^8$: $\tilde{\Phi}_I \equiv \tilde{\Phi}_I + 2\pi n_I$, for any integer n_I. This equivalence may alternatively be described as an invariance

(of operators constructed out of the "Chevalley" bosons) under large gauge transformations. Using the R-transformation, the "Cartan-Weyl" bosons $\boldsymbol{\phi} = (\phi_1, \ldots, \phi_8)$ have the equivalence $\phi_j \equiv \phi_j + 2\pi(R^{-1})^I_j n_I$, where the vector $\mathbf{r} = R^{-1}\mathbf{n}$ lives inside the lattice $\mathcal{R}$ that contains the E_8 root vectors $\boldsymbol{\alpha}$ as primitive lattice vectors. $\mathcal{R}$ consists of vectors $\mathbf{r} = (r_1, \ldots, r_8)$ with all integral or all half-integral entries and even trace $\sum_{j=1}^8 r_j$. A vertex operator $e^{im^j\phi_j}$ is local if and only if it is invariant under all large gauge transformations, i.e., $\mathbf{m}\cdot\mathbf{r}$ is integral. Since the lattice $\mathcal{R}$ is self-dual, $e^{im^j\phi_j}$ is local and integral if and only if $\mathbf{m}$ lives in $\mathcal{R}$. Therefore the "Cartan-Weyl" bosons $\boldsymbol{\phi} = (\phi_1, \ldots, \phi_8)$ live in the compactified torus $T_{E_8} = \mathbb{R}^8/2\pi\mathcal{R}$. If the theory (3.30) were 8 free local Dirac fermions, $\boldsymbol{\phi}$ would live in a different torus $T_{U(1)^8} = \mathbb{R}^8/2\pi\mathbb{Z}^8$. T_{E_8} and $T_{U(1)^8}$ are not related by unimodular transformation and therefore the corresponding Hilbert spaces are different. Consequently, the bosonic $(E_8)_1$ theory is inequivalent to the theory of 8 free (local) Dirac fermions, and the $(E_8)_1$ Hilbert space is spanned by fermion bilinear or even spinor excitations.

The coupled-wire model of the E_8 state is completed by including inter-wire E_8 current backscattering interactions $\mathcal{H}_{\text{inter}}$. Summarizing, the full Hamiltonian density (including for completeness the "integrated" fermion modes) $\mathcal{H} = \mathcal{H}_0 + \mathcal{H}_{\text{intra}} + \mathcal{H}_{\text{inter}}$ consists of the bare Hamiltonian $\mathcal{H}_0$ (3.21), the "integrated" fermion gap-generating term $\mathcal{H}^f_{\text{intra}}$ (3.22) that removes all local fermion excitations below the energy scale $E_g^1 \sim u_{\text{intra}}$, and the E_8

backscattering interactions,

$$\begin{aligned}\mathcal{H}_{\text{inter}} &= u_{\text{inter}} \sum_y \mathbf{J}^R_y \cdot \mathbf{J}^L_{y+1} \\ &= u_{\text{inter}} \sum_y \left(\sum_{j=1}^{8} [\mathtt{H}_{E_8}]^{R\ \dagger}_{y,j} [\mathtt{H}_{E_8}]^L_{y+1,j} + \sum_{\boldsymbol{\alpha}} [\mathtt{E}_{E_8}]^{R\ \dagger}_{y,\boldsymbol{\alpha}} [\mathtt{E}_{E_8}]^L_{y+1,\boldsymbol{\alpha}} \right) \\ &= u_{\text{inter}} \sum_y \left[\sum_{j=1}^{8} \partial_{\mathrm{x}} \phi^R_{y,j} \partial_{\mathrm{x}} \phi^L_{y+1,j} - \sum_{\boldsymbol{\alpha}} \cos\left(\boldsymbol{\alpha} \cdot \boldsymbol{\theta}_{y+1/2}\right) \right].\end{aligned} \tag{3.35}$$

The interactions in (3.35) are analogous to those in the $O(N)$ Gross-Neveu model [GN74, SZT16]. The entries of $\boldsymbol{\theta}_{y+1/2} = (\theta_{y+1/2,1}, \ldots, \theta_{y+1/2,8})$ are the sine-Gordon angle variables $\theta_{y+1/2,j} = \phi^R_{y,j} - \phi^L_{y+1,j}$, and the sum over $\boldsymbol{\alpha}$ ranges over all 240 roots of E_8. Like $\mathcal{H}_0$ and $\mathcal{H}^f_{\text{intra}}$, the inter-wire interactions are combinations of integral products of electron operators because $[\mathtt{H}_{E_8}]^\sigma_{ya}$ and $[\mathtt{E}_{E_8}]^\sigma_{y\boldsymbol{\alpha}}$ are. Because the roots $E^{R\dagger}_{\boldsymbol{\alpha}}$ and $E^L_{\boldsymbol{\alpha}}$ have opposite electric charge, $\mathcal{H}_{\text{inter}}$ conserves charge. The last identity of (3.35) holds when the Fermi momenta appearing in the E_8 roots (3.24), (3.33) and (3.34) cancel, i.e., $k^R_{y,j} = k^L_{y+1,j}$ in the "Cartan-Weyl" basis (or equivalently $\tilde{k}^R_{y,I} = \tilde{k}^L_{y+1,I}$ in the "Chevalley" basis). These momentum conservation conditions of $\mathcal{H}_{\text{inter}}$ and the ones from $\mathcal{H}^f_{\text{intra}}$, $\tilde{k}^R_{y,n+8} = \tilde{k}^L_{y,n+8}$ for $n = 1, 2, 3$, require the electron bare Fermi momenta $k_{F,a}$ (see (3.7)) to take a particular form:

$$k_{F,a} = \frac{1}{2} \frac{eBd}{\hbar c} \sum_{J,J'=1}^{8} \left(U^{++}_{Ja} + U^{+-}_{Ja}\right) \left(K^{-1}_{E8}\right)^{JJ'} \tilde{q}_{J'}, \tag{3.36}$$

where U is the unimodular matrix (3.16) that defines the E_8 simple roots, and $\tilde{q}_J$ are the electric charges (3.19) of the simple roots. The momentum conservation condition (3.36) also guarantees that the filling number (3.8) agrees with (3.29).

With $u_{\text{inter}} > 0$, the sine-Gordon potentials in (3.35) are marginally relevant in the renormalization group sense at the 1-loop level due to the E_8 current OPE (3.26) and generate a mass gap [LQHT19]. The potentials simultaneously pin the angle variables $\boldsymbol{\theta}_{y+1/2} = (\theta_{y+1/2,1}, \ldots, \theta_{y+1/2,8})$. The ground state expectation value $\langle \boldsymbol{\theta}_{y+1/2} \rangle$ sits inside the lattice $2\pi\mathcal{R}$ so that $\langle \boldsymbol{\alpha} \cdot \boldsymbol{\theta}_{y+1/2} \rangle$ are integers multiple of 2π, for all E_8 roots, and minimize the sine-gordon potentials. The angle variables can be shifted by the large gauge transformation $\phi^R_{y,j} \to \phi^R_{y,j} + 2\pi r_j$ for any lattice vector $\mathbf{r}$ in $\mathcal{R}$. Therefore, up to the large gauge transformation, there is a unique potential minimum and ground state. The inter-wire E_8 current backscattering strength sets the finite energy scale $E^0_g \sim u_{\text{inter}}$ of bulk excitations of the E_8 state. Throughout this paper, we assume the excitation energy gap is much smaller than the fermion gap $E^1_g \sim u_{\text{intra}}$. For the E_8 quantum Hall state, all excitations between E^0_g and E^1_g are bosonic even combinations of electrons.

If the coupled-wire model is defined on a closed torus where $\mathsf{x} \equiv \mathsf{x} + l$ and $y \equiv y + \mathsf{L}$ are both periodic, the summation of the inter-wire interactions in (3.35) runs over all wires $y = 1, \ldots, \mathsf{L}$. The unique ground state is separated from all excitations by the bulk gap $E^0_g \sim u_{\text{inter}}$. On the other hand, if the model is defined on a cylinder where the y direction is open, the summation in (3.35) runs from $y = 1, \ldots, \mathsf{L} - 1$. $\mathcal{H}_{\text{inter}}$ leaves behind the gapless left (right) propagating chiral E_8 level 1 WZW CFTs on the open boundaries at $y = 1$ (resp. $y = \mathsf{L}$). All low-energy edge excitations are bosonic and have even electric charge.

This can in principle be experimentally verified by shot-noise tunneling at a quantum point contact.

Lastly, we remark that certain sub-collections of sine-Gordon potentials in the inter-wire interaction (3.35) are sufficient to introduce the bulk excitation energy gap. For example, instead of backscattering the entire E_8 current algebra, a gap opens if only the eight E_8 simple roots are back-scattered, $\sum_{I=1}^{8} \cos\big(\boldsymbol{\alpha}_I \cdot \boldsymbol{\theta}_{y+1/2}\big)$. This is because the eight independent terms obey Haldane's nullity condition [Hal95], $\big[\boldsymbol{\alpha}_I \cdot \boldsymbol{\theta}_{y+1/2}, \boldsymbol{\alpha}_J \cdot \boldsymbol{\theta}_{y+1/2}\big] = 0$, and completely gap the eight-component boson theory. Alternatively, instead of summing over all the 240 E_8 roots $\boldsymbol{\alpha}$ in (3.35), one can restrict the sum to include only the 112 $SO(16)$ roots. Despite only involving the $SO(16)_1$ currents, the model will still leave behind the chiral E_8 level 1 WZW CFTs on the edges, and the quantum Hall state constructed will still carry the same short-ranged entangled $(E_8)_1$ topological order, i.e., an absence of fractionalization. This is because the even spinors of $SO(16)_1$ are still local operators that are integral combinations of electrons and extend $SO(16)_1$ to $(E_8)_1$. In other words, the even spinors are "condensed" in the anyon condensation picture [BS09, Bur18]. The $SO(16)_1$ topological order is killed. This is because the odd spinor and odd fermion excitations, which carry mutual semionic braiding statistics with the even spinor, are confined by the locality of the even spinor. Moreover, the $SO(16)_1$ sine-Gordon potentials pin the angle variables $\theta_{y+1/2,j}$ to the same minimum since the large gauge transformation $\theta_{y+1/2,j} \equiv \theta_{y+1/2,j} + 2\pi r_j$, for any $\mathbf{r}$ in $\mathcal{R}$, are still set by the locality of the $(E_8)_1$ current operators. Therefore, the ground state remains unique and is identical to that of the $(E_8)_1$ state.

3.3 Fractional bosonic states

We now present a family of bosonic fractional quantum Hall (bFQH) states that "partially fill" this E_8 state. These bFQH states can be viewed as bosonic analogues of the fermionic fractional quantum Hall (fFQH) states that occur when the Landau level is partially filled. Examples of fFQH states include the Abelian Laughlin states [Lau83] at filling $\nu = 1/m$, for m odd, and their particle-hole conjugates at filling $\nu = 1 - 1/m$, as well as the non-Abelian Moore-Read Pfaffian state [MR91b, GWW91] at filling $\nu = 1/2$ and its particle-hole conjugate, the anti-Pfaffian state [LHR07, LRNF07]. These states are topologically ordered and long-range entangled. They support fractional quasiparticle excitations that are not local integral combinations of electrons and that must exist non-locally in conjugate pairs (or multiplets). These excitations can carry fractional electric charge and exhibit anyonic (i.e., not bosonic or fermionic) statistics.

The bFQH states constructed in this section are also topologically ordered and support fractionalization. Like the parent E_8 state, the bFQH states differ from the fFQH states by the presence of a fermionic energy gap E_g^1, below which all local bulk and edge excitations are even (i.e., bosonic) combinations of electrons. Excitations of the bFQH states have a minimum energy gap $0 \leq E_g^0 < E_g^1$ above the ground state energy (taken here to be zero). As long as the energy of an excited state is below the fermion gap E_g^1, the excitation must have the same fermion parity as the ground state. This requirement excludes the filled Landau level, the Laughlin states, and the Pfaffian states from our constructions because

the gapless edge of these fermionic states (where $E_g^0 = 0$) support odd-electron excitations with arbitrarily small energy in the thermodynamic limit.

There are two related senses in which the bFQH states considered in this section "partially fill" the E_8 state. The first is simply that filling fractions of the bFQH states are less than or equal to the E_8 filling fraction $\nu_{E_8} = 16$. The second is that the bFQH edge states are described by WZW theories with a KM symmetry $\mathcal{G}$ that is a subalgebra of $(E_8)_1$ symmetry. This $\mathcal{G}$ symmetry is generated by KM current operators $J^i_{\mathcal{G}}$, which are even combinations of electrons and together form a subcollection (of linear combinations) of the E_8 currents. Similar to the E_8 algebra (c.f. 3.26), the $\mathcal{G}$ subalgebra has a closed OPE (up to non-singular terms),

$$J^i_{\mathcal{G}}(z) J^j_{\mathcal{G}}(w) = \frac{k\delta^{ij}}{(z-w)^2} + \frac{if^{ijk}}{z-w} J^k_{\mathcal{G}}(w) + \ldots, \tag{3.37}$$

where the integer k, known as the level of the WZW algebra, is 1 unless specified otherwise, f^{ijk} are the structure constants of the Lie algebra of $\mathcal{G}$, and $z = e^{2\pi(\tilde{v}\tau + ix)/l}$ (similarly for w) is the complex spacetime coordinate along the edge. Since $\mathcal{G}$ sits inside E_8, the filling number and central charge that determine the electric and thermal transport (3.2) of the corresponding bFQH state must be less than or equal to the E_8 values:

$$\nu \leq \nu_{E_8} = 16, \quad c \leq c_{E_8} = 8. \tag{3.38}$$

Moreover, we restrict our focus to subalgebras $\mathcal{G}$ whose "particle-hole conjugate" coset $E_8/\mathcal{G}$ is also a subalgebra of E_8. In other words, the edge WZW theory $\mathcal{G}$ of the bFQH state must

be one of the two components of a bipartite conformal embedding into E_8,

$$\mathcal{G}_A \times \mathcal{G}_B \subseteq E_8. \tag{3.39}$$

This implies the energy momentum tensors combine as $T_{\mathcal{G}_A} + T_{\mathcal{G}_B} = T_{E_8}$, and the two sectors decouple from each other so that the OPE of currents belonging to the A and B subalgebras $J_A(z)J_B(w)$ are non-singular. Eq. (3.39) implies the particle-hole pair have conjugate electrical and thermal transport:

$$\nu_A + \nu_B = 16, \quad c_A + c_B = 8. \tag{3.40}$$

These relations generalize those in the lowest Landau level of electrons, $\nu_X + \nu_{\bar{X}} = 1$ and $c_X + c_{\bar{X}} = 1$, where X is a fFQH state, $\bar{X}$ is its particle-hole conjugate, and the filling number and central charge of the filled lowest Landau level are $\nu_{\mathrm{LLL}} = c_{\mathrm{LLL}} = 1$.

In this paper, we consider the following (bipartite) conformal embeddings of E_8 at level 1:

$$\mathcal{G}_A \times \mathcal{G}_B = \begin{cases} SU(3) \times E_6, \\ SU(2) \times E_7, \\ SU(5) \times SU(5), \\ SO(M) \times SO(16-M), \\ G_2 \times F_4, \\ U(1)_8 \times SU(8), \\ SU(2)_4 \times Sp(8), \end{cases} \tag{3.41}$$

for $M = 1, \ldots, 8$, where all the KM algebras are level 1 except the two orbifold theories, $U(1)_8 = SU(2)_1/\mathbb{Z}_2$ and $SU(2)_4 = SU(3)_1/\mathbb{Z}_2$. The exceptional E_6 and E_7 algebras at level 1 and their particle-hole conjugates, $SU(3)_1$ and $SU(2)_1$, the D-series $D_r = SO(2r)$ at level 1 for $r = 1, \ldots, 7$, and the orbifold theory $SU(8)_1 = (E_7)_1/\mathbb{Z}_2$ and its particle-hole conjugate $U(1)_8 = SU(2)_1/\mathbb{Z}_2$ are Abelian states, where all anyonic excitations have quantum dimension $d = 1$ and exhibit single-channel fusion rules. The B-series $B_r = SO(2r+1)$ at level 1, for $r = 1, \ldots, 6$, have non-Abelian Ising topological orders and support Ising anyons [NW96] σ with quantum dimension $d_\sigma = \sqrt{2}$ and the two-channel fusion rule $\sigma \times \sigma = 1 + \psi$. The $Sp(8)_1 = (E_6)_1/\mathbb{Z}_2$ orbifold theory and its particle-hole conjugate $SU(2)_4 = SU(3)_1/\mathbb{Z}_2$ have non-Abelian topological order and host metaplectic anyons [HNW13] Σ with quantum dimension $d_\Sigma = \sqrt{3}$ and the multi-channel fusion rule $\Sigma \times \Sigma = 1 + E + E^2$. The exceptional G_2 and F_4 algebras at level 1 host non-Abelian

Fibonacci anyons [SB01], whose fusion rule $\tau \times \tau = 1 + \tau$ and non-Abelian braiding allow for universal topological quantum computation [NSS+08b].

Given a conformal embedding $\mathcal{G}_A \times \mathcal{G}_B \subseteq E_8$, the $\mathcal{G}_A$ bFQH state can be constructed using the Hamiltonian,

$$\mathcal{H}[\mathcal{G}_A] = \mathcal{H}_0 + \mathcal{H}^f_{\text{intra}} + \mathcal{H}^B_{\text{intra}} + \mathcal{H}^A_{\text{inter}}, \tag{3.42}$$

that only back-scatters the $\mathcal{G}_A$ currents between adjacent wires by

$$\mathcal{H}^A_{\text{inter}} = u_{\text{inter}} \sum_y \mathbf{J}^R_{y,A} \cdot \mathbf{J}^L_{y+1,A}, \tag{3.43}$$

and backscatters the $\mathcal{G}_B$ currents within each wire by

$$\mathcal{H}^B_{\text{intra}} = u_{\text{intra}} \sum_y \mathbf{J}^R_{y,B} \cdot \mathbf{J}^L_{y,B}. \tag{3.44}$$

In an open cylinder geometry of L wires, while (3.44) sums over all wires, the inter-wire interaction sum in (3.43) only involves $y = 1, \ldots, \mathsf{L}-1$. The model gaps all bulk excitations, but leaves behind chiral $\mathcal{G}_A$ WZW CFTs on the boundary edges. The particle-hole conjugate $\mathcal{G}_B$ phase can be constructed similarly by exchanging the A and B sectors.

In the following, we construct (i) the conformal embeddings in (3.41) and present the (ii) the charge assignments of the KM currents and primary fields of the respective WZW theories. Similar to the E_8 state, the coupled wire models are exactly-solvable when the backscattering interactions preserve momentum conservation. In each model studied below,

we detail (iii) the the electron Fermi momenta that ensures momentum along the wire is conserved and connect the edge electric transport $\sigma_{xy} = \nu e^2/h$ to the bulk electron filling number $\nu = N_e/N_B$. We begin with the $SU(3) \times E_6$ decomposition of E_8; this construction is then straightforwardly generalized to all other the Abelian states in (3.41). After this, we then construct non-Abelian bFQH states of E_8 with Ising, Fibonacci, and metaplectic topological orders.

3.3.1 Abelian states

The Abelian $\mathbb{Z}_3$ $SU(3)$ and E_6 states

We begin with the $\mathcal{G}_A \times \mathcal{G}_B = SU(3) \times E_6$ decomposition of the E_8 WZW algebra at level 1. We present in detail the inequivalent $SU(3) \times E_6$ conformal embeddings in E_8 and the corresponding $SU(3)_1$ and $(E_6)_1$ bosonic fractional quantum Hall states. This decomposition demonstrates most features that appear in general Abelian bipartitions $\mathcal{G}_A \times \mathcal{G}_B \subseteq E_8$ using simpy-laced WZW algebras $\mathcal{G}_{A/B}$. We rely on the Cartan-Weyl representation of E_8 using the eight non-local Dirac fermions $d^\sigma_{yj}(\mathsf{x}) = e^{i\phi^\sigma_{yj}(\mathsf{x}) + ik^\sigma_{yj}\mathsf{x}}$, for $j = 1, \ldots, 8$, defined in (3.27). Recall the chiral E_8 algebra is generated by the eight Cartan generators $\partial_\mathsf{x}\phi_j$ in (3.31) and the 240 roots $e^{i\alpha^j(\phi_j(\mathsf{x}) + k_j\mathsf{x})}$ in (3.32). (The wire index y and chiral sector label $\sigma = R, L$ are fixed and suppressed.) The E_8 root vectors $\boldsymbol{\alpha} = (\alpha^1, \ldots, \alpha^8)$ all have length $|\boldsymbol{\alpha}| = \sqrt{2}$. The set of E_8 root vectors Δ_{E_8} consists of 112 $SO(16)$ root vectors, where $\alpha^j = 0, \pm 1$, and 128 $SO(16)$ even spinors, where $\alpha^j = \varepsilon^j/2 = \pm 1/2$ with $\prod_{j=1}^8 \varepsilon^j = +1$. An $SU(3) \times E_6$

embedding in E_8 is a particular assignment of $SU(3)$ and E_6 current operators inside the E_8 algebra.

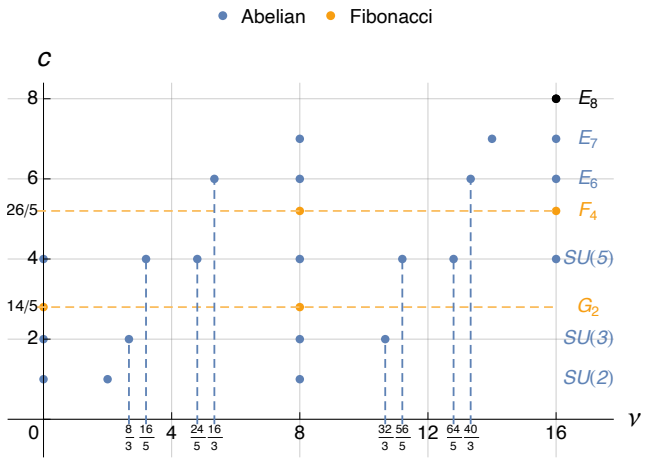

Figure 3.3: The filling numbers ν and central charges c of bosonic fractional quantum Hall (bFQH) states involving the exceptional Lie algebras G_2, F_4, $E_{6,7,8}$ as well as $A_4 = SU(5)$.

We start by choosing a particular subset of E_8 current operators that generate an $SU(3)$ subalgebra. The $SU(3)$ Lie algebra has rank 2 and dimension 8. It is generated by 2 Cartan generators and 6 roots. It suffices to choose, from the E_8 root lattice, 2 simple root vectors $\boldsymbol{\alpha}_1$ and $\boldsymbol{\alpha}_2$ of $SU(3)$, so that the inner products $K_{IJ} = \boldsymbol{\alpha}_I \cdot \boldsymbol{\alpha}_J$ are the entries of the $SU(3)$ Cartan matrix,

$$K_{SU(3)} = (K_{IJ})_{2\times 2} = \begin{pmatrix} 2 & -1 \\ -1 & 2 \end{pmatrix}. \tag{3.45}$$

Roots $\boldsymbol{\alpha}_1$ and $\boldsymbol{\alpha}_2$ generate the $SU(3)$ root lattice $\Delta_{SU(3)}$, which consists of the 6 root vectors $\boldsymbol{\alpha}_{SU(3)} = \pm\boldsymbol{\alpha}_1$, $\pm\boldsymbol{\alpha}_2$ and $\pm(\boldsymbol{\alpha}_1 + \boldsymbol{\alpha}_2)$. It can be shown from properties of a root system that each of these roots is an E_8 root vector. For example, $\boldsymbol{\alpha}_1 + \boldsymbol{\alpha}_2 = \boldsymbol{\alpha}_1 - 2\left(\frac{\boldsymbol{\alpha}_2\cdot\boldsymbol{\alpha}_1}{\boldsymbol{\alpha}_2\cdot\boldsymbol{\alpha}_2}\right)\boldsymbol{\alpha}_2$ is

the reflection of $\boldsymbol{\alpha}_1$ on the hyperplane normal to $\boldsymbol{\alpha}_2$. It lies in the E_8 root lattice because a root system, in general, is invariant under the reflection about the hyperplane normal to any root vector.

In general, the 6 root operators of $SU(3)$ are the vertex operators $\left[\mathtt{E}_{SU(3)}(\mathtt{x})\right]_{\boldsymbol{\alpha}_{SU(3)}} = e^{i\alpha^j_{SU(3)}(\phi_j(\mathtt{x})+k_j\mathtt{x})}$, corresponding to the 6 $SU(3)$ root vectors. The 2 Cartan generators of $SU(3)$ are $\left[\mathtt{H}_{SU(3)}(\mathtt{x})\right]_a = \beta^j_a\partial_{\mathtt{x}}\phi_j$, for $a = 1, 2$, where $\boldsymbol{\beta}_1, \boldsymbol{\beta}_2$ is an orthonormal basis of the space spanned by $\boldsymbol{\alpha}_1, \boldsymbol{\alpha}_2$. We take $\boldsymbol{\beta}_1 = \boldsymbol{\alpha}_1/\sqrt{2}$ and $\boldsymbol{\beta}_2 = (\boldsymbol{\alpha}_1 + 2\boldsymbol{\alpha}_2)/\sqrt{6}$. The Cartan generators and the real and imaginary parts of the root operators are the current operators $J_{SU(3)}$ that generate the (real) $SU(3)$ WZW algebra at level 1 and obey the OPE (3.37).

We choose the 2 simple root vectors of $SU(3)$ to be

$$\boldsymbol{\alpha}_1 = \mathbf{e}_1 - \mathbf{e}_2, \quad \boldsymbol{\alpha}_2 = \mathbf{e}_2 - \mathbf{e}_3. \tag{3.46}$$

These simple roots define the rows of a 2×8 matrix $A_{SU(3)}$. The root operators of $SU(3)$ are then

$$\left[\mathtt{E}_{SU(3)}(\mathtt{x})\right]_{\boldsymbol{\alpha}_{SU(3)}} = e^{i(\phi_a(\mathtt{x})-\phi_b(\mathtt{x}))+i(k_a-k_b)\mathtt{x}}, \tag{3.47}$$

where $\boldsymbol{\alpha}_{SU(3)} = \mathbf{e}_a - \mathbf{e}_b$ are the 6 $SU(3)$ roots, and a, b are distinct integers that range from 1 to 3. Given the simple roots (3.46), the Cartan generators are

$$\begin{aligned}\left[\mathtt{H}_{SU(3)}(\mathtt{x})\right]_1 &= \frac{\partial_{\mathtt{x}}\phi_1 - \partial_{\mathtt{x}}\phi_2}{\sqrt{2}},\\ \left[\mathtt{H}_{SU(3)}(\mathtt{x})\right]_2 &= \frac{\partial_{\mathtt{x}}\phi_1 + \partial_{\mathtt{x}}\phi_2 - 2\partial_{\mathtt{x}}\phi_3}{\sqrt{6}}.\end{aligned} \tag{3.48}$$

It can be shown that any alternative choice of simple root vectors $\boldsymbol{\alpha}'_{1,2}$ of $SU(3)$ inside the E_8 root lattice is related to the one above, $\boldsymbol{\alpha}'_J = w\boldsymbol{\alpha}_J$, by a rotation or reflection w inside the automorphism group of the E_8 root lattice Δ_{E_8},

$$\mathrm{Aut}(E_8) = \{w \in O(8) : w(\Delta_{E_8}) = \Delta_{E_8}\}. \tag{3.49}$$

This automorphism group is identical to the Weyl group [CS13], $W(E_8)$ of E_8 that is generated by reflections about hyperplanes perpendicular to the E_8 root vectors. Consequently, all $SU(3)$ root embeddings $\Delta_{SU(3)} \subseteq \Delta_{E_8}$ are equivalent up to the Weyl symmetry.

The E_6 sector is the orthogonal complement of $SU(3)$ in E_8. The E_6 Lie algebra has rank 6 and dimension 78. It is generated by 6 Cartan generators and 72 roots. The Cartan generators $[\mathtt{H}_{E_6}(\mathtt{x})]_b = \gamma_b^j \partial_{\mathtt{x}}\phi_j$, for $b = 1, \ldots, 6$, can be chosen using an orthonormal basis $\boldsymbol{\gamma}_1, \ldots, \boldsymbol{\gamma}_6$ of the subspace perpendicular to the $SU(3)$ root system $\Delta_{SU(3)}$. The E_6 roots,

$$\left[\mathtt{E}_{E_6}(\mathtt{x})\right]_{\boldsymbol{\alpha}_{E_6}} = e^{i\alpha^j_{E_6}(\phi_j(\mathtt{x}) + k_j\mathtt{x})}, \tag{3.50}$$

are the E_8 roots whose root vectors are perpendicular to those in $SU(3)$: $\boldsymbol{\alpha}_{E_6} \cdot \boldsymbol{\alpha}_{SU(3)} = 0$. Specifically, the set of E_6 root vectors Δ_{E_6} consists of (i) 40 integral vectors of the form $\boldsymbol{\alpha}_{E_6} = (0, 0, 0, \alpha^4, \ldots, \alpha^8)$, where two of $\alpha^{4,\ldots,8}$ are ± 1 and the rest are 0, and (ii) 32 half integral vectors $\boldsymbol{\alpha}_{E_6} = (\varepsilon^1, \ldots, \varepsilon^8)/2$ where $\varepsilon^j = \pm 1$, $\varepsilon^1 = \varepsilon^2 = \varepsilon^3$ and $\prod_{j=1}^{8} \varepsilon^j = +1$. The E_6 root system Δ_{E_6} can be generated by the 6 simple root vectors $\boldsymbol{\alpha}_{J=1,\ldots,6}$ that are the rows of the following matrix,

$$A_{E_6} = \begin{pmatrix} & & & 1 & -1 & & & \\ & & & & 1 & -1 & & \\ & & & & & 1 & -1 & \\ & & & & & & 1 & -1 \\ \frac{1}{2} & \frac{1}{2} & \frac{1}{2} & -\frac{1}{2} & -\frac{1}{2} & -\frac{1}{2} & -\frac{1}{2} & \frac{1}{2} \\ & & & & & & 1 & 1 \end{pmatrix}. \tag{3.51}$$

The inner products $K_{IJ} = \boldsymbol{\alpha}_I \cdot \boldsymbol{\alpha}_J$ are identical to the entries of the Cartan matrix of E_6

$$K_{E_6} = A_{E_6} A_{E_6}^T = \begin{pmatrix} 2 & -1 & & & & & \\ -1 & 2 & -1 & & & & \\ & -1 & 2 & -1 & & & -1 \\ & & -1 & 2 & -1 & & \\ & & & -1 & 2 & & \\ & & -1 & & & & 2 \end{pmatrix}. \tag{3.52}$$

The Cartan generators $[\mathtt{H}_{E_6}]_{b=1,\dots,6}$ and the real and imaginary parts of the root operators $[\mathtt{E}_{E_6}]_{\boldsymbol{\alpha}_{E_6}}$ are the current operators J_{E_6} that generate the (real) E_6 WZW algebra at level 1 and obey the OPE (3.37). Since the $SU(3)$ and E_6 root systems are orthogonal, the current operators have non-singular mutual OPE $J_{SU(3)}(z)J_{E_6}(w)$ and the current modes mutually commute. Because the $SU(3)$ (E_6) theory is generated by 2 (resp. 6) independent bosonized variables, their central charges are $c_{SU(3)_1} = 2$ and $c_{(E_6)_1} = 6$. Not only do the central charges add up to $c_{(E_8)_1} = 8$, the Sugawara energy-momentum tensors obey $T_{SU(3)_1} + T_{(E_6)_1} = T_{(E_8)_1}$. Equivalently, the two CFTs are $(E_8)_1$ coset duals of each other,

$$SU(3)_1 = \frac{(E_8)_1}{(E_6)_1}, \quad (E_6)_1 = \frac{(E_8)_1}{SU(3)_1}. \tag{3.53}$$

Moreover, as all $SU(3)$ root embeddings $\Delta_{SU(3)} \subseteq \Delta_{E_8}$ are equivalent up to the Weyl symmetry (3.49), the same equivalence holds for the E_6 root embeddings $\Delta_{E_6} = \Delta^{\perp}_{SU(3)}$.

Having completed the definition of the conformal embedding $SU(3) \times E_6 \subseteq E_8$, the $SU(3)$ and E_6 level 1 quantum Hall states can be constructed using the coupled-wire Hamiltonians in (3.42). For example, the $SU(3)_1$ model Hamiltonian $\mathcal{H}[SU(3)]$ contains the inter-wire (intra-wire) backscattering of $SU(3)$ (resp. E_6) currents:

$$\begin{aligned}
\mathcal{H}^{SU(3)}_{\text{inter}} &= u_{\text{inter}} \sum_y \left[\sum_{a=1}^{2} \left[\mathtt{H}_{SU(3)}\right]^{R\ \dagger}_{y,a} \left[\mathtt{H}_{SU(3)}\right]^{L}_{y+1,a} - \sum_{\boldsymbol{\alpha}_{SU(3)}} \cos\left(\boldsymbol{\alpha}_{SU(3)} \cdot \boldsymbol{\theta}_{y+1/2}\right) \right], \\
\mathcal{H}^{E_6}_{\text{intra}} &= u_{\text{intra}} \sum_y \left[\sum_{b=1}^{6} \left[\mathtt{H}_{E_6}\right]^{R\ \dagger}_{y,b} \left[\mathtt{H}_{E_6}\right]^{L}_{y,b} - \sum_{\boldsymbol{\alpha}_{E_6}} \cos\left(\boldsymbol{\alpha}_{E_6} \cdot \boldsymbol{\theta}_{y}\right) \right],
\end{aligned} \tag{3.54}$$

where the entries of $\boldsymbol{\theta}_{y+1/2} = (\theta_{y+1/2,1}, \ldots, \theta_{y+1/2,8})$ and $\boldsymbol{\theta}_y = (\theta_{y,1}, \ldots, \theta_{y,8})$ are the inter-wire and intra-wire sine-Gordon variables $\theta_{y+1/2,j} = \phi^R_{y,j} - \phi^L_{y+1,j}$ and $\theta_{y,j} = \phi^R_{y,j} - \phi^L_{y,j}$, respectively. With the density interactions in $\mathcal{H}_0 + \mathcal{H}^f_{\text{intra}}$ that give rise to the conformal E_8 fixed point, the current backscattering interactions in (3.54) are marginally relevant in the RG sense if $u_{\text{inter/intra}} > 0$. The sums of roots $\boldsymbol{\alpha}_{SU(3)}$ and $\boldsymbol{\alpha}_{E_6}$ in the sine-Gordon potentials in (3.54) can be restricted to only include the simple roots $\boldsymbol{\alpha}^{SU(3)}_{1,2}$ in (3.46) for the $SU(3)$ sector and $\boldsymbol{\alpha}^{E_6}_{J=1,\ldots,6}$ in (3.51) for the E_6 sector. This restricted set of sine-Gordon potentials pins the ground state expectation values of the angle variables $\Theta^{SU(3)}_{y+1/2,I=1,2} = \boldsymbol{\alpha}^{SU(3)}_I \cdot \boldsymbol{\theta}_{y+1/2}$ and $\Theta^{E_6}_{y,J=1,\ldots,6} = \boldsymbol{\alpha}^{E_6}_J \cdot \boldsymbol{\theta}_y$ to lie at an integral multiple of 2π. Since all roots are integral combinations of simple ones, the other sine-Gordon potentials in (3.54) with non-simple roots do not compete, as they share the same minima. On a closed torus geometry, the angle variables $\Theta^{SU(3)}_{y+1/2,I=1,2}$ and $\Theta^{E_6}_{y,J=1,\ldots,6}$ form a maximal set of independent commuting bosonized operators and therefore the sine-Gordon potentials in (3.54) introduce a finite bulk excitation energy gap.

Unlike the E_8 quantum Hall state, $\mathcal{H}[SU(3)]$ has three degenerate ground states on a torus. The bosonized variables are compactified and identified by large gauge transformations $\phi^\sigma_{y,j} \equiv \phi^\sigma_{y,j} + 2\pi r^\sigma_{y,j}$, where $\mathbf{r}^\sigma_y = (r^\sigma_{y,1}, \ldots, r^\sigma_{y,8})$ is a vector inside the lattice $\mathcal{R} = \text{span}_{\mathbb{Z}}(\Delta_{E_8})$ generated by the E_8 roots. Up to large gauge transformations, all ground state expectation values $\left\langle \Theta^{E_6}_{y,J=1,\ldots,6} \right\rangle$ that minimize $\mathcal{H}^{E_6}_{\text{intra}}$ are equivalent. On the other hand, there are three gauge inequivalent sets of ground state expectation values $\left\langle \Theta^{SU(3)}_{y+1/2,I=1,2} \right\rangle$ that minimize

$\mathcal{H}_{\text{inter}}^{SU(3)}$. They correspond to the three anyon classes of bulk quasiparticle excitations,

$$\mathbb{Z}_3 = \left\{1, \mathcal{E}, \overline{\mathcal{E}}\right\}, \tag{3.55}$$

and the three primary fields in the chiral edge CFTs when the model is defined on an open cylinder with boundaries. Non-trivial primary fields and anyons $\mathcal{E}$ and $\overline{\mathcal{E}}$ cannot appear alone and must come in conjugate pairs $\mathcal{E} \times \overline{\mathcal{E}} = 1$, triplets $\mathcal{E} \times \mathcal{E} \times \mathcal{E} = \overline{\mathcal{E}} \times \overline{\mathcal{E}} \times \overline{\mathcal{E}} = 1$, or any multiplets that fuse to the trivial sector 1. On the chiral edge, each non-trivial primary field $\mathcal{E}$ is a super-selection sector of vertex operators $\mathcal{E}^p$ that rotate irreducibly under the $SU(3)$ WZW algebra. Specifically, $\mathcal{E}$ is spanned by three non-local fields

$$\mathcal{E} = \text{span}\left\{e^{i(\phi_1+\phi_2-2\phi_3)/3}, e^{i(\phi_1-2\phi_2+\phi_3)/3}, e^{i(-2\phi_1+\phi_2+\phi_3)/3}\right\}. \tag{3.56}$$

Fields inside the same super-selection sector obey the current OPE

$$J_g(z)\mathcal{E}^p(w) = \frac{\rho(g)_q^p}{z-w}\mathcal{E}^q(w) + \ldots, \tag{3.57}$$

where g is a Lie algebra element, $J_g(z)$ is its corresponding WZW current operator, and $\rho(g)$ is a matrix representation of g. For example, the $SU(3)$ root operator $[\mathtt{E}_{SU(3)}(z)]_{\boldsymbol{\alpha}_1} =$

$e^{i(\phi_1(z)-\phi_2(z))}$ rotates $e^{i\mathbf{m}\cdot\boldsymbol{\phi}} = e^{i(-2\phi_1+\phi_2+\phi_3)/3}$ into

$$\begin{aligned}\left[\mathtt{E}_{SU(3)}(z)\right]_{\boldsymbol{\alpha}_1} e^{i\mathbf{m}\cdot\boldsymbol{\phi}(w)} &= e^{i(\boldsymbol{\alpha}_1+\mathbf{m})\cdot\boldsymbol{\phi}(w)-\langle\boldsymbol{\alpha}_1\cdot\boldsymbol{\phi}(z),\mathbf{m}\cdot\phi(w)\rangle+\ldots} \\ &= e^{i(\phi_1(w)-2\phi_2(w)+\phi_3(w))/3-\log(z-w)+\ldots} \\ &\propto \frac{1}{z-w} e^{i(\phi_1(w)-2\phi_2(w)+\phi_3(w))/3}+\ldots\end{aligned} \tag{3.58}$$

(up to non-singular terms and oscillations factors involving $e^{ik_f x}$) using the correlation $\langle\phi_i(z)\phi_j(w)\rangle = -\delta_{ij}\log(z-w)+\ldots$. The exact constant phase in "$\propto$" depends on the non-singular pieces in the above correlator that guarantee the fermion fields $d^j = e^{i\phi_j}$ mutually anti-commute. These phases are unimportant in this paper and will be omitted. The primary super-sector $\mathcal{E}$ transforms under the fundamental 3D irreducible representation of $SU(3)$, while its conjugate sector $\overline{\mathcal{E}} = \mathcal{E}^\dagger$ transforms under the conjugate representation. They both carry fractional spin (i.e., conformal scaling dimensions) $h_{\mathcal{E}} = h_{\overline{\mathcal{E}}} = 1/3$. Fields within the same primary sector differ from each other by the local $SU(3)$ currents, which are integral combinations of electrons. On the other hand, fields belonging to different primary sectors are not related by any local integral product of electrons.

The particle-hole conjugate coupled-wire model $\mathcal{H}[E_6]$ can be constructed by reversing the role of $SU(3)$ and E_6 so that the former (latter) is gapped by an intra-wire (inter-wire) backscattering interaction. The E_6 quantum Hall state also has three degenerate ground states on a closed torus geometry. They correspond to the three anyon classes of bulk quasiparticle excitations and primary field super-selection sectors $1, \mathcal{E}, \overline{\mathcal{E}}$ on the chiral edge

CFT. Specifically, the primary super-sector $\mathcal{E}$ is spanned by 27 non-local fields

$$\begin{aligned}\mathcal{E} = \text{span} &\left\{ e^{i2(\phi_1+\phi_2+\phi_3)/3} \right\} \\ &\cup \left\{ e^{i(\phi_1+\phi_2+\phi_3)/6+\sum_{j=4}^{8}\varepsilon^j\phi_j/2} \right\}_{\varepsilon^{j=4,\ldots,8}=\pm 1, \prod_{j=4}^{8}\varepsilon^j=-1} \\ &\cup \left\{ e^{-i(\phi_1+\phi_2+\phi_3)/3\pm\phi_j} \right\}_{j=4,\ldots,8}.\end{aligned} \tag{3.59}$$

These fields transform irreducibly under the OPE of the E_6 current algebra (see (3.57)). The conjugate primary super-sector $\overline{\mathcal{E}} = \mathcal{E}^\dagger$ forms another irreducible representation. They both carry spin $h_{\mathcal{E}} = h_{\overline{\mathcal{E}}} = 2/3$. The product of primary fields $\mathcal{E}_{SU(3)} \times \mathcal{E}_{E_6}$ and $\overline{\mathcal{E}}_{SU(3)} \times \overline{\mathcal{E}}_{E_6}$ generate the remaining 162 E_8 roots in the complement $\Delta_{E_8} \backslash (\Delta_{SU(3)} \cup \Delta_{E_6})$. Therefore, if both $SU(3)$ and E_6 were gapped by inter-wire backscattering interactions, their anyons would pairwise condense as local bosons and the resulting quantum Hall phase would be identical to the topologically trivial E_8 state.

We complete the construction of the $SU(3)$ and E_6 models by presenting their charge fractionalization and the momentum arrangement of electrons on each wire. For this, there are two issues to address in our coupled-wire construction. First, the R matrix used in (3.28)—that enables the non-local Dirac fermion presentation of E_8 in (3.27) by providing the transformation $\widetilde{\mathbf{\Phi}} = R\boldsymbol{\phi}$ between the Chevalley and Cartan-Weyl basis—has not been specified. Second, the root operators in (3.47) and (3.50) carry oscillation factors $e^{i\alpha^j k_j \times}$. Like the E_8 model, the exact cancellation of these factors in the sine-Gordon interactions in (3.54) requires a specific arrangement of electron Fermi momentum.

The construction of the E_8 quantum Hall state in §3.2 did not depend on the choice of the non-local Dirac fermions $d^j = e^{i\phi_j}$ presented in (3.27). This is because the E_8 current operators in (3.23) and (3.24), and in particular, the simple roots $e^{i\tilde{\Phi}_I}$ in (3.18) are fixed by their electronic origin. Here, however, the $SU(3)$ and E_6 models are constructed using a preferred set of simple roots in (3.46) and (3.51) based on a particular choice of non-local Dirac fermions, or equivalently, their Cartan-Weyl bosonized variables ϕ_j. While different choices are related by symmetries in the E_8 Weyl group (3.49), they lead to distinct bFQH states with inequivalent charge fractionalizations. This is because the fixed electric charges $\tilde{q}_I$ in (3.19) of the E_8 simple roots $e^{i\tilde{\Phi}_I}$ are not preserved by all E_8 Weyl symmetries. Given a specific choice of the non-local Dirac fermions d_j, their electric charges q_j define a charge vector $\mathbf{q} = (q_1, \ldots, q_8)$. The collection of charge vectors for the various choices of d_j was exhaustively presented above equation (3.29). Among them, they generate four inequivalent sets of $SU(3)$ and E_6 bFQH states with distinct filling numbers ν and quasiparticle charge assignments.

In general, electric charge splits in the $SU(3) \times E_6 \subseteq E_8$ decomposition. From the electric response on the edge, $\sigma = \nu e^2/h$, the filling numbers of the $SU(3)$ and E_6 bFQH states can be read off from the length of the charge vector when projecting it onto the $SU(3)$ and E_6 subspaces (c.f. (3.29) for the E_8 state):

$$\begin{aligned} \nu_{SU(3)} &= \left|P_{SU(3)}\mathbf{q}\right|^2 = \mathbf{q}^{SU(3)} \cdot K^{-1}_{SU(3)} \mathbf{q}^{SU(3)}, \\ \nu_{E_6} &= \left|P_{E_6}\mathbf{q}\right|^2 = \mathbf{q}^{E_6} \cdot K^{-1}_{E_6} \mathbf{q}^{E_6}. \end{aligned} \tag{3.60}$$

Here, $P_{SU(3)}$ and $P_{E_6} = \mathbb{I}_8 - P_{SU(3)}$ are the projection matrices (each obeying $P^2 = P$) onto subspaces spanned by the $SU(3)$ and E_6 roots, respectively:

$$\begin{aligned} P_{SU(3)} &= A_{SU(3)}^T K_{SU(3)}^{-1} A_{SU(3)}, \\ P_{E_6} &= A_{E_6}^T K_{E_6}^{-1} A_{E_6}, \end{aligned} \tag{3.61}$$

where the rows of $A_{SU(3)}$ and A_{E_6} are the the simple roots in the Euclidean 8-space chosen in (3.46) and (3.51). The electric charge of the simple roots of the two algebras are the entries of the charge vectors $\mathbf{q}^{SU(3)} = (q_{M=1,2}^{SU(3)}) = A_{SU(3)}\mathbf{q}$ and $\mathbf{q}^{E_6} = (q_{N=1,\ldots,6}^{E_6}) = A_{E_6}\mathbf{q}$. Since the $SU(3)$ and E_6 roots are orthogonal, $P_{SU(3)}\mathbf{q} \perp P_{E_6}\mathbf{q}$. Thus, the filling numbers in (3.60) obey the particle-hole conjugation relation:

$$\nu_{SU(3)} + \nu_{E_6} = |\mathbf{q}|^2 = \nu_{E_8} = 16. \tag{3.62}$$

Let's see specifically how this works for the charge vector $\mathbf{q} = (4,0,0,0,0,0,0,0)$ of a set of non-local Dirac fermions chosen using the R matrix

$$R = \begin{pmatrix} -1 & 0 & 0 & 1 & 0 & 0 & 0 & 0 \\ \frac{1}{2} & \frac{1}{2} & \frac{1}{2} & -\frac{1}{2} & \frac{1}{2} & -\frac{1}{2} & \frac{1}{2} & -\frac{1}{2} \\ 0 & 0 & 0 & 0 & -1 & 0 & 0 & 1 \\ 0 & 0 & 0 & 0 & 0 & 0 & -1 & -1 \\ -\frac{1}{2} & -\frac{1}{2} & \frac{1}{2} & -\frac{1}{2} & \frac{1}{2} & \frac{1}{2} & \frac{1}{2} & \frac{1}{2} \\ \frac{1}{2} & \frac{1}{2} & -\frac{1}{2} & \frac{1}{2} & -\frac{1}{2} & \frac{1}{2} & \frac{1}{2} & -\frac{1}{2} \\ 0 & -1 & 0 & 0 & 0 & -1 & 0 & 0 \\ \frac{1}{2} & \frac{1}{2} & -\frac{1}{2} & \frac{1}{2} & \frac{1}{2} & -\frac{1}{2} & -\frac{1}{2} & \frac{1}{2} \end{pmatrix}. \tag{3.63}$$

In this case, the bFQH models constructed have filling numbers $\nu_{SU(3)} = 32/3$ and $\nu_{E_6} = 16/3$. The charge vector $\mathbf{q}$ also dictates the charge assignments of a vertex field operator, $Q(e^{i\mathbf{m}\cdot\boldsymbol{\phi}}) = \mathbf{m}\cdot\mathbf{q}$. This decomposes the $SU(3)$ and E_6 WZW current algebras and their primary field super-selection sectors into subspaces with different electric charges. For example, with the same charge vector as above, the eight-dimensional $SU(3)$ WZW algebra—which is spanned by the two Cartan generators (3.48) and the six roots (3.47)—splits into $8 = 4(0)\oplus 2(+4)\oplus 2(-4)$, a four-dimensional neutral subspace, a two-dimensional subspace of charge 2 currents and a two-dimensional subspace of charge -2 currents. The three dimensional $SU(3)$ primary sector $\mathcal{E}$ in (3.56) decomposes into $3 = 2(4/3)\oplus 1(-8/3)$, a two-dimensional subspace of charge $4/3$ fields and a one-dimensional subspace of charge $-8/3$ fields. For the particle-hole conjugate E_6 state, its 78-dimensional WZW current alge-

bra splits into $78 = 46(0) \oplus 16(+2) \oplus 16(-2)$, and its primary sector $\mathcal{E}$ in (3.59) decomposes into $27 = 1(8/3) \oplus 16(2/3) \oplus 10(-4/3)$. As above, the numbers in each term $*$ $(\star)$ specify the dimension $*$ of the subspace consisting of fields with charge $\star$.

Under an E_8 Weyl symmetry, the set of reflected/rotated non-local Dirac fermions obtain a new charge vector. The $SU(3)$ and E_6 subalgebras are subsequently reflected/rotated and may lead to different electric responses from before. The four distinct classes of $SU(3)$ and E_6 bFQH states can be represented by the following four charge vectors:

$$\begin{aligned} \mathbf{q} = &(0,0,0,0,0,0,0,4), \quad (4,0,0,0,0,0,0,0), \\ &(2,0,0,0,2,2,2,0), \quad (2,-2,0,0,2,2,0,0). \end{aligned} \tag{3.64}$$

The bFQH coupled-wire models constructed have, respectively, the distinct filling numbers

$$\nu_{SU(3)} = 0,\ \frac{32}{3},\ \frac{8}{3},\ 8, \quad \nu_{E_6} = 16,\ \frac{16}{3},\ \frac{40}{3},\ 8, \tag{3.65}$$

as summarized in Fig.3.3 along with central charges of $SU(3)_1$ and $(E_6)_1$. The charge assignments of the WZW current algebras and primary field super-selection sectors are summarized in Tables A.1 and A.4. The E_8 Weyl inversion that flips $\mathbf{q} \to -\mathbf{q}$ corresponds to the $\mathbb{Z}_2$ anyonic symmetry [KTH14, Teo16] (also referred to as outer automorphism) of the topological phases that relabels the anyon classes $\mathcal{E} \leftrightarrow \overline{\mathcal{E}}$. Since $\overline{\mathcal{E}} = \mathcal{E}^\dagger$, the two conjugate classes carry fields with conjugate electric charges. The charge assignment pattern of each primary field sector is invariant (changed) under the $\mathbb{Z}_2$ inversion flip for the bFQH states with integral (fractional) filling numbers. Therefore, the $\mathbb{Z}_2$ symmetry is preserved

(resp. broken) by the electric charge assignment. Since switching the anyon labels $\mathcal{E} \leftrightarrow \overline{\mathcal{E}}$ does not alter the fusion and statistics data, the bFQH states constructed from opposite charge vectors are indistinguishable in the absence of other physical symmetries.

Next, we address the momentum conservation in the coupled-wire model. The $SU(3)$ and E_6 root operators (3.47) and (3.50) carry oscillation factors $e^{i\alpha^j k_j \times}$. The same goes for the integrated fermions $f_{n=1,2,3}$. These factors cancel and do not appear in the sine-Gordong interactions (3.54) and (3.22) when the bare Fermi momenta $k_{F,a}$ of the electron channels (see (3.7)) take a set of specific values. Given any fixed R matrix (3.28), the momentum conserving $SU(3)_1$ model is constructed with bare Fermi momenta,

$$k_{F,a} = \frac{1}{2}\frac{eBd}{\hbar c} \sum_{j,j',J=1}^{8} \left(U^{++}_{Ja} + U^{+-}_{Ja}\right) \left(R^{-1}\right)^{j}_{J} P^{jj'}_{SU(3)} q_{j'}, \tag{3.66}$$

where only the first 8 rows of the $U^{+\pm}$ matrices in (3.16) are summed. The E_6 model is constructed with a different set of $k_{F,a}$, which are obtained by replacing the projection matrix $P_{SU(3)} \to P_{E_6}$ in (3.66). Using these $k_{F,a}$, the filling number (3.8) reproduces the value (3.60) predicted from the edge-state response.

The Abelian $\mathbb{Z}_2$ $SU(2)$ and E_7 states

We now construct the $SU(2)_1$ and $(E_7)_1$ bFQH states. The construction method is identical to the $SU(3)_1$ and $(E_6)_1$ states presented above. Here, we highlight the essential features and results. First, these bFQH states rely on the $SU(2) \times E_7$ conformal bipartition of E_8. The $SU(2)_1$ and $(E_7)_1$ WZW subalgebras can be chosen by fixing two decoupled subsets of

current operators inside $(E_8)_1$. Using the non-local Dirac fermions $d_j \sim e^{i\phi_j}$ (see (3.27)), we fix the $SU(2)_1$ by choosing its generators

$$\begin{aligned}\left[\mathtt{H}_{SU(2)}(\mathtt{x})\right] &= \frac{\partial_{\mathtt{x}}\phi_1 - \partial_{\mathtt{x}}\phi_2}{\sqrt{2}}, \\ \left[\mathtt{E}_{SU(2)}(\mathtt{x})\right]^{\pm} &= e^{\pm i(\phi_1(\mathtt{x})-\phi_2(\mathtt{x})+(k_1-k_2)\mathtt{x})}.\end{aligned} \tag{3.67}$$

The $SU(2)$ root system $\Delta_{SU(2)}$ contains the positive root $\boldsymbol{\alpha}_{SU(2)} = \mathbf{e}_1 - \mathbf{e}_2$ and the negative one $-\boldsymbol{\alpha}_{SU(2)}$. They correspond to the raising and lowering operators $[\mathtt{E}_{SU(2)}]^{\pm} = e^{\pm i\boldsymbol{\alpha}_{SU(2)}\cdot\boldsymbol{\phi}}$. The Cartan matrix of $SU(2)$ is $K_{SU(2)} = \boldsymbol{\alpha}_{SU(2)}\cdot\boldsymbol{\alpha}_{SU(2)} = 2$. Since the $SU(2)_1$ WZW CFT is generated by a single bosonized variable, it is identical to $U(1)_2$. The $(E_7)_1$ theory is the subalgebra in $(E_8)_1$ that commutes with the $SU(2)_1$. The E_7 root system Δ_{E_7} consists of root vectors in E_8 that are orthogonal to $\boldsymbol{\alpha}_{SU(2)}$. It is the union of the following three sets: (i) the 2 vectors $\pm(\mathbf{e}_1 + \mathbf{e}_2)$, (ii) the 60 integral vectors of the form $(0, 0, \alpha^3, \ldots, \alpha^8)$, where two of the $\alpha^{3,\ldots,8}$ are ± 1 and the rest are 0, and (iii) the 64 half-integral vectors $(\varepsilon^1, \ldots, \varepsilon^8)/2$, where $\varepsilon^j = \pm 1$, $\varepsilon^1 = \varepsilon^2$ and $\prod_{j=1}^{8} \varepsilon^j = +1$. Δ_{E_7} can be generated by the set of simple root vectors that form the rows of the following matrix

$$A_{E_7} = \begin{pmatrix} 1 & -1 & & & & & & \\ & 1 & -1 & & & & & \\ & & 1 & -1 & & & & \\ & & & 1 & -1 & & & \\ & & & & 1 & 1 & & \\ -1/2 & -1/2 & -1/2 & -1/2 & -1/2 & -1/2 & -1/2 & -1/2 \\ & & & & & & 1 & -1 \end{pmatrix} \tag{3.68}$$

and produce the Cartan matrix

$$K_{E_7} = A_{E_7} A_{E_7}^T = \begin{pmatrix} 2 & -1 & & & & & & \\ -1 & 2 & -1 & & & & & \\ & -1 & 2 & -1 & & & & \\ & & -1 & 2 & -1 & & -1 & \\ & & & -1 & 2 & -1 & & \\ & & & & -1 & 2 & & \\ & & & -1 & & & 2 & \end{pmatrix} \tag{3.69}$$

The $(E_7)_1$ WZW subalgebra is spanned by the 126 root operators,

$$[\mathtt{E}_{E_7}(\mathsf{x})]_{\boldsymbol{\alpha}_{E_7}} = e^{i\alpha^j_{E_7}(\phi_j(\mathsf{x})+k_j\mathsf{x})}, \quad \boldsymbol{\alpha}_{E_7} \in \Delta_{E_7} \tag{3.70}$$

and the 7 Cartan generators $[\mathtt{H}_{E_7}]_{b=1,\ldots,7} = \gamma^j_b \partial_{\mathsf{x}} \phi_j$, where $\boldsymbol{\gamma}_{b=1,\ldots,7} = (\gamma^1_b, \ldots, \gamma^8_b)$ is an orthonormal basis of the E_7 root subspace.

The coupled-wire Hamiltonians of the $SU(2)_1$ and $(E_7)_1$ bFQH states are constructed in a similar fasion as the $SU(3)_1$ and $(E_6)_1$ states. The model Hamiltonian (3.42) contains the intra-wire backscattering $\mathcal{H}^f_{\text{intra}}$ of the integrated fermions defined in (3.22), and the intra-wire and inter-wire backscattering of the two current algebras (c.f. (3.54) for the $SU(3)_1$ state). For the $SU(2)$ state, the inter-wire backscattering interactions involve the $SU(2)$ currents, whereas the intra-wire ones involve the E_7 currents. For the particle-hole conjugate E_7 state, the backscattering pattern of the two current algebras are switched. The resulting topological phases have a finite bulk excitation energy gap and chiral gapless boundary edges described by corresponding $SU(2)_1$ or $(E_7)_1$ CFTs. The thermal responses κ_{xy} (3.2) of the bFQH states are determined by the central charges $c_{SU(2)_1} = 1$ and $c_{(E_7)_1} = 7$, which are identical to the ranks of the simply-laced Lie algebras.

The two bFQH states have a $\mathbb{Z}_2 = \{1, \mathcal{S}\}$ topological order and each supports a semion quasiparticle excitation $\mathcal{S}$. It obey the fusion rule $\mathcal{S} \times \mathcal{S} = 1$ and therefore is its own anti-partner. $\mathcal{S}$ has spin $h = 1/4$ in the $SU(2)_1$ state or $h = 3/4$ in the $(E_7)_1$ state. The semion primary field super-selection sector in $SU(2)_1$ is spanned by the two non-local vertex fields $e^{\pm i\boldsymbol{\alpha}_{SU(2)}\cdot\boldsymbol{\phi}/2}$, which together rotate irreducibly under the $SU(2)_1$ algebra (see (3.57)). The

semion primary super-sector in $(E_7)_1$ is spanned by 56 non-local fields

$$\mathcal{S} = \text{span}\left\{e^{\pm i(\phi_1+\phi_2)/2 \pm i\phi_j}\right\}_{j=3,\ldots,8} \cup \left\{e^{i\sum_{j=3}^{8}\varepsilon^j\phi_j/2}\right\}_{\varepsilon^{j=3,\ldots,8}=\pm 1, \prod_{j=3}^{8}\varepsilon^j=-1}, \tag{3.71}$$

which irreducibly represent E_7. Like in the previous $SU(3)\times E_6$ case, if both the $SU(2)$ and E_7 currents were gapped by inter-wire backscattering interactions, the $2\times 56 = 112$ semion pairs from $SU(2)\times E_7$ would anyon condense [BS09, Bur18] to form the remaining E_8 root currents outside of $SU(2)\times E_7$. The resulting state would have trivial bosonic topological order equivalent to $(E_8)_1$. We notice in passing that semion primary super-sectors $\mathcal{S}$ in $SU(2)_1$ as well as $(E_7)_1$ are closed under the $\mathbb{Z}_2$ involution symmetry $\phi_j \to -\phi_j$ in the Weyl group $\text{Aut}(E_8)$. The involution acts differently on the $SU(3)_1$ and $(E_6)_1$ states where the non-trivial anyon classes are flipped, $\mathcal{E} \leftrightarrow \overline{\mathcal{E}}$, under the symmetry.

The filling numbers and electric charge assignments of the bFQH states depend on the R matrix that specifies the E_8 simple roots $e^{i\tilde{\Phi}_J} = e^{iR^j_J\phi_j}$ in Euclidean 8-space and defines the non-local Dirac fermions $d_j \sim e^{i\phi_j}$ (see (3.27)). The allowed charge vectors $\mathbf{q} = (q_{j=1,\ldots,8})$ of the fermions were presented above (3.29). There are three inequivalent classes of the $SU(2)_1$ and $(E_7)_1$ states, where the filling numbers are

$$\nu_{SU(2)} = 0,\ 2,\ 8, \quad \nu_{E_7} = 16 - \nu_{SU(2)}. \tag{3.72}$$

The three classes can be respectively represented by three particular charge vectors

$$\mathbf{q} = 4\mathbf{e}_8, \quad 2\mathbf{e}_1 + 2\mathbf{e}_3 + 2\mathbf{e}_5 + 2\mathbf{e}_7, \quad 4\mathbf{e}_1. \tag{3.73}$$

The electric charge assignments of the WZW currents and the primary fields are summarized in Tables A.1 and A.3.

Lastly, the coupled-wire models are exactly solvable when the bare electron momenta $k_{F,a}$ (see (3.7)) take a set of specific values. These values can be computed by applying the projection matrix $P_A = P_{SU(2)}$ or P_{E_7} on the Euclidean 8-space. Small deviations away from these fine-tuned values are perturbations that should not alter the topological phases, assuming they are not strong enough the overcome the bulk excitation energy gap.

The Abelian $\mathbb{Z}_5$ $SU(5)$ states

Next we consider the Abelian $\mathbb{Z}_5$ $SU(5)$ bFQH states. These bFQH states are based on the conformal embedding of $SU(5)^A \times SU(5)^B$ in E_8. Starting with the A sector, the simply-laced Lie algebra is spanned by its 4 Cartan generators and 20 root operators

$$\begin{aligned}\left[\mathtt{H}_{SU(5)^A}(\mathsf{x})\right]_{b=1,\ldots,4} &= \frac{1}{\sqrt{b(b+1)}}\left[\sum_{a=1}^{b}\partial_{\mathsf{x}}\phi_a - b\partial_{\mathsf{x}}\phi_{b+1}\right],\\ \left[\mathtt{E}_{SU(5)^A}(\mathsf{x})\right]_{\boldsymbol{\alpha}_{SU(5)}} &= e^{i\alpha^j_{SU(5)}(\phi_j(\mathsf{x})+k_j\mathsf{x})}.\end{aligned} \tag{3.74}$$

The $SU(5)$ root system $\Delta_{SU(5)^A}$ is composed of root vectors $\boldsymbol{\alpha}_{SU(5)} = \pm(\mathbf{e}_a - \mathbf{e}_b)$ where $1 \le a < b \le 5$. The simple roots $\mathbf{e}_j - \mathbf{e}_{j+1}$, for $j = 1, \ldots, 4$, form the rows of the 4×8 matrix $A_{SU(5)^A}$. The Cartan matrix of $SU(5)$ is the Gram matrix

$$K_{SU(5)} = A_{SU(5)^A} A^T_{SU(5)^A} = \begin{pmatrix} 2 & -1 & & \\ -1 & 2 & -1 & \\ & -1 & 2 & -1 \\ & & -1 & 2 \end{pmatrix}. \tag{3.75}$$

The $SU(5)^B$ algebra is the complement of $SU(5)^A$ in E_8. The Cartan generators

$$\left[\mathtt{H}_{SU(5)^B(\mathtt{x})}\right]_b = \gamma_b^j \partial_{\mathtt{x}} \phi_j \tag{3.76}$$

in the B sector can be chosen with orthonormal vectors $\boldsymbol{\gamma}_{b=1,2,3,4}$ perpendicular to the $SU(5)^A$ root system. For example, one can set $\boldsymbol{\gamma}_1 = \mathbf{e}_6$, $\boldsymbol{\gamma}_2 = \mathbf{e}_7$, $\boldsymbol{\gamma}_3 = \mathbf{e}_8$ and $\boldsymbol{\gamma}_4 = \sum_{i=1}^5 \mathbf{e}_i/\sqrt{5}$. The $SU(5)^B$ root system $\Delta_{SU(5)^B}$ consists of the E_8 roots that are perpendicular to $\Delta_{SU(5)^A}$. $\Delta_{SU(5)^B}$ contains $\pm\mathbf{e}_a \pm \mathbf{e}_b$ for $6 \leq a < b \leq 8$ and $\varepsilon^a \mathbf{e_a}/2$ where $\varepsilon_a = \pm 1$, $\prod_a \varepsilon^a = +1$ and $\varepsilon^1 = \ldots = \varepsilon^5$. The simple roots of $SU(5)^B$ can be chosen to be the rows of

$$A_{SU(5)^B} = \begin{pmatrix} & & & & & 1 & -1 & \\ & & & & & & 1 & -1 \\ 1/2 & 1/2 & 1/2 & 1/2 & 1/2 & -1/2 & -1/2 & 1/2 \\ -1/2 & -1/2 & -1/2 & -1/2 & -1/2 & -1/2 & -1/2 & -1/2 \end{pmatrix}, \tag{3.77}$$

so that their scalar product recovers $K_{SU(5)} = A_{SU(5)^B} A_{SU(5)^B}^T$ in (3.75). The mutual OPEs between current operators in the A and B sectors are non-singular while OPEs within the same sector obey the $SU(5)$ WZW current algebra at level 1 (c.f. (3.37)). The two sectors are decoupled. Their Sugawara energy-momentum tensors add up to $T_{SU(5)_1^A} + T_{SU(5)_1^B} = T_{(E_8)_1}$ and thus the central charges are $c_{SU(5)^A} = c_{SU(5)^B} = 4$, which is half of that of $(E_8)_1$.

The $SU(5)$ bFQH states can be constructed by the coupled-wire Hamiltonians $\mathcal{H}[SU(5)]$ that contain the inter- and intra-wire current backscattering interactions $\mathcal{H}_{\text{inter}}^{SU(5)^A} + \mathcal{H}_{\text{intra}}^{SU(5)^B}$. The interactions are analogous to those in (3.54). They are non-competing sine-Gordon interactions that create a finite excitation energy gap in the bulk, but leave behind gapless chiral edge states on the boundaries described by the $SU(5)_1$ WZW CFT. Like the previous Abelian models, the $SU(5)$ bFQH state depends on the choice of the non-local Dirac

fermions $d_j \sim e^{i\phi_j}$ and their electric charges q_j. These choices give rise to different $SU(5)_1$ bFQH states at various fillings with distinct charge assignments.

The topological phase carries $|K_{SU(5)}| = 5$ primary field super-selection sectors. Each sector, labelled by $\mathcal{E}^{m=-2,-1,0,1,2}$, forms a $C^5_{|m|} = 5!/(|m|!(5-|m|)!)$ dimensional irreducible representation of $SU(5)$. $\mathcal{E}^0$ is the trivial vacuum sector. In $SU(5)^A_1$, for $m > 0$,

$$\mathcal{E}^m = \text{span}\left\{e^{-i\sum_{i=1}^m \phi_{j_i} + im\sum_{l=1}^5 \phi_l/5}\right\}_{1\leq j_1<\ldots<j_m\leq 5}. \tag{3.78}$$

For $m < 0$, $\mathcal{E}^m = (\mathcal{E}^{-m})^\dagger$. The vertex fields in $\mathcal{E}^m$ all carry spins (scaling dimensions) $h_m = |m|(5-|m|)/10$. Primary fields in the same super-sector can be rotated irreducibly into one another under the $SU(5)$ current OPE (c.f. (3.57)). These bFQH states have the Abelian $\mathbb{Z}_5$ topological order. Their anyon classes follow the fusion rules $\mathcal{E}^m \times \mathcal{E}^{m'} = \mathcal{E}^{[m+m']}$ where $[m+m'] = -2,-1,0,1,2$ and $[m+m'] \equiv m+m'$ modulo 5.

The possible Hall conductivities of the $SU(5)$ bosonic states can be exhausted by applying the projection operator $P_{SU(5)^A} = A_{SU(5)^A} K^{-1}_{SU(5)} A_{SU(5)^A}$ to the possible charge vectors $\mathbf{q} = (q_{i=1,\ldots,8})$ that were presented above (3.29). The resulting filling numbers of the $SU(5)_1$ states are

$$\nu_{SU(5)_1} = |P_{SU(5)^A}\mathbf{q}|^2 = \frac{4}{5}\sum_{j=1}^5 q_j^2 - \frac{2}{5}\sum_{1\leq i<j\leq 5} q_i q_j = 0, \frac{16}{5}, \frac{24}{5}, 8, \frac{56}{5}, \frac{64}{5}, 16. \tag{3.79}$$

Pairs of bFQH states with fillings ν and $16-\nu$ are related by particle-hole conjugation. The $SU(5)_1$ state at filling $\nu = 8$ is particle-hole symmetric. The electric charge assignments of the $SU(5)$ WZW currents and the primary fields are summarized in Table A.5 and A.6.

Since $\mathcal{E}^{-m} = (\mathcal{E}^m)^\dagger$, the primary fields in the conjugate sectors $\mathcal{E}^{1,2}$ and $\mathcal{E}^{-1,-2}$ carry opposite electric charges. At the same time, the E_8 Weyl inversion that flips $\phi_j \to -\phi_j$ corresponds to the $\mathbb{Z}_2$ anyonic symmetry (or outer automorphism) [KTH14, Teo16] of $SU(5)_1$ that switches the anyon classes $\mathcal{E}^m \leftrightarrow \mathcal{E}^{-m}$. Similar to the $SU(3)_1$ and $(E_6)_1$ states, the charge assignments of $\mathcal{E}^m$ and $\mathcal{E}^{-m}$, for $m \neq 0$, are opposite (identical) when the filling number $\nu_{SU(5)}$ is fractional (resp. integral). Thus, at fractional fillings, the $\mathbb{Z}_2$ anyonic symmetry is broken by the primary field charge assignments. Although there are opposite charge patterns in each of these fractional cases, the two bFQH states are physically indistinguishable and can be identified by relabeling the anyon classes $m \leftrightarrow -m$.

The fractional filling $\nu = 64/5$ is special. There are multiplicities in the charge patterns of the WZW current operators as well as the primary fields that are *not* mutually related by the $\mathbb{Z}_2$ charge flip. (Similar multiplicities of charge assignments will also later appear in $SU(8)_1$ and $SO(N)_1$, for $N = 9, \ldots, 15$.) In case (i), the 24 WZW currents decompose into $24 = 16(0) \oplus 4(+4) \oplus 4(-4)$, where the numbers inside the parentheses indicate the electric charge. In case (ii), the charge decomposition is $24 = 10(0) \oplus 4(+2) \oplus 4(-2) \oplus 3(+4) \oplus 3(-4)$. The charge decompositions of the primary fields of cases (i) and (ii) are also $\mathbb{Z}_2$ inequivalent (see table A.6). Despite the charge differences, these two cases belong in the same bFHQ phase. When juxtaposing states (i) and (ii), the shared 1D edge is gappable by charge-preserving higher-order interactions. Since the $SU(5)$ currents in (i) and (ii) have

unequal charges, they cannot all backscatter on the shared edge without violating charge conservation. Alternatively, the shared edge can be gapped by the charge-conserving sine-Gordon interactions

$$\mathcal{U} = -u\sum_{\ell=1}^{3}\cos\left(\phi_\ell^R - \phi_{\ell+1}^R - \phi_\ell^L + \phi_{\ell+1}^L\right) - u\cos\left(\sum_{\ell=1}^{4}\phi_\ell^R - 4\phi_5^R + \sum_{\ell=1}^{4}\phi_\ell^L - 4\phi_5^L\right). \quad (3.80)$$

Here, we assume the Dirac fermions $d_j^R \sim e^{i\phi_j^R}$ in case (i) carries charge

$$q_j = (0,0,0,-4,0,0,0,0), \quad (3.81)$$

and the fermions $d_j^L \sim e^{i\phi_j^L}$ in case (ii) carries

$$q_j = (2,2,2,-2,0,0,0,0). \quad (3.82)$$

The last sine-Gordon potential back-scatters a non-primitive boson with scaling dimension $h = 10$. It becomes relevant in the RG sense given a sufficiently strong density-density interaction.

The Abelian $SO(2r)$ states and emergent Dirac fermions

We now construct the $SO(2r)_1$ bFQH states, for $r = 1,\ldots,7$. The construction relies on the $SO(2r) \times SO(16-2r)$ conformal decomposition of E_8. Given a particular choice of non-local Dirac fermions $d_j \sim e^{i\phi_j}$, for $j = 1,\ldots,8$, in each wire (see (3.27)), the splitting is set by generating the $SO(2r)_1$ by $d_{l=1,\ldots,r}$ and $d^\dagger_{l=1,\ldots,r}$ and its particle-hole conjugate

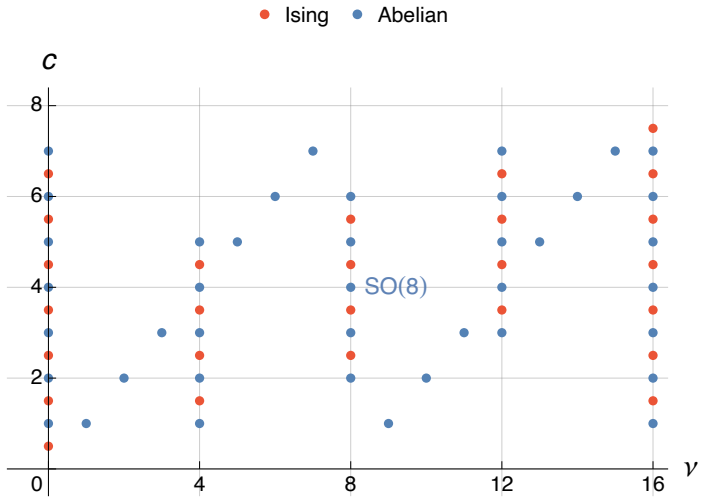

Figure 3.4: Bosonic fractional quantum Hall (bFQH) states $SO(N)_1$. All $SO(2r)_1$ states are Abelian (blue dots); and all $SO(2r+1)_1$ states have non-Abelian Ising topological orders (red dots). The bFQH states are related under the particle-hole conjugation $(\nu, c) \leftrightarrow (16-\nu, 8-c)$ about the PH symmetric $SO(8)_1$ at $(\nu, c) = (8, 4)$.

$SO(16-2r)_1$ by $d_{m=r+1,\ldots,8}$ and $d^\dagger_{m=r+1,\ldots,8}$. The WZW current operators of $SO(2r)_1$ are the fermion bilinears $d_l d_{l'}$, $d_l d^\dagger_{l'}$, $d^\dagger_l d_{l'}$ and $d^\dagger_l d^\dagger_{l'}$ for $1 \le l \le l' \le r$. They can be bosonized into r Cartan generators and $2r(r-1)$ root operators:

$$\begin{aligned} \big[\mathtt{H}_{SO(2r)}(\mathsf{x})\big]_l &= d_l(\mathsf{x})^\dagger d_l(\mathsf{x}) = \partial_{\mathsf{x}}\phi_l(\mathsf{x}), \\ \big[\mathtt{E}_{SU(2r)}(\mathsf{x})\big]_{\boldsymbol{\alpha}_{SO(2r)}} &= e^{i\alpha^j_{SO(2r)}(\phi_j(\mathsf{x})+k_j\mathsf{x})}. \end{aligned} \tag{3.83}$$

The root system $\Delta_{SO(2r)}$ contains the integral length $\sqrt{2}$ vectors $\boldsymbol{\alpha}_{SO(2r)} = \pm\mathbf{e}_l \pm \mathbf{e}_{l'}$, where $1 \le l < l' \le r$. They are integral combinations of a set of simple roots $\boldsymbol{\alpha}_1 = \mathbf{e}_1 - \mathbf{e}_2, \ldots, \boldsymbol{\alpha}_{r-1} = \mathbf{e}_{r-1} - \mathbf{e}_r$, and $\boldsymbol{\alpha}_r = \mathbf{e}_{r-1} + \mathbf{e}_r$ that produce the Cartan matrix by scalar

product:

$$K_{ll'}^{SO(2r)} = \boldsymbol{\alpha}_l \cdot \boldsymbol{\alpha}_{l'} = \begin{pmatrix} 2 & -1 & & & & & \\ -1 & 2 & & & & & \\ & & \ddots & & & & \\ & & & 2 & -1 & & \\ & & & -1 & 2 & -1 & -1 \\ & & & & -1 & 2 & \\ & & & & -1 & & 2 \end{pmatrix}. \tag{3.84}$$

The conjugate $SO(16-2r)_1$ sector commutes with $SO(2r)_1$. The root system $\Delta_{SO(16-2r)}$ consists of E_8 root vectors that are perpendicular to $\Delta_{SO(2r)}$. In other words, $\boldsymbol{\alpha}_{SO(16-2r)} = \pm\mathbf{e}_m \pm \mathbf{e}_{m'}$, where $r+1 \leq m < m' \leq 8$.

The coupled-wire model of the $SO(2r)_1$ state is constructed in a similar fashion as the previous Abelian quantum Hall states. The inter-wire and intra-wire current backscattering terms in the exactly solvable model Hamiltonian (3.42) involve the $SO(2r)_1$ and $SO(16-2r)_1$ sector respectively. Generically, they are the two-fermion backscattering Gross-Neveu-type interactions:

$$\begin{aligned} \mathcal{H}_{\text{inter}}^{SO(2r)} &= u_{\text{inter}} \sum_y \sum_{1\leq p<q\leq 2r} \psi_{yp}^R \psi_{yq}^R \psi_{y+1,p}^L \psi_{y+1,q}^L, \quad \text{for } r = 2,\ldots,7 \qquad (3.85) \\ &= u_{\text{inter}} \sum_y \left[\sum_{l=1}^{r} \left[\mathtt{H}_{SO(2r)}\right]_{yl}^R \left[\mathtt{H}_{SO(2r)}\right]_{y+1,l}^L - \sum_{\boldsymbol{\alpha}_{SO(2r)}} \cos\left(\boldsymbol{\alpha}_{SO(2r)} \cdot \boldsymbol{\theta}_{y+1/2}\right) \right], \end{aligned}$$

$$\begin{aligned} \mathcal{H}_{\text{intra}}^{SO(16-2r)} &= u_{\text{inter}} \sum_y \sum_{2r+1\leq p<q\leq 16} \psi_{yp}^R \psi_{yq}^R \psi_{yp}^L \psi_{yq}^L, \quad \text{for } r = 1,\ldots,6 \qquad (3.86) \\ &= u_{\text{intra}} \sum_y \left[\sum_{m=r+1}^{16} \left[\mathtt{H}_{SO(16-2r)}\right]_{ym}^R \left[\mathtt{H}_{SO(16-2r)}\right]_{ym}^L \right. \qquad (3.87) \\ &\quad \left. - \sum_{\boldsymbol{\alpha}_{SO(16-2r)}} \cos\left(\boldsymbol{\alpha}_{SO(16-2r)} \cdot \boldsymbol{\theta}_y\right) \right]. \end{aligned}$$

Here, ψ are the real and imaginary Majorana components of the complex Dirac fermions $d_j = (\psi_{2j-1} + i\psi_{2j})/\sqrt{2}$; $\boldsymbol{\theta}_{y+1/2} = \boldsymbol{\phi}_y^R - \boldsymbol{\phi}_{y+1}^L$; and $\boldsymbol{\theta}_y = \boldsymbol{\phi}_y^R - \boldsymbol{\phi}_y^L$. Similar to the $SU(3)_1$ and $(E_6)_1$ states previously presented in (3.54), the sine-Gordon interactions here are marginally relevant when $u > 0$. They introduce a finite excitation energy gap in the bulk and leave behind the chiral gapless $SO(2r)_1$ WZW CFTs on boundary edges. The thermal response κ_{xy} (3.2) is determined by the central charge $c_{SO(2r)_1} = r$, which is the rank of the simply-laced $SO(2r)$ Lie algebra. The model Hamiltonian of the particle-hole conjugate $SO(16 - 2r)_1$ state can be constructed by interchanging the intra-wire and inter-wire gapping pattern between the $SO(2r)$ and $SO(16 - 2r)$ sectors.

Cases involving $SO(2)_1$ when $r = 1$ or 7 are special. This is because the $SO(2)$ algebra is Abelian and the $SO(2)_1 = U(1)_4$ WZW algebra is generated by a single current operator $\partial_x \phi$. The current backscattering interaction $\partial_x \phi^R \partial_x \phi^L$ is a density interaction that does not open an energy gap by itself. Instead, the $SO(2)_1$ inter-wire or intra-wire gapping potential is

$$\mathcal{U}^{SO(2)} = u \partial_x \phi_y^R \partial_x \phi_{y'}^L - u' \cos(4\theta), \tag{3.88}$$

where $2\theta = \phi_y^R - \phi_{y'}^L$ (the factor of 2 is adopted here to match with the usual convention in Luttinger liquid theory), and $y' = y$ ($y' = y + 1$) for an intra-wire (resp., inter-wire) interaction. The sine-Gordon potential here back-scatters the spin-2 local bosons $e^{i2\phi^\sigma}$ rather than spin-1 currents in (3.85) and (3.86). It becomes relevant when the density interaction u becomes "repulsive" (i.e., negative) enough so that the Luttinger parameter

$g = \sqrt{\frac{1+2\pi u/\tilde{v}}{1-2\pi u/\tilde{v}}}$ is smaller than $1/2$, where $\tilde{v}$ is the velocity of the fermions d_j appeared in (3.30). Odd fermion backscattering terms, such as the single fermion backscattering $\cos(2\theta) \sim (d^R)^\dagger d^L + h.c.$, are non-local for both the inter- and intra-wire cases, and do not have an integral electron origin. Higher order even terms $\cos(4n\theta)$, for $n \geq 2$, are irrelevant or less relevant.

The $SO(2r)_1$ WZW CFT has four primary field super-selection sectors. The non-trivial ones consist of the spin $h = 1/2$ fermion sector f spanned by the Dirac fermions $d_{l=1,\ldots,r}$ and $d^\dagger_{l=1,\ldots,r}$, and the spin $h = r/8$ even $(+)$ and odd $(-)$ spinor sector $s_\pm$ spanned by the vertex operators $e^{i\varepsilon^l \phi_l/2}$, where $\varepsilon^{l=1,\ldots,r} = \pm 1$ and $\prod_{l=1}^r \varepsilon^a = \pm 1$. Fields within the same super-selection sector differ from each other by local bosons and can be rotated into each other by the WZW algebra (c.f. (3.57)). For even r, they follow the $\mathbb{Z}_2 \times \mathbb{Z}_2$ fusion rules, where $(s_\pm)^2 = f^2 = 1$ and $s_\pm \times f = s_\mp$. For odd r, they follow the $\mathbb{Z}_4$ fusion rules, $s_\pm \times s_\mp = f^2 = 1$ and $s_\pm \times f = s_\mp$. Unlike the previously considered $SU(2)_1$, $SU(3)_1$ and $(E_{6,7,8})_1$ states, the non-local Dirac fermions $d_{a=1,\ldots,r}$ now emerge as quasiparticle excitations in $SO(2r)_1$ and exist in the form of deconfined anyons in the bulk and primary fields on the edge.

The $SO(2r)_1$ WZW CFT is generically symmetric under a twofold outer automorphism and the topological phase has the corresponding $\mathbb{Z}_2$ anyonic relabelling symmetry. The outer automorphism can be generated by the involution symmetry w in $\mathrm{Aut}(E_8)$ that flips $\phi_r \to -\phi_r$ and $\phi_8 \to -\phi_8$ while keeping the rest of the bosonized variables $\phi_{j\neq r,8}$ unchanged. The involution acts as a reflection on the $SO(2r)$ root system. But the mirror plane is not perpendicular to any $SO(2r)$ root and the reflection falls outside of the Weyl group of $SO(2r)$. The reflection flips the simple roots $\boldsymbol{\alpha}_{r-1} \leftrightarrow \boldsymbol{\alpha}_r$ and leaves $\boldsymbol{\alpha}_{l=1,\ldots,r-2}$ unchanged.

It can be represented by the matrix $M = \mathbb{I}_{r-2} \oplus \sigma_x$, which commutes with the Cartan matrix (3.84). The fermion primary sector f of $SO(2r)_1$ is closed under the $\mathbb{Z}_2$ symmetry, but the even and odd spinor sectors are switched, $s_+ \leftrightarrow s_-$ (c.f. the switching action $\mathcal{E} \leftrightarrow \overline{\mathcal{E}}$ in $SU(3)_1$ and $(E_6)_1$). The $SO(8)_1$ theory is special and carries a triality S_3 symmetry. This is because, when $r = 4$, in addition to the w symmetry, the $SO(8) \times SO(8)$ root system is also preserved by another twofold symmetry $w' = (H_4 \oplus H_4)/2$ in $\mathrm{Aut}(E_8)$, where H_4 is the Hadamard matrix

$$H_4 = \begin{pmatrix} 1 & 1 & 1 & 1 \\ 1 & -1 & 1 & -1 \\ 1 & 1 & -1 & -1 \\ 1 & -1 & -1 & 1 \end{pmatrix}. \tag{3.89}$$

Combining the two, ww' is a threefold symmetry that rotates the primary field sectors $f \to s_- \to s_+ \to f$. It is not a coincidence that all three non-trivial primary sectors in $SO(8)_1$ have identical spin $h = 1/2$ and interchangeable fusion rules so that the theory is symmetric under the permutation group S_3 of three elements.

The electric response of the $SO(2r)_1$ bFQH states depend on the choice of the eight non-local Dirac fermions in (3.27), $d_j \sim e^{i\phi_j}$, which are specified by the R matrix that corresponds to the E_8 simple roots $e^{i\tilde{\Phi}_J} = e^{iR^j_J \phi_j}$. The allowed charge vectors $\mathbf{q} = (q_{j=1,\ldots,8})$ of the fermions were presented above (3.29). The filling numbers of the $SO(2r)_1$ state and its

particle-hole conjugate $SO(16-2r)_1$ are

$$\nu_{SO(2r)_1} = \sum_{j=1}^{r} q_j^2, \quad \nu_{SO(16-2r)_1} = \sum_{j=r+1}^{8} q_j^2, \tag{3.90}$$

which add up to $\nu_{E_8} = 16$. Fig.3.4 summarizes the possible filling numbers and central charges of the Abelian $SO(2r)_1$ and $SO(16-2r)_1$ bFQH states. The electric charge assignments of the WZW currents and the primary fields are summarized in Tables A.12 and A.13. The $SO(2)_1$ algebra does not contain any roots. Instead of listing the trivial electric charge of its only current operator $\partial_x\phi_1$, the $SO(2)$ column in Table A.12 counts the electric charges $\pm q_1$ of the smallest local boson $e^{\pm i2\phi_1}$.

We highlight two observations in our results. First, there are two distinct states at filling fraction $\nu = 16$ for $SO(2r)_1 = SO(10)_1$, $SO(12)_1$, or $SO(14)_1$, where the WZW current operators either (i) carry electric charges $0, \pm 4$ or (ii) carry charges $0, \pm 2, \pm 4$ (see Table A.12). The coupled-wire models of case (i) are constructed with the charge vector $\mathbf{q} = (q_{j=1,\ldots,8})$ of non-local Dirac fermions that contains one and only one non-zero entry $q_j = 4$ and is within the $SO(2r)$ subspace. Models in case (ii) are constructed with $\mathbf{q}$ that contains four non-zero entries $q_j = \pm 2$ in the $SO(2r)$ subspace. The two cases also have unequal charge assignments for their primary fields. For case (i), the fermion sector f contains fields with charges $0, \pm 4$ and the spinor sectors $s_\pm$ carry charges ± 2. For case (ii), f has charges $0, \pm 2$ and $s_\pm$ have charges $0, \pm 2, \pm 4$ (see Table A.13). Despite the distinct charge assignments, the two cases belong in the same bFQH phase at $\nu = 16$. When juxtaposing the two states, the shared edge is gappable. Because the WZW currents in cases (i) and

(ii) have different charge assignments, current backscattering interactions (that include all currents) on the shared edge generally violate charge conservation. To gap the shared edge in a way that preserves charge conservation, an alternative set of interactions needs to be considered: There exist sine-Gordon potentials that backscatter higher-spin bosons with the same charges between the (i) and (ii) boundaries. To demonstrate this, we consider $SO(2r)_1 = SO(10)_1$ where the shared edge carries 5 counter propagating pairs of non-local Dirac fermions $d^{\sigma}_{j=1,\ldots,5} \sim e^{i\phi^{\sigma}_j}$. The fermion charges are $q^R_{j=1,\ldots,5} = (0,0,0,0,4)$ and $q^L_{j=1,\ldots,5} = (2,2,2,2,0)$. The shared edge can be gapped by the charge-preserving, local sine-Gordon potentials:

$$\mathcal{U} = -u\sum_{l=1}^{3}\cos\left(\phi^R_l - \phi^R_{l+1} - \phi^L_l + \phi^L_{l+1}\right) - u\cos\left(2\phi^L_5 + \sum_{l=1}^{4}\phi^R_l\right) - u\cos\left(2\phi^R_5 - \sum_{l=1}^{4}\phi^L_l\right). \tag{3.91}$$

$\mathcal{U}$ breaks the $SO(10)$ symmetry. The last two terms in $\mathcal{U}$ backscatter spin-2 bosons; these terms are relevant for sufficiently strong density-density interactions. Therefore, the two states (i) and (ii) are only distinguishable when the $SO(10)$ symmetry is preserved.

Second, in Table A.13, we observe that a $SO(2r)_1$ state may carry multiple distinct charge assignment patterns for its anyons or edge primary fields at the same filling number. For example, for $SO(4)_1$ at filling $\nu = 2$, the charges of the even spinors $q(s_+) = \pm 1$ while the odd ones are neutral $q(s_-) = 0$ in one state, but the charge pattern is reversed with $q(s_+) = 0$ and $q(s_-) = \pm 1$ in another state. For $SO(6)_1$ at filling $\nu = 3$, the charges of the spinors are $q(s_\pm) = \mp 3/2, \pm 1/2$ for one state, but are flipped to $q(s_\pm) = \pm 3/2, \mp 1/2$

for another. This degeneracy stems from the $\mathbb{Z}_2$ outer automorphism (anyonic symmetry) of $SO(2r)_1$ that switches between the $s_+ \leftrightarrow s_-$ anyon classes. Each state in the above examples illustrates a weak $\mathbb{Z}_2$ symmetry breaking by electric charge in the sense that the charge assignments of two anyon classes related by the $\mathbb{Z}_2$ symmetry are not identical (even up to charge 2 local bosons). In addition, the spinors $s_\pm$ are self-conjugate $(s_\pm)^2 = 1$ when r is even, and are anti-partners of each other $s_+ \times s_- = 1$ when r is odd. This requires the charges of each of $s_\pm$ to be closed under $q \to -q$ when r is even or requires $s_\pm$ to have opposite charges when r is odd. For $SO(8)_1$, the S_3 symmetry that permutes the fermions f, s_+, s_- gives rise to the three charge patterns for some filling numbers. For example in any given $SO(8)_1$ state at $\nu = 4$, one fermion class carries odd charges while the other two carry even charges. The S_3 symmetry is weakly broken down by the charge assignments into $\mathbb{Z}_2$, which switches the two even-charged fermion classes. There are filling numbers where the charge pattern is non-degenerate and the anyonic symmetry of the state is preserved by electric charge. In particular, the particle-hole symmetric $SO(8)_1$ state at filling $\nu = 8$ fully preserves its S_3 triality symmetry where the three fermion classes f, s_+, s_- have identical charges.

Lastly, we address the momentum conservation of the backscattering interactions in the coupled-wire models. They conserve x-momentum when the bare electron momenta $k_{F,a}$ (see (3.7)) take a set of specific values. This allows the L and R non-local Dirac fermions to have the same x-momentum if they are pairwise back-scattered within a wire, or different momenta that are commensurate with the magnetic field, $k_j^R - k_j^L = \frac{eBd}{\hbar c} q_j$, if they are pairwise back-scattered between wires.

The Abelian orbifold $U(1)_8$ and $SU(8)_1$ states

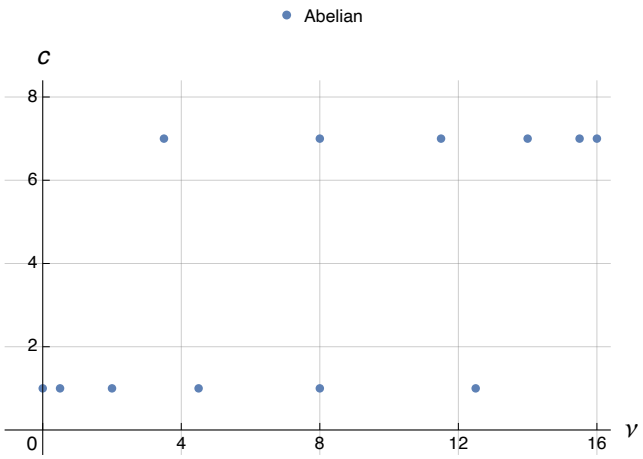

Figure 3.5: $SU(8)_1$ bFQH states with central charge $c = 7$ and $U(1)_8$ with central charge $c = 1$.

We demonstrate the concept of symmetry "gauging" [THF15a, BBCW19a] by constructing the Abelian orbifold bFQH states

$$U(1)_8 = \frac{SU(2)_1}{\mathbb{Z}_2}, \quad SU(8)_1 = \frac{(E_7)_1}{\mathbb{Z}_2}. \tag{3.92}$$

These are the simplest examples originating from the $\mathbb{Z}_2$ symmetry that flips the signs of the eight non-local Dirac fermions, $d_j \to -d_j$. It is an internal symmetry because all local operators, including the WZW currents in E_8 and any of its subalgebras, are unchanged under the symmetry. In §3.3.1, we constructed the $SU(2)_1$ and $(E_7)_1$ bFQH states. The corresponding WZW theories contain $U(1)_8$ and $SU(8)_1$ as subalgebras. Together, $U(1)_8 \times SU(8)_1$ conformally splits $(E_8)_1$. The two sectors can be gapped within a wire or in between wires by sine-Gordon potentials or current backscattering interactions. However, the coupled-wire

models constructed this way do not carry the $U(1)_8$ and $SU(8)_1$ topological orders. This is because both subalgebras carry spin-1 bosonic primary field sectors that are local integral combinations of electrons. These spin-1 local fields "anyon condense" [BS09, Bur18] and then extend the WZW algebras from $U(1)_8$ to $SU(2)_1$ and from $SU(8)_1$ to $(E_7)_1$. Therefore, the bFQH states still carry the $SU(2)_1$ and $(E_7)_1$ topological order.

Here, we will construct $U(1)_8$ and $SU(8)_1$ bFQH states by designing a conformal embedding $U(1)_8 \times SU(8)_1 \subseteq (E_8)_1$ that cannot be extended to $SU(2)_1 \times (E_7)_1$ without violating electron locality. The spin-1 bosonic primary fields will be non-local and therefore will not be able to "anyon condense." These bosons will be odd under the $\mathbb{Z}_2$ symmetry and will be identified as $\mathbb{Z}_2$ gauge charges. Deconfined gauge fluxes will emerge in the topological phases as anyons that exhibit π monodromy with the gauge charges.

We begin by defining a mixed set of non-local Dirac fermions. Starting with $d_j \sim e^{i\phi_j}$, $j = 1, \ldots, 8$, in (3.27), we consider the following basis transformation of the Cartan-Weyl bosonized variables

$$\tilde{\phi}_{2l-1} = \phi_{2l-1}, \quad \tilde{\phi}_{2l} = \frac{1}{2} \sum_{l'=1}^{4} (H_4)_l^{l'} \, \phi_{2l'} \tag{3.93}$$

where $l = 1, 2, 3, 4$ and H_4 is the Hadarmard matrix (3.89). The new bosonized variables $\tilde{\phi}$ are still described by the same free theory (3.30) as the old ones, and obey the same equal-time commutation relations $\left[\tilde{\phi}_j^{\sigma}(\mathsf{x}), \partial\tilde{\phi}_{j'}^{\sigma'}(\mathsf{x})\right] = 2\pi i \sigma \delta^{\sigma\sigma'} \delta_{jj'} \delta(\mathsf{x} - \mathsf{x}')$. However, the basis transformation is *not* a Weyl group symmetry in $\mathrm{Aut}(E_8)$. Not all E_8 root vectors $\boldsymbol{\alpha}$ in Δ_{E_8} correspond to local vertex operators $e^{i\alpha^j \tilde{\phi}_j}$. In particular, the $\mathbb{Z}_2$ gauge transformation

$\phi_j \to \phi_j + \pi$ (i.e., $d_j \to -d_j$), for all $j = 1, \ldots, 8$, now only alters the signs of the new fermions $\tilde{d}_j = e^{i\tilde{\phi}_j} \to (-1)^j \tilde{d}_j$ with odd indices because

$$\mathbb{Z}_2 : \tilde{\phi}_j \to \tilde{\phi}_j + \pi g_j, \tag{3.94}$$

for $g_{j=1,\ldots,8} = (1, 2, 1, 0, 1, 0, 1, 0)$. Operators such as $\tilde{d}_1 \tilde{d}_2 \sim e^{i(\tilde{\phi}_1 + \tilde{\phi}_2)}$ are no longer local because they are odd under $\mathbb{Z}_2$. A root operator $e^{i\alpha^j \tilde{\phi}_j}$ is a local integral electronic combination only when $\boldsymbol{\alpha}$ has even product with $\mathbf{g}$, i.e., $\alpha^j g_j \equiv 0 \bmod 2$. There are 112 such even root vectors, and they form a root system for $SO(16)$. We caution that the $SO(16)_1$ algebra generated by these local roots is a sub-algebra sitting inside the $(E_8)_1$. One of the spinor sectors of the $SO(16)_1$ contains local fields that extend $SO(16)_1$ back to the original $(E_8)_1$. Consequently, a coupled-wire model that back-scatters the $SO(16)_1$ between wires would still belong in the $(E_8)_1$ phase with trivial topological order. On the other hand, if the $SO(16)_1$ is split by some conformal embedding $\mathcal{G}_A \times \mathcal{G}_B \subseteq SO(16)_1$, which we are going to perform in this subsection, the coupled-wire models of $\mathcal{G}_A$ and $\mathcal{G}_B$ may exhibit an orbifold structure in which a deconfined $\mathbb{Z}_2$ gauge theory emerges.

First, we consider the $SU(2) \times E_7$ algebra by replacing ϕ in §3.3.1 by the mixed variables $\tilde{\phi}$ defined in (3.93). Since ϕ and $\tilde{\phi}$ are described by the same Lagrangian density, the $SU(2)$ and E_7 currents still obey the same OPEs. However, only the root operators that are invariant under $\mathbb{Z}_2$ are local. The $\mathbb{Z}_2$ even current operators span the $U(1)_8$ and $SU(8)_1$ subalgebras of $SU(2)_1$ and $(E_7)_1$, respectively. To see this, we begin with the substitution $\phi \to \tilde{\phi}$ in the $SU(2)_1$ currents in (3.67). While the Cartan generator $\mathtt{H}_0 = \partial_x(\tilde{\phi}_1 - \tilde{\phi}_2)/\sqrt{2}$

is even under (3.94), the raising and lowering operators,

$$\mathtt{E}^{\pm} = e^{\pm i(\tilde{\phi}_1 - \tilde{\phi}_2)} = e^{\pm i[\phi_1 - (\phi_2+\phi_4+\phi_6+\phi_8)/2]}, \tag{3.95}$$

are $\mathbb{Z}_2$ odd and no longer local. Instead, the primitive local bosons are $e^{\pm 2i(\tilde{\phi}_1 - \tilde{\phi}_2)}$, which have spin 4. It generates the $U(1)_8$ CFT, which we will later identify as the $SU(2)_1/\mathbb{Z}_2$ orbifold.

Performing the same substitution $\phi \to \tilde{\phi}$ for the $(E_7)_1$ currents in (3.70), the $\mathbb{Z}_2$ symmetric root operators $e^{i\alpha^j \tilde{\phi}_j}$ are associated with the even root vectors $\boldsymbol{\alpha}_{SU(8)}$ that form the root system,

$$\Delta_{SU(8)} = \left\{ \boldsymbol{\alpha} \in \Delta_{E_7} : \alpha^j g_j \equiv 0 \bmod 2 \right\}. \tag{3.96}$$

A set of simple root vectors $\boldsymbol{\alpha}_{l=1,\ldots,7}$ can be chosen to be the rows of the rectangular matrix,

$$A_{SU(8)} = \begin{pmatrix} & & & & 1 & & 1 & \\ & 1 & & & -1 & & & \\ & & & & 1 & & -1 & \\ -1/2 & -1/2 & -1/2 & 1/2 & -1/2 & 1/2 & 1/2 & 1/2 \\ & & & -1 & & -1 & & \\ & & & & & 1 & & -1 \\ & & & 1 & & -1 & & \end{pmatrix}. \tag{3.97}$$

The scalar products,

$$K^{SU(8)}_{ll'} = \boldsymbol{\alpha}_l \cdot \boldsymbol{\alpha}_{l'} = 2\delta_{ll'} - \delta_{l,l'+1} - \delta_{l,l'-1}, \tag{3.98}$$

are the entries of the Cartan matrix of $SU(8)$. The local roots $e^{i\alpha^j_{SU(8)}\tilde{\phi}_j}$ and the Cartan generators $\mathtt{H}_1 = \partial_{\mathtt{x}}(\tilde{\phi}_1 + \tilde{\phi}_2)/\sqrt{2}$, $\mathtt{H}_2 = \partial_{\mathtt{x}}\tilde{\phi}_3$, …, $\mathtt{H}_7 = \partial_{\mathtt{x}}\tilde{\phi}_8$ span the $SU(8)_1$ WZW algebra.

We will identify this CFT with the $(E_7)_1/\mathbb{Z}_2$ orbifold after constructing the coupled-wire models.

Like all models in this paper, the Hamiltonian begins with $\mathcal{H}_0 + \mathcal{H}^f_{\text{intra}}$ that reduces the electron wires to counter-propagating pairs of E_8 CFTs (see (3.11), (3.22) and (3.42)). Ignoring the gapped integrated fermions $f_{n=1,2,3}$, the free theory is described by (3.30). Since the basis transformation (3.93) is orthogonal, the form of the free Lagrangian density (3.30) is unchanged under the substitution $\phi \to \tilde{\phi}$. Using the splitting $U(1)_8 \times SU(8)_1 \subseteq (E_8)_1$, the two decoupled sectors can be gapped by backscattering interactions in different sectors. To construct the $U(1)_8$ state, the interactions are

$$\begin{aligned} \mathcal{H}^{SU(8)_1}_{\text{intra}} &= u_{\text{intra}} \left[\sum_{l=1}^{7} \mathtt{H}^R_{l,y} \mathtt{H}^L_{l,y} - \sum_{\boldsymbol{\alpha}_{SU(8)}} \cos\left(\alpha^j_{SU(8)} \theta_{y,j} \right) \right], \\ \mathcal{H}^{U(1)_8}_{\text{inter}} &= u_{\text{inter}} \mathtt{H}^R_{0,y} \mathtt{H}^L_{0,y+1} - u'_{\text{inter}} \cos\left(2\theta^{U(1)_8}_{y+1/2} \right), \end{aligned} \tag{3.99}$$

where $\theta^{U(1)_8}_{y+1/2} = \tilde{\phi}^R_{y,1} - \tilde{\phi}^R_{y,2} - \tilde{\phi}^L_{y+1,1} + \tilde{\phi}^L_{y+1,2}$ and $\theta_{y,j} = \tilde{\phi}^R_{y,j} - \tilde{\phi}^L_{y,j}$. The intra-wire $SU(8)_1$ current backscattering interaction is marginally relevant when $u_{\text{intra}} > 0$. The sine-Gordon potential simultaneously pins the ground state expectation values $\langle \boldsymbol{\alpha}_{SU(8)} \cdot \boldsymbol{\theta}_y \rangle$ and gaps the $SU(8)_1$ sector on all wires. The inter-wire $U(1)_8$ sine-Gordon interaction back-scatters the spin-4 local boson $e^{\pm 2i(\tilde{\phi}_1 - \tilde{\phi}_2)}$. Because of its higher spin $h > 1$, this interaction is only relevant when the density interaction u_{inter} is negative enough so that the Luttinger parameter $g = \sqrt{\frac{1+2\pi u/\tilde{v}}{1-2\pi u/\tilde{v}}}$ is smaller than $1/4$. Under this condition, the inter-wire sine-Gordon interaction pins $\langle \theta^{U(1)_8}_{y+1/2} \rangle$ and gaps all $U(1)_8$ sector modes except the right and left moving ones on the top and bottom boundary edges. The particle-hole conjugate $SU(8)_1$

state can be constructed by a coupled-wire model that exchanges the inter-wire and intra-wire backscattering roles of $U(1)_8$ and $SU(8)_1$.

Next, we justify the orbifold identifications (3.92). From §3.2, we see that electron locality implies the large gauge invariance is $\phi_j \equiv \phi_j + 2\pi r_j$, where $\mathbf{r} = (r_1, \ldots, r_8)$ lives inside the lattice $\mathcal{R} = \text{span}_{\mathbb{Z}}(\Delta_{E_8})$ generated by the E_8 root vectors in Euclidean 8-space. This allows the bosonized variable $\phi_1 - \phi_2$ that generates $SU(2)_1$ (see (3.67) in §3.3.1) to be shifted by any integer multiple of 2π. The substitution $\phi \to \tilde{\phi}$ in (3.93) imposes the additional identification:

$$\tilde{\phi}_1 - \tilde{\phi}_2 \equiv \tilde{\phi}_1 - \tilde{\phi}_2 + \pi. \tag{3.100}$$

Hence, the $U(1)_8$ bosonized variable $\tilde{\phi}_1 - \tilde{\phi}_2$ is compactified on the circle $\mathbb{R}/\pi\mathbb{Z}$, which has half the circumference of the closed circle $\mathbb{R}/2\pi\mathbb{Z}$ where the $SU(2)_1$ variable $\phi_1 - \phi_2$ lives. A similar distinction of compactifications applies to $(E_7)_1$ and $SU(8)_1$. The bosonized variables $(A_{E_7})_l^j \phi_j$ that generate the simple roots of E_7 in (3.68), for $l = 1, \ldots, 7$, are left unchanged under the large gauge transformation $(A_{E_7})_l^j \phi_j \equiv (A_{E_7})_l^j \phi_j + 2\pi n_l$, for any integers n_l. However, with the substitution $\phi \to \tilde{\phi}$, the large gauge transformation rules are modified to include

$$(A_{E_7})_l^j \tilde{\phi}_j \equiv (A_{E_7})_l^j \tilde{\phi}_j + \pi, \tag{3.101}$$

for all l, in addition to the ones above. Thus, while the $(E_7)_1$ bosonized variables $(A_{E_7})_l^j \phi_j$ are compactified on the torus $\mathbb{R}^7/2\pi\mathbb{Z}^7$, the new ones $(A_{E_7})_l^j \tilde{\phi}_j$ that generate $SU(8)_1$ live

on the torus $\mathbb{R}^7/2\pi\text{BCC}$ of half the size. Here, BCC is the 7-dimensional lattice containing vectors with all integral or all half-integral entries. The new compactifications (3.100) and (3.101) are associated with the orbifold CFTs $SU(2)_1/\mathbb{Z}_2$ and $(E_7)_1/\mathbb{Z}_2$, where $\mathbb{Z}_2$ is the quotient groups $\mathbb{Z}/2\mathbb{Z}$ and $\text{BCC}/\mathbb{Z}^7$ that differentiate the new large gauge transformations from the old ones.

The orbifolding of the CFTs corresponds to the gauging of anyon structures. Both the $U(1)_8$ and the $SU(8)_1$ topological states support eight Abelian anyon classes $\mathcal{E}^m$, for $m = -3, \ldots, 4$. Their total quantum dimension is $\sqrt{8}$, which is larger than that of $SU(2)_1$ and $(E_7)_1$ by a factor of 2, the order of the gauge group $\mathbb{Z}_2$. For $U(1)_8$, the anyons correspond to the the fractional vertex operators $\mathcal{E}^m = e^{im(\tilde{\phi}_1 - \tilde{\phi}_2)/4}$ of the edge CFT. They carry spins $h_m = m^2/16$. The spin-1 vertex $\mathcal{E}^4$ is exactly the raising operator $\mathtt{E}^+$ of $SU(2)_1$; it carries unit $\mathbb{Z}_2$ gauge charge. For $SU(8)_1$, the anyons correspond to 8 primary field super-selection sectors on the edge. Each super-sector is spanned by a collection of vertex fields that irreducibly "rotate" under the $SU(8)_1$ current OPE (c.f. (3.57)). They have spins $h_m = m(8-m)/16$. In particular, the super-sector $\mathcal{E}^4$ has 70 spin-1 primary fields that are odd under $\mathbb{Z}_2$. They are the $\mathbb{Z}_2$ gauge charges and are non-local boson fields that would extend $SU(8)_1$ to $(E_7)_1$ had they been integral. The anyon classes in both $U(1)_8$ and $SU(8)_1$ follow the $\mathbb{Z}_8$ fusion rules

$$\mathcal{E}^m \times \mathcal{E}^{m'} = \mathcal{E}^{[m+m']}, \tag{3.102}$$

where $[n]$ puts n back in the range $-3, \ldots, 4$ by subtracting or adding an integer multiple of 8. The anyons $\mathcal{E}^m$ with odd index $m = \pm 1, \pm 3$ all carry a $\mathbb{Z}_2$ flux because of their π monodromy with the $\mathbb{Z}_2$ charge $\mathcal{E}^4$. The remaining anyons $\mathcal{E}^{\pm 2}$ are semions with spin 1/4 for $U(1)_8$ or 3/4 for $SU(8)_1$. They have trivial monodromy with the $\mathbb{Z}_2$ charge and therefore have a trivial flux component. They are associated with the semions $\mathcal{S}$ in the un-gauged theories $SU(2)_1$ and $(E_7)_1$. Each $\mathbb{Z}_2$ gauge flux must square under fusion into a semion instead of the trivial vacuum class. This property reflects the "non-symmorphic" nature of the quantum $\mathbb{Z}_2$ symmetry [THF15a] and is captured as a non-trivial element in the group cohomology $H^2(\mathbb{Z}_2, \mathcal{A}) = \mathbb{Z}_2$, where $\mathcal{A} = \mathbb{Z}_2 = \{1, \mathcal{S}\}$ is the fusion group of Abelian anyons in $SU(2)_1$ and $(E_7)_1$.

Now we present the electric responses of the $U(1)_8$ and $SU(8)_1$ bFQH states. The coupled-wire model depends on the particular choice of the eight non-local Dirac fermions in (3.27), $d_j \sim e^{i\phi_j}$, which are related to the local E_8 simple roots by $e^{i\tilde{\Phi}_J} = e^{iR^j_J \phi_j}$ for some R matrix. The allowed charge vectors $\mathbf{q} = (q_{j=1,\ldots,8})$ of the fermions d_j were presented above (3.29). Since the $U(1)_8$ is in the $\phi_1 - (\phi_2 + \phi_4 + \phi_6 + \phi_8)/2$ direction, its filling number can be deduced by the length square of the projection the $\mathbf{q}$ vector along this direction. The filling number of $SU(8)_1$ is the length square of the orthogonal projection. We have:

$$\begin{aligned} \nu_{U(1)_8}(\mathbf{q}) &= \frac{1}{8}(2q_1 - q_2 - q_4 - q_6 - q_8)^2, \\ \nu_{SU(8)_1}(\mathbf{q}) &= 16 - \nu_{U(1)_8}(\mathbf{q}). \end{aligned} \tag{3.103}$$

Fig.3.5 summarizes the possible filling numbers and central charges of the Abelian orbifold $U(1)_8$ and $SU(8)_1$ states. The electric charge assignments of the $SU(8)_1$ WZW currents are

summarized in Table A.7. Like the $SO(2)_1$ algebra in the previous subsection, the $U(1)_8$ algebra also does not contain any roots, and the $U(1)_8$ column in the same table counts the electric charges $\pm(2q_1 - q_2 - q_4 - q_6 - q_8)$ of the smallest local boson $e^{\pm i(2\phi_1 - \phi_2 - \phi_4 - \phi_6 - \phi_8)}$. The electric charges carried by the primary fields $\mathcal{E}^m$ of $U(1)_8$ and $SU(8)_1$ are summarized in Table A.8. In particular, we notice that the charge and anyon data for the $U(1)_8$ bFQH state at $\nu = 1/2$ agrees with the strongly paired state that theoretically may occupy the half-filled Landau level.

We observe that there are multiplicities in the charge assignments. First, primary fields in the conjugate sectors $\mathcal{E}^m$ and $\mathcal{E}^{-m}$ carry opposite charges. Therefore, unless the set of primary fields' charges within a super-selection sector $\mathcal{E}^m$ is closed under $q \to -q$, fields in the conjugate sector $\mathcal{E}^{-m}$ must carry unequal charges. This imbalance occurs for all primary sectors in $U(1)_8$ in all filling numbers and in most cases in $SU(8)_1$. Thus, the electric charge assignment weakly breaks the conjugation symmetry $\mathcal{E}^m \leftrightarrow \mathcal{E}^{-m}$. Conversely, the conjugation $\phi_j \to -\phi_j$ inverts the charge for each individual primary sector and leads to the double degeneracy of charge assignments in all filling numbers in Table A.8. The same phenomenon was observed for the previous $SU(3)_1$, $(E_6)_1$, and $SO(2r)_1$ states.

Second, an additional multiplicity arises for $SU(8)_1$ at filling numbers 14 and 31/2. Table A.7 shows two distinct charge patterns for the $SU(8)_1$ WZW currents at each of these fillings. The two states also have unequal charge assignments for their primary fields that cannot be attributed to the conjugation symmetry. Similar degeneracy was seen for $SO(10)_1$, $SO(12)_1$ and $SO(14)_1$ at filling 16. Like the previous cases, the two $SU(8)_1$ states still belong in the same bFQH phase. When juxtaposing the two states, the shared boundary

edge is gappable by interactions that backscatter higher spin bosons and break the $SU(8)$ symmetry.

3.3.2 Non-Abelian states

We now construct non-Abelian bosonic fractional quantum Hall (bFQH) states that partially fill the E_8 state. The construction is similar to the previous examples (c.f. (3.42)) and relies on the bipartite conformal embeddings $\mathcal{G}_A \times \mathcal{G}_B \subseteq E_8$ (see (3.41)). Here, the topological states $\mathcal{G}_{A/B}$ support non-Abelian quasiparticle excitations. They exhibit multi-channel fusion rules and carry non-unit quantum dimensions, $d > 1$. The anyon braiding operations do not all mutually commute. We focus on three classes of non-Abelian bFQH states: Ising, Fibonacci, and metaplectic topological orders. The chiral CFTs on the boundary edges of all but one of these states are affine WZW simple Lie algebras $\mathcal{G}$ at level 1 that are *not* simply-laced. The exceptional case is the metaplectic orbifold state $SO(3)_2 = SU(2)_4 = SU(3)_1/\mathbb{Z}_2$. Each long root current operator in $\mathcal{G}$ is an E_8 root, but each short root in $\mathcal{G}$ is a linear combination of multiple E_8 roots. Consequently, the inter/intra-wire current backscattering interactions (3.43) and (3.44) consist of competing sine-Gordon potentials that collectively gap degrees of freedom carrying fractional central charges c.

The $SO(2r+1)$ Ising states and emergent Majorana fermions

We now construct the $SO(2r+1)_1$ bFQH states, for $r = 0, 1, \ldots, 7$. They all carry an Ising-like topological order [NW96, Kit06]. In the generic range for $r = 1, \ldots, 6$, the bFQH

state has an edge-state theory described by the $SO(2r+1)$ WZW theory at level 1. $SO(15)_1$ and its particle-hole conjugate the Ising CFT, which we denote by $SO(1)_1$, require a special treatment (because the Ising CFT is not a WZW theory) and will therefore be presented last.

The generic construction for $r = 1, \ldots, 6$ relies on the $SO(2r+1) \times SO(15-2r)$ conformal bipartition of E_8. A particular decomposition is chosen by fixing a set of non-local Dirac fermions $d_{j=1,\ldots,8} \sim e^{i\phi_j}$ (see (3.27)) that represent the E_8 WZW CFT in each chiral sector $\sigma = R, L$ on each wire. Each Dirac fermion can be formally split into real and imaginary Majorana components, $d_j = (\psi_{2j-1} + i\psi_{2j})/\sqrt{2}$. The $SO(2r+1)_1$ sector is generated by the first $2r+1$ Majorana fermions $\psi_{p=1,\ldots,2r+1}$. The (real) WZW algebra is spanned by the current operators $J_{pq} = i\psi_p\psi_q$, for $1 \leq p < q \leq 2r+1$. Similarly, the $SO(15-2r)_1$ sector is generated by the remaining fermions $\psi_{p=2r+2,\ldots,16}$.

The (complexified) $SO(2r+1)_1$ algebra can be obtained by first bosonizing the $SO(2r)_1$ subalgebra generated by $\psi_{p=1,\ldots,2r}$. The Cartan generators and root operators of $SO(2r)_1$ were presented in (3.83). These operators coincide with the Cartan generators and long root operators of $SO(2r+1)_1$. Because the $SO(2r+1)_1$ algebra extends $SO(2r)_1$, we must also include the following current operators:

$$\left[\mathtt{E}_{SO(2r+1)}(\mathtt{x})\right]_{\pm\mathbf{e}_j} = i\psi_{2r+1}e^{\pm i(\phi_j(\mathtt{x})+k_j\mathtt{x})}, \tag{3.104}$$

which pair the Majorana fermion ψ_{2r+1} with one of the Dirac fermions $d_{j=1,\ldots,r}$ or $d^\dagger_{j=1,\ldots,r}$ in $SO(2r)_1$. Each of the additional currents in (3.104), referred to as a short root operator,

is a linear combination of two E_8 root operators:

$$\left[\mathtt{E}_{SO(2r+1)}(\mathsf{x})\right]_{\pm\mathbf{e}_j} = e^{i(\pm\phi_j(\mathsf{x})+\phi_{2r+1}(\mathsf{x}))\pm ik_j\mathsf{x}} + e^{i(\pm\phi_j(\mathsf{x})-\phi_{2r+1}(\mathsf{x}))\pm ik_j\mathsf{x}}, \tag{3.105}$$

because $\psi_{2r+1} = (d_{r+1} + d_{r+1}^\dagger)/\sqrt{2}$. In order for the short root current backscattering to preserve charge and momentum conservation, the two E_8 roots must carry identical charge and momentum; this ensures the linear combination transforms homogeneously. This requires $d_{r+1} \sim e^{i\phi_{r+1}}$ to be electrically neutral and have trivial momentum:

$$q_{r+1} = k_{r+1} = 0. \tag{3.106}$$

The conjugate $SO(15-2r)_1$ algebra can be organized in a similar manner. It contains the bosonized $SO(14-2r)_1$ subalgebra, which is generated by $\psi_{p=2r+3,\ldots,16}$ and is associated with the long root vectors $\boldsymbol{\alpha}_{SO(14-2r)} = \pm\mathbf{e}_j \pm \mathbf{e}_{j'}$, for $r+2 \le j < j' \le 8$. $SO(15-2r)_1$ extends $SO(14-2r)_1$ by including the short roots

$$\left[\mathtt{E}_{SO(15-2r)}(\mathsf{x})\right]_{\pm\mathbf{e}_j} = i\psi_{2r+2}e^{\pm i(\phi_j(\mathsf{x})+k_j\mathsf{x})}, \tag{3.107}$$

for $j = r+2, \ldots, 8$.

The coupled-wire model of the $SO(2r+1)_1$ bFQH state follows the recipe given in (3.42). Each 11-channel electron wire is turned into the bosonic E_8 CFT by the intra-wire backscattering interaction $\mathcal{H}^f_{\text{intra}}$ from (3.22) that gaps all odd fermion excitations. The $(E_8)_1$ WZW algebra is split into $SO(2r+1)\times SO(15-2r)$, and the two decoupled sectors are gapped by

inter-wire and intra-wire current backscattering interactions (3.43) and (3.44). Similar to the $SO(2r)$ theory (c.f. (3.85) and (3.86)), these current backscattering terms are quartic in the fermions, as in the Gross-Neveu model [GN74, SZT16],

$$\begin{aligned}
\mathcal{H}_{\text{inter}}^{SO(2r+1)} &= u_{\text{inter}} \sum_{y} \sum_{1\le p<q\le 2r+1} \psi_{yp}^{R}\psi_{yq}^{R}\psi_{y+1,p}^{L}\psi_{y+1,q}^{L}, \quad \text{for } r=1,\dots,6 \\
&= u_{\text{inter}} \sum_{y} \Bigg[\sum_{l=1}^{r} \big[\mathtt{H}_{SO(2r)}\big]_{y,l}^{R} \big[\mathtt{H}_{SO(2r)}\big]_{y+1,l}^{L} - \sum_{\boldsymbol{\alpha}_{SO(2r)}} \cos\big(\boldsymbol{\alpha}_{SO(2r)}\cdot\boldsymbol{\theta}_{y+1/2}\big) \\
&\quad - 2i\psi_{y,2r+1}^{R}\psi_{y+1,2r+1}^{L} \sum_{j=1}^{r} \cos\big(\mathbf{e}_j\cdot\boldsymbol{\theta}_{y+1/2}\big) \Bigg],
\end{aligned} \tag{3.108}$$

$$\begin{aligned}
\mathcal{H}_{\text{intra}}^{SO(15-2r)} &= u_{\text{intra}} \sum_{y} \sum_{2r+2\le p<q\le 16} \psi_{yp}^{R}\psi_{yq}^{R}\psi_{yp}^{L}\psi_{yq}^{L}, \quad \text{for } r=1,\dots,6 \\
&= u_{\text{intra}} \sum_{y} \Bigg[\sum_{m=r+2}^{8} \big[\mathtt{H}_{SO(14-2r)}\big]_{y,m}^{R} \big[\mathtt{H}_{SO(14-2r)}\big]_{y,m}^{L} \\
&\quad - \sum_{\boldsymbol{\alpha}_{SO(14-2r)}} \cos\big(\boldsymbol{\alpha}_{SO(14-2r)}\cdot\boldsymbol{\theta}_{y}\big) \\
&\quad - 2i\psi_{y,2r+2}^{R}\psi_{y,2r+2}^{L} \sum_{j=r+2}^{8} \cos\big(\mathbf{e}_j\cdot\boldsymbol{\theta}_{y}\big) \Bigg].
\end{aligned} \tag{3.109}$$

The sine-Gordon vector variables have entries $\theta_{y+1/2,j} = \phi_{y,j}^{R} - \phi_{y+1,j}^{L}$ and $\theta_{y,j} = \phi_{y,j}^{R} - \phi_{y,j}^{L}$, for $j = 1,\dots,8$. There is no sum over long roots $\boldsymbol{\alpha}_{SO(2r)} = \pm\mathbf{e}_j \pm \mathbf{e}_{j'}$ ($\boldsymbol{\alpha}_{SO(14-2r)}$) when $r = 1$ ($r = 6$) because $SO(2)$ does not have a root system. The second line of (3.108) is identical to the inter-wire interactions $\mathcal{H}_{\text{inter}}^{SO(2r)}$ encountered in (3.85). They are marginally relevant when $u_{\text{inter}} > 0$ and simultaneously pin the ground-state expectation values $\big\langle\theta_{y+1/2,j}(\mathsf{x})\big\rangle = \pi n_j$, for $j = 1,\dots,r$, where $n_{j=1,\dots,r}$ are either all even integers or all odd integers. Terms in the last line of (3.108) back-scatter the short roots. At low energies, they effectively become

the single-fermion backscattering interaction,

$$\begin{aligned} &- 2u_{\text{inter}} \sum_y i\psi^R_{y,2r+1}\psi^L_{y+1,2r+1} \sum_{j=1}^{r} \left\langle \cos\left(\theta_{y+1/2,j}\right)\right\rangle \\ &= -2ru_{\text{inter}} \sum_y (-1)^{n_{y+1/2,j}} i\psi^R_{y,2r+1}\psi^L_{y+1,2r+1}, \end{aligned} \tag{3.110}$$

which gaps the remaining Majorana fermions, and pins

$$\left\langle i\psi^R_{y,2r+1}(\mathsf{x})\psi^L_{y+1,2r+1}(\mathsf{x})\right\rangle \sim (-1)^{n_{y+1/2,j}}. \tag{3.111}$$

The intra-wire interactions (3.109) similarly gaps all degrees of freedom in $SO(15-2r)_1$. Together, $\mathcal{H}^{SO(2r+1)}_{\text{inter}}$ and $\mathcal{H}^{SO(15-2r)}_{\text{intra}}$ produce a state with a finite bulk excitation energy gap and leave behind the gapless chiral $SO(2r+1)_1$ WZW CFT on the edge.

The $SO(2r+1)_1$ topological phase has an Ising topological order that corresponds to the $SO(2r+1)_1$ WZW CFT on any boundary edge. There are three super-selection sectors of primary fields (anyons) 1, f, and σ. The fermion sector f has spin $h = 1/2$ and is spanned by the $2r+1$ Majorana fermions $\psi_{p=1,\ldots,r+1}$. The Ising twist field (also known as Ising anyon) σ has spin $h = (2r+1)/16$. The Ising sector consists of spinor fields

$$\sigma = \text{span}\left\{ \sigma_{2r+1} \exp\left(\frac{i}{2}\sum_{j=1}^{r} \varepsilon^j \phi_j\right) : \varepsilon_{j=1,\ldots,r} = \pm 1 \right\}. \tag{3.112}$$

Here, the vertex field $e^{i\varepsilon^j\phi_j/2}$ is the spinor field $s_\pm$ of $SO(2r)_1$. There is a π-monodromy between this field and any of the first $2r$ Majorana fermions $\psi_{p=1,\ldots,2r}$. It corresponds to a π-kink in $\langle\theta_j(\mathsf{x})\rangle$ where the ground state expectation value jumps by an odd integer

multiple of π from one side to another. The Majorana mass $2r(-1)^{n_j}u_{\text{inter}}$ of ψ_{2r+1} in (3.110) therefore changes sign at the kink, and traps a Majorana zero mode at the domain wall. This corresponds to the Ising twist field σ_{2r+1} that has a π-monodromy with ψ_{2r+1}. Since the fermion pairs $\psi_p\psi_{2r+1}$ are local on any given wire in each chiral sector, the Ising twist field σ_{2r+1} and the spinor field $s_\pm = e^{i\varepsilon^j\phi_j/2}$ are confined together. σ_{2r+1} has spin $1/16$ while $s_\pm$ has spin $r/8$. They add up to the total spin $h_{\boldsymbol{\sigma}} = (2r+1)/16$. The three anyon sectors have the fusion rules:

$$f \times f = 1, \quad f \times \sigma = \sigma, \quad \sigma \times \sigma = 1 + f. \tag{3.113}$$

Next, we address the charge and momentum conservation of the $SO(2r+1)_1$ coupled-wire model. The model relies on a particular set of non-local Dirac fermions $d_j \sim e^{i\phi_j}$ (see (3.27)) that are defined using a R matrix that specifies the E_8 simple roots $e^{i\tilde{\Phi}_J} = e^{iR^j_J\phi_j}$ in Euclidean 8-space. Unlike the previous Abelian models, in order for d_{r+1} to split into Majorana components ψ_{2r+1} and ψ_{2r+2} that back-scatter in different direction, the R-matrix must be chosen so that d_{r+1} is electrically neutral, i.e. $q_{r+1} = (R^{-1})^J_{r+1}\tilde{q}_J = 0$ where the simple root electric charges $\tilde{q}_J$ were presented in (3.19). The model conserves momentum when the electron Fermi momenta $k_{F,a}$ are set under the projection $P_A^{jj'} = 1$ if $1 \le j = j' \le r$ and 0 otherwise. This ensures (i) $d^R_{y,j}$ and $d^L_{y+1,j}$ have identical momenta for $j = 1, \ldots, r$, (ii) $d^R_{y,j}$ and $d^L_{y,j}$ have identical momenta for $j = r+2, \ldots, 8$, and (iii) $d^\sigma_{y,r+1}$ has vanishing momentum. Since ψ_{2r+1} is electrically neutral, $d_{j=1,\ldots,r}$ are responsible for the charge response of the chiral $SO(2r+1)_1$ WZW CFT on the boundary edge. Therefore,

the filling number is

$$\nu_{SO(2r+1)} = \sum_{j=1}^{r} q_j^2. \tag{3.114}$$

Moreover, as $q_{r+1} = 0$ and $\nu_{E_8} = \sum_{j=1}^{8} q_j^2 = 16$, the particle-hole conjugate $SO(15-2r)$ carries the conjugate filling number $\nu_{SO(15-2r)} = 16 - \nu_{SO(2r+1)}$. Fig. 3.4 summarizes the possible filling numbers and central charges $c_{SO(2r+1)} = (2r+1)/2$ of the various $SO(2r+1)_1$ bFQH states.

The allowed electric charges q_j of the non-local Dirac fermions were presented above (3.29). With the additional charge neutral condition $q_{r+1} = 0$, the electric charge of the WZW currents and primary fields of $SO(2r+1)_1$ can be read-off from their $SO(2r)$ components. The charge assignments are summarized in Tables A.10 and A.11. Similar to the Abelian $SO(10)_1$, $SO(12)_1$, and $SO(14)_1$, we notice that there are two distinct charge patterns at filling $\nu = 16$ for each of $SO(9)_1$, $SO(11)_1$, $SO(13)_1$ and $SO(15)_1$. The two cases correspond to the two charge vectors $\mathbf{q} = (4,0,0,0,0,0,0,0)$ and $(2s_1, 2s_2, 2s_3, 2s_4, 0, 0, 0, 0)$, for $s_j = \pm 1$, of the non-local Dirac fermions. When the two states are put side by side so that they share a boundary, the distinct WZW current charge patterns forbid all currents to be back-scattered from one state to another without violating charge conservation. On the other hand, there may exist alternative gapping interactions on the shared edge that involve the backscattering of higher-spin bosons. For example, this has been seen in (3.91) for the two $SO(10)_1$ states at filling 16.

We now present such an alternative gapping interaction on the shared edge of the two $SO(11)_1$ states at filling 16:

$$\mathcal{U}' = \mathcal{U} + iu\psi_{11}^R\psi_{11}^L \cos\left(\phi_3^R + \phi_4^R + \phi_5^R - \phi_3^L - \phi_4^L + \phi_5^L\right), \tag{3.115}$$

where the potential $\mathcal{U}$ was defined in (3.91). $\mathcal{U}$ gaps the $SO(10)_1$ sub-sector consisting of the Dirac fermions $d^{L/R}_{j=1,\ldots,5} = e^{i\phi^{L/R}_{j=1,\ldots,5}}$. The last term in (3.115) is an integral electronic combination because it is proportional to the 4-body backscattering $(\psi_{11}^R d_3^R d_4^R d_5^R)(\psi_{11}^L d_3^{R\dagger} d_4^{R\dagger} d_5^R)$ and any fermion pair from the same edge is local. The sine-Gordon variable combination $\langle\phi_3^R + \phi_4^R + \phi_5^R - \phi_3^L - \phi_4^L + \phi_5^L\rangle$ takes a finite ground state expectation value in $\pi\mathbb{Z}$ because it can be expressed as a half-integral linear combination of the five sine-Gordon variables in potential $\mathcal{U}$ defined in (3.91). Therefore, at low energies, the last term of (3.115) is effectively the Majorana fermion backscattering $\pm i\psi_{11}^R\psi_{11}^L$, which gaps the remaining Majorana sector in $SO(11)_1$.

Similar to (3.115), alternative gapping potentials on the shared edges of the two $\nu = 16$ $SO(13)_1$ states and the two $\nu = 16$ $SO(15)_1$ states exist. The two $SO(9)_1$ states at filling 16 are special. The $SO(9)_1$ shared edge with distinct charge patterns between the left and right WZW currents cannot be gapped while preserving charge conservation. There is no even-body fermion backscattering involving ψ_9^R and ψ_9^L that preserves charge. However, the shared edge is gappable under an edge reconstruction that extends $SO(9)_1$ and includes additional counter-propagating fermion channels without changing the bulk topological order. For example, the R edge, consisting of $\psi^R_{p=1,\ldots,9}$, can be extended to $\psi_1^R, \ldots, \psi_{10}^R, \psi_{10}^L$,

where any fermion pair within the set is local. The shared edge can then be gapped after extending both the L and R edges by a potential similar to (3.115). To summarize, the two distinct charge patterns at filling 16 for each of the $SO(9)_1$, $SO(11)_1$, $SO(13)_1$ and $SO(15)_1$ state belong in the same bFQH phase. They are distinguishable only when the $SO(2r+1)$ symmetry is preserved.

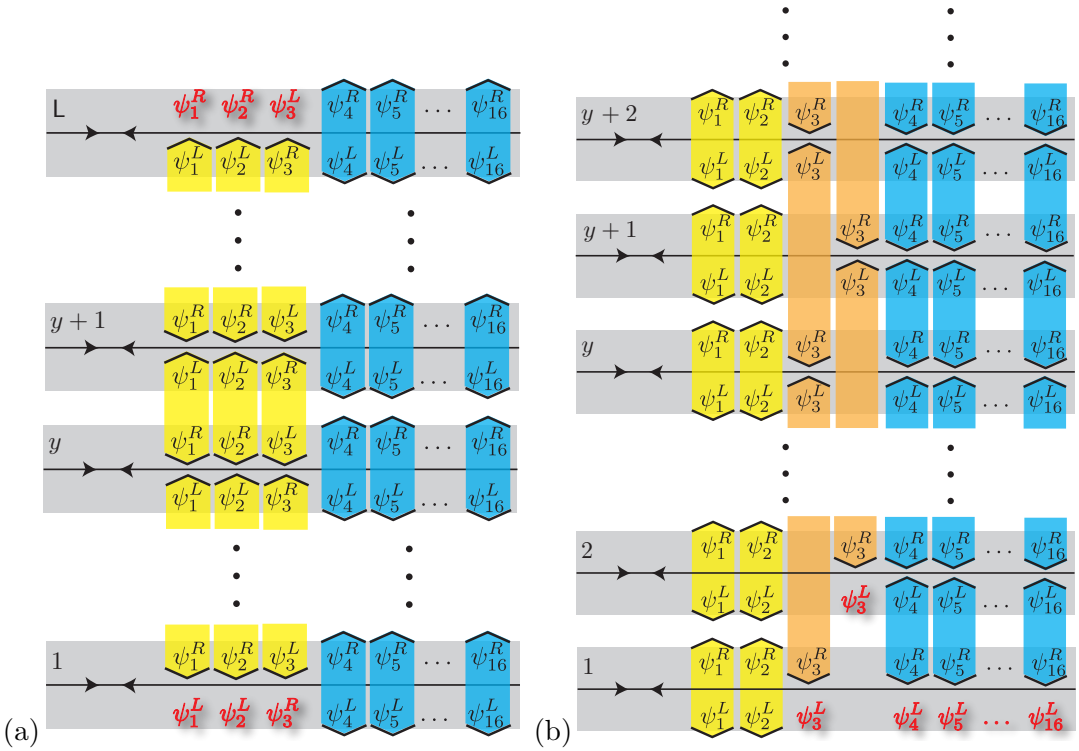

Figure 3.6: Fermion bilinears take finite ground state expectation values $\langle \psi^R_{yp} \psi^L_{y'p} \rangle$ in the (a) $SO(1)_1$ and (b) $SO(15)_1$ coupled-wire models. The chiral Majorana fermions in red near the boundary edges remain gapless.

Lastly, we address the coupled-wire construction of the $SO(15)_1$ and $SO(1)_1$ states. Recall that $SO(1)_1$ refers to the $c = 1/2$ Ising minimal model CFT $\mathcal{M}(4,3)$ [FMS12], which consists of a single Majorana fermion. This CFT is *not* a WZW theory. Although $SO(1)_1 \times SO(15)_1$ still conformally embeds into $(E_8)_1$, in the sense that the energy-momentum tensor

decomposes $T_{E_8} = T_{SO(15)} + T_{SO(1)}$, a coupled-wire model cannot be constructed based on the splitting. This is because the Ising sector cannot be gapped by backscattering local currents. Single Majorana fermion backscattering $\psi^L\psi^R$ within the same wire or between wires is *not* local because the Majorana fermion is not an integral combination of electrons. Here, we present an alternative construction for the $SO(15)_1$ bFQH state at filling 16 and the electrically neutral $SO(1)_1$ = Ising states. They support anyon quasiparticle excitations f and σ in the bulk that follow the fusion rules (3.113). They have spins $h_f = 1/2$ and $h_\sigma = 15/16$ or $1/16$ for $SO(15)_1$ or $SO(1)_1$ respectively.

The coupled-wire models are based on the same 11-channel electron wire arrays, as before. The intra-wire backscattering $\mathcal{H}^f_{\text{intra}}$ in (3.22) gaps the three integrated fermions and leave behind the E_8 WZW CFTs on each wire. To construct the $SO(1)_1$ state, the model Hamiltonian $\mathcal{H}[SO(1)_1] = \mathcal{H}_0 + \mathcal{H}^f_{\text{intra}} + \mathcal{H}_{\text{inter}} + \mathcal{H}_{\text{intra}}$ in (3.42) consists of the following inter-wire and intra-wire backscattering interactions.

$$\begin{aligned}
\mathcal{H}_{\text{intra}} &= -u_{\text{intra}} \sum_y \sum_{4\le p<q\le 16} \psi^R_{y,p}\psi^R_{y,q}\psi^L_{y,p}\psi^L_{y,q}, \\
\mathcal{H}_{\text{inter}} &= -u_{\text{inter}} \sum_y \Big[\psi^R_{y,1}\psi^R_{y,2}\psi^L_{y+1,1}\psi^L_{y+1,2} \\
&\quad + \lambda_0^2 \psi^R_{y,1}\psi^R_{y+1,3}\psi^L_{y+1,1}\psi^L_{y,3}\psi^R_{y,4}\psi^L_{y,4}\psi^R_{y+1,4}\psi^L_{y+1,4} \\
&\quad + \lambda_0^2 \psi^R_{y,2}\psi^R_{y+1,3}\psi^L_{y+1,2}\psi^L_{y,3}\psi^R_{y,4}\psi^L_{y,4}\psi^R_{y+1,4}\psi^L_{y+1,4} \Big].
\end{aligned} \tag{3.116}$$

The model preserves charge and momentum conservation when (i) the R-matrix is chosen so that the Dirac fermion $d_2 = (\psi_3 + i\psi_4)/\sqrt{2}$ has zero electric charge, $q_2 = (R^{-1})^J_2 \tilde{q}_J = 0$, and (ii) the electron Fermi momenta $k_{F,a}$ are set by the projection $P_A^{jj'} = 1$ if $j =$

$j' = 1$ and 0 otherwise. $\mathcal{H}_{\text{intra}}$ contains local $SO(13)_1$ current backscattering terms that collectively gap the fermions $\psi_{4,\ldots,16}$ within a wire. At low-energy, fermion pairs $i\psi^R_{y,p}\psi^L_{y,p}$, for $p = 4, \ldots, 16$, can be replaced by their ground state (mean-field) expectation values $\langle i\psi^R_{y,p}\psi^L_{y,p}\rangle = (-1)^{s_y}/\lambda$. Here, the sign is uniform and independent from p, and λ is some finite positive scalar with units of length.

The inter-wire interactions $\mathcal{H}_{\text{inter}}$ are a combination of products of local fermion pairs $\psi^\sigma_{y,r}\psi^\sigma_{y,p}$. The two 4-body terms in (3.116) consist of products of the form:

$$(\psi^R_{y,r}\psi^R_{y,4})(\psi^R_{y+1,3}\psi^R_{y+1,4})(\psi^L_{y+1,r}\psi^L_{y+1,4})(\psi^L_{y,3}\psi^L_{y,4}), \tag{3.117}$$

for $r = 1, 2$, where the two fermions in each parentheses have the same wire and chiral labels and thus the pair is a local integral combination of electrons. The scalar λ_0 has units of length so that the two 4-body terms share the same dimension as the two-body one. Although the 4-body terms are by themselves irrelevant, they become marginally relevant when $u_{\text{inter}} > 0$ in the presence of $\mathcal{H}_{\text{intra}}$. This is because, at low-energy, the fermion bilinears $\psi^R_4\psi^L_4$ take finite expectation values, and in the mean-field approximation, $\mathcal{H}_{\text{inter}}$

becomes the two-body interaction,

$$\begin{aligned}\mathcal{H}^{\rm mf}_{\rm inter} &= -u_{\rm inter}\sum_{y=1}^{\mathsf{L}-1}\Big[\psi^R_{y,1}\psi^R_{y,2}\psi^L_{y+1,1}\psi^L_{y+1,2}\\ &\quad+\lambda_0^2\psi^R_{y,1}\psi^R_{y+1,3}\psi^L_{y+1,1}\psi^L_{y,3}\langle\psi^R_{y,4}\psi^L_{y,4}\rangle\langle\psi^R_{y+1,4}\psi^L_{y+1,4}\rangle\\ &\quad+\lambda_0^2\psi^R_{y,2}\psi^R_{y+1,3}\psi^L_{y+1,2}\psi^L_{y,3}\langle\psi^R_{y,4}\psi^L_{y,4}\rangle\langle\psi^R_{y+1,4}\psi^L_{y+1,4}\rangle\Big]\\ &= -u_{\rm inter}\sum_{y=1}^{\mathsf{L}-1}\Big[\psi^R_{y,1}\psi^R_{y,2}\psi^L_{y+1,1}\psi^L_{y+1,2}\\ &\quad+(-1)^{1+s_y+s_{y+1}}\frac{\lambda_0^2}{\lambda^2}\psi^R_{y,1}\psi^R_{y+1,3}\psi^L_{y+1,1}\psi^L_{y,3}\\ &\quad+(-1)^{1+s_y+s_{y+1}}\frac{\lambda_0^2}{\lambda^2}\psi^R_{y,2}\psi^R_{y+1,3}\psi^L_{y+1,2}\psi^L_{y,3}\Big].\end{aligned}\tag{3.118}$$

It is crucial to recognize that the last two terms in $\mathcal{H}^{\rm mf}_{\rm inter}$ are not local because the four fermions in each term all have different wire and chirality indices. Therefore, $\mathcal{H}^{\rm mf}_{\rm inter}$ cannot be directly used in the electron-based coupled-wire model, and instead has to originate from the full many-body interactions in (3.116). The signs $(-1)^{1+s_y+s_{y+1}}$ depend on the ground states of $\mathcal{H}_{\rm intra}$. When $(-1)^{1+s_y+s_{y+1}}\lambda_0^2/\lambda^2 = 1$, the mean-field Hamiltonian is identical to the current backscattering $\mathcal{H}^{\rm mf}_{\rm inter} = u_{\rm inter}\mathbf{J}^R_{SO(3)_1}\cdot\mathbf{J}^L_{SO(3)_1}$, where the R-chiral (L-chiral) $SO(3)_1$ currents are generated by fermion pairs within the chiral set $\psi^R_{y,1},\psi^R_{y,2},\psi^R_{y+1,3}$ (resp. $\psi^L_{y+1,1},\psi^L_{y+1,2},\psi^L_{y,3}$). It gaps the three counter-propagating pairs of Majorana fermions. In general, by bosonizing $(\psi^R_{y,1}+i\psi^R_{y,2})/\sqrt{2}\sim e^{i\phi^R_{y,1}}$ and $(\psi^L_{y+1,1}+i\psi^R_{y+1,2})/\sqrt{2}\sim e^{i\phi^L_{y+1,1}}$, the mean-field Hamiltonian (3.118) can be expressed as

$$\begin{aligned}\mathcal{H}^{\rm mf}_{\rm inter} = u_{\rm inter}\sum_y\Big[&\partial_{\mathsf{x}}\phi^R_{y,1}\partial_{\mathsf{x}}\phi^L_{y+1,1}\\ &-(-1)^{1+s_y+s_{y+1}}\frac{\lambda_0^2}{\lambda^2}i\psi^R_{y+1,3}\psi^L_{y,3}\cos\theta_{y+1/2,1}\Big],\end{aligned}\tag{3.119}$$

where $\theta_{y+1/2,1} = \phi^R_{y,1} - \phi^L_{y+1,1}$. Similar to (3.110), in order to minimize the energy (3.119), the sine-Gordon angle parameter and Majorana mass must have correlated ground state expectation values:

$$\begin{aligned} \langle \theta_{y+1/2,1}(\mathsf{x}) \rangle &= \pi m_{y+1/2}, \\ \left\langle i\psi^R_{y+1,3}(\mathsf{x})\psi^L_{y,3}(\mathsf{x}) \right\rangle &\sim (-1)^{m_{y+1/2}}, \end{aligned} \tag{3.120}$$

where $m_{y+1/2}$ is an integer. The sine-Gordon term fixes the same sign $(-1)^{m_{y+1/2}}$ for $\langle i\psi^R_{y,1}\psi^L_{y,1}\rangle$ and $\langle i\psi^R_{y,2}\psi^L_{y,2}\rangle$.

We now see that $\mathcal{H}_{\text{inter}} + \mathcal{H}_{\text{intra}}$ gaps all bulk Majorana fermions in a closed torus geometry. On the other hand, in an open geometry with boundary edges at $y = 1$ and $y = \mathsf{L}$, the sum of wires in $\mathcal{H}_{\text{inter}}$ only runs over $y = 1, \ldots, \mathsf{L} - 1$. There remains gapless Majorana fermions $\psi^L_{y=1,1}$, $\psi^L_{y=1,2}$, $\psi^R_{y=1,3}$ on the bottom edge and $\psi^R_{y=\mathsf{L},1}$, $\psi^R_{y=\mathsf{L},2}$, $\psi^L_{y=\mathsf{L},3}$ on the top edge as indicated in Fig. 3.6(a). At neutral filling $\nu = 0$ when the Dirac fermion $d^\sigma_{y,1} = (\psi^\sigma_{y,1} + i\psi^\sigma_{y,2})/\sqrt{2}$ is electrically neutral, the edge states are unstable to the local edge perturbation,

$$\begin{aligned} \mathcal{U}_{\text{edges}} &= -u\psi^R_{1,3}\psi^R_{1,4}\psi^L_{1,2}\psi^L_{1,4} - u\psi^R_{\mathsf{L},3}\psi^R_{\mathsf{L},4}\psi^L_{\mathsf{L},2}\psi^L_{\mathsf{L},4} \\ &\to u\psi^R_{1,3}\psi^L_{1,2}\langle\psi^R_{1,4}\psi^L_{1,4}\rangle + u\psi^R_{\mathsf{L},3}\psi^L_{\mathsf{L},2}\langle\psi^R_{\mathsf{L},4}\psi^L_{\mathsf{L},4}\rangle. \end{aligned} \tag{3.121}$$

The pair $\langle\psi^R_{y,4}\psi^L_{y,4}\rangle$ takes finite ground state expectation values from $\mathcal{H}_{\text{intra}}$. $\mathcal{U}_{\text{edges}}$ introduces a Majorana mass for ψ^σ_2 and $\psi^{-\sigma}_3$ on the top and bottom edges. This leaves behind the single chiral Ising CFT $SO(1)_1$ on the boundaries, generated by the lone $\psi^L_{y=1,1}$ on the bottom edge and $\psi^R_{y=\mathsf{L},1}$ on the top edge.

On the other hand, at non-zero fillings $\nu = 1, 4, 9, 16$ when $d^{\sigma}_{y,1}$ carries electric charge $q_1 = \pm 1, \pm 2, \pm 3, \pm 4$ respectively, (3.121) does not preserve charge conservation. The edge CFT $U(1)_4 \times \overline{\text{Ising}}$—consisting of the charge carrying forward moving $d_1 = (\psi_1 + i\psi_2)/\sqrt{2} \sim e^{i\phi_1}$ and neutral backward moving $\bar{\psi}_3$—cannot be reduced. The fermions $\psi_{1,2}$ and $\bar{\psi}_3$ differs from each other by local bosons (up to the ground state expectation value $\langle \psi_4^R \psi_4^L \rangle$) and belong to the same fermion anyon class f. The spinor fields $e^{\pm i\phi_1/2}$ (spin 1/8) and the Ising twist field $\bar{\sigma}_3$ (spin $-1/16$) of $\bar{\psi}_3$ are confined together and can only appear simultaneously. The combinations belong in the Ising anyon class σ, which has spin $h_\sigma = 1/8 - 1/16 = 1/16$. This recovers the $SO(1)_1$ topological order. Unlike the electrically neutral case, the superselection sectors f and σ now each contain a collection of fields with mixed chirality and electric charges, $Q_f = \{\pm q_1, 0\}$ and $Q_\sigma = \{\pm q_f/2\}$. These charged $SO(1)_1$ bFQH states are not included in Figs. 3.1, 3.4 and Tables A.10, A.11.

Moving on to the construction of the $SO(15)_1$ bFQH state, we apply the particle-hole conjugation on the $SO(1)_1$ state by shifting the wire and chiral labels in the Hamiltonian (3.116) from $\psi^L_{y,p} \to \psi^R_{y,p}$ and $\psi^R_{y,p} \to \psi^R_{y+1,p}$. The model Hamiltonian $\mathcal{H}[SO(15)_1] = \mathcal{H}_0 + \mathcal{H}^f_{\text{intra}} + \mathcal{H}_{\text{inter}} + \mathcal{H}_{\text{intra}}$ consists of the following shifted inter-wire and intra-wire backscat-

tering terms (see also Fig. 3.6(b)):

$$\begin{aligned}
&\mathcal{H}_{\text{intra}} + \mathcal{H}_{\text{inter}} \\
&= -u \sum_y \sum_{4\le p<q\le 16} \psi^L_{y+1,p}\psi^L_{y+1,q}\psi^R_{y,p}\psi^R_{y,q} \\
&\quad - u \sum_y \Big[\psi^L_{y,1}\psi^L_{y,2}\psi^R_{y,1}\psi^R_{y,2} \\
&\quad + \lambda_0^2 \psi^L_{y+1,1}\psi^L_{y+2,3}\psi^R_{y+1,1}\psi^R_{y,3}\psi^L_{y+1,4}\psi^R_{y,4}\psi^L_{y+2,4}\psi^R_{y+1,4} \\
&\quad + \lambda_0^2 \psi^L_{y+1,2}\psi^L_{y+2,3}\psi^R_{y+1,2}\psi^R_{y,3}\psi^L_{y+1,4}\psi^R_{y,4}\psi^L_{y+2,4}\psi^R_{y+1,4}\Big].
\end{aligned} \tag{3.122}$$

The model preserves charge and momentum conservation. Using a similar mean-field analysis as in (3.118), the model gaps all fermions in the bulk but leaves behind gapless Majorana fermions on the boundary. Since the model involves second nearest wire interactions, the Majorana fermions that remain gapless near the bottom edge are $\psi^L_{y=1,p=1,\ldots,16}$, $\psi^R_{y=1,p=1,2}$, and $\psi^L_{y=2,p=3}$. Two pairs of Majoranan fermions can further be gapped by the edge potential at $y = 1$:

$$\mathcal{U}_{\text{edge}} = u\partial_x\phi^R_1\partial_x\phi^L_1 - u'\cos\left[2\left(\phi^R_1 - \phi^L_1\right)\right], \tag{3.123}$$

for a sufficiently strong "repulsive" interaction $u < -\frac{3\tilde{v}}{10\pi}$, so that the sine-Gordon potential is relevant. There remains 15 chiral Majoranan fermions $\psi^L_{y=1,p=3,\ldots,16}$ and $\psi^L_{y=2,p=3}$ (see Fig. 3.6(b)). They generate the chiral $SO(15)_1$ WZW CFT on the edge. All 15 fermion fields belong to the same anyon class f. For instance, $\psi^L_{y=1,p}$ and $\psi^L_{y=2,3}$ differ from each other by local bosons and ground state expectation values $\langle\psi^L_{y=2,4}\psi^R_{y=1,4}\rangle$. The Ising twist fields of each of the 15 fermions must appear simultaneously due to electron locality. Therefore, the

bFQH state carries the $SO(15)_1$ topological order. Although the possible filling numbers of the $SO(15)_1$ bFQH models are $\nu = 16, 15, 12, 7, 0$, depending on the electric charge $q_1 = 0, 1, 2, 3, 4$ of the Dirac fermion $d_1 = (\psi_1 + i\psi_2)/\sqrt{2}$, we only include the filling 16 case in Figs. 3.1, 3.4 and Tables A.10, A.11. This is because it is the only bFQH state that is particle-hole conjugate to the neutral $\nu = 0$ $SO(1)_1$ Ising state.

The G_2 and F_4 Fibonacci states

We now construct bosonic fractional quantum Hall (bFQH) states with Fibonacci topological order. These phases support Fibonacci anyon excitations [RR99, SB01]. The gapless edge modes are described by either the G_2 or F_4 WZW CFT at level 1. These states were first constructed by the coupled-wire approach in Ref. [LQHT19] at filling $\nu = 8$. We begin by briefly reviewing this construction. Then, we present the following newly-discovered properties of these (and related) Fibonacci states: (i) the explicit charge assignments of the G_2 and F_4 currents and Fibonacci primary fields, (ii) the new Fibonacci states at filling $\nu = 0$ and 16, and (iii) the realization of bulk Fibonacci anyons using an open string of local boson operators.

The coupled-wire models begin with the embedding of the $(G_2)_1$ and $(F_4)_1$ WZW subalgebras in $(E_8)_1$. With the help of the 8 non-local fermions $d_j \sim e^{i\phi_j}$ that represent the E_8 (see (3.27)), the embedding makes use of the "parafermion" decomposition of the current

algebra [Gep87],

$$(G_2)_1 \simeq SU(3)_1 \times \mathbb{Z}_3, \tag{3.124}$$

where "$\mathbb{Z}_3$" stands for the $\mathbb{Z}_3$ parafermion CFT [ZF85] with central charge $c = 4/5$. G_2 has 2 Cartan generators, 6 long roots, and 6 short roots. The Cartan generators and long roots of G_2 coincide with those of $SU(3)_1$, presented in (3.47) and (3.48) in §3.3.1. The $(G_2)_1$ WZW algebra extends $SU(3)_1$ by the $\mathbb{Z}_3$ parafermion CFT, which is the coset $SU(2)_3/U(1)_6$ (or equivalently, $(G_2)_1/SU(3)_1$). The $\mathbb{Z}_3$ parafermion primary field Ψ and its hermitian conjugate $\Psi^\dagger$ carry spin $h = 2/3$ and obey the 3-nilpotent fusion rule. The latter means that $\Psi^3 = (\Psi^\dagger)^3 = \Psi \times \Psi^\dagger = 1$ belong in the trivial primary sector of local fields. The parafermion field can be chosen to be the linear combination of vertex operators

$$\Psi = \frac{1}{\sqrt{3}} \left[-e^{-i2(\phi_1+\phi_2+\phi_3)/3} + 2e^{i(\phi_1+\phi_2+\phi_3)/3} \sin\phi_4 \right] \tag{3.125}$$

for each wire y and chiral sector $\sigma = R, L$. The coefficients of the linear combination are chosen so that, the parafermion fields obey the OPE

$$\begin{aligned} \Psi(z)\Psi^\dagger(w) &= \frac{1}{(z-w)^{4/3}} \left[1 + \frac{5}{3}(z-w)^2 T_{\mathbb{Z}_3}(w) \right] + \ldots, \\ \Psi(z)\Psi(w) &= \frac{2/\sqrt{3}}{(z-w)^{2/3}} \Psi^\dagger(w) + \ldots, \end{aligned} \tag{3.126}$$

where $T_{\mathbb{Z}_3}(z)$ is the energy-momentum tensor of the $\mathbb{Z}_3$ parafermion CFT. The 6 short roots of $(G_2)_1$ are the decoupled products $\mathcal{E}^\dagger\Psi$ and $\mathcal{E}\Psi^\dagger$, where $\mathcal{E}$ is the $SU(3)_1$ primary

field triplet defined in (3.56). We choose the positive short roots to be

$$\begin{aligned}
[\mathbf{E}_{G_2}]_1 &= e^{-i(\phi_1+\phi_2-2\phi_3)/3}\Psi, \\
[\mathbf{E}_{G_2}]_2 &= e^{-i(\phi_1-2\phi_2+\phi_3)/3}\Psi, \\
[\mathbf{E}_{G_2}]_3 &= e^{i(-2\phi_1+\phi_2+\phi_3)/3}\Psi^\dagger.
\end{aligned} \tag{3.127}$$

The negative short roots are the Hermitian conjugates of the positive ones. These operators have spin $h = h_{\mathcal{E}} + h_\Psi = 1/3 + 2/3 = 1$, appropriate for a boson. Moreover, each of them is a linear combination of three E_8 roots and therefore is an even integral combination of local electrons. The locality of the G_2 short roots means the bosonic pairs $\mathcal{E}\Psi^\dagger$ and $\mathcal{E}^\dagger\Psi$ in the tensor product (3.124) are "anyon condensed" [BS09, Bur18]. Together with the $SU(3)_1$ currents, they span the closed G_2 WZW algebra at level 1. In the coupled-wire model, in order for the short root current backscattering to conserve charge and momentum, all three vertex operator components of each short root must have identical charge and x-momentum. This requires $d_1 d_2 d_3 \sim e^{i(\phi_1+\phi_2+\phi_3)}$ and $d_4 \sim e^{i\phi_4}$ to both have zero charge and vanishing momentum.

We define the $(F_4)_1$ WZW subalgebra as the complement subalgebra of $(G_2)_1$ in $(E_8)_1$. The $(F_4)_1$ WZW algebra has 4 Cartan generators, 24 long roots, and 24 short roots. It is an extension of $SO(9)_1$,

$$(F_4)_1 \simeq \mathcal{M}(5,4) \times SO(9)_1, \tag{3.128}$$

where $\mathcal{M}(5,4)$ is the tricritical Ising CFT [FMS12] with central charge $c = 7/10$. Here, we have taken $SO(9)_1$ to be generated by $\psi_8, \ldots, \psi_{16}$. $(F_4)_1$ contains the simply-laced algebra $SO(8)_1$, which is generated by $d_{j=5,\ldots,8} = (\psi_{2j-1} + i\psi_{2j})/\sqrt{2} \sim e^{i\phi_{5,\ldots,8}}$. The 4 Cartan generators of $(F_4)_1$ are those of $SO(8)_1$: $[\mathtt{H}_{F_4}]_l = \partial_{\mathsf{x}}\phi_{4+l}$, for $l = 1, \ldots, 4$. The 24 long roots of $(F_4)_1$ are the $SO(8)_1$ roots:

$$[\mathtt{E}_{F_4}(\mathsf{x})]_{\boldsymbol{\alpha}_{SO(8)}} = e^{i\boldsymbol{\alpha}_{SO(8)}\cdot(\boldsymbol{\phi}(\mathsf{x})+\boldsymbol{k}\mathsf{x})}, \tag{3.129}$$

where the long root vectors are $\boldsymbol{\alpha}_{SO(8)} = \{\pm(\mathbf{e}_i \pm \mathbf{e}_j) : 5 \leq i < j \leq 8\}$ and $\boldsymbol{\phi} = (\phi_5, \ldots, \phi_8)$. The 24 short roots pair the 8 vector fermions $e^{\pm i\phi_{5,\ldots,8}}$ and 16 spinors $e^{i\boldsymbol{\varepsilon}\cdot\boldsymbol{\phi}/2}$ of $SO(8)_1$ with Majorana fermions ψ_8 and $\psi_\pm$, respectively [LQHT19]:

$$\begin{aligned}
[\mathtt{E}_{F_4}(\mathsf{x})]_{\pm j} &= \psi_8(\mathsf{x})e^{\pm i(\phi_{4+j}(\mathsf{x})+k_{4+j}\mathsf{x})}, \quad j = 1, \ldots, 4, \\
[\mathtt{E}_{F_4}(\mathsf{x})]_{\boldsymbol{\varepsilon}_\pm} &= \psi_\pm(\mathsf{x})e^{i\varepsilon_\pm^j(\phi_{4+j}(\mathsf{x})+k_{4+j}\mathsf{x})/2},
\end{aligned} \tag{3.130}$$

where $\varepsilon_\pm^j = 1$ or -1 and $\prod_{j=1}^4 \varepsilon_\pm^j = \pm 1$. The 8 short roots in the first line of (3.130) are the short roots of $SO(9)_1$ (c.f. (3.104) in section 3.3.2). The remaining 16 short roots in the second line extend $SO(9)_1$ to $(F_4)_1$. The Majorana fermions $\psi_\pm$ are

$$\psi_\pm = \frac{1}{\sqrt{2}}\omega_\pm e^{i(\phi_1+\phi_2+\phi_3\pm\phi_4)/2} + h.c., \tag{3.131}$$

where $\omega_+ = e^{i3\pi/8}$ and $\omega_- = e^{-i\pi/8}$. The F_4 short roots are linear combinations of E_8 roots. In the coupled-wire model, the current backscattering conserves charge and momentum

when all vertex components in a given short root have identical charge and momentum. Like the G_2 case, this condition is satisfied when $d_1d_2d_3$ and d_4 both have vanishing charge and momentum.

The fermions $\psi_\pm$ are clearly decoupled from $SO(8)_1$ because they involve disjoint sets of bosonized variables. Moreover, $\psi_\pm$ are also decoupled from $SU(3)_1$, which is generated by the traceless combinations $\phi_1-\phi_2$, $\phi_2-\phi_3$ and $\phi_3-\phi_1$ that have non-singular correlations with $\phi_1+\phi_2+\phi_3$. The phases $\omega_\pm$ are chosen so that the OPE $\Psi(z)\psi_\pm(w)$ and $\Psi^\dagger(z)\psi_\pm(w)$ with the $\mathbb{Z}_3$ parafermion Ψ in (3.125) are non-singular. This ensures the $(G_2)_1$ and $(F_4)_1$ currents have non-singular mutual OPE. It is essential to recognize that, although $\psi_8,\psi_\pm$ each has self-fermionic statistics and obeys the 2-nilpotent fusion rules, $\psi_8^2=\psi_\pm^2=1$, the three fermions have mutual *semionic* statistics due to the cross fusion rule, $\psi_8\times\psi_\pm=\psi_\mp$, that is due to the OPE, $\psi_8(z)\psi_\pm(w)\sim(z-w)^{-1/2}\psi_\mp(w)+\ldots$. The short roots $[\mathtt{E}_{F_4}]_{\boldsymbol{\varepsilon}_\pm}$ in (3.130) can be decomposed in terms of primary fields in $\mathcal{M}(5,4)$ and $SO(9)_1$:

$$[\mathtt{E}_{F_4}]_{\boldsymbol{\varepsilon}_\pm}\sim\left[\frac{7}{16}\right]\otimes\left[\frac{9}{16}\right]_{\boldsymbol{\varepsilon}_\pm}. \tag{3.132}$$

$[7/16]$ is the primary field with spin $h=7/16$ at position $(r,s)=(2,1)$ on the conformal grid of the tricritical Ising CFT $\mathcal{M}(5,4)$ [FMS12]. $[9/16]_{\boldsymbol{\varepsilon}_\pm}$ is the spinor field $\sigma_{\boldsymbol{\varepsilon}_\pm}=\sigma_8 e^{i\varepsilon_\pm^j\phi_{4+j}/2}$ with spin $h=9/16$ in $SO(9)_1$, where σ_8 is the Ising twist field associated to ψ_8. The locality of $[\mathtt{E}_{F_4}]_{\boldsymbol{\varepsilon}_\pm}$ means the bosonic pairs (3.132) in the tensor product (3.128) are "anyon condensed" [BS09, Bur18].

Having defined the WZW algebra embedding $(G_2)_1 \times (F_4)_1 \subseteq (E_8)_1$, we are ready to review the coupled-wire construction of the Fibonacci bFQH states [LQHT19]. Following (3.42), the electron-based models begin with the intra-wire backscattering $\mathcal{H}^f_{\text{intra}}$ of the integrated fermions (see (3.22)). This gaps all local odd fermion degrees of freedom and leaves behind the counter-propagating $(E_8)_1$ bosons on each wire. The Fibonacci states are constructed by back-scattering the $(G_2)_1$ currents and $(F_4)_1$ currents in complementary ways.

For example, the $(G_2)_1$ model consists of the inter-wire and intra-wire interactions $\mathcal{H}^{G_2}_{\text{inter}} + \mathcal{H}^{F_4}_{\text{intra}}$:

$$\begin{aligned}\mathcal{H}^{G_2}_{\text{inter}} &= u_{\text{inter}} \sum_y \boldsymbol{J}^R_{y,G_2} \cdot \boldsymbol{J}^L_{y+1,G_2} \qquad (3.133)\\ &= \mathcal{H}^{SU(3)}_{\text{inter}} + u_{\text{inter}} \sum_y \left(\mathcal{O}^{SU(3)}_{y+1/2} \Psi^{R\dagger}_y \Psi^L_{y+1} + h.c. \right),\\ \mathcal{H}^{F_4}_{\text{intra}} &= u_{\text{intra}} \sum_y \boldsymbol{J}^R_{y,F_4} \cdot \boldsymbol{J}^L_{y,F_4} \qquad (3.134)\\ &= \mathcal{H}^{SO(9)}_{\text{intra}} + u_{\text{intra}} \sum_y \sum_{\boldsymbol{\varepsilon}_\pm} {[\mathbb{E}_{F_4}]^R_{y,\boldsymbol{\varepsilon}_\pm}}^\dagger [\mathbb{E}_{F_4}]^L_{y,\boldsymbol{\varepsilon}_\pm},\end{aligned}$$

where $\mathcal{H}^{SU(3)}_{\text{inter}}$ and $\mathcal{H}^{SU(3)}_{\text{inter}}$ were defined in (3.54) and (3.109) respectively. The operator $\mathcal{O}^{SU(3)}_{y+1/2}$ is the combination of the sine-Gordon vertex operators,

$$e^{i(\theta_1+\theta_2-2\theta_3)/3} + e^{i(\theta_1-2\theta_2+\theta_3)/3} + e^{i(-2\theta_1+\theta_2+\theta_3)/3},$$

where $\theta_j = \phi^R_{y,j} - \phi^L_{y+1,j}$. It is the singlet non-chiral product $\mathcal{E}^R_y \cdot {\mathcal{E}^L_{y+1/2}}^\dagger$ of $SU(3)_1$ primary fields in (3.56); it is pinned at a finite ground state expectation value under $\mathcal{H}^{SU(3)}_{\text{inter}}$. At low energies, the short root part of $\mathcal{H}^{G_2}_{\text{inter}}$ is approximated by the $\mathbb{Z}_3$ parafermion backscattering

terms,

$$\mathcal{H}^{G_2}_{\text{inter}} \to u_{\text{inter}} \sum_y \left\langle \mathcal{O}^{SU(3)}_{y+1/2} \right\rangle \Psi^{R\dagger}_y \Psi^L_{y+1} + h.c. \tag{3.135}$$

This gaps the counter-propagating $\mathbb{Z}_3$ parafermion sectors [FAT91].

Next, we focus on the F_4 sector. The Gross-Neveu interaction $\mathcal{H}^{SO(9)}_{\text{intra}}$ in (3.134) gaps the counter-propagating $SO(9)_1$ CFT on each wire (c.f. (3.109) in §3.3.2). On any given wire y, the non-chiral singlet combination,

$$\sum_{\boldsymbol{\varepsilon}_\pm} \sigma^R_{\boldsymbol{\varepsilon}_\pm} \sigma^L_{-\boldsymbol{\varepsilon}_\pm} = \sum_{\boldsymbol{\varepsilon}_\pm} \sigma^R_8 \sigma^L_8 e^{i\varepsilon^j_\pm (\phi^R_{4+j} - \phi^L_{4+j})}, \tag{3.136}$$

takes a finite ground state expectation value [SZT16]. Therefore, using the identification (3.132), the backscattering terms for the remaining F_4 short roots $[\mathtt{E}_{F_4}]_{\boldsymbol{\varepsilon}_\pm}$ are approximated at low energy by

$$\mathcal{H}^{F_4}_{\text{intra}} \to u_{\text{intra}} \sum_y \left[\sum_{\boldsymbol{\varepsilon}_\pm} \left\langle \sigma^R_{y,\boldsymbol{\varepsilon}_\pm} \sigma^L_{y,-\boldsymbol{\varepsilon}_\pm} \right\rangle \right] \sigma'_y, \tag{3.137}$$

where $\sigma' = \Phi_{\frac{7}{16},\frac{7}{16}}$ is the diagonal non-chiral product $[7/16]^R[7/16]^L$. The field σ' is identical to the (subleading) magnetization operator in the tricritical Ising model. Perturbation by this term is known to deform the model away from its critical point into a gapped phase [LMC91].

$\mathcal{H}^{G_2}_{\text{inter}} + \mathcal{H}^{F_4}_{\text{intra}}$ together introduce a finite excitation energy gap in the bulk of the coupled-wire model. In an open cylinder geometry, chiral G_2 WZW CFTs at level 1 are left behind

on the two boundaries. The particle-hole conjugate F_4 bFQH state can be constructed by switching the inter-wire and intra-wire backscattering patterns between G_2 and F_4. Charge conservation requires $d_1 d_2 d_3$ and d_4 to be electrically neutral. Hence, the charge vector $\mathbf{q} = (q_1, \ldots, q_8)$ of the 8 non-local Dirac fermions (see above (3.29)) must be further restricted by $q_1 + q_2 + q_3 = q_4 = 0$. This forces $(q_1, q_2, q_3) = (0, 0, 0)$ or $(\pm 2, \mp 2, 0)$. The filling numbers of the Fibonacci bFQH states are

$$\begin{aligned} \nu_{G_2} &= \sum_{j=1}^{3} q_j^2 = 0 \text{ or } 8, \\ \nu_{F_4} &= \sum_{j=5}^{8} q_j^2 = 16 - \nu_{G_2}. \end{aligned} \tag{3.138}$$

The quantized thermal Hall conductances are determined by the chiral central charges of the level 1 WZW algebras $c_{G_2} = 14/5$ and $c_{F_4} = 26/5$. The G_2 coupled-wire model conserves momentum along the x direction when the Fermi momenta take under the projection matrix $P_A = P_{SU(3)_1}$. The same goes for the F_4 model by substituting $P_A = P_{SO(8)_1} = O_4 \oplus \mathbb{I}_4$.

Both G_2 and F_4 states have Fibonacci topological order: These states support Fibonacci anyons that follow the fusion rule $\tau \times \tau = 1 + \tau$ and carry the golden ratio quantum dimension $d_\tau = (1 + \sqrt{5})/2$. The Fibonacci primary fields of the $(G_2)_1$ and $(F_4)_1$ WZW CFTs can be found in Ref. [LQHT19]. They can be summarized as follows. The G_2 Fibonacci superselection sector is the 7-dimensional irreducible representation of the G_2 algebra spanned

by

$$
\begin{aligned}
[\tau] &= (1 \otimes \tau) \oplus (\mathcal{E} \otimes \tau\Psi^\dagger) \oplus (\mathcal{E}^\dagger \otimes \tau\Psi) \\
&= \text{span} \left\{ \begin{array}{c} \tau, e^{i(\phi_1+\phi_2-2\phi_3)/3}\tau\Psi^\dagger, \\ e^{i(\phi_2+\phi_3-2\phi_1)/3}\tau\Psi^\dagger, e^{i(\phi_3+\phi_1-2\phi_2)/3}\tau\Psi^\dagger, \\ e^{-i(\phi_1+\phi_2-2\phi_3)/3}\tau\Psi, e^{-i(\phi_2+\phi_3-2\phi_1)/3}\tau\Psi, \\ e^{-i(\phi_3+\phi_1-2\phi_2)/3}\tau\Psi \end{array} \right\}.
\end{aligned} \tag{3.139}
$$

Here, the tensor product splits each field in the $\mathbb{Z}_3$ parafermion CFT sector and $SU(3)_1$ sector (see (3.124)). τ is the spin 2/5 primary field in the $\mathbb{Z}_3$ parafermion CFT. $\tau\Psi$ and $\tau\Psi^\dagger$ are the two primary fields with spin 1/15. The vertex operators are $SU(3)_1$ primary fields in $\mathcal{E}$ and $\mathcal{E}^\dagger$ (see (3.56)). The F_4 Fibonacci super-selection sector is the 26-dimensional irreducible representation of F_4 algebra spanned by

$$
[\bar{\tau}] = \left(\Phi_{(1,3)} \otimes 1\right) \oplus \left(\Phi_{(1,2)} \otimes f\right) \oplus \left(\Phi_{(2,2)} \otimes \sigma\right), \tag{3.140}
$$

where the fields are split in the tricritical Ising sector and $SO(9)_1$ sector (see (3.128)). Here, $\Phi_{(r,s)}$ are the primary fields located at the (r,s) entry in the conformal grid of the CFT minimal model $\mathcal{M}(5,4)$. $\Phi_{(1,3)} = \bar{\tau}$, $\Phi_{(1,2)}$ and $\Phi_{(2,2)}$ have spins 3/5, 1/10 and 3/80, respectively. f is the $SO(9)_1$ vector spanned by ψ_8 and $e^{\pm i\phi_{j=5,\ldots,8}}$. σ is the $SO(9)_1$ spinor spanned by $\sigma_8 e^{i\varepsilon^j\phi_{4+j}}$, for $\varepsilon^{j=1,\ldots,4} = \pm$. The electric charges of the fields in (3.139) and (3.140) are completely determined by their vertex component. The charge assignments of the G_2 and F_4 currents and their Fibonacci primary fields are summarized in Tables A.1 and A.2.

We conclude this section by showing Fibonacci anyon pairs can be created in the bulk by applying an open string $\mathcal{S}$ of electron operators on the ground state. This operator string makes use of the E_8 currents that lie outside of the $G_2 \times F_4$ subalgebra. The E_8 algebra has dimension 248, while $G_2 \times F_4$ has dimension $14 + 52 = 66$. The complement $(G_2 \times F_4)^\perp$ is spanned by $182 = 7 \times 26$ current fields that can be decomposed into the Fibonacci pair $[\tau][\bar{\tau}]$ from (3.139) and (3.140). The operator string is a product $\mathcal{S} = \prod_{y=y_1}^{y_2} \mathcal{O}_y^R(\mathsf{x}_0)\mathcal{O}_y^L(\mathsf{x}_0)$, where $\mathcal{O}$ is a current operator in $(G_2 \times F_4)^\perp$. For example, we take $\mathcal{O} = \partial_{\mathsf{x}}(\phi_1 + \phi_2 + \phi_3)$. This operator is a $SU(3)_1 \times SO(9)_1$ singlet and has trivial OPE with the $SU(3)_1$ and $SO(9)_1$ currents. Therefore, it splits into the product $\mathcal{O} \sim \tau\bar{\tau}$, where τ is the primary field with spin 2/5 in the $\mathbb{Z}_3$ parafermion CFT and $\bar{\tau} = \Phi_{(1,3)}$ is the primary field with spin 3/5 in the tricritical Ising CFT. The string operator becomes

$$\mathcal{S} \sim \prod_{y=y_1}^{y_2} \tau_y^R(\mathsf{x}_0)\bar{\tau}_y^R(\mathsf{x}_0)\tau_y^L(\mathsf{x}_0)\bar{\tau}_y^L(\mathsf{x}_0). \tag{3.141}$$

To demonstrate this, we will now apply this operator to the ground state of the G_2 model. (The F_4 model has a similar structure.) The inter-wire $\mathbb{Z}_3$ parafermion backscattering interaction (3.135) introduces the finite ground state expectation value $\langle \tau_y^R(\mathsf{x}_0)\tau_{y+1}^L(\mathsf{x}_0)\rangle$. At the same time, the intra-wire $\sigma' = \Phi_{\frac{7}{16},\frac{7}{16}}$ interaction in (3.137) pins the ground state expectation value $\langle \bar{\tau}_y^R(\mathsf{x}_0)\bar{\tau}_y^L(\mathsf{x}_0)\rangle$. To see this, we use the effective Landau-Ginzburg description of minimal CFT models [FMS12]:

$$\mathcal{L}_{2D} = \frac{1}{2}(\nabla\Phi)^2 + V(\Phi). \tag{3.142}$$

The relevant minimal models here are the tricritical Ising model $\mathcal{M}(5,4)$ with

$$V(\Phi) = \Phi^6 - \lambda_3 \Phi^3, \tag{3.143}$$

and the 3-state Potts model $\mathcal{M}(6,5)$ with

$$V(\Phi) = \Phi^8 - \lambda_6 \Phi^6. \tag{3.144}$$

When $\lambda_{3,6} = 0$, the models are at their conformal critical points. The λ_3 term in (3.143) deforms the tricritical Ising model by the subleading magnetization operator $\Phi^3 \sim \sigma' = \Phi_{\frac{7}{16},\frac{7}{16}}$ that appears in (3.137). (Here, "subleading" means that σ' is the next-most-relevant, in the renormalization group sense, magnetization operator of the tricritical Ising model [FMS12]. A similar definition of "subleading" applies below.) For nonzero $\lambda_3 > 0$, the Landau-Ginzburg variable takes a nonzero ground state expectation value, and consequently, so too does the (tricritical Ising) subleading thermal operator $\langle \Phi^4 \rangle \sim \langle \varepsilon' \rangle = \langle \Phi_{\frac{3}{5},\frac{3}{5}} \rangle = \langle \bar{\tau}^R \bar{\tau}^L \rangle$. The λ^6 term in (3.144) corresponds to the $\mathbb{Z}_3$ parafermion backscattering $\Phi^6 \sim \Phi_{\frac{2}{3},\frac{2}{3}} = \Psi^{R\dagger}\Psi^L$ in (3.135). It pins the Landau-Ginzburg field and introduces the finite ground state expectation value for the (3-state Potts) thermal operator $\langle \Phi^4 \rangle \sim \langle \varepsilon \rangle = \langle \Phi_{\frac{2}{5},\frac{2}{5}} \rangle = \langle \tau^R \tau^L \rangle$.

By replacing $\tau_y^R \tau_{y+1}^L$ and $\bar{\tau}_y^R \bar{\tau}_y^L$ by scalar ground state expectation values, the operator string $\mathcal{S}$ in (3.141) at low energy becomes

$$\mathcal{S} \to \tau_{y_2}^R(\mathsf{x}_0)\tau_{y_1}^L(\mathsf{x}_0) \times \prod_{y=y_1}^{y_2-1} \left\langle \tau_y^R(\mathsf{x}_0)\tau_{y+1}^L(\mathsf{x}_0) \right\rangle \prod_{y=y_1}^{y_2} \left\langle \bar{\tau}_y^R(\mathsf{x}_0)\bar{\tau}_y^L(\mathsf{x}_0) \right\rangle .$$

The Fibonacci field operators $\tau^R_{y_2}(\mathsf{x}_0)\tau^L_{y_1}(\mathsf{x}_0)$ create a pair of gapped excitations, one between y_2 and y_2+1 and another between y_1-1 and y_1.

The $SU(2)_4$ and $Sp(8)_1$ metaplectic states

We construct the non-Abelian orbifold bFQH states

$$SU(2)_4 = \frac{SU(3)_1}{\mathbb{Z}_2}, \quad Sp(8)_1 = \frac{(E_6)_1}{\mathbb{Z}_2} \tag{3.145}$$

by gauging the $\mathbb{Z}_2$ outer automorphism symmetry of $SU(3)_1$ and $(E_6)_1$. The concepts of orbifolding and gauging were introduced in the contexts of CFTs [DHVW85, DHVW86, Gin88, DVV88, MS89, CRTR17] and topological field theories [BBCW19a, THF15a]. In §3.3.1, we discussed the Abelian orbifold bFHQ states, $U(1)_8 = SU(2)_1/\mathbb{Z}_2$ and $SU(8)_1 = (E_7)_1/\mathbb{Z}_2$, where the $\mathbb{Z}_2$ symmetry is an inner automorphism that does not alter the anyon classes of $SU(2)_1$ and $(E_7)_1$. In contrast, the $\mathbb{Z}_2$ symmetry in $SU(3)_1$ and $(E_6)_1$ in (3.145) is an outer automorphism [TKV16, Teo16] that conjugates the anyon classes $\mathcal{E} \leftrightarrow \mathcal{E}^\dagger$. When such a symmetry is gauged, the topological phase is promoted to a non-Abelian orbifold phase, referred to as a twist liquid [THF15a]. The edge-state theory of a twist liquid is an orbifold CFT. Ref. [TH23] considered the coupled-wire construction of non-Abelian dihedral twist liquids, such as the $SU(2)_4 = SO(3)_2 = SU(3)_1/\mathbb{Z}_2$ states. Here, we study bFQH symplectic $Sp(8)_1$ and $SU(2)_4$ states that arise from the E_8 state.

The origin of the $\mathbb{Z}_2$ symmetry is the internal gauge symmetry in the non-local Dirac fermion presentation (3.27) of the E_8 state. The symmetry, for any give wire y and chiral sector

$\sigma = R, L$, flips the signs of all eight non-local Dirac fermions, $d_j \to -d_j$, through a shift of the bosonized variables $\phi_j \to \phi_j + \pi$. All local operators must be even under this $\mathbb{Z}_2$ symmetry. This includes, in particular, all E_8 current operators. In (3.93) (see section 3.3.1), we defined a new set of bosonized variables $\tilde{\phi}_{2l-1} = \phi_{2l-1}$, $\tilde{\phi}_{2l} = (H_4)^{l'}_{l}\, \phi_{2l'}/2$, where H_4 is the Hadamard matrix (3.89). These bosons were associated with the non-local Dirac fermions $\tilde{d}_j = (\tilde{\psi}_{2j-1} + i\tilde{\psi}_{2j})/\sqrt{2} \sim e^{i\tilde{\phi}_j}$ that transformed according to the $\mathbb{Z}_2$ symmetry as $\tilde{d}_j \to (-1)^j \tilde{d}_j$. Here, in addition, we assume that fermions $\tilde{d}_{1,2,3,4}$ carry zero electric charge and zero x-momentum. This allows us to introduce a different basis of fermions:

$$\begin{aligned} &\bar{d}_1 = \frac{\tilde{\psi}_3 + i\tilde{\psi}_1}{\sqrt{2}}, \quad \bar{d}_2 = \frac{\tilde{\psi}_4 + i\tilde{\psi}_2}{\sqrt{2}}, \\ &\bar{d}_3 = \frac{\tilde{\psi}_7 + i\tilde{\psi}_5}{\sqrt{2}}, \quad \bar{d}_4 = \frac{\tilde{\psi}_8 + i\tilde{\psi}_6}{\sqrt{2}}, \\ &\bar{d}_5 = \tilde{d}_5, \quad \bar{d}_6 = \tilde{d}_7, \quad \bar{d}_7 = \tilde{d}_6, \quad \bar{d}_8 = \tilde{d}_8. \end{aligned} \tag{3.146}$$

These fermions are bosonized as $\bar{d}_j \sim e^{i\bar{\phi}_j}$. The local $\mathbb{Z}_2$ symmetry acts as follows:

$$\begin{aligned} &\bar{d}_{1,2,3,4} \to \bar{d}^{\dagger}_{1,2,3,4}, \quad \bar{\phi}_{1,2,3,4} \to -\bar{\phi}_{1,2,3,4}, \\ \mathbb{Z}_2: \quad &\bar{d}_{5,6} \to -\bar{d}_{5,6}, \quad \bar{\phi}_{5,6} \to \bar{\phi}_{5,6} + \pi, \\ &\bar{d}_{7,8} \to \bar{d}_{7,8}, \quad \bar{\phi}_{7,8} \to \bar{\phi}_{7,8}. \end{aligned} \tag{3.147}$$

We now revisit the $SU(3)_1$ and $(E_6)_1$ WZW algebras (studied in §3.3.1) to show how the $SU(2)_4$ and $Sp(8)_1$ symmetries arise. These algebras are generated by current operators $\partial_{\mathsf{x}}\bar{\phi}_j$ and $e^{i\alpha^j\bar{\phi}_j}$, obtained from those in §3.3.1 by replacing the bosonized variables $\phi_j \to \bar{\phi}_j$. Not all current operators are local because they may not be even under the internal $\mathbb{Z}_2$

symmetry (3.147). For example, the Cartan generators $\partial\bar{\phi}_{1,2,3,4}$ are now odd under $\mathbb{Z}_2$ and therefore are *not* local integral combinations of electrons. The local $(E_8)_1$ currents constructed by electrons are still the original ones associated with the old bosonized variables ϕ_j. The local sub-algebras of $SU(3)_1$ and $(E_6)_1$—consisting of current operators that are even under the internal $\mathbb{Z}_2$ symmetry and lie inside the local $(E_8)_1$ algebra—are $SU(2)_4$ and $Sp(8)_1$, respectively. To see this, we start with the $SU(3)_1$ algebra, which is generated by $\mathtt{H}_1 = \partial_{\mathtt{x}}(\bar{\phi}_1 - \bar{\phi}_2)/\sqrt{2}$, $\mathtt{H}_2 = \partial_{\mathtt{x}}(\bar{\phi}_1 + \bar{\phi}_2 - 2\bar{\phi}_3)/\sqrt{6}$, and the roots $e^{\pm i(\bar{\phi}_a - \bar{\phi}_b)}$ for $1 \le a < b \le 3$. Its $\mathbb{Z}_2$ even sub-algebra is spanned by $J_1 = 2\sqrt{2}\cos\left(\bar{\phi}_2 - \bar{\phi}_3\right)$, $J_2 = 2\sqrt{2}\cos\left(\bar{\phi}_3 - \bar{\phi}_1\right)$, and $J_3 = 2\sqrt{2}\cos\left(\bar{\phi}_1 - \bar{\phi}_2\right)$. $J_{1,2,3}$ obey the $SU(2)_4$ current OPE,

$$J_a(z)J_b(w) = \frac{4\delta_{ab}}{(z-w)^2} + \frac{i\sqrt{2}\epsilon_{abc}}{z-w}J_c(w) + \ldots, \tag{3.148}$$

where ϵ_{abc} is the Levi-Civita symbol for $a, b, c = 1, 2, 3$, and the coefficient of the most singular term specifies the level $k = 4$ of the $SU(2)$ WZW algebra.

Next, we consider the $(E_6)_1$ algebra. Among its Cartan generators $\mathtt{H}_b = \gamma_b^j \partial_{\mathtt{x}}\bar{\phi}_j$, only $\partial_{\mathtt{x}}\bar{\phi}_{5,6,7,8}$ are even under the $\mathbb{Z}_2$ symmetry (3.147). In addition, there are 32 root operator combinations of E_6 that are even under the $\mathbb{Z}_2$. They are

$$\begin{aligned}
&e^{\pm i(\bar{\phi}_5+\bar{\phi}_6)}, e^{\pm i(\bar{\phi}_5-\bar{\phi}_6)}, e^{\pm i(\bar{\phi}_7+\bar{\phi}_8)}, e^{\pm i(\bar{\phi}_7-\bar{\phi}_8)},\\
&\chi_0 e^{\pm i\bar{\phi}_7}, \chi_0 e^{\pm i\bar{\phi}_8}, \eta_0 e^{\pm i\bar{\phi}_5}, \eta_0 e^{\pm i\bar{\phi}_6},\\
&\eta_\pm e^{i\sum_{j=5}^8 \varepsilon_\pm^j \bar{\phi}_j/2}, \quad \text{if } \varepsilon_\pm^5 = \varepsilon_\pm^6,\\
&\chi_\pm e^{i\sum_{j=5}^8 \varepsilon_\pm^j \bar{\phi}_j/2}, \quad \text{if } \varepsilon_\pm^5 = -\varepsilon_\pm^6,
\end{aligned} \tag{3.149}$$

where $\varepsilon_{\pm}^{j=5,6,7,8} = \pm 1$ with $\prod_{j=5}^{8} \varepsilon_{\pm}^{j} = \pm 1$. The Majorana fermions are

$$\begin{aligned}
\chi_0 &= \sqrt{2}\cos\bar{\phi}_4, \quad \eta_0 = \sqrt{2}\sin\bar{\phi}_4, \\
\chi_\pm &= \sqrt{2}\cos\left[\left(\bar{\phi}_1 + \bar{\phi}_2 + \bar{\phi}_3 \pm \bar{\phi}_4\right)/2\right], \\
\eta_\pm &= \sqrt{2}\sin\left[\left(\bar{\phi}_1 + \bar{\phi}_2 + \bar{\phi}_3 \pm \bar{\phi}_4\right)/2\right].
\end{aligned} \tag{3.150}$$

While $\chi_{0,\pm}$ and $\eta_{0,\pm}$ have neutral charge and zero momentum, $\bar{d}_{5,6,7,8} \sim e^{i\bar{\phi}_{5,6,7,8}}$ can carry charge and momentum, in general. Thus, $\bar{\phi}_j$ in the vertex components in (3.149) are really abbreviations for $\bar{\phi}_j(\mathsf{x}) + \bar{k}_j\mathsf{x}$ for $j = 5, 6, 7, 8$. The root operators (3.149) can be put in a more familiar form using the basis transformation,

$$\begin{pmatrix} X_1 \\ X_2 \\ X_3 \\ X_4 \end{pmatrix} = \frac{1}{2}\begin{pmatrix} 1 & 1 & 0 & 0 \\ 1 & -1 & 0 & 0 \\ 0 & 0 & 1 & 1 \\ 0 & 0 & 1 & -1 \end{pmatrix}\begin{pmatrix} \bar{\phi}_5 \\ \bar{\phi}_6 \\ \bar{\phi}_7 \\ \bar{\phi}_8 \end{pmatrix}, \tag{3.151}$$

after which these operators become

$$\begin{aligned}
&e^{\pm 2iX_1}, e^{\pm 2iX_2}, e^{\pm 2iX_3}, e^{\pm 2iX_4}, \\
&\chi_0 e^{\pm i(X_3 \pm X_4)}, \eta_0 e^{\pm i(X_1 \pm X_2)}, \\
&\eta_+ e^{\pm i(X_1 \pm X_3)}, \chi_+ e^{\pm i(X_2 \pm X_4)}, \\
&\eta_- e^{\pm i(X_1 \pm X_4)}, \chi_- e^{\pm i(X_2 \pm X_3)}.
\end{aligned} \tag{3.152}$$

The $\mathbb{Z}_2$ symmetry acts as

$$\mathbb{Z}_2 : \begin{array}{l} X_1 \to X_1 + \pi, \quad X_{2,3,4} \to X_{2,3,4}, \\ \chi_\pm \to \chi_\pm, \quad \eta_\pm \to -\eta_\pm. \end{array} \tag{3.153}$$

The vertex components $e^{i\alpha^l X_l}$ are associated with the root vectors $\boldsymbol{\alpha} = (\alpha^1, \alpha^2, \alpha^3, \alpha^4)$ of $C_4 = Sp(8)$. The operators in the first line of (3.152) corresponds to the 8 long roots, $\boldsymbol{\alpha} = \pm 2\mathbf{e}_{1,2,3,4}$ of length 2. The remaining operators in (3.152) correspond to the 24 short roots, $\boldsymbol{\alpha} = \pm\mathbf{e}_l \pm \mathbf{e}_{l'}$ with length $\sqrt{2}$, for $1 \le l < l' \le 4$. Together with the 4 Cartan generators, $\mathtt{H}_l = \sqrt{2}\partial_{\mathtt{x}} X_l$, these operators span the $Sp(8)$ WZW current algebra at level 1.

The coupled-wire models of the $SU(2)_4$ and $Sp(8)_1$ states follow the general strategy in (3.42). The models begin with the intra-wire backscattering $\mathcal{H}^f_{\text{intra}}$ of the integrated fermions (see (3.22)). The remaining counter-propagating modes of the $(E_8)_1$ CFT on each wire are gapped by backscattering the $SU(2)_4$ and $Sp(8)_1$ currents in opposite directions. For

example, for the $Sp(8)_1$ bFQH model, the backscattering interactions are the sum of

$$\begin{aligned}
\mathcal{H}_{\text{intra}}^{SU(2)_4} &= -u_{\text{intra}} \sum_y \sum_{1\le a<b\le 3} \cos\left(\bar{\phi}_{ya}^R - \bar{\phi}_{yb}^R\right) \cos\left(\bar{\phi}_{ya}^L - \bar{\phi}_{yb}^L\right) \\
&= -\frac{u_{\text{intra}}}{2} \sum_y \sum_{1\le a<b\le 3} \left(\cos\theta_{ab}^y + \cos\varphi_{ab}^y\right), \\
\mathcal{H}_{\text{inter}}^{Sp(8)_1} &= u_{\text{inter}} \sum_y \Bigg\{ \sum_{l=1}^4 \mathtt{H}_{y,l}^R \mathtt{H}_{y+1,l}^L - 2\sum_{l=1}^4 \cos\left(2\Xi_l^{y+1/2}\right) \\
&\quad - 2i\eta_{y,0}^R \eta_{y+1,0}^L \sum_{s=\pm} \cos\left(\Xi_1^{y+1/2} + s\Xi_2^{y+1/2}\right) \\
&\quad - 2i\chi_{y,0}^R \chi_{y+1,0}^L \sum_{s=\pm} \cos\left(\Xi_3^{y+1/2} + s\Xi_4^{y+1/2}\right) \\
&\quad - 2i\eta_{y,+}^R \eta_{y+1,+}^L \sum_{s=\pm} \cos\left(\Xi_1^{y+1/2} + s\Xi_3^{y+1/2}\right) \\
&\quad - 2i\chi_{y,+}^R \chi_{y+1,+}^L \sum_{s=\pm} \cos\left(\Xi_2^{y+1/2} + s\Xi_4^{y+1/2}\right) \\
&\quad - 2i\eta_{y,-}^R \eta_{y+1,-}^L \sum_{s=\pm} \cos\left(\Xi_1^{y+1/2} + s\Xi_4^{y+1/2}\right) \\
&\quad - 2i\chi_{y,-}^R \chi_{y+1,-}^L \sum_{s=\pm} \cos\left(\Xi_2^{y+1/2} + s\Xi_3^{y+1/2}\right) \Bigg\},
\end{aligned} \tag{3.154}$$

(3.155)

where $\theta_{ab}^y = \bar{\phi}_{ya}^R - \bar{\phi}_{yb}^R - \bar{\phi}_{ya}^L + \bar{\phi}_{yb}^L$, $\varphi_{ab}^y = \bar{\phi}_{ya}^R - \bar{\phi}_{yb}^R + \bar{\phi}_{ya}^L - \bar{\phi}_{yb}^L$, and $\Xi_l^{y+1/2} = X_{y,l}^R - X_{y+1,l}^L$.

The gapping of the $SU(2)_4 = SO(3)_2$ sector by current backscattering was shown in Ref. [TH23]. The interaction (3.154) fixes the finite ground state expectation values,

$$s_y = \left\langle \sin\left(\bar{\phi}_{ya}^R - \bar{\phi}_{yb}^R\right) \sin\left(\bar{\phi}_{ya}^L - \bar{\phi}_{yb}^L\right) \right\rangle, \tag{3.156}$$

for $1 \le a < b \le 3$, where $S_{ab} = \sin\left(\bar{\phi}_a - \bar{\phi}_b\right)$ are non-local spin-1 primary fields that are odd under the $\mathbb{Z}_2$ symmetry and thus carry a non-trivial $\mathbb{Z}_2$ gauge charge. Applying the $\mathbb{Z}_2$

symmetry to one of the two chiral sectors produces a new ground state and flips the sign of s_y. Depending on the sign of the expectation value s_y, either θ^y_{ab} or φ^y_{ab} is pinned.

$$\begin{aligned} s_y > 0: &\quad \left\langle \cos\theta^y_{ab} \right\rangle > 0, \quad \left\langle \cos\varphi^y_{ab} \right\rangle = 0, \\ s_y < 0: &\quad \left\langle \cos\theta^y_{ab} \right\rangle = 0, \quad \left\langle \cos\varphi^y_{ab} \right\rangle > 0. \end{aligned} \tag{3.157}$$

We now explain the gapping of the $Sp(8)_1$ sector. The first line of (3.155) introduces the finite ground state expectation values $\langle \Xi_l^{y+1/2} \rangle = \pi n_l^{y+1/2}$, where $n_l^{y+1/2}$ is an integer. Subsequently, the second line of (3.155) is approximately proportional to

$$i\left(\chi^R_{y,0}\chi^L_{y+1,0} + s_{y+1/2}\eta^R_{y,0}\eta^L_{y+1,0}\right) = 2\cos\left(\bar{\phi}^R_{y,4} - s_{y+1/2}\bar{\phi}^L_{y+1,4}\right), \tag{3.158}$$

where the sign is

$$s_{y+1/2} = (-1)^{n_1^{y+1/2}+n_2^{y+1/2}+n_3^{y+1/2}+n_4^{y+1/2}} = \pm 1. \tag{3.159}$$

The terms in the second line therefore pin either $\theta_4^{y+1/2} = \bar{\phi}^R_{y,4} - \bar{\phi}^L_{y+1,4}$ or $\varphi_4^{y+1/2} = \bar{\phi}^R_{y,4} + \bar{\phi}^L_{y+1,4}$. The $\mathbb{Z}_2$ symmetry, say in the R sector on wire y, shifts $X^R_{y,1} \to X^R_{y,1} + \pi$, while leaving $X^R_{y,l=2,3,4}$ unchanged. Therefore, it produces a new ground state, changes $n_1^{y+1/2} \to n_1^{y+1/2} + 1$, and switches the sign $s_{y+1/2}$. Similarly, depending on the sign $s_{y+1/2}$, the last

two lines of (3.155) at low energies become

$$
\begin{aligned}
& i\left(\chi^R_{y,\pm}\chi^L_{y+1,\pm} + s_{y+1/2}\eta^R_{y,\pm}\eta^L_{y+1,\pm}\right) \\
& \to 2\cos\left(\theta^{y+1/2}_{123} \pm \left\langle \theta^{y+1/2}_{4} \right\rangle /2\right) \\
& \quad \text{or } 2\cos\left(\varphi^{y+1/2}_{123} \pm \left\langle \varphi^{y+1/2}_{4} \right\rangle /2\right),
\end{aligned}
\tag{3.160}
$$

where $\theta^{y+1/2}_{123} = \sum_{a=1}^{3}\left(\bar{\phi}^R_{y,a} - \bar{\phi}^L_{y+1,a}\right)/2$ and $\varphi^{y+1/2}_{123} = \sum_{a=1}^{3}\left(\bar{\phi}^R_{y,a} + \bar{\phi}^L_{y+1,a}\right)/2$.

The coupled-wire model (3.154) and (3.155) describes a bFHQ state with $Sp(8)_1$ topological order. Recall that the model construction assumes $\tilde{d}_{5,6,7,8}$ are the only Dirac fermions that carry electric charge. They are responsible for the charge response of the entire E_8 sector. Since $\tilde{d}_{5,6,7,8}$ are all within the $Sp(8)_1$ sector and are decoupled from the $SU(2)_4$ sector, the $Sp(8)_1$ bFQH state must have the same filling number as the full E_8 state, $\nu_{Sp(8)_1} = 16$. The central charge of the $Sp(8)_1$ CFT is identical to its parents state $(E_6)_1$. Therefore, $c_{Sp(8)_1} = 6$. The intra-wire and inter-wire current backscattering interactions (3.154) and (3.155) preserve charge and momentum conservation when the Dirac fermions $\tilde{d}_{1,2,3,4}$ have vanishing electric charge and x-momentum.

The coupled-wire model for the particle-hole conjugate state with $SU(2)_4$ topological order can be constructed by reversing the intra-wire and inter-wire backscattering patterns of (3.154) and (3.155). It has trivial filling $\nu_{SU(2)_4} = 0$ because the $SU(2)_4$ sector is electrically neutral. The chiral central charge is $c_{SU(2)_4} = 3$ and is the same as its parent CFT $SU(3)_1$.

We now discuss the primary fields and anyon excitations of the $Sp(8)_1$ and $SU(2)_4$ theory. We first present the primary field content of $SU(2)_4 = SU(3)_1/\mathbb{Z}_2$ state. The 5 primary

field super-selection sectors $[j]$ can be labeled by the $SU(2)$ "spins" $j = 0, 1/2, 1, 3/2, 2$. Each primary sector $[j]$ is spanned by $2j+1$ primary fields that irreducibly rotate among each other under the $SU(2)_4$ current algebra (c.f. (3.57)). The conformal scaling dimensions (or spins) of the primary fields are $h_j = j(j+1)/6$, where the denominator $6 = k + h_{SU(2)}$ is set by the dual Coxeter number $h_{SU(2)} = 2$ and level $k = 4$ of the WZW algebra. We begin with the free field representation of the bosonic Abelian primary fields in [2], which is identified as the pure $\mathbb{Z}_2$ gauge charge sector in the orbifold theory. [2] is the complement of $SU(2)_4$ in $SU(3)_1$:

$$\begin{aligned}[2] = \text{span}\left\{\frac{\partial\bar{\phi}_1 - \partial\bar{\phi}_2}{\sqrt{2}}, \frac{\partial\bar{\phi}_1 + \partial\bar{\phi}_2 - 2\partial\bar{\phi}_3}{\sqrt{6}}\right\} \\ \cup \left\{\sin\left(\bar{\phi}_a - \bar{\phi}_b\right) : 1 \le a < b \le 3\right\},\end{aligned} \tag{3.161}$$

which consists of the current operators that are odd under the internal $\mathbb{Z}_2$ symmetry (3.147). These fields obey the fusion rule $[2] \times [2] = [0]$ because any even combination is even under $\mathbb{Z}_2$ and is local.

The $SU(3)_1$ primary sectors $\mathcal{E}$ and $\mathcal{E}^\dagger$ (by replacing $\phi \to \bar{\phi}$ in (3.56)) now becomes the primary sector [1]. Since $\mathcal{E} \leftrightarrow \mathcal{E}^\dagger$ are flipped under the internal $\mathbb{Z}_2$ symmetry, they are now the same primary sector in $SU(3)_1/\mathbb{Z}_2$. They obey the fusion rules

$$[2] \times [1] = [1], \quad [1] \times [1] = [0] + [1] + [2]. \tag{3.162}$$

The former originates from the $SU(3)_1$ current OPE of $\mathcal{E}$ and $\mathcal{E}^\dagger$. The latter holds because (i) operator products from $\mathcal{E} \times \mathcal{E}^\dagger$ produce both local bosons, such as $SU(2)_4$ currents, as

well as $\mathbb{Z}_2$ charges in [2]; and (ii) pair products in $\mathcal{E} \times \mathcal{E}$ give fields in $\mathcal{E}^\dagger$ that now also belong in [1]. [1/2] and [3/2] are twist fields (also known as $\mathbb{Z}_2$ fluxes). They have spin 1/8 and 5/8 respectively, and follow the fusion rules

$$\begin{aligned} &[1/2] \times [1/2] = [0] + [1], \\ &[1] \times [1/2] = [1/2] + [3/2], \\ &[2] \times [1/2] = [3/2]. \end{aligned} \tag{3.163}$$

The twist fields in $SU(2)_4$ do not have free field representations. However, we will see below that they can be paired with twist fields in $Sp(8)_1$ to form local E_8 currents. Since $SU(2)_4$ is electrically neutral, so are all of its primary fields.

We now present the primary fields of $Sp(8)_1 = (E_6)_1/\mathbb{Z}_2$. Particle-hole symmetry dictates that $Sp(8)_1$ and $SU(2)_4$ have the same number of primary field super-selection sectors, identical fusion rules, and conjugate spins. We label the 5 primary sectors of $Sp(8)_1$ by $1, \sigma, \mathsf{E}, \tau, S$, which are the particle-hole conjugates of $[0], [1/2], [1], [3/2], [2]$, respectively. Each sector is spanned by # primary fields that rotate irreducibly under the $Sp(8)_1$ current algebra (c.f. (3.57)). The spin h, quantum dimension d, and the number of fields # in each primary sector are listed in Table 3.1. The fusion rules mirror $SU(2)_4$:

$$\begin{aligned} &S^2 = 1, \quad S \times \sigma = \tau, \quad S \times \mathsf{E} = \mathsf{E}, \\ &\mathsf{E} \times \mathsf{E} = 1 + \mathsf{E} + S, \quad \mathsf{E} \times \sigma = \sigma + \tau, \\ &\sigma \times \sigma = 1 + \mathsf{E}. \end{aligned} \tag{3.164}$$

	σ	E	τ	S
h	$3/8$	$2/3$	$7/8$	1
d	$\sqrt{3}$	2	$\sqrt{3}$	1
$\#$	8	27	48	42

Table 3.1: The spin h, quantum dimension d, and the number of fields $\#$ of each non-trivial primary sector of $Sp(8)_1$.

We begin with the free field representation of the $\mathbb{Z}_2$ charges in sector S, which is the complement of $Sp(8)_1$ in $(E_6)_1$. S is spanned by the 42 fields:

$$\begin{aligned}
&\frac{\partial\bar{\phi}_1+\partial\bar{\phi}_2+\partial\bar{\phi}_3}{\sqrt{3}}, \partial\bar{\phi}_4,\\
&e^{\pm i(\bar{\phi}_5+\bar{\phi}_7)}, e^{\pm i(\bar{\phi}_5-\bar{\phi}_7)}, e^{\pm i(\bar{\phi}_5+\bar{\phi}_8)}, e^{\pm i(\bar{\phi}_5-\bar{\phi}_8)},\\
&e^{\pm i(\bar{\phi}_6+\bar{\phi}_7)}, e^{\pm i(\bar{\phi}_6-\bar{\phi}_7)}, e^{\pm i(\bar{\phi}_6+\bar{\phi}_8)}, e^{\pm i(\bar{\phi}_6-\bar{\phi}_8)},\\
&\chi_0 e^{\pm i\bar{\phi}_5}, \chi_0 e^{\pm i\bar{\phi}_6}, \eta_0 e^{\pm i\bar{\phi}_7}, \eta_0 e^{\pm i\bar{\phi}_8},\\
&\chi_\pm e^{i\sum_{j=5}^{8}\varepsilon_\pm^j\bar{\phi}_j/2}, \quad \text{if } \varepsilon_\pm^5=\varepsilon_\pm^6,\\
&\eta_\pm e^{i\sum_{j=5}^{8}\varepsilon_\pm^j\bar{\phi}_j/2}, \quad \text{if } \varepsilon_\pm^5=-\varepsilon_\pm^6.
\end{aligned} \tag{3.165}$$

The electric charges of these operators can be read off from that of the Dirac fermions $\bar{d}_{5,6,7,8}=e^{i\bar{\phi}_{5,6,7,8}}$: one possibility is that all these fermions carry ±2 charge; another possibility is to have one carry charge ±4 with the remaining fermions neutral. Next, we move on to the E sector. It originates from the $(E_6)_1$ primary field sectors $\mathcal{E}$ and $\mathcal{E}^\dagger$ by replacing $\phi\to\bar{\phi}$ in (3.59). Like the $SU(2)_4$ primaries, these fields are flipped and conjugated $\mathcal{E}\leftrightarrow\mathcal{E}^\dagger$ under the internal $\mathbb{Z}_2$ symmetry, and therefore both $\mathcal{E}$ and $\mathcal{E}^\dagger$ now belong in the same sector E. It forms a 27 dimensional irreducible representation of the $Sp(8)$ Lie algebra, and is invariant under the encompassing E_6, which includes the $\mathbb{Z}_2$ charges in S. The electric

charge assignment is identical to the primary field $\mathcal{E}$ of E_6 at filling 16. The charge pattern of the E and S sectors can be found in Table A.9.

In §3.3.1, we noted the decomposition of the 248-dimensional $(E_8)_1$ algebra into the 8-dimensional $SU(3)_1$ algebra, the 78-dimensional $(E_6)_1$ algebra, and the two tensor product spaces $\mathcal{E}_{SU(3)} \otimes \mathcal{E}_{E_6}$ and $\mathcal{E}^\dagger_{SU(3)} \otimes \mathcal{E}^\dagger_{E_6}$, each with dimension $3 \times 27 = 81$. Any $(E_8)_1$ current operator is a linear combination of a $SU(3)_1$ current, a $(E_6)_1$ current, and primary field pair product in $\mathcal{E}_{SU(3)} \otimes \mathcal{E}_{E_6}$ and $\mathcal{E}^\dagger_{SU(3)} \otimes \mathcal{E}^\dagger_{E_6}$. Here, in this section, the conformal embedding $(E_8)_1 \supseteq Sp(8)_1 \times SU(2)_4$ of orbifold theories splits the E_8 algebra into the direct sum:

$$\begin{aligned}(E_8)_1 \supseteq\ & Sp(8)_1 \oplus SU(2)_4 \\ & \oplus (\sigma \otimes [3/2]) \oplus (\tau \otimes [1/2]) \oplus (\mathsf{E} \otimes [1])\,.\end{aligned} \tag{3.166}$$

The first line embeds the $Sp(8)_1$ and $SU(2)_4$ algebras, which add up to dimension $36 + 3 = 39$. The tensor space $\mathsf{E} \otimes [1]$ pairs the spin 2/3 and 1/3 primary fields together and it contains $27 \times 3 = 81$ E_8 currents that have integral monodromy (i.e., trivial braiding) with the $\mathbb{Z}_2$ charges in S and [2]. The twist fields (i.e., $\mathbb{Z}_2$ gauge fluxes) in the $Sp(8)_1$ sectors σ and τ can be paired with those in [3/2] and [1/2] in $SU(2)_4$ to make up the remaining 128 E_8 currents that have π-monodromy with the $\mathbb{Z}_2$ charges. For instance, the spins of the paired twist fields add up to $1 = 3/8 + 5/8 = 7/8 + 1/8$, and the dimensions of the two tensor spaces of twist fields add up to $8 \times 4 + 48 \times 2 = 128$. (While not included in the E_8 algebra, the pair product of $\mathbb{Z}_2$ charges in $S \otimes [2]$ are spin-2 local bosons.) Knowing fields in [1/2] and [3/2] are electrically neutral allows us to read off the electric charge assignments

of twist fields in σ and τ. The charge pattern is listed in Table A.9. The $\mathbb{Z}_2$ fluxes σ and τ are referred to as metaplectic anyons [HNW13, HNW14].

3.4 Discussion and Conclusion

In this paper, we explored the analogy between the integer quantum Hall state of electrons and the (bosonic) E_8 quantum Hall state. In particular, we gave explicit constructions of the "partially-filled" E_8 state—summarized in Fig. 3.1 —using the coupled-wire approach. The topological orders of the various fractional E_8 states include Abelian and non-Abelian varieties. Our approach in this paper for finding fractional E_8 states relied on the theory of conformal embeddings. This theory details the various possible (bipartite) symmetry decompositions $\mathcal{G}_A \times \mathcal{G}_B \subseteq E_8$. We then showed how the bulk-boundary correspondence (through the coupled-wire construction) allowed for the explicit construction of $\mathcal{G}_A$ and $\mathcal{G}_B$ fractional E_8 states. These states have edge-state theories with $\mathcal{G}_A$ or $\mathcal{G}_B$ Kac-Moody symmetry. Furthermore, the $\mathcal{G}_A$ and $\mathcal{G}_B$ states are related by a generalized "particle-hole" symmetry similar to particle-hole conjugate states ν and $1-\nu$ in the lowest Landau level.

Our approach, using conformal embeddings, provides for a systematic understanding of the various possible fractional E_8 states. This approach relies on the E_8 Kac-Moody symmetry of the edge-state theory. This conformal embedding approach may be straightforwardly applied to construct fractional states of topological orders with edge-state theories possessing other Kac-Moody symmetries, e.g., $U(N)_1$ for N filled Landau levels of electrons.

It is unclear whether the conformal embedding approach might provide a complementary avenue for understanding topological phases in the lowest Landau level. What symmetry group can be embedded into $U(1)$? One possibility is to consider a dual description [HS16] of the $\nu = 1$ integer quantum Hall state of electrons. This dual description is in terms of a $U(N)_1 \times U(1)_{N+1}$ Chern-Simons gauge theory (see Appendix B of [HKM19]). Here N is an arbitrary integer; a physical interpretation of N can be given in terms of partons [Wen91b]. We may then imagine applying the conformal embedding approach to the $U(N)_1$ Chern-Simons theory. It would be interesting to know how such constructions might be related to the composite fermion/boson approach to fractional quantum Hall states (for a recent review and references therein, [Jai20]).

Related to this is the question of whether there might be a gapless parent state for various fractional E_8 states found in this paper. Here, we (again) have in mind an E_8 state analogy for the composite fermion theory at $\nu = 1/2$. Half-filling of the E_8 state occurs at $\nu = 8$. We have shown both Abelian and non-Abelian topological states can exist at $\nu = 8$. We do not yet have a candidate gapless parent state.

The bosonic topological states considered in this paper (summarized in Fig. 3.2 and Eq. (3.1)) do *not* exhaust all fractional states of E_8. Below are some possible examples not studied in this paper. (i) In this paper, we only considered bipartitions $\mathcal{G}_A \times \mathcal{G}_B \subset (E_8)_1$ where the WZW algebras $\mathcal{G}_A$ and/or $\mathcal{G}_B$ have level $k = 1$. The E_8 state can be decomposed by into multi-partitions $\mathcal{G}_A \times \mathcal{G}_B \times \mathcal{G}_C \times \ldots$ of WZW theories with levels $k \geq 1$. This may produce new bFQH states. (ii) In §3.3.1 and 3.3.2, we constructed $SO(N)_1$ bFQH states, where $N = 1, \ldots, 15$. The coupled-wire model construction for $SO(15)_1$, in particular, that

includes longer-range inter-wire interactions, may allow generalization to $SO(N)_1$ states with $N \geq 16$.

(iii) The exploration of orbifold bFQH states with twist liquid topological orders is incomplete. First, in our constructions of the $(E_8)_1$ wires, we do not find any $SO(16)_1$ subalgebras whose even and odd spinors are non-local. Therefore, the $SO(16)_1$ bFQH state, which is the orbifold state $(E_8)_1/\mathbb{Z}_2$ is missing in this paper. The construction of this state may be facilitated by introducing additional electron channels on each wire or allowing longer-range interactions. Second, in §3.3.2, we may not have exhausted all possible variations of the metaplectic orbifold embedding $SU(2)_4 \times Sp(8)_1 \subseteq (E_8)_1$. A more thorough investigation may discover more filling numbers with $\nu_{SU(2)_4} > 0$ and $\nu_{Sp(8)_1} < 16$. Third, in this paper, we only consider $\mathbb{Z}_2$ orbifold CFTs that are also WZW theories, such as $(E_6)_1/\mathbb{Z}_2 = Sp(8)_1$ and $(E_7)_1/\mathbb{Z}_2 = SU(8)_1$. There may be orbifold theories with higher-order gauge groups G that are not WZW theories that decompose $(E_8)_1$. Fourth, it is very likely that there are $\mathbb{Z}_2$ orbifold CFTs that are also WZW theories but are not covered in this paper. One probable example is the orbifold state $SU(5)_1/\mathbb{Z}_2 = SO(5)_2 = Sp(4)_2$. Spin liquid or superconducting $SO(5)_2$ states have been constructed by coupled-wire models in ref. [TH23]. We anticipate charged $SO(5)_2$ bFQH states to occupy filling $\nu = 16$. It would be interesting to see if such state can also occupy the particle-hole symmetric filling $\nu = 8$. If so, such a metaplectic topological state can serve as the bosonic anolog of particle-hole symmetric Pfaffian state at $\nu = 1/2$ that half-fills the Landau level.

Lastly, the E_8 state is not the only short-range entangled integer quantum Hall state. For example, the D_{16}^+ lattice [CS13] at $c = 16$, the Leech lattice and Niemeier lattices at $c = 24$

are even unimodular lattices that can describe other bosonic short-range entangled integer quantum Hall states with unequal filling numbers and central charges, $\nu \neq c$. Just like the E_8, they also can be fractionally occupied by long-range entangled states. There can also be fermionic short-range entangled integer quantum Hall states corresponding to odd unimodular lattices, such as the D_{12}^+ lattice [CS13] at $c = 12$ and $(E_7 \times E_7)^+$ lattice at $c = 14$. They are postulated [HST] to occupy filling $\nu = 4$ and $\nu = 6$, which are much closer to experimentally observable regime than $\nu_{E_8} = 16$.

Chapter 4

TOPOLOGICAL ORDER WITH CLASSICAL LIE GROUPS

This chapter is to be published as [Pak Kau Lim, Michael Mulligan, Jeffrey C.Y. Teo, "Topological orders with classical Lie group edge symmetries from coupling electron wires".]

4.1 Introduction

The purpose of this paper is to apply this program to other topological phases with classical Lie group edge-state symmetries, different from the E_8 quantum Hall state. Specifically, we will consider "parent" $\mathcal{G}$-states with $\mathcal{G} = \mathrm{SU}(mn)_1$, $\mathrm{SO}(mn)_1$, or $\mathrm{SO}(4mn)_1$ edge-state

symmetries and the symmetry decompositions:

$$\begin{cases} \mathrm{SU}(m)_n \times \mathrm{SU}(n)_m \subset \mathrm{SU}(mn)_1, \\ \mathrm{SO}(m)_n \times \mathrm{SO}(n)_m \subset \mathrm{SO}(mn)_1, \\ \mathrm{Sp}(2m)_n \times \mathrm{Sp}(2n)_m \subset \mathrm{SO}(4mn)_1. \end{cases} \tag{4.1}$$

Here, m and n are positive integers. Note that states with $\mathrm{SO}(N)$ symmetry group do not have electrical U(1) symmetry. Following the procedure outlined above for the E_8 quantum Hall state, we will use these symmetry decompositions to engineer quantum Hall liquids, topological superconductors, or spin liquids with, respectively, $\mathrm{SU}(N)_k$, $\mathrm{SO}(N)_k$, or $\mathrm{Sp}(N)_k$ edge-state symmetry, for some positive integer k. We thereby provide explicit constructions of various states with Abelian or non-Abelian topological orders.

4.2 A_r series and partons

In this section, we show how fractional quantum Hall states with $\mathrm{U}(1)_{mn} \times \mathrm{SU}(m)_n$ topological order can arise from "partially occupying" the deconfined parton FQH states [SSCT19] with $\mathrm{U}(mn)_1/\mathbb{Z}_{mn} = \mathrm{U}(1)_{mn} \times \mathrm{SU}(mn)_1$ topological order.

4.2.1 Generalized Parton Construction

We begin with a description of the parton FQH states. Prior work [SSCT19] constructed such states with $\mathrm{U}(3)_1/\mathbb{Z}_3$ topological order; we will generalize this to $\mathrm{U}(mn)_1/\mathbb{Z}_{mn}$, for

arbitrary positive integers m, n. The parton phase can be motivated by imagining the fractionalization of a fundamental or elementary fermion (boson) Ψ_{el} into fermionic partons d^a, for $a = 1, \ldots, mn$:

$$\Psi_{el} = d^1 d^2 \ldots d^{mn}. \tag{4.2}$$

A FQH phase of the fundamental fermion (boson) is then realized as a particular topological ordering of the partons. (In the simplest of instances, a FQH phase can form when the partons enter an IQH phase.) Ψ_{el} is "fundamental" in the sense that it is composed of an integral combination of electron operators. We will study cases where Ψ_{el} carries electric charge e ($2e$), when Ψ_{el} is fermionic (bosonic). By "electron operators," we are referring to spin-polarized electron creation/annihilation operators for the electrons in the underlying coupled-wire array that produce the parton FQH phase. The factor of 2 for even mn reflects the fact that Ψ_{el} is composed of an even number of electron operators.

One route to the parton phase (used in [SSCT19]) begins with the parton decomposition (4.2). This decomposition has a $\mathbb{Z}_{mn}$ gauge redundancy by which $d^a \to e^{2\pi i/mn} d^a$. Describing the parton phase by its edge-state theory, we may systematically obtain the correct edge-state Lagrangian by first treating $\mathbb{Z}_{mn}$ as a global symmetry to obtain a $\mathrm{U}(mn)_1$ edge-state theory (i.e., an edge-state theory with $\mathrm{U}(mn)_1$ KM symmetry) and subsequently gauging the $\mathbb{Z}_{mn}$ symmetry to obtain the edge-state theory for the parton FQH phase with

$\mathrm{U}(mn)_1/\mathbb{Z}_{mn}$ KM symmetry. The edge-state Lagrangian for the parton FQH phase is

$$\mathcal{L}_{\mathrm{U}(mn)_1/\mathbb{Z}_{mn}} = \frac{1}{4\pi} K_{IJ} \partial_t \tilde{\phi}^I \partial_{\mathsf{x}} \tilde{\phi}^J - \frac{1}{4\pi} \tilde{V}_{IJ} \partial_{\mathsf{x}} \tilde{\phi}^I \partial_{\mathsf{x}} \tilde{\phi}^J. \tag{4.3}$$

Here, $\tilde{\phi}^I$ are chiral (left-moving) bosons, $K = (K_{IJ})$ is the mn-dimensional Cartan matrix of $\mathrm{U}(mn)_1/\mathbb{Z}_{mn} = \mathrm{U}(1)_{mn} \times \mathrm{SU}(mn)_1$,

$$K = K_{\mathrm{U}(1)_{mn}} \oplus K_{\mathrm{SU}(mn)_1} = \begin{pmatrix} K_{\mathrm{U}(1)_{mn}} & 0 \\ 0 & K_{\mathrm{SU}(mn)_1} \end{pmatrix} \tag{4.4}$$

$$K_{\mathrm{U}(1)_{mn}} = mn, \quad K_{\mathrm{SU}(mn)} = \begin{pmatrix} 2 & -1 & & & \\ -1 & 2 & -1 & & \\ & -1 & 2 & & \\ & & & \ddots & \\ & & & & \begin{matrix} 2 & -1 \\ -1 & 2 \end{matrix} \end{pmatrix},$$

where $I, J \in \{0, \ldots, mn-1\}$. Elements of K above, not indicated explicitly, e.g., elements K_{1p} for $p = 2, \ldots, mn-1$, are zero; we will use this notation throughout whenever convenient. The Einstein summation convention is assumed, unless otherwise specified. The positive symmetric velocity matrix $\tilde{V}_{IJ}$ can be set to be proportional to K_{IJ} by appropriate short-ranged density-density interactions, so that the free theory (4.3) has the $\mathrm{U}(mn)$ KM symmetry. The above Lagrangian implies the bosons satisfy the equal-time commutation algebra:

$$[\partial_{\mathsf{x}} \tilde{\phi}^I(\mathsf{x}), \tilde{\phi}^J(\mathsf{x}')] = 2\pi i (K^{-1})^{IJ} \delta(\mathsf{x} - \mathsf{x}'). \tag{4.5}$$

The bosons $\tilde{\phi}^I$ are 2π-periodic: $\tilde{\phi}^I \sim \tilde{\phi}^I + 2\pi N^I$, where N^I is an arbitrary integer vector. This periodicity implies that general quasiparticle creation/annihilation operators along the

edge are given by vertex operatos of the form $e^{im_I\tilde{\phi}^I}$, for arbitrary integer vectors m_I; local fermion/boson operators are of the form $e^{in^IK_{IJ}\tilde{\phi}^J}$, for arbitrary integer vectors n^I. Local operators have trivial monodromy with any other operator and may be understood to be a product of an integral number of elementary fermion/boson operators.

The parton phase has a conserved electric U(1) symmetry and a corresponding characteristic electrical Hall response. This response is determined by a so-called charge vector t_I. In the coupled-wire construction of the parton FQH phase that we will describe later, the charge vector is

$$t_I = \begin{cases} (1,0,\ldots,0), & (mn \text{ odd}) \\ (2,0,\ldots,0), & (mn \text{ even}). \end{cases} \tag{4.6}$$

This charge vector implies that $\tilde{\phi}^0$ of the $\mathrm{U}(1)_{mn}$ sector carries all of the electric charge along an edge; the $\mathrm{SU}(mn)_1$ sector is electrically neutral. The fundamental fermion (boson) operator in the Lauglin charged sector is $\Psi_{el} = e^{imn\tilde{\phi}^0}$. The electrical Hall conductivity is

$$\sigma_{xy} = \nu\frac{e^2}{h}, \tag{4.7}$$

where $\nu = t_I(K^{-1})^{IJ}t_J$. In the parton phase, $\nu = \nu_{mn}$, with

$$\nu_{mn} = \begin{cases} \frac{1}{mn}, & (mn \text{ odd}), \\ \frac{4}{mn}, & (mn \text{ even}). \end{cases} \tag{4.8}$$

Here, ν_{mn} is also the filling fraction that counts the ratio between the number of electric charge and number of magnetic flux quanta in this FQH phase. In addition to the electrical response, the parton FQH phase has a thermal response characterized by the thermal Hall conductivity [KF97, CHZ02],

$$\kappa_{xy} = c\frac{\pi^2 k_B^2}{3h}T, \tag{4.9}$$

where c is the chiral central chaerge of the state and T is the applied temperature gradient. In the parton phase, $c = c_{mn} = mn$, which is the total number of edge modes.

The U(mn) symmetry becomes apparent under the following invertible transformation from the "Chevalley" basis $\tilde{\phi}$ to the "Cartan-Weyl" basis ϕ.

$$\phi^r = R^r_I \tilde{\phi}^I, \tag{4.10}$$

where

$$R = \begin{pmatrix} 1 & 1 & & & & \\ 1 & -1 & 1 & & & \\ 1 & & -1 & 1 & & \\ \vdots & & & \ddots & & \\ 1 & & & & & -1 \end{pmatrix}. \tag{4.11}$$

Here $r = 1, \ldots, mn$ and $I = 0, \ldots, mn-1$ labels the rows and columns of the matrix. The columns of R are the simple roots of $\mathrm{U}(1)_{mn} \times \mathrm{SU}(mn)_1$, such that the K-matrix in (4.4)

decomposes into $K_{IJ} = \sum_r R^r_I R^r_J$. Note that R is not unimodular and has determinant mn. In the Cartan-Weyl basis, the Lagrangian (4.3) becomes

$$\mathcal{L}_{\mathrm{U}(mn)_1/\mathbb{Z}_{mn}} = \frac{1}{4\pi}\delta_{rs}\partial_t\phi^r\partial_{\mathsf{x}}\phi^s - \frac{1}{4\pi}V_{rs}\partial_{\mathsf{x}}\phi^r\partial_{\mathsf{x}}\phi^s, \tag{4.12}$$

where $V_{rs} = (R^{-1})^I_r\tilde{V}_{IJ}(R^{-1})^J_s = v\delta_{rs}$ is diagonal so that the theory is U(mn) symmetric. The Cartan-Weyl bosons obey the equal-time commutation relation

$$[\partial_{\mathsf{x}}\phi^r(\mathsf{x}), \phi^s(\mathsf{x}')] = 2\pi i\delta^{rs}\delta(\mathsf{x}-\mathsf{x}'). \tag{4.13}$$

The Cartan-Weyl bosons have more complicated compactification conditions that mix various species $\tilde{\phi}^I$ according to the R matrix ($\phi^r \sim \phi^r + 2\pi R^r_I N^I$). The parton fermions are the vertex fields $d^r \sim e^{i\phi^r}$. (The $\sim$ symbol here indicates that we are suppressing a non-universal constant of engineering dimension 1/2.) The fundamental fermion (boson) operator is now $\Psi_{el} = e^{i\phi^1}\cdots e^{i\phi^{mn}}$, which recovers the parton decomposition (4.2). The partons are non-local fractional fields. They transform according to an internal $\mathbb{Z}_{mn}$ discrete gauge symmetry that sends $\phi^r \to \phi^r + 2\pi/(mn)$. Any local vertex operator that is an integral combination of electrons must be $\mathbb{Z}_{mn}$ neutral and therefore invariant under the $\mathbb{Z}_{mn}$ transformation.

We close this subsection by presenting the $\mathrm{U}(mn)_1/\mathbb{Z}_{mn} = \mathrm{U}(1)_{mn} \times \mathrm{SU}(mn)_1$ edge-state symmetry currents of the parton FQH phase. These currents (and the notation we use to present them) are used in the coupled-wire construction of the parton FQH phase; analogous

ideas will be used in constructing the $\mathrm{SU}(m)_n$ phases (and the other phases considered in later sections).

Using standard Lie algebra terminology, there are two types of currents: Cartan and root currents. The Cartan current of $\mathrm{U}(1)_{mn}$ is

$$\begin{aligned} \mathtt{H}_{\mathrm{U}(1)_{mn}} &= \frac{1}{\sqrt{mn}} \sum_{r=1}^{mn} \partial_{\mathtt{x}} \phi^r \sim (d^r)^\dagger X^{\mathrm{U}(1)_{mn}}_{rs} d^s, \\ X^{\mathrm{U}(1)_{mn}}_{rs} &= \delta_{rs}/\sqrt{mn} \end{aligned} \tag{4.14}$$

where $r, s = 1, \ldots, mn$. The Cartan currents of $\mathrm{SU}(mn)_1$ are

$$\left[\mathtt{H}_{\mathrm{SU}(mn)_1}\right]_p = \frac{1}{\sqrt{p(p+1)}} \left(\sum_{r=1}^{p} \partial_{\mathtt{x}} \phi^r - p \partial_{\mathtt{x}} \phi^{p+1} \right) \sim (d^\dagger)^r X^p_{rs} d^s, \tag{4.15}$$

$$X^p_{rs} = \begin{cases} 1/\sqrt{p(p+1)}, & \text{for } 1 \le r = s \le p \\ -p/\sqrt{p(p+1)}, & \text{for } r = s = p+1 \\ 0, & \text{otherwise} \end{cases},$$

where $p = 1, \ldots, mn-1$. These Cartan currents form a maximal set of commuting operators in the affine Lie algebra. They span the operator space generated by diagonal parton densities $(d^r)^\dagger d^r$.

The root currents of $\mathrm{SU}(mn)_1$ are the off-diagonal bilinear parton products

$$\begin{aligned} [\mathtt{E}_{\mathrm{SU}(mn)_1}]_{\boldsymbol{\alpha}_{\mathrm{SU}(mn)_1}} &= e^{i(\phi^r - \phi^s)} \sim d^r (d^s)^\dagger = d^{r'} X^{rs}_{r's'} (d^{s'})^\dagger \\ X^{rs}_{r's'} &= \delta^r_{r'} \delta^s_{s'} \end{aligned} . \tag{4.16}$$

Here, $\boldsymbol{\alpha}_{\mathrm{SU}(mn)_1} = \mathbf{e}_r - \mathbf{e}_s$ are the root vectors of $\mathrm{SU}(mn)$, where r, s are distinct integers between 1 and mn. $\mathbf{e}_k$ is the unit mn-vector whose k^{th} element equals 1 and is zero elsewhere.

4.2.2 Coupled-Wire Construction of Parton FQH States

In the last subsection, we defined the $\mathrm{U}(mn)_1/\mathbb{Z}_{mn} = \mathrm{U}(1)_{mn} \times \mathrm{SU}(mn)_1$ parton CFT. In this subsection, we present a theoretical model based on electrons where the parton CFT emerges. In particular, we present the coupled-wire construction of the parton FQH phase with $\mathrm{U}(1)_N \times \mathrm{SU}(N)_1$ edge-state theory, for integer $N = mn > 1$. (Recall by "$\mathrm{U}(1)_N \times \mathrm{SU}(N)_1$ edge-state theory," we mean an edge-state theory with $\mathrm{U}(1)_N \times \mathrm{SU}(N)_1$ KM symmetry.)

Following [SSCT19], we introduce a 2D array of electron wires, aligned parallel to the x axis and in the presence of a transverse magnetic field $\mathbf{B} = B\hat{\mathbf{z}}$. We choose the gauge $\mathbf{A} = -B\mathsf{y}\hat{\mathbf{x}}$. The wires are grouped into bundles, each containing $N+2$ wires $j = 0, 1, \ldots, N+1$ and regularly spaced along the y axis. The vertical positions of the wires are $\mathsf{y} = yd + \delta_j$, where $y \in \mathbb{Z}$ labels the bundle, d is the spacing between neighboring bundles, and δ_j is the relative vertical position of the j^{th} wire in a given bundle. Each wire (y, j) carries a spin-polarized electron. At low energies, each electron decomposes into a single Dirac electron, with one left (L) and one right (R) moving component. We denote by $c^{\sigma}_{yj}(\mathsf{x})$ the $\sigma = R/L = \pm 1$

chiral component of the Dirac electron of wire j of bundle y at the Fermi momentum point,

$$k_{yj}^{\sigma} = \frac{eB}{\hbar c}\left(yd + \delta_j\right) + \sigma k_{F,j}. \tag{4.17}$$

Here $k_{F,j}$ is the "bare" Fermi momentum that sets the electron number density (per unit length) $n_j^0 = 2k_{F,j}/(2\pi)$ on wire j.

We write the Dirac electrons in terms of chiral bosons Φ_{yj}^{σ} as

$$c_{yj}^{\sigma}(\mathsf{x}) \sim \exp\left[i\big(\Phi_{yj}^{\sigma}(\mathsf{x}) + k_{yj}^{\sigma}\mathsf{x}\big)\right]. \tag{4.18}$$

Before introducing interactions that couple the wires together, the free Lagrangian is

$$\mathcal{L} = \frac{1}{4\pi}\sum_{y}\sum_{\sigma=\pm}\sum_{j=0}^{N+1}\sigma\partial_t\Phi_{yj}^{\sigma}\partial_{\mathsf{x}}\Phi_{yj}^{\sigma} - \mathcal{H}_0, \tag{4.19}$$

where $\mathcal{H}_0$ is the kinetic Hamiltonian including density-density interactions between electrons within a bundle of wires,

$$\mathcal{H}_0 = \sum_{y}\sum_{\sigma,\sigma'=\pm}\sum_{j,j'=0}^{N+1} v_{\sigma\sigma'}^{jj'}\partial_{\mathsf{x}}\Phi_{yj}^{\sigma}\partial_{\mathsf{x}}\Phi_{yj'}^{\sigma'}, \tag{4.20}$$

and $v_{\sigma\sigma'}^{jj'}$ is a positive definite symmetric matrix to be specified shaortly.

The parton FQH phase is achieved by coupling together nearby bundles of wires in a particular way. To motivate the necessary inter-bundle interaction, we first perform a basis

transformation,

$$\begin{aligned}
&\tilde{\Phi}^{\sigma}_{y\mu} = \sum_{\sigma' j} U^{\sigma\sigma'}_{\mu j} \Phi^{\sigma'}_{yj}, \\
&\tilde{\Phi}^{\sigma}_{y\rho} = N\tilde{\phi}^{\sigma,0}_{y}, \quad \tilde{\Phi}^{\sigma}_{yI} = (K_{\mathrm{SU}(N)_1})_{IJ}\tilde{\phi}^{\sigma,J}_{y}, \\
&\tilde{\Phi}^{\sigma}_{yc_1} = K_{c_1}\tilde{\phi}^{\sigma}_{yc_1}, \quad \tilde{\Phi}^{\sigma}_{yc_2} = N\tilde{\phi}^{\sigma}_{yc_2},
\end{aligned} \tag{4.21}$$

where $\mu = \rho, c_1, c_2, 1, 2, \ldots, N-1$ and $I, J = 1 \ldots, N-1$. The K-matrix is the Cartan matrix of U(N) presented in (4.4). $K_{c_1} = N$ if N is odd, and $K_{c_1} = 1$ if N is even. $U^{\sigma\sigma'} = \left(U^{\sigma\sigma'}_{\mu j}\right)$ are $(N+2)\times(N+2)$ matrices with integral entries. Since $\tilde{\Phi}^{\sigma}_{y\mu}$ is an integral linear combination of the $\Phi^{\sigma'}_{yj}$, vertex operators of the form $\exp\left(in^{\mu}\tilde{\Phi}^{\sigma}_{y\mu}\right)$, for arbitrary integer-vector n_μ, are local.

The U transformation allows the embedding of the parton Lagrangian $\mathcal{L}_{\mathrm{U}(N)_1/\mathbb{Z}_N}$ (4.3) inside a bundle of $N+2$ electron wires. After the basis transformation, the free Lagrangian (4.19) becomes

$$\begin{aligned}
\mathcal{L} = &\frac{1}{4\pi}\sum_{y}\sum_{\sigma=\pm}\sum_{I,J=0}^{N-1}\sigma K_{IJ}\partial_t\tilde{\phi}^{\sigma,I}_{y}\partial_{\mathrm{x}}\tilde{\phi}^{\sigma,J}_{y} \\
&+ \frac{1}{4\pi}\sum_{y}\sum_{\sigma=\pm}\sigma\left(K_{c_1}\partial_t\tilde{\phi}^{\sigma}_{yc_1}\partial_{\mathrm{x}}\tilde{\phi}^{\sigma}_{yc_1} + N\partial_t\tilde{\phi}^{\sigma}_{yc_2}\partial_{\mathrm{x}}\tilde{\phi}^{\sigma}_{yc_2}\right) \\
&- \mathcal{H}_0,
\end{aligned} \tag{4.22}$$

where $K = K_{\mathrm{U}(1)_N} \oplus K_{\mathrm{SU}(N)}$ is the N-dimensional matrix in (4.4). The velocity tensor $v^{jj'}_{\sigma\sigma'}$ in (4.20) is tuned so that the free Hamiltonian becomes

$$\mathcal{H}_0 = \frac{1}{4\pi} \sum_y \sum_{\sigma=\pm} \sum_{I,J=0}^{N-1} \tilde{V}_{IJ} \partial_{\mathrm{x}} \tilde{\phi}^{\sigma,I}_y \partial_{\mathrm{x}} \tilde{\phi}^{\sigma,J}_y + \sum_y \sum_{\sigma=\pm} \sum_{l,l'=1,2} (V_C)^{ll'}_{\sigma\sigma'} \partial_{\mathrm{x}} \tilde{\Phi}^{\sigma}_{y,c_l} \partial_{\mathrm{x}} \tilde{\Phi}^{\sigma'}_{y,c_{l'}}, \tag{4.23}$$

where $\tilde{V}_{IJ}$ is identical to the U(N) symmetric velocity tensor in (4.12), and $(V_C)^{ll'}_{\sigma\sigma'}$ is chosen so that an intra-bundle gapping interactions defined below in (4.26) are relevant in the renormalization group sense.

We here present one particular integral U matrix that transforms (4.19) into (4.22). For odd N,

$$U^{++} = \begin{pmatrix} \frac{1+N}{2}\mathbf{e}_{N+2} \\ \frac{1+N}{2}\mathbf{e}_1 \\ \sum_{a=1}^{N}(2a-N)\mathbf{e}_{a+1} \\ 2\mathbf{e}_2 \\ \vdots \\ 2\mathbf{e}_N \end{pmatrix}, \quad U^{+-} = \begin{pmatrix} \frac{1-N}{2}\mathbf{e}_{N+2} \\ \frac{1-N}{2}\mathbf{e}_1 \\ \sum_{a=1}^{N}(N-2a+1)\mathbf{e}_{a+1} \\ -\mathbf{e}_2-\mathbf{e}_3 \\ \vdots \\ -\mathbf{e}_N-\mathbf{e}_{N+1} \end{pmatrix}, \tag{4.24}$$

$U^{--} = U^{++}\Lambda$, and $U^{-+} = U^{+-}\Lambda$, where Λ is the $(N+2)\times(N+2)$ anti-diagonal matrix

$$\Lambda = \begin{pmatrix} & & & 1 \\ & & \iddots & \\ & 1 & & \\ 1 & & & \end{pmatrix}.$$

$\mathbf{e}_a$ is the unit (row) vector in $\mathbb{R}^{N+2}$ whose a^{th} entry is 1 (where $a = j-1$, for $j = 0, 1, \ldots, N+1$). For even N,

$$
\begin{aligned}
U^{++} &= \begin{pmatrix} \frac{N}{2}\mathbf{e}_1+\mathbf{e}_{N+2} \\ -\mathbf{e}_1+\mathbf{e}_{N+2} \\ \sum_{a=1}^{N}(2a-N)\mathbf{e}_{a+1} \\ 2\mathbf{e}_2 \\ \vdots \\ 2\mathbf{e}_N \end{pmatrix}, \quad U^{+-} = \begin{pmatrix} \frac{2-N}{2}\mathbf{e}_1 \\ \mathbf{e}_1 \\ \sum_{a=1}^{N}(N-2a+1)\mathbf{e}_{a+1} \\ -\mathbf{e}_2-\mathbf{e}_3 \\ \vdots \\ -\mathbf{e}_N-\mathbf{e}_{N+1} \end{pmatrix}, \\
U^{--} &= \begin{pmatrix} \frac{2+N}{2}\mathbf{e}_1 \\ \mathbf{e}_{N+2} \\ \sum_{a=1}^{N}(N-2a+2)\mathbf{e}_{a+1} \\ 2\mathbf{e}_{N+1} \\ \vdots \\ 2\mathbf{e}_3 \end{pmatrix}, \quad U^{-+} = \begin{pmatrix} -\frac{N}{2}\mathbf{e}_1+\mathbf{e}_{N+2} \\ \mathbf{0} \\ \sum_{a=1}^{N}(2a-N-1)\mathbf{e}_{a+1} \\ -\mathbf{e}_N-\mathbf{e}_{N+1} \\ \vdots \\ -\mathbf{e}_2-\mathbf{e}_3 \end{pmatrix}.
\end{aligned}
\tag{4.25}
$$

The "integrated" modes $\tilde{\Phi}^{\sigma}_{c_1}$ and $\tilde{\Phi}^{\sigma}_{c_2}$ within each bundle are gapped using the following charge and momentum preserving sine-Gordon interactions.

$$
\mathcal{H}^{(c_1,c_2)}_{\text{intra}} = \sum_y \left(u_I \cos\Theta^{(I)}_y + u_{II} \cos\Theta^{(II)}_y \right), \tag{4.26}
$$

where

$$
\Theta^{(I)}_y = \tilde{\Phi}^R_{c_1} - \tilde{\Phi}^L_{c_1}, \quad \Theta^{(II)}_y = \tilde{\Phi}^R_{c_2} - \tilde{\Phi}^L_{c_2}. \tag{4.27}
$$

The remaining boson modes $\tilde{\phi}^{\sigma,I}_y$, for $I = 0, \ldots, N-1$, generate the left and right propagating $\mathrm{U}(N)_1/\mathbb{Z}_N = \mathrm{U}(1)_N \times \mathrm{SU}(N)_1$ parton CFTs on each bundle.

The Dirac partons d^r, $r = 1, \ldots, N$, and Laughlin quasiparticle λ on each bundle y and each chiral sector $\sigma = R, L$ can be expressed as the vertex operators

$$d_y^{\sigma,r} = e^{i\phi_y^{\sigma,r}}, \quad \lambda_y^{\sigma} = e^{i\sum_{r=1}^{N}\phi_y^{\sigma,r}/N}, \tag{4.28}$$

where $\phi_y^{\sigma,r} = R_I^r \tilde{\phi}_y^{\sigma,I}$ (see (4.10) and (4.11)). These operators carry fractional electric charge $1/N$. They are non-local operators that can only appears in conjugate pairs of mutiplets. On any given bundle, the following chiral field combinations are (with a fixed σ) are integral combinations of electrons.

$$\begin{aligned} (\lambda_y^{\sigma})^N &\sim d_y^{\sigma,1} \ldots d_y^{\sigma,1} \sim e^{i\sum_{r=1}^{N}\left(\phi_y^{\sigma,r}(\mathsf{x})+k_y^{\sigma,r}\mathsf{x}\right)} = e^{i\left(\tilde{\Phi}_{y\rho}^{\sigma}(\mathsf{x})+\tilde{k}_{y\rho}^{\sigma}\mathsf{x}\right)}, \\ d_y^{\sigma,r} d_y^{\sigma,r+1\dagger} &\sim e^{i\left(\phi_y^{\sigma,r}(\mathsf{x})-\phi_y^{\sigma,r+1}(\mathsf{x})\right)+i\left(k_y^{\sigma,r}-k_y^{\sigma,r+1}\right)\mathsf{x}} = e^{i\left(\tilde{\Phi}_{y,I=r}^{\sigma}(\mathsf{x})+\tilde{k}_{y,r}^{\sigma}\mathsf{x}\right)}. \end{aligned} \tag{4.29}$$

This is because the Chevalley bosons $\tilde{\Phi}$ are integral combinations of the electron bosonized variables Φ from the U transformation in (4.21). The locality of the second identity in (4.29) implies all parton conjugate pairs $d^r d^{r'\dagger}$ on any given wire and chiral sector are integral. In addition, the non-chiral conjugate pairs of Laughlin quasiparticles $\lambda_y^R \lambda_y^{L\dagger}$ and Dirac partons $d_y^{R,r} d_y^{L,r'\dagger}$, for any $r, r' = 1, \ldots, N$, are effectively local at energies lower than that of the intra-bundle potential. Each of these conjugate pairs operators is a vertex operator $e^{i\sum_{\sigma,r} a_{\sigma r}\phi_y^{\sigma r}}$, whose exponent $\sum_{\sigma,r} a_{\sigma r}\phi_y^{\sigma r}$ equals an integral linear combination of the electron bosonized variable Φ_{yj}^{σ} plus a (fractional) combination $b_I\Theta_y^{(I)} + b_{II}\Theta_y^{(II)}$ of the sine-Gordon angle variables in (4.27). Under the intra-bundle potential (4.26), the sine-Gordon angle variables are pinned to their ground state expectation values $\langle\Theta_y^{(I)}\rangle$ and

$\langle\Theta_y^{(II)}\rangle$ at energies $\ll u_I, u_{II}$. Therefore, the non-chiral conjugate pairs $\lambda_y^R\lambda_y^{L\dagger}$ and $d_y^{R,r}d_y^{L,r'\dagger}$ are effectively integral electronic (up to the phase $e^{i(b_I\langle\Theta_y^{(I)}\rangle+b_{II}\langle\Theta_y^{(II)}\rangle)}$).

By further backscattering the left and right moving $\mathrm{U}(1)_N \times \mathrm{SU}(N)_1$ currents in opposite directions between neighboring wires, we obtain the parton FQH state with a fully gapped bulk. The charge and momentum preserving inter-bundle current backscattering interactions are

$$\mathcal{H}[\mathrm{U}(1)_N \times \mathrm{SU}(N)_1] = \mathcal{H}_0 + \mathcal{H}_{\text{intra}}^{(c_1,c_2)} + \mathcal{H}_{\text{inter}}^{\mathrm{U}(1)_N} + \mathcal{H}_{\text{inter}}^{\mathrm{SU}(N)_1} \tag{4.30}$$

where

$$\begin{aligned}\mathcal{H}_{\text{inter}}^{\mathrm{U}(1)_N} &= u_{\text{inter}}\sum_y \left[\mathtt{H}_{\mathrm{U}(1)_N}\right]_y^{R\dagger}\left[\mathtt{H}_{\mathrm{U}(1)_N}\right]_{y+1}^{L} \\ &\quad + u_{\text{inter}}\sum_y\left(\left[\mathtt{E}_{\mathrm{U}(1)_N}\right]_{y,,\boldsymbol{\alpha}_{\mathrm{U}(1)_N}}^{R\dagger}\left[\mathtt{E}_{\mathrm{U}(1)_N}\right]_{y+1,\boldsymbol{\alpha}_{\mathrm{U}(1)_N}}^{L} + h.c.\right) \\ &= u_{\text{inter}}\sum_y\left(\frac{1}{mn}\sum_{r,s=1}^{N}\partial_{\mathrm{x}}\phi_{y,r}^R\partial_{\mathrm{x}}\phi_{y+1,s}^L - 2\cos\left(\boldsymbol{\alpha}_{\mathrm{U}(1)_N}\cdot\boldsymbol{\theta}_{y+1/2}\right)\right),\end{aligned} \tag{4.31}$$

and

$$\begin{aligned}\mathcal{H}_{\text{inter}}^{\mathrm{SU}(N)_1} &= u_{\text{inter}}\sum_y\left(\sum_{p=1}^{N-1}\left[\mathtt{H}_{\mathrm{SU}(N)_1}\right]_{y,p}^{R\dagger}\left[\mathtt{H}_{\mathrm{SU}(N)_1}\right]_{y+1,p}^{L}\right. \\ &\quad \left. + \sum_{\boldsymbol{\alpha}_{\mathrm{SU}(N)_1}}\left[\mathtt{E}_{\mathrm{SU}(N)_1}\right]_{y,\boldsymbol{\alpha}}^{R\dagger}\left[\mathtt{E}_{\mathrm{SU}(N)_1}\right]_{y+1,\boldsymbol{\alpha}}^{L}\right) \\ &= u_{\text{inter}}\sum_y\left(\sum_{p=1}^{N-1}\left[\mathtt{H}_{\mathrm{SU}(N)_1}\right]_{y,p}^{R\dagger}\left[\mathtt{H}_{\mathrm{SU}(N)_1}\right]_{y+1,p}^{L} - \sum_{\boldsymbol{\alpha}_{\mathrm{SU}(N)_1}}\cos\left(\boldsymbol{\alpha}_{\mathrm{SU}(N)_1}\cdot\boldsymbol{\theta}_{y+1/2}\right)\right).\end{aligned} \tag{4.32}$$

Above, $\left[\mathtt{H}_{\mathrm{U}(1)_N}\right]_y^{L,R}$, $\left[\mathtt{H}_{\mathrm{SU}(N)_1}\right]_y^{L,R}$, and $\left[\mathtt{E}_{\mathrm{SU}(N)_1}\right]_y^{L,R}$ are L,R KM currents on bundle y of the form given in Eqs. (4.14), (4.15), and (4.16); $\left[\mathtt{E}_{\mathrm{U}(1)_N}\right]_y^{L,R}$ is a vertex operator of the form in (4.16) with root vector $\boldsymbol{\alpha}_{\mathrm{U}(1)_N} = \sum_{j=1}^{N} \mathbf{e}_j$. The arguments of the cosine potentials are $\boldsymbol{\theta}_{y+1/2} = (\theta_{y+1/2,1}, \ldots, \theta_{y+1/2,N})$ where $\theta_{y+1/2,a} \equiv \phi^R_{y,a} - \phi^L_{y+1,a}$. The arguments of the cosine potentials mutually commute and may therefore be pinned. This pinning gaps out the bulk degrees of freedom, while the modes living on the top ($y_{\max}$) and bottom ($y_{\min}$) bundles of wires remain gapless with chiral edge-state Lagrangian of the form (4.12).

We notice in passing that the electrically neutral $\mathrm{SU}(N)_1$ currents carry vanishing $\mathtt{x}$-momentum and therefore can also be backscattered within the same bundle by an intra-bundle interaction $\mathcal{H}^{\mathrm{SU}(N)_1}_{\mathrm{intra}} \sim [\mathbf{J}_{\mathrm{SU}(N)_1}]^L_y \cdot [\mathbf{J}_{\mathrm{SU}(N)_1}]^R_y$. In this case, the resulting FQH state $\mathcal{H}[\mathrm{U}(1)_N] = \mathcal{H}^{\mathrm{U}(1)_N}_{\mathrm{inter}} + \mathcal{H}^{\mathrm{SU}(N)_1}_{\mathrm{intra}}$ will only carry chiral edge mode for $\mathrm{U}(1)_N$, and not for $\mathrm{SU}(N)_1$. It will belong in the same FQH phase as the Laughlin $\nu = 1/N$ state, where the partons are confined. On the other hand, our current model (4.30) describes a distinct FQH state where the $1/N$-charged partons can emerge as deconfined gapped excitations in the bulk. The $\mathcal{H}^{\mathrm{SU}(N)_1}_{\mathrm{intra}}$ and $\mathcal{H}^{\mathrm{SU}(N)_1}_{\mathrm{inter}}$ interactions in general can be present simultaneously and compete. The complete model $\mathcal{H}^{\mathrm{U}(1)_N}_{\mathrm{inter}} + \mathcal{H}^{\mathrm{SU}(N)_1}_{\mathrm{intra}} + \mathcal{H}^{\mathrm{SU}(N)_1}_{\mathrm{inter}}$ may provide a platform to study the critical transition of parton decomfinement.

4.2.3 Conformal Embedding and Descendant Topological Order

In this subsection, we will use the conformal embedding (also referred to as level-rank duality) $\mathrm{SU}(m)_n \times \mathrm{SU}(n)_m \subseteq \mathrm{SU}(mn)_1$ to demonstrate how FQH states with $\mathrm{U}(1)_{mn} \times$

$\mathrm{SU}(m)_n$ or $\mathrm{U}(1)_{mn} \times \mathrm{SU}(n)_m$ non-Abelian topological order can arise from partially filling the parton FQH state $\mathrm{U}(1)_{mn} \times \mathrm{SU}(mn)_1$.

Symmetry embedding

We first consider the embeddings of matrix tensor products $gl(m,\mathbb{C}) \times gl(n,\mathbb{C}) \subset gl(mn,\mathbb{C})$. Let $\mathbb{I}_p$ be the $p \times p$ identity matrix. Then, for any $m \times m$ matrix A_{ab} in $gl(m,\mathbb{C})$ and $n \times n$ matrix B_{cd} in $gl(n,\mathbb{C})$, they can be embedded into matrices of the tensor space $\mathbb{C}^{mn} = \mathbb{C}^m \otimes \mathbb{C}^n$ by the mappings $A \to (A \otimes \mathbb{I}_n)$ and $B \to (\mathbb{I}_m \otimes B)$. Moreover, the two embeddings commute because $A \otimes B = (A \otimes \mathbb{I}_n)(\mathbb{I}_m \otimes B) = (\mathbb{I}_m \otimes B)(A \otimes \mathbb{I}_n)$. We adopt the following notation for tensor products: $(A \otimes B)_{rs} = A_{ab} B_{cd} \delta_r^{(a-1)n+c} \delta_s^{(b-1)n+d}$, where $r, s = 1, \ldots, mn$. The counting of rows in $(A \otimes B)$, indexed by (a, c), is determined by $r = (a-1)n+c$; the counting of columns, indexed by (b, d), is determined by $s = (b-1)n+d$. Thus, the matrix embeddings are

$$\begin{aligned} (A \otimes \mathbb{I}_n)_{rs} &= A_{ab} \delta_{cd} \delta_r^{(a-1)n+c} \delta_s^{(b-1)n+d}, \\ (\mathbb{I}_m \otimes B)_{rs} &= \delta_{ab} B_{cd} \delta_r^{(a-1)n+c} \delta_s^{(b-1)n+d}. \end{aligned} \tag{4.33}$$

Let's apply this to $\mathrm{SU}(m)_n \times \mathrm{SU}(n)_m \subset \mathrm{SU}(mn)_1$. The $\mathrm{SU}(m)$ Lie algebra is spanned by traceless Hermitian m-dimensional matrices X, and they can be embedded inside the $\mathrm{SU}(mn)$ Lie algebra, $X \to X^A = (X \otimes \mathbb{I}_n)$, using the first equation in (4.33). In particular, the Cartan generators X^p and root matrices X^{ab} defined in (4.15) and (4.16) now lives

inside SU(mn) using

$$(X^A)^p_{rs} = \frac{1}{\sqrt{p(p+1)}} \sum_{c=1}^{n} \Big(\sum_{q=1}^{p} \delta_r^{(q-1)n+c} \delta_s^{(q-1)n+c} - p \delta_r^{pn+c} \delta_s^{pn+c} \Big). \tag{4.34}$$

$$(X^A)^{pq}_{rs} = (X^{pq})_{ab} \delta_{cd} \delta_r^{(a-1)n+c} \delta_s^{(b-1)n+c} = \sum_{c=1}^{n} \delta_r^{(p-1)n+c} \delta_s^{(q-1)n+c}. \tag{4.35}$$

We can apply this matrix embedding technology to the parton edge-state theory described in Sec. 4.2.1 to define the $\mathrm{SU}(m)_n \times \mathrm{SU}(n)_m$ currents to be parton bilinears. We begin with $\mathrm{SU}(m)_n$. In terms of the partons d^a, the Cartan operators are $(d^r)^\dagger (X^A)^p_{rs} d^s$; the ladder operators are $d^r (X^A)^{pq}_{rs} (d^s)^\dagger$ and $(d^r)^\dagger (X^A)^{pq}_{rs} d^s$. In terms of the Cartan-Weyl bosons ϕ_a, these Cartan and root operators are:

$$\begin{aligned} [\mathtt{H}_{\mathrm{SU}(m)_n}]_p &= \sum_{c=1}^{n} \frac{1}{\sqrt{p(p+1)}} \left(\sum_{a=1}^{p} \partial_{\mathsf{x}} \phi_{(a-1)n+c} - p \partial_{\mathsf{x}} \phi_{pn+c} \right), \\ [\mathtt{E}_{\mathrm{SU}(m)_n}]_{ab} &= \sum_{c=1}^{n} e^{i(\alpha^c_{ab})^j (\phi_j(\mathsf{x}) + k_j \mathsf{x})}. \end{aligned} \tag{4.36}$$

Here, $p = 1, \ldots, m-1$, where $m-1$ is the rank of SU(m), and

$$\boldsymbol{\alpha}^c_{ab} = \pm \left(\mathbf{e}_{(a-1)n+c} - \mathbf{e}_{(b-1)n+c} \right), \tag{4.37}$$

for $1 \le a < b \le m$ and $c = 1, \ldots, n$, with n the level of SU(m), and $\mathbf{e}_\ell$ are the unit vectors in $\mathbb{R}^{mn}$.

The same construction applies to $\mathrm{SU}(n)_m$. The matrix representations of Cartan generators and root operators are

$$\begin{aligned}(X^B)^p_{rs} &= \delta_{ab}(X^p)_{cd}\delta_r^{(a-1)n+c}\delta_s^{(b-1)n+d},\\ (X^B)^{pq}_{rs} &= \delta_{ab}(X^{pq})_{cd}\delta_r^{(a-1)n+c}\delta_s^{(b-1)n+d},\end{aligned} \tag{4.38}$$

respectively, which can be used to construct the corresponding currents in terms of partons, as above. Written in terms of the Cartan-Weyl bosons, these operators are:

$$\begin{aligned}[\mathtt{H}_{\mathrm{SU}(n)_m}]_q &= \sum_{a=1}^{m}\frac{1}{\sqrt{q(q+1)}}\left(\sum_{b=1}^{q}\partial_{\mathtt{x}}\phi_{(a-1)n+b} - q\partial_{\mathtt{x}}\phi_{(a-1)n+q+1}\right),\\ [\mathtt{E}_{\mathrm{SU}(n)_m}]_{cd} &= \sum_{a=1}^{m} e^{i(\alpha^a_{cd})^j(\phi_j(\mathtt{x})+k_j\mathtt{x})}.\end{aligned} \tag{4.39}$$

Here, $q = 1, \ldots, n-1$, where $n-1$ is the rank of $\mathrm{SU}(n)$, and

$$\boldsymbol{\alpha}^a_{cd} = \pm\left(\mathbf{e}_{(a-1)n+c} - \mathbf{e}_{(a-1)n+d}\right), \tag{4.40}$$

for $1 \le c < d \le n$ and $a = 1, \ldots, m$.

Descendant states

We now apply this technology to construct fractional quantum Hall states with $\mathrm{U}(1)_{mn} \times \mathrm{SU}(m)_n$ or $\mathrm{U}(1)_{mn} \times \mathrm{SU}(n)_m$ topological orders. The starting point is the free Lagrangian of the electron wires in (4.22). By introducing $\mathcal{H}^{(c_1,c_2)}_{\mathrm{intra}}$ in (4.26), the integrated fermion modes $\tilde{\Phi}^{\sigma}_{yc_1}$ and $\tilde{\Phi}^{\sigma}_{yc_1}$ are gapped. On each bundle there remains a non-chiral $\mathrm{U}(1)_{mn} \times \mathrm{SU}(mn)_1$

parton theory into which we embed $\mathrm{U}(1)_{mn} \times \mathrm{SU}(m)_n \times \mathrm{SU}(n)_m$. Note that the embedded symmetry currents are local since they are combinations of the integral vertex operators appearing in (4.29).

The full model Hamiltonians for the $\mathrm{U}(1)_{mn} \times \mathrm{SU}(m)_n$ or $\mathrm{U}(1)_{mn} \times \mathrm{SU}(n)_m$ states, using current backscattering potentials, is

$$\mathcal{H}\left[\mathrm{U}(1)_N \times \mathrm{SU}(m)_n\right] = \mathcal{H}_0 + \mathcal{H}_{\text{intra}}^{(c_1,c_2)} + \mathcal{H}_{\text{intra}}^{\mathrm{SU}(n)_m} + \mathcal{H}_{\text{inter}}^{\mathrm{U}(1)_N} + \mathcal{H}_{\text{inter}}^{\mathrm{SU}(m)_n}. \tag{4.41}$$

The intra- and inter-wire potentials of the neutral sectors are defined by

$$\mathcal{H}_{\text{intra}}^{\mathrm{SU}(n)_m} = u_{\text{intra}} \sum_y \left(\sum_{q=1}^{n-1} [\mathtt{H}_{\mathrm{SU}(n)_m}]_{y,q}^{R\dagger} [\mathtt{H}_{\mathrm{SU}(n)_m}]_{y,q}^{L} + \sum_{\boldsymbol{\alpha}_{\mathrm{SU}(n)}} \left[\mathtt{E}_{\mathrm{SU}(n)_m}\right]_{y,\boldsymbol{\alpha}}^{R\dagger} \left[\mathtt{E}_{\mathrm{SU}(n)_m}\right]_{y,\boldsymbol{\alpha}}^{L} \right), \tag{4.42}$$

$$\mathcal{H}_{\text{inter}}^{\mathrm{SU}(m)_n} = u_{\text{inter}} \sum_y \left(\sum_{p=1}^{m-1} [\mathtt{H}_{\mathrm{SU}(m)_n}]_{y,p}^{R\dagger} [\mathtt{H}_{\mathrm{SU}(m)_n}]_{y+1,p}^{L} + \sum_{\boldsymbol{\alpha}_{\mathrm{SU}(m)}} \left[\mathtt{E}_{\mathrm{SU}(m)_n}\right]_{y,\boldsymbol{\alpha}}^{R\dagger} \left[\mathtt{E}_{\mathrm{SU}(m)_n}\right]_{y+1,\boldsymbol{\alpha}}^{L} \right), \tag{4.43}$$

where $\mathcal{H}_{\text{inter}}^{\mathrm{U}(1)_N}$ is given in (4.31). The $\mathrm{U}(1)_{mn} \times \mathrm{SU}(n)_m$ state can be obtained by exchanging $\mathrm{SU}(m)_n \leftrightarrow \mathrm{SU}(n)_m$ in the formulas above. We conjecture that the $\mathrm{SU}(m)_n$ and $\mathrm{SU}(n)_m$ current backscattering potentials gap all neutral degrees of freedom in the bulk. If so, the model leaves behind an edge-state theory on each boundary with $\mathrm{U}(1)_{mn} \times \mathrm{SU}(m)_n$ KM symmetry. The Hamiltonian above preserves momentum and charge conservation. The

latter follows from the fact that current operators $[\mathtt{E}_{\mathcal{G}}]^R_{\boldsymbol{\alpha}}$ and $[\mathtt{E}_{\mathcal{G}}]^L_{\boldsymbol{\alpha}}$ carry equal electric charge.

4.2.4 Topological Order Examples

In this subsection, we will present the topological order carried by the parton FQH states as well as its non-Abelian descendants.

Emergent $\mathbb{Z}_N$ gauge theory in the Abelian $\mathrm{U}(1)_N \times \mathrm{SU}(N)_1$

The topological order of $\mathrm{U}(1)_N \times \mathrm{SU}(N)_1$ is identical to the $\mathbb{Z}_N$ orbifold of $\mathrm{U}(N)_1$ because of the deconfined partons $d^a = e^{i\phi^a}$. Each parton field is rotated by a complex phase $e^{2\pi i/N}$ under the discrete $\mathbb{Z}_N$ gauge transformation, whereas the local electronic field operator $\Psi_{\mathrm{el}} = e^{i(\phi^1+\ldots+\phi^N)}$ is gauge neutral. The different partons all belong in the same anyon class $[d] = \mathrm{span}\{d^1, \ldots, d^N\}$. Because the $\mathrm{SU}(N)_1$ current $d^a(d^b)^\dagger$ is an integral local field and belong to the vacuum anyon class. The parton anyon class $[d]$ can be regarded as the fundamental gauge charge. (It can be made bosonic by combining the fermionic parton with an electron.) It obeys the fusion rule $[d]^N = 1$ because $\Psi_{\mathrm{el}} = d^1 \ldots d^N$ belongs to the trivial vacuum class 1.

The Laughlin quasiparticle $\lambda = e^{i(\phi^1+\ldots+\phi^N)/N}$, which is the primitive non-local field in $\mathrm{U}(1)_N$, carries a gauge flux component. It has non-trivial mutual braiding statistics with

the gauge charge $[d]$

$$\langle \lambda(z) d^a(w) \rangle = \frac{1}{(z-w)^{1/N}} \tag{4.44}$$

with the monodromy phase $e^{2\pi i/N}$. It obeys the order N fusion rule $\lambda^N = 1$ and carries spin $h_\lambda = \frac{1}{2N}$. Combinations of the Laughlin quasiparticle λ and the deconfined parton $[d]$ generate all anyon classes in the $\mathrm{U}(1)_N \times \mathrm{SU}(N)_1$ topological order. For example, the primitive primary field sector in $\mathrm{SU}(N)_1$ consists of the vertex fields $e^{i\phi^a - i\sum_{b=1}^N \phi^b/N}$, for $a = 1, \ldots, N$. This sector is the fusion of $\mathcal{E}^1 = [d] \times \lambda^{-1}$.

Emergent Ising, Fibonacci and metaplectic anyons in $\mathrm{SU}(2)_n \times \mathrm{SU}(n)_2 \subseteq \mathrm{SU}(2n)_1$

Here we consider the example of topological orders that arise from the embedding of $\mathrm{SU}(2)_n \times \mathrm{SU}(n)_2$ in $\mathrm{SU}(2n)_1$. This is motivated by: (i) the $\mathbb{Z}_N$ parafermion decomposition of $\mathrm{SU}(2)_n$ current operators, where the parafermions CFT is the coset $\mathrm{SU}(2)_n/\mathrm{U}(1)_{2n}$; (ii) and the emergence of Fibonacci and metaplectic topological orders.

The root operators of $\mathrm{SU}(2)_n$ in (4.36) are the decomposable raising operators

$$\mathtt{E}^+_{\mathrm{SU}(2)_n} = \sum_{c=1}^{n} e^{i(\phi_c - \phi_{n+c})} = \xi \times \Psi, \tag{4.45}$$

and the lowering operator $\mathtt{E}^- = (\mathtt{E}^+)^\dagger$. The second identity above suggests the parafermion decomposition [Gep87, Gin88], with ξ a primary field in a $\mathrm{U}(1)_{2n}$ sector, and Ψ the $\mathbb{Z}_n$

parafermion primary field in the $\mathrm{SU}(2)_n/\mathrm{U}(1)_{2n}$ coset. For any given level n, we have

$$\xi = \sqrt{n} e^{i\theta_\perp/n}, \quad \Psi = \frac{1}{\sqrt{n}} \sum_{c=1}^{n} e^{i(\theta_c - \theta_\perp/n)}, \tag{4.46}$$

where $\theta_\perp = \theta_1 + \cdots + \theta_n$, and $\theta_c = \phi_c - \phi_{n+c}$. To obtain a $\mathbb{Z}_n$ primary field

$$\Psi_k = \frac{1}{\sqrt{C_k^n}} \sum_{1 \le j_1 < \ldots < j_k \le n} e^{i(\theta_{j_1} + \ldots + \theta_{j_k} - k\theta_\perp/n)}, \tag{4.47}$$

we fuse Ψ k-time with itself, where $k = 1, \ldots, n-1$. $\sqrt{C_k^n}$ is the normalized constant scaled by $C_k^n = n!/[k!(n-k)!]$.

Interactions of the $\mathrm{SU}(2)_n$ model can be now expressed by backscattering opposite chiral $\mathbb{Z}_n$ parafermion fields and coupling to a sine-Gordon potential. The operator $\mathcal{O}_{y+\epsilon}^{\mathrm{U}(1)_{2n}}$ is introduced through opposite chiral backscattering of ξ from the U(1) sector. We adopt the notation that when $\epsilon = 0$, it refers to the intrawire backscattering; and when $\epsilon = 1$ it refers to the interwire backscattering. Hence,

$$\begin{aligned}
\mathcal{U}_\epsilon^{\mathrm{SU}(2)_n} &= u_\epsilon \sum_y \left([\mathtt{H}_{\mathrm{SU}(2)_n}]_y^{R\dagger} [\mathtt{H}_{\mathrm{SU}(2)_n}]_{y+\epsilon}^{L} + \left(\left(J^+\right)_y^R \left(J^-\right)_{y+\epsilon}^L + h.c. \right) \right) \\
&= u_\epsilon \sum_y \left([\mathtt{H}_{\mathrm{SU}(2)_n}]_y^{R\dagger} [\mathtt{H}_{\mathrm{SU}(2)_n}]_{y+\epsilon}^{L} + \sum_{s=+,-} \left[\mathtt{E}^s_{\mathrm{SU}(2)_n}\right]_y^{R\dagger} \left[\mathtt{E}^s_{\mathrm{SU}(2)_n}\right]_{y+\epsilon/2}^{L} \right) \\
&\to u_\epsilon \sum_y \left([\mathtt{H}_{\mathrm{SU}(2)_n}]_y^{R\dagger} [\mathtt{H}_{\mathrm{SU}(2)_n}]_{y+\epsilon}^{L} + \left\langle \mathcal{O}_{y+\epsilon}^{\mathrm{U}(1)_{2n}} \right\rangle \Psi_y^{R\dagger} \Psi_{y+\epsilon}^{L} \right).
\end{aligned} \tag{4.48}$$

The sine-Gordon potential is pinned at a finite ground state expectation value. Subsequently, (4.48) opens up a mass gap for the counter-propagating $\mathbb{Z}_n$ parafermions sector [FAT91].

In the B sector, based on (4.39), the $\mathrm{SU}(n)_2$ root operator is

$$\left[\mathtt{E}_{\mathrm{SU}(n)_2}\right]^{\sigma}_{y,cd} \sim d^{\sigma}_{y,c} d^{\sigma\dagger}_{y,d} + d^{\sigma}_{y,n+c} d^{\sigma\dagger}_{y,n+d}. \tag{4.49}$$

Backscattering opposite chiral root operators gives the gapping potential

$$\mathcal{U}^{\mathrm{SU}(n)_2}_{\epsilon} = u_{\epsilon} \sum_{y} \left(\left[\mathtt{H}_{\mathrm{SU}(n)_2}\right]^{R\dagger}_{y} \left[\mathtt{H}_{\mathrm{SU}(n)_2}\right]^{L}_{y+\epsilon} + \Big(\sum_{1\le c<d\le n} \left[\mathtt{E}_{\mathrm{SU}(n)_2}\right]^{R\dagger}_{y,cd} \left[\mathtt{E}_{\mathrm{SU}(n)_2}\right]^{L}_{y+\epsilon,cd} + h.c. \Big) \right) \tag{4.50}$$

For the rest of the discussion on topological orders, we assume that (4.50) opens up a finite bulk excitation energy gap.

The topological order in the bulk corresponds to the conformal field theory on the edge. First, the $\mathrm{SU}(N)_1$ topological phase for general N can be constructed from (4.30) using the neutral modes in (4.29). The topological phase supports N Abelian anyons superselection sector $\mathcal{E}^m$ each containing C^N_m independent primary fields,

$$\mathcal{E}^m = \mathrm{span} \left\{ e^{i\left(\phi_{a_1} + \ldots + \phi_{a_m} - m\phi_{\perp}/N\right)} \right\}_{1\le a_1 < \ldots < a_m \le N}, \tag{4.51}$$

with $\phi_{\perp} = \phi_1 + \ldots + \phi_N$. They carry spin $h(\mathcal{E}^m) = m(N-m)/2N$, and obey fusion rules $\mathcal{E}^k \times \mathcal{E}^{\ell} = \mathcal{E}^{k+\ell}$ and $\mathcal{E}^0 = \mathcal{E}^N = 1$. Primary fields within a superselection sector are closed under the rotation of $\mathrm{SU}(N)_1$ WZW KM algebra. When $N = 2n$, we here present the three examples of the decomposition $\mathrm{SU}(2)_n \times \mathrm{SU}(n)_2$ for $n = 2, 3, 4$. They contain

Ising, Fibonacci, metaplectic anyons respectively. Each one of them is a primary field in the respective WZW algebras:

(I) $\mathrm{SU}(2)_2 = \mathrm{SO}(3)_1 = \mathrm{Sp}(2)_2$,

(II) $\mathrm{SU}(2)_3$ and $\mathrm{SU}(3)_2$,

(III) $\mathrm{SU}(2)_4 = \mathrm{SO}(3)_2 = \mathrm{SU}(3)_1/\mathbb{Z}_2$ and $\mathrm{SU}(4)_2 = \mathrm{SO}(6)_2 = \mathrm{SU}(6)_1/\mathbb{Z}_2$.

For case (I), when $n = 2$, the parafermion Ψ_y^σ has spin $1/2$ and is self-conjugate, i.e. is its own anti-particle. $\Psi_y^\sigma = (\Psi_y^\sigma)^\dagger$ is a Majorana fermion. The $\mathrm{SU}(2)_2$ and $\mathrm{SO}(3)_1$ WZW algebras are identical. The $\mathrm{SU}(2)_2$ current interaction (4.48) is the two-fermion backscattering potential $i(\xi^R)^\dagger \xi^L \Psi^R \Psi^L$, which under a mean-field approximation becomes the single-fermion potential $m_\xi (\xi^R)^\dagger \xi^L + i m_\Psi \Psi^R \Psi^L$, where $m_\xi = \langle i \Psi^R \Psi^L \rangle$ and $m_\Psi = \langle (\xi^R)^\dagger \xi^L \rangle$. The resulting topological phase under (4.41) and (4.48) supports Ising topological order. The edge chiral $\mathrm{SU}(2)_2$ CFT carries primary fields superselection sectors $1, [f], [\sigma]$ corresponding to the vacuum, the emergent fermion, and the Ising sectors.

Using the parafermion decomposition, the superselection sectors of fermion and Ising twist field in $\mathrm{SU}(2)_2$ (the A-sector, i.e. the first SU(2) in the $\mathrm{SU}(2)_2 \times \mathrm{SU}(2)_2 \subseteq \mathrm{SU}(4)_1$ embedding) are

$$\begin{aligned} [f] &= \mathrm{span}\Big\{ \xi, \xi^\dagger, \Psi \Big\}, \quad \xi = e^{i(\phi_1+\phi_2-\phi_3-\phi_4)/2}, \\ [\sigma] &= \mathrm{span}\Big\{ \sigma e^{\pm i(\phi_1+\phi_2-\phi_3-\phi_4)/4} \Big\}. \end{aligned} \tag{4.52}$$

They form the $j = 1$ and $j = 1/2$ irreducible representations of $\mathrm{SU}(2)_2$. Ψ is the emergent Majorana/$\mathbb{Z}_2$ parafermion. σ in the above equation is the Ising twist field of Ψ carrying spin $h = 1/16$. It has a π-monodromy with the Majorana fermion Ψ. The vertex fields $e^{\pm i(\phi_1+\phi_2-\phi_3-\phi_4)/4}$ are twist fields of the Dirac fermion ξ. Each one of them carries spin $h = 1/8$, and has a π-monodromy with ξ. The two twist fields σ and $e^{\pm i(\phi_1+\phi_2-\phi_3-\phi_4)/4}$ are bound to each other and cannot be individually present without the other. This is because each one has a π-braiding phase with the local boson $\xi\Psi$, which is the raising current operator of $\mathrm{SU}(2)_2$. Combining them, the total spin of the primary fields in the superselection sector $[\sigma]$ is $h_{[\sigma]} = 3/16$. The primary field presentation for the B-sector – the second SU(2) in the $\mathrm{SU}(2)_2 \times \mathrm{SU}(2)_2 \subseteq \mathrm{SU}(4)_1$ embedding – follows a similar structure. The primary fields satisfy fusion rules

$$f \times f = 1, \quad f \times \sigma = \sigma, \quad \sigma \times \sigma = 1 + f. \tag{4.53}$$

The spins, quantum dimensions, and dimensions of the superselection sectors are summarized in Table 4.1.

Table 4.1: The spin h, quantum dimension d, and number of fields # of each non-trivial primary sector of $\mathrm{SU}(2)_2$.

	f	σ
h	$\frac{1}{2}$	$\frac{3}{16}$
d	1	$\sqrt{2}$
#	3	2

Now we move on to case (II) – the topological phases with $\mathrm{SU}(2)_3$ and $\mathrm{SU}(3)_2$ edge CFTs constructed from the $\mathrm{SU}(2)_3 \times \mathrm{SU}(3)_2 \subseteq \mathrm{SU}(6)_1$ embedding. The $\mathrm{SU}(2)_3$ theory from

the A sector can be decomposed into a $\mathrm{U}(1)_6$ sector and a $\mathbb{Z}_3$ parafermion CFT, which is the coset $\mathrm{SU}(2)_3/\mathrm{U}(1)_6$. The primary fields in the U(1) sector can be generated by $\Xi = e^{i(\phi_1-\phi_4+\phi_2-\phi_5+\phi_3-\phi_6)/6}$. The $\mathbb{Z}_3$ parafermion CFT is connected to the chiral sector of three-state Potts model at criticality [DF84, Zam90] with central charge $c = 4/5$. Operators of the three-state Potts model can be generated by the energy density (τ) and spin (σ) operators of the $\mathbb{Z}_3$ model [DF84]. The spin operators can be obtained from the OPEs of the energy density operator and the $\mathbb{Z}_3$ parafermionic primaries, namely, $\sigma^+ = \tau \times \Psi$ and $\sigma^- = \tau \times \Psi^2$. τ has conformal dimension of $2/5$, and $\sigma^\pm$ are of $1/15$. The $\mathbb{Z}_3$ parafermionic primaries Ψ, Ψ^2 has conformal dimension of $2/3$ and can be identified with the charged fields Σ^+, Σ^- in the three-state Potts. Alternatively, these aforementioned primaries are the scaling fields $\Phi_{r,s}$ of the minimal model $\mathcal{M}(6,5)$ at central charge $4/5$, where $\Phi_{2,1} = \tau$, $\Phi_{3,3} = \sigma^\pm$, and $\Phi_{4,3} = \Sigma^\pm$. The locality of the $\mathrm{SU}(2)_3$ current (4.45) allows the following primary fields from the tensor product of $\mathrm{U}(1)_6 \times \mathbb{Z}_3$, and they are the non-trivial primary fields of $\mathrm{SU}(2)_3$.

$$\begin{aligned}
[j = 1/2] &= \mathrm{span}\left\{\Xi^\dagger\sigma^+, \Xi\sigma^-\right\}, \\
[j = 1] &= \mathrm{span}\left\{\tau, \Xi^2\sigma^+, (\Xi^2)^\dagger\sigma^-\right\}, \\
[j = 3/2] &= \mathrm{span}\left\{\Xi^3, \Xi\Psi^2, \Xi^\dagger\Psi, (\Xi^3)^\dagger\right\}.
\end{aligned} \tag{4.54}$$

They obey the following fusion rules [FMS12]:

$$\begin{gathered}
[3/2]\times[3/2]=1, \quad [3/2]\times[1]=[1/2], \\
[1/2]\times[1]=[3/2], \quad [1]\times[1]=1+[1], \\
[1]\times[1/2]=[3/2]+[1/2], \quad [1/2]\times[1/2]=1+[1],
\end{gathered} \tag{4.55}$$

where $1=[j=0]$ is the vacuum class. The primary fields $[j=\frac{1}{2}]$ and $[j=1]$ have the quantum dimension of golden ratio carried by the Fibonacci anyon τ, which has spin $h_\tau=2/5$, quantum dimension $d_\tau=(1+\sqrt{5})/2$ and lives inside the [1] class. Fields in [3/2] are Abelian semions and all have free field vertex operator representations. The $\mathrm{SU}(2)_3$ primaries are summarized in 4.2.

Table 4.2: The spin h, quantum dimension d, and number of fields # of each non-trivial primary sector of $\mathrm{SU}(2)_3$.

	$[\frac{1}{2}]$	$[1]$	$[\frac{3}{2}]$
h	$\frac{3}{20}$	$\frac{2}{5}$	$\frac{3}{4}$
d	$\frac{1+\sqrt{5}}{2}$	$\frac{1+\sqrt{5}}{2}$	1
#	2	3	4

We now present the anyon classes of $\mathrm{SU}(3)_2$. By using the coset identification $\mathrm{SU}(3)_2=\mathrm{SU}(6)_1/\mathrm{SU}(2)_3$ (which comes from the conformal embedding $\mathrm{SU}(2)_3\times\mathrm{SU}(3)_2\subseteq\mathrm{SU}(6)_1$), the topological order of $\mathrm{SU}(3)_2$ is identical to the reduced tensor product $\mathrm{SU}(6)_1\boxtimes\overline{\mathrm{SU}(2)_3}$. Here $\overline{\mathrm{SU}(2)_3}$ is the time-reversal conjugate of $\mathrm{SU}(2)_3$. Its anyons $\overline{[j]}$ have the fusion rules as those in $\mathrm{SU}(2)_3$, but they have conjugated spins $h_{\overline{[j]}}=-h_{[j]}$ (mod 1) and braiding phases. The tensor product $\boxtimes$ is relative to the anyon condensation [BS09] of the local bosonic pair of semions $b=\mathcal{E}^3\times\overline{[j=3/2]}$ in $\mathrm{SU}(6)_1\times\overline{\mathrm{SU}(2)_3}$, where $\mathcal{E}^3$ is the semion class in $\mathrm{SU}(6)_1$

(see (4.51) for the primary fields $\mathcal{E}^m$ of $\mathrm{SU}(N)_1$). The anyon selection rule restricts the deconfined anyons of $\mathrm{SU}(3)_2$ to be the anyon tensor products $\mathcal{E}^m \times \overline{[j]}$ in $\mathrm{SU}(6)_1 \times \overline{\mathrm{SU}(2)_3}$ that have trivial monodromy braiding with the local boson b. The non-trivial $\mathrm{SU}(3)_2$ anyons are

$$\begin{aligned}
[a] &= \mathcal{E}^2 \times \overline{[0]} \equiv \mathcal{E}^5 \times \overline{[3/2]}, \\
[a^*] &= \mathcal{E}^4 \times \overline{[0]} \equiv \mathcal{E}^1 \times \overline{[3/2]}, \\
[\bar{\tau}] &= \mathcal{E}^0 \times \overline{[1]} \equiv \mathcal{E}^3 \times \overline{[1/2]}, \\
[E] &= \mathcal{E}^2 \times \overline{[1]} \equiv \mathcal{E}^5 \times \overline{[1/2]}, \\
[E^*] &= \mathcal{E}^4 \times \overline{[1]} \equiv \mathcal{E}^1 \times \overline{[1/2]},
\end{aligned} \tag{4.56}$$

where anyon products are equivalent $\equiv$ modulo the local boson b. The spins and fusion rules of the $\mathrm{SU}(3)_2$ anyons can be determined by the product structure. The spins and quantum dimensions are summarized in table 4.3. The fusion rules are

$$\begin{aligned}
&[a] \times [a] = [a^*], \quad [a^*] \times [a^*] = [a], \quad [a] \times [a^*] = 1 \\
&[\bar{\tau}] \times [\bar{\tau}] = 1 + [\bar{\tau}], \quad [a] \times [\bar{\tau}] = [E], \quad [a^*] \times [\bar{\tau}] = [E^*].
\end{aligned} \tag{4.57}$$

Table 4.3: The spin h, quantum dimension d, and number of fields $\#$ of each non-trivial primary sector of $\mathrm{SU}(3)_2$.

	$[a]$ or $[a^*]$	$[\bar{\tau}]$	$[E]$ or $[E^*]$
h	$\frac{2}{3}$	$\frac{3}{5}$	$\frac{4}{15}$
d	1	$\frac{1+\sqrt{5}}{2}$	$\frac{1+\sqrt{5}}{2}$
$\#$	6	8	3

Each $SU(3)_2$ primary is a superselection sector of fields that rotate irreducibly under the $SU(3)_2$ WZW algebra. We begin with the Abelian $[a]$ and $[a^*]$ sectors. The primary fields in $[a]$ are linear combinations of the following six vertex fields

$$\mathcal{E}^2_{14}, \mathcal{E}^2_{25}, \mathcal{E}^2_{36}, \frac{\mathcal{E}^2_{15}+\mathcal{E}^2_{24}}{\sqrt{2}}, \frac{\mathcal{E}^2_{16}+\mathcal{E}^2_{34}}{\sqrt{2}}, \frac{\mathcal{E}^2_{26}+\mathcal{E}^2_{35}}{\sqrt{2}}, \tag{4.58}$$

where $\mathcal{E}^2_{j_1 j_2} = e^{i(\phi_{j_1}+\phi_{j_2}-2\phi_\perp/6)}$ are the vertex fields in the $\mathcal{E}^2$ class of $SU(6)_1$ (see (4.51)). These six fields are the ones in $\mathcal{E}^2$ that are decoupled from the $SU(2)_3$ sub-algebra of $SU(6)_1$. They have trivial OPE with the $SU(2)_3$ currents and therefore solely represent the $SU(3)_2$ sub-algebra. The primary fields in $[a^*]$ are spanned by the Hermitian conjugate of the vertices in (4.58).

Next, we move on to the Fibonacci super-selection sector $[\bar{\tau}]$ in $SU(3)_2$. It is spanned by eight primary fields. To see this, we observe the field products in $[\tau] \times [\bar{\tau}]$, – where $[\tau] = [j = 1]$ is the Fibonacci primary field sector in $SU(2)_3$ – are the $SU(6)_1$ WZW currents outside of those in $SU(2)_3 \times SU(3)_2$. On each bundle in each chiral sector, the field product pairs in $[\tau] \times [\bar{\tau}]$ are local spin $h = 2/5 + 3/5 = 1$ bosons that extend the $SU(2)_3 \times SU(3)_2$ WZW algebra to the full $SU(6)_1$ WZW algebra. The difference in dimensions of $SU(6)$ and $SU(2) \times SU(3)$ is $35 - (3 + 8) = 24$. There are 3 linearly independent fields in $[\tau] = [j = 1]$. Therefore, there must be $24/3 = 8$ linearly independent fields in $[\bar{\tau}]$ so that the product $[\tau] \times [\bar{\tau}]$ accounts for the 24 missing currents outside of $SU(2)_3 \times SU(3)_2$ in $SU(6)_1$. The eight fields in $[\bar{\tau}]$ form the adjoint representation of $SU(3)$. The affine $SU(6)_1$ Lie algebra,

as a vector space of the currents, decomposes into

$$\mathrm{SU}(6)_1 = \mathrm{SU}(2)_3 \oplus \mathrm{SU}(3)_2 \oplus ([\tau] \times [\bar{\tau}])\,. \tag{4.59}$$

We notice this field counting method holds for general $\mathrm{SU}(m)_n \times \mathrm{SU}(n)_m \subseteq \mathrm{SU}(mn)_1$ embeddings. The conformal dimension of a primary field sector (R) in $\mathrm{SU}(m)$ at level n is given by [Gin88, FMS12]:

$$h_{(R)} = \frac{C_{(R)}/2}{n+g} \tag{4.60}$$

where $C_{(R)}$ is the quadratic Casimir invariant of the irreducible representation (R), and g the dual Coxeter number of the algebra. $g = m$ for $\mathrm{SU}(m)$. In particular, the adjoint representation A of $\mathrm{SU}(m)$ has dimension $\dim(A) = \dim(\mathrm{SU}(m)) = m^2-1$ and the quadratic Casimir invariant $C_{(A)} = 2m$ [FMS12]. It corresponds to a primary field sector $[A]$ in the $\mathrm{SU}(m)_n$ WZW CFT if $n \geq 2$. The scaling dimension according to (4.60) is $h_A = m/(m+n)$. Therefore, in the conformal embedding where $\mathrm{SU}(m)_n \times \mathrm{SU}(n)_m \subseteq \mathrm{SU}(mn)_1$, the scaling dimensions of the adjoint primary fields in the two sectors combine to

$$h_A^{\mathrm{SU}(m)_n} + h_A^{\mathrm{SU}(n)_m} = \frac{m}{n+m} + \frac{n}{m+n} = 1. \tag{4.61}$$

There are $(m^2-1)(n^2-1)$ fields in the pair tensor product $[A]_{\mathrm{SU}(m)_n} \times [A]_{\mathrm{SU}(n)_m}$. This number equals the difference in the numbers of current operators, $\dim(\mathrm{SU}(mn)) - \dim(\mathrm{SU}(m)) - \dim(\mathrm{SU}(n))$. The spin-1 bosons in the adjoint pair are exactly the currents in $\mathrm{SU}(mn)_1$ out-

side of $\mathrm{SU}(m)_n$ and $\mathrm{SU}(n)_m$. This is summarized by the branching rule

$$\mathrm{SU}(mn)_1 = \mathrm{SU}(m)_n \oplus \mathrm{SU}(n)_m \oplus \left([A]_{\mathrm{SU}(m)_n} \times [A]_{\mathrm{SU}(n)_m}\right) \tag{4.62}$$

that generalizes (4.59). Since all $\mathrm{SU}(mn)_1$ currents are local bosons in the coupled-wire constructions, so are the field pair product in $[A]_{\mathrm{SU}(m)_n} \times [A]_{\mathrm{SU}(n)_m}$.

Going back to the case when $m = 2$ and $n = 3$, the identification of Fibonacci pairs $[\tau] \times [\bar{\tau}]$ in $\mathrm{SU}(2)_3 \times \mathrm{SU}(3)_2$ as local $\mathrm{SU}(6)_1$ currents, $J_y^\sigma \sim \tau_y^\sigma \bar{\tau}_y^\sigma$ on each bundle y and in each chiral sector $\sigma = R, L$, allows us to write down an explicit string of local boson operators that creates a Fibonacci anyon excitation at each end.

$$\begin{aligned} \mathcal{S} = \prod_{y=y_1}^{y_2} J_y^L(\mathsf{x}) J_y^R(\mathsf{x})^\dagger \sim \prod_{y=y_1}^{y_2} \tau_y^L \tau_y^R \prod_{y=y_1}^{y_2} \bar{\tau}_y^L \bar{\tau}_y^R \\ \xrightarrow{\text{at low energy}} \tau_{y_1}^L \left(\prod_{y=y_1}^{y_2-1} \langle \tau_y^R \tau_{y+1}^L \rangle \right) \tau_{y_2}^R \left(\prod_{y=y_1}^{y_2-1} \langle \bar{\tau}_y^L \bar{\tau}_y^R \rangle \right), \end{aligned} \tag{4.63}$$

where J_y^σ can be chosen to be an arbitrary current operator in $\mathrm{SU}(6)_1$ that falls outside of $\mathrm{SU}(2)_3 \times \mathrm{SU}(3)_2$ (see (4.59)), i.e. the most singular terms in the OPE of $J_y^\sigma(z)$ and currents from $\mathrm{SU}(2)_3$ or $\mathrm{SU}(3)_2$ are proportional to $1/(z-w)$ and not $1/(z-w)^2$. Neighboring Fibonacci field pairs from opposite chiral sectors at low energy are pinned to the ground state expectation values by the $\mathrm{SU}(2)_3$ and $\mathrm{SU}(3)_2$ current backscattering potentials. In the $\mathrm{SU}(2)_3$ phase where $\mathrm{SU}(2)_3$ (or $\mathrm{SU}(3)_2$) currents are back-scattered between (resp. within) bundles, $\tau_y^L \tau_{y+1}^R \to \langle \tau_y^L \tau_{y+1}^R \rangle$ and $\bar{\tau}_y^L \bar{\tau}_y^R \to \langle \bar{\tau}_y^L \bar{\tau}_y^R \rangle$. This leaves behind two dangling Fibonacci modes $\tau_{y_2}^L$ and $\tau_{y_1}^R$ at the two ends of the string. (See figure 4.1.)

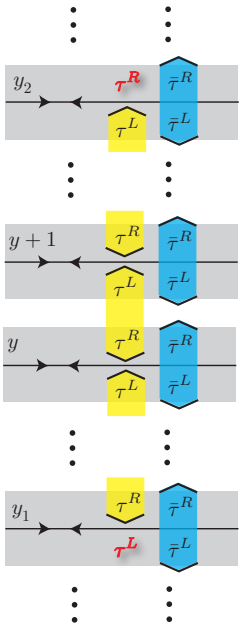

Figure 4.1: Fibonacci excitation pair created by the string of local operators $\mathcal{S}$ in (4.63). Yellow (blue) brackets are ground state expectation values of Fibonacci pairs as a result of the inter-wire (intra-wire) potential. The unpaired Fibonacci fields (highlighted in red) $\tau^L_{y_1}$ and $\tau^R_{y_2}$ become anyon excitations at the two ends of the string.

As for the remaining primary field super-selection sectors $[E]$ and $[E^*]$ in $\mathrm{SU}(3)_2$, they correspond to the two fundamental three-dimensional irreducible representations of SU(3). To see this, under the conformal embedding $\mathrm{SU}(2)_3 \times \mathrm{SU}(3)_2 \subseteq \mathrm{SU}(6)_1$, the $\mathrm{SU}(6)_1$ primary field sector $\mathcal{E}^2$ splits into two parts (c.f. (4.56))

$$\mathcal{E}^2 = ([j=0] \times [a]) \oplus ([j=1] \times [E])\,. \tag{4.64}$$

For instance, the spin of $[j=1] \times [E]$ combines to $2/5 + 4/15 = 2/3$, which is identical to that of $\mathcal{E}^2$ and $[a]$. There are $C_2^6 = 15$ linearly independent primary fields in $\mathcal{E}^2$. The six of them in (4.58) generate $[a] = [j=0] \times [a]$. The remaining nine generate $[j=1] \times [E]$. Since $[j=1]$ is the three-dimensional vector representation of $\mathrm{SU}(2)_3$ (see (4.54)), $[E]$ must be of dimension $9/3 = 3$. The same counting holds for $[E^*]$ because $\mathcal{E}^4$ splits into $[a^*]$ and $[j=1] \times [E^*]$. Apart from (4.64), the other $\mathrm{SU}(6)_1$ primary field super-selection sectors split into $\mathrm{SU}(2)_3 \times \mathrm{SU}(3)_2$ components according to the branching rules

$$\begin{aligned} \mathcal{E}^1 &= [j=1/2] \times [E^*]\,, \\ \mathcal{E}^3 &= ([j=3/2] \times 1) \oplus ([j=1/2] \times [\bar{\tau}])\,, \end{aligned} \tag{4.65}$$

and similarly for the conjugates $\mathcal{E}^4 = (\mathcal{E}^2)^\dagger$ and $\mathcal{E}^5 = (\mathcal{E}^1)^\dagger$.

The branching rules (4.64) and (4.65) allow us to write down strings of electron operators that create the anyon excitations on each end. These open strings are similar to those that created the Fibonacci anyons in (4.63) and figure 4.1. They are products of local operators

over a range of consecutive bundles

$$\mathcal{S}^m = \prod_{y=y_1}^{y_2} \mathcal{E}_y^{L,m}(\mathsf{x})\mathcal{E}_y^{R,m}(\mathsf{x})^\dagger, \tag{4.66}$$

where $m = 1, \ldots, 5$. On each wire in low-energy, the conjugate pair of $\mathrm{SU}(6)_1$ primaries $\mathcal{E}_y^{L,m}\mathcal{E}_y^{R,m\,\dagger}$ is effectively an integral product of electrons up to ground state expectation values $\langle\Theta_y^{(I)}\rangle$ and $\langle\Theta_y^{(II)}\rangle$ of the gapped $c_{1,2}$ modes. Any arbitrary anyon conjugate pair can be created by choosing an appropriate primary field in $\mathcal{E}^m$ and applying the operator string $\mathcal{S}^m$ on a ground state. We here demonstrate the pair creation of the Abelian anyon $[a]$ and the non-Abelian anyon $[E]$ in a $\mathrm{U}(1)_6 \times \mathrm{SU}(3)_2$ FQH model. First, we apply the string $\mathcal{S}^2$ in (4.66) and choose the $\mathrm{SU}(6)_1$ primary $\mathcal{E}^2$ on each chiral sector and bundle to be one (or any normalized linear combination) of the primary fields in (4.58). Since these fields all belong in the $[a]$ primary field sector in $\mathrm{SU}(3)_2$, the string in low-energy decomposes into

$$\mathcal{S}^2 \xrightarrow{\text{at low energy}} a_{y_1}^L \left(\prod_{y=y_1}^{y_2-1} \left\langle a_y^{R\dagger} a_{y+1}^L \right\rangle \right) a_{y_2}^{R\,\dagger} \tag{4.67}$$

where a_y^σ is the chosen primary field $\mathcal{E}^2$ in (4.58) at (y, σ). By the inter-bundle backscattering $\mathcal{H}_{\text{inter}}^{\mathrm{SU}(3)_2}$, conjugate field pairs between neighboring bundles are pinned to their ground state expectation values $\langle a_y^{R\dagger} a_{y+1}^L \rangle$, which is a U(1) phase. This leaves behind the unpaired fields $a_{y_1}^L$ and $a_{y_2}^{R\,\dagger}$ at the two ends and creates the separated conjugate pair of Abelian anyon excitations.

Next, we again apply the string $\mathcal{S}^2$ in (4.66) but instead choose a new $\mathrm{SU}(6)_1$ primary $\mathcal{E}^2$ that is orthogonal to the $[a]$ sector (i.e. the most singular term in its OPE with any of the

fields in (4.58) is at most proportional to $1/(z-w)^h$ but not $1/(z-w)^{2h}$, where $h=2/3$ is the spin of $\mathcal{E}^2$). According to the branching rule (4.64), this field $\mathcal{E}^2$ decomposes into the tensor product $\tau \times E$, where τ belongs to the $[j=1]$ sector in $\mathrm{SU}(2)_3$ and E belongs to the $[E]$ sector in $\mathrm{SU}(3)_2$. Therefore, in low-energy,

$$\mathcal{S}^2 \sim \prod_{y=y_1}^{y_2} \tau_y^L \tau_y^R \prod_{y=y_1}^{y_2} E_y^L E_y^{R\dagger} \xrightarrow{\text{at low energy}} \left(\prod_{y=y_1}^{y_2} \langle \tau_y^L \tau_y^R \rangle \right) \times E_{y_1}^L \left(\prod_{y=y_1}^{y_2-1} \left\langle E_y^{R\dagger} E_{y+1}^L \right\rangle \right) E_{y_2}^{R\,\dagger}, \tag{4.68}$$

where the ground state expectation values are pinned by the intra/inter-bundle current backscattering potentials $\mathcal{H}_{\text{intra}}^{\mathrm{SU}(2)_3}$ and $\mathcal{H}_{\text{inter}}^{\mathrm{SU}(3)_2}$. This leaves behind the separated conjugate pair of non-Abelian excitations in anyon classes $[E]$ and $[E^*]$ at the two ends of the string. If the same string is applied to the $\mathrm{SU}(2)_3$ state instead of $\mathrm{SU}(3)_2$, it will create a pair of Fibonacci anyons τ. All other anyon pairs can be created using different string operators $\mathcal{S}^m$ in (4.66) with appropriate choices of primary fields $\mathcal{E}^m$ and branching rules (4.65).

Lastly, we present case (III) – the topological phases with $\mathrm{SU}(2)_4$ and $\mathrm{SU}(4)_2$ edge CFTs constructed from the $\mathrm{SU}(2)_4 \times \mathrm{SU}(4)_2 \subseteq \mathrm{SU}(8)_1$ embedding. The $\mathrm{SU}(2)_4$ theory can be decomposed into a $\mathrm{U}(1)_8$ sector and a $\mathbb{Z}_4$ parafermion CFT, which is the coset $\mathrm{SU}(2)_4/\mathrm{U}(1)_8$. The $\mathrm{SU}(2)_4$ current raising operator can be decomposed according to (4.45). We now define $\Xi \equiv e^{i\sum_{j=1}^4 \theta_j/8}$ where $\theta_j = \phi_j - \phi_{4+j}$ that generates $\mathrm{U}(1)_8$. They carry spin $h_{\Xi^q} = q^2/16$ for $q = -3, \ldots, 4$. For Ψ_k, the corresponding spin is $h_k = k(4-k)/4$ with $k = 0, 1, 2, 3$. The primary fields of the $\mathbb{Z}_4$ parafermion CFT was described in [DVVV89, TH23] by identifying the theory with the $\mathrm{U}(1)_6/\mathbb{Z}_2$ orbifold CFT. They are the spin 1/3 vertex operators $\phi_3^{1,2}$,

that can be identified with $\Psi_{1,3}$; spin 1 operator j that can be identified with Ψ_2; the rest are the operators $\phi_{1,2}$, twist fields $\sigma_{1,2}$ and $\tau_{1,2}$, which are non-Abelian and do not have free field expression. Their conformal and quantum dimensions are included in Table 4.4.

Table 4.4: The spin h and quantum dimension d of $\mathbb{Z}_4$ parafermion CFT. Notation of primary fields are based on [DVVV89].

	$\phi_3^{1,2}$	j	ϕ_1	ϕ_2	$\sigma_{1,2}$	$\tau_{1,2}$
h	$\frac{3}{4}$	1	$\frac{1}{12}$	$\frac{1}{3}$	$\frac{1}{16}$	$\frac{9}{16}$
d	1	1	2	2	$\sqrt{3}$	$\sqrt{3}$

The $\mathrm{SU}(2)_4$ topological order can now be obtained from the reduced tensor product $\mathrm{U}(1)_8 \times \mathbb{Z}_4$ relative to the anyon condensation of the bosonic product $\Xi^2 \times \phi_3^1$, which is the raising current operator $\mathtt{E}^+_{\mathrm{SU}(2)_4}$ (along with its conjugate $\mathtt{E}^-_{\mathrm{SU}(2)_4} = {\mathtt{E}^+_{\mathrm{SU}(2)_4}}^\dagger$ and its square $\Xi^4 \times j$). The primary field superselection sector of $\mathrm{SU}(2)_4$ is labeled by $[j]$, with $j = 0, 1/2, 1, 3/2, 2$ with spin $h_j = j(j+1)/6$. Under the parafermion decomposition, each of the $\mathrm{SU}(2)_3$ super-sector is spanned by a set of primary field products in $\mathrm{U}(1)_8 \times \mathbb{Z}_4$ that rotate irreducibly under $\mathtt{E}^\pm_{\mathrm{SU}(2)_4}$.

$$\begin{aligned}
[j = 1/2] &= \mathrm{span}\left\{\Xi\sigma_1, \Xi^{-1}\sigma_2\right\}, \\
[j = 1] &= \mathrm{span}\left\{\phi_2, \Xi^2\phi_1, \Xi^{-2}\phi_1\right\}, \\
[j = 3/2] &= \mathrm{span}\left\{\Xi\tau_1, \Xi^{-1}\tau_2, \Xi^3\sigma_2, \Xi^{-3}\sigma_1\right\}, \\
[j = 2] &= \mathrm{span}\left\{\Xi^4, \Xi^2\phi_3^2, j, \Xi^{-2}\phi_3^1, \Xi^{-4}\right\}.
\end{aligned} \tag{4.69}$$

Alternatively, modular data like quantum dimensions and fusion algebras of a WZW KM algebras are readily encoded in the modular $\mathcal{S}$-matrix. The modular $\mathcal{S}$-matrix can be obtained from the ribbon identity that relates the 2π braiding phase of anyon j, j' over a

fixed fusion channel k [Kit06]. Specifically,

$$\mathcal{S}_{ij} = \frac{1}{\mathcal{D}} \sum_k d_k N_{ij}^k \frac{\theta_k}{\theta_i \theta_j}, \tag{4.70}$$

where d_k is the quantum dimension of a superselection sector, and $\mathcal{D} = \sqrt{\sum_k d_k^2}$ is the total quantum dimension. $\theta_k = e^{2\pi i h_k}$ is the topological spin of anyone k, where h_k is the conformal scaling dimension of its corresponding primary field. The general formula for the modular $\mathcal{S}$-matrix of $\mathrm{SU}(2)_n$ is given by the formula [FMS12]

$$\mathcal{S}_{j,j'}(n) = \sqrt{\frac{2}{n+2}} \sin \frac{(2j+1)(2j'+1)\pi}{n+2}. \tag{4.71}$$

For $n = 4$, we have

$$\mathcal{S}_{j,j'} = \frac{2}{\sqrt{3}} \sin \frac{(2j+1)(2j'+1)\pi}{6} \tag{4.72}$$

where $j, j', k = 0, 1/2, \ldots, 2$. Using the Verlinde formula [Ver88], one can obtain all fusion algebra, and quantum dimensions of anyons, by computing the fusion tensor

$$\mathcal{N}_{jj'}^k = \sum_\sigma \frac{\mathcal{S}_{j\sigma} \mathcal{S}_{j'\sigma} \mathcal{S}_{k\sigma}^*}{\mathcal{S}_{0\sigma}}. \tag{4.73}$$

The topological data of $\mathrm{SU}(2)_4$ is summarized in Table.4.5. The $\mathrm{SU}(2)_4$ anyons obey the fusion rules

$$\begin{gathered}
[1/2]\times[1/2]=[0]+[1],\quad [1/2]\times[2]=[3/2],\\
[2]\times[2]=[0],\\
[1/2]\times[1]=[1/2]+[3/2],\\
[1]\times[1]=[0]+[1]+[2].
\end{gathered}\tag{4.74}$$

$\mathrm{SU}(2)_4$ supports metaplectic topologial order [HNW13, CW15, BRU16]. It is identical to the $\mathrm{SO}(3)_2$ WZW algebra and the $\mathrm{SU}(3)_1/\mathbb{Z}_2$ orbifold CFT [TH23]. It has two spin 1 bosons, and two metaplectic anyons with quantum dimension of $\sqrt{3}$ and one with quantum dimension of 2. The metaplectic anyon $[j=1]$, which has integral quantum dimension, is capable of computing the Kauffman polynomial that is #P-hard [HNW13].

Table 4.5: The spin h, quantum dimension d, and number of fields # of each non-trivial primary sector of $\mathrm{SU}(2)_4$.

	$[\frac{1}{2}]$	$[1]$	$[\frac{3}{2}]$	$[2]$
h	$\frac{1}{8}$	$\frac{1}{3}$	$\frac{5}{8}$	1
d	$\sqrt{3}$	2	$\sqrt{3}$	1
#	2	3	4	5

Now we move on to $\mathrm{SU}(4)_2$. From the conformal embedding $\mathrm{SU}(2)_4\times\mathrm{SU}(4)_2\subseteq\mathrm{SU}(8)_1$, the $\mathrm{SU}(2)_4$ CFT is identical to the coset $\mathrm{SU}(8)_1/\mathrm{SU}(2)_4$. Its topological order is the same as the reduced tensor product $\mathrm{SU}(8)_1\boxtimes\overline{\mathrm{SU}(2)_4}$ between $\mathrm{SU}(8)_1$ and the time-reversal conjugate of $\mathrm{SU}(2)_4$. The tensor product is relative to the anyon condensation of the boson pair $\mathcal{E}^4\times\overline{[j=2]}$ (see (4.51) for the $\mathrm{SU}(N)_1$ primary fields $\mathcal{E}^m$). The $\mathrm{SU}(4)_2$ primary fields

are in 1-1 correspondence with the deconfined anyons in $\mathrm{SU}(8)_1 \boxtimes \overline{\mathrm{SU}(2)_4}$ that have trivial mutual statistics with the condensed boson $\mathcal{E}^4 \times \overline{[j=2]}$. The Abelian ones are (up to the condensed boson) $[a] = \mathcal{E}^4 \times \overline{[j=0]}$ that has spin $h = 1$ as well as $[b] = \mathcal{E}^2 \times \overline{[0]}$ and its anti-particle $[b^*] = \mathcal{E}^6 \times \overline{[0]}$ that both have spin $h = 3/4$. Primary fields in these Abelian superselection sectors have free field expressions. The $\mathrm{SU}(8)_1$ primary field sectors of $\mathcal{E}^2$ and $\mathcal{E}^4$ consist of vertex operators $\mathcal{E}^2_{j_1 j_2} \equiv e^{i(\phi_{j_1}+\phi_{j_2}-2\phi_\perp/8)}$ for $1 \le j_1 < j_2 \le 8$, and $\mathcal{E}^4_{j_1 j_2 j_3 j_4} \equiv e^{i(\sum_{k=1}^4 \phi_{j_k}-4\phi_\perp/8)}$ for $1 \le j_1 < j_2 < j_3 < j_4 \le 8$. The 20 dimensional superselection sector $[a]$ is spanned by the vertex fields combinations

$$[a] = \left\{ \begin{array}{c} \mathcal{E}^4_{1256}, \mathcal{E}^4_{1357}, \mathcal{E}^4_{1458}, \mathcal{E}^4_{2367}, \mathcal{E}^4_{2468}, \mathcal{E}^4_{3478}, \\ \frac{\mathcal{E}^4_{1257}+\mathcal{E}^4_{1356}}{\sqrt{2}}, \frac{\mathcal{E}^4_{1258}+\mathcal{E}^4_{1456}}{\sqrt{2}}, \frac{\mathcal{E}^4_{1267}+\mathcal{E}^4_{2356}}{\sqrt{2}}, \frac{\mathcal{E}^4_{1268}+\mathcal{E}^4_{2456}}{\sqrt{2}}, \\ \frac{\mathcal{E}^4_{1358}+\mathcal{E}^4_{1457}}{\sqrt{2}}, \frac{\mathcal{E}^4_{1367}+\mathcal{E}^4_{2357}}{\sqrt{2}}, \frac{\mathcal{E}^4_{1378}+\mathcal{E}^4_{3457}}{\sqrt{2}}, \frac{\mathcal{E}^4_{1468}+\mathcal{E}^4_{2458}}{\sqrt{2}}, \\ \frac{\mathcal{E}^4_{1478}+\mathcal{E}^4_{3458}}{\sqrt{2}}, \frac{\mathcal{E}^4_{2368}+\mathcal{E}^4_{2467}}{\sqrt{2}}, \frac{\mathcal{E}^4_{2378}+\mathcal{E}^4_{3467}}{\sqrt{2}}, \frac{\mathcal{E}^4_{2478}+\mathcal{E}^4_{3468}}{\sqrt{2}}, \\ \frac{\mathcal{E}^4_{1278}+\mathcal{E}^4_{3456}+\mathcal{E}^4_{1368}+\mathcal{E}^4_{2457}}{2}, \frac{\mathcal{E}^4_{1368}+\mathcal{E}^4_{2457}+\mathcal{E}^4_{1467}+\mathcal{E}^4_{2358}}{2} \end{array} \right\} \tag{4.75}$$

in $\mathcal{E}^4$ that are decoupled from and have non-singular OPE with the $\mathrm{SU}(2)_4$ WZW subalgebra. Similarly, $[b]$ is the 10 dimensional superselection sector spanned by the $\mathrm{SU}(2)_4$-invariant vertex fields

$$[b] = \left\{ \begin{array}{c} \mathcal{E}^2_{15}, \mathcal{E}^2_{26}, \mathcal{E}^2_{37}, \mathcal{E}^2_{48}, \frac{\mathcal{E}^2_{16}+\mathcal{E}^2_{25}}{\sqrt{2}}, \frac{\mathcal{E}^2_{17}+\mathcal{E}^2_{35}}{\sqrt{2}}, \\ \frac{\mathcal{E}^2_{18}+\mathcal{E}^2_{45}}{\sqrt{2}}, \frac{\mathcal{E}^2_{27}+\mathcal{E}^2_{36}}{\sqrt{2}}, \frac{\mathcal{E}^2_{28}+\mathcal{E}^2_{46}}{\sqrt{2}}, \frac{\mathcal{E}^2_{38}+\mathcal{E}^2_{47}}{\sqrt{2}} \end{array} \right\}. \tag{4.76}$$

Fields within each sector can be rotated irreducibly into one another by the $\mathrm{SU}(4)_2$ KM currents. The Abelian supersector $[b^*]$ is the Hermitian conjugate of $[b]$.

For the non-Abelian primary field superselection sectors of $\mathrm{SU}(4)_2$, we label them by borrowing the notations from table 4.4. First, we label the twist fields to be $[\bar{\tau}_1]$, $[\bar{\tau}_2]$, $[\bar{\sigma}_1]$, and $[\bar{\sigma}_2]$. They can be identified (up to the condensed boson) with the following pair product anyons in $\mathrm{SU}(8)_1 \times \overline{\mathrm{SU}(2)_4}$.

1. $[\bar{\sigma}_1] = \mathcal{E}^5 \times \overline{[j = 3/2]}$ and $[\bar{\sigma}_2] = \mathcal{E}^3 \times \overline{[j = 3/2]}$. Both carry spin $h = 5/16$.

2. $[\bar{\tau}_1] = \mathcal{E}^5 \times \overline{[j = 1/2]}$ and $[\bar{\tau}_2] = \mathcal{E}^5 \times \overline{[j = 1/2]}$. Both carry spin $h = 13/16$.

Second, we label the remaining metaplectic [CW15, BRU16] primary fields to be $[\bar{\phi}_2] = \mathcal{E}^4 \times \overline{[j = 1]}$, which carries spin $h = 2/3$, and $[\bar{\phi}_1] = \mathcal{E}^2 \times \overline{[j = 1]}$, which carries spin $h = 5/12$. The fusion rules of $\mathrm{SU}(4)_2$ are generated by

$$
\begin{gathered}
[a] \times [a] = 1, \quad [a] \times [b] = [b^*], \quad [b] \times [b] = [a] \\
[b] \times [\bar{\phi}_1] = [\bar{\phi}_2], \quad [b] \times [\bar{\phi}_2] = [\bar{\phi}_1], \\
[b] \times [\bar{\sigma}_1] = [\bar{\tau}_2], \quad [b] \times [\bar{\tau}_2] = [\bar{\tau}_1], \\
[b] \times [\bar{\tau}_1] = [\bar{\sigma}_2], \quad [b] \times [\bar{\sigma}_2] = [\bar{\sigma}_1] \\
[\bar{\sigma}_1] \times [\bar{\sigma}_2] = [\bar{\tau}_1] \times [\bar{\tau}_2] = 1 + [\bar{\phi}_2], \\
[\bar{\phi}_i] \times [\bar{\phi}_i] = 1 + [a] + [\bar{\phi}_2] \\
[\bar{\phi}_2] \times [\bar{\sigma}_j] = [\bar{\phi}_2] \times [\bar{\tau}_j] = [\bar{\sigma}_j] + [\bar{\tau}_j]
\end{gathered}
\tag{4.77}
$$

where $i, j = 1, 2$.

The corresponding modular $\mathcal{S}$-matrix is:

$$\mathcal{S}_{j,j'} = \frac{1}{2\sqrt{6}} \begin{pmatrix} 1 & 1 & 1 & 1 & \sqrt{3} & \sqrt{3} & \sqrt{3} & \sqrt{3} & 2 & 2 \\ 1 & -1 & 1 & -1 & -i\sqrt{3} & i\sqrt{3} & -i\sqrt{3} & i\sqrt{3} & 2 & -2 \\ 1 & 1 & 1 & 1 & -\sqrt{3} & -\sqrt{3} & -\sqrt{3} & -\sqrt{3} & 2 & 2 \\ 1 & -1 & 1 & -1 & i\sqrt{3} & -i\sqrt{3} & i\sqrt{3} & -i\sqrt{3} & 2 & -2 \\ \sqrt{3} & -i\sqrt{3} & -\sqrt{3} & i\sqrt{3} & \sqrt{\frac{3}{2}}(1-i) & -\sqrt{\frac{3}{2}}(1+i) & -\sqrt{\frac{3}{2}}(1-i) & \sqrt{\frac{3}{2}}(1+i) & 0 & 0 \\ \sqrt{3} & i\sqrt{3} & -\sqrt{3} & -i\sqrt{3} & -\sqrt{\frac{3}{2}}(1+i) & \sqrt{\frac{3}{2}}(1-i) & \sqrt{\frac{3}{2}}(1+i) & -\sqrt{\frac{3}{2}}(1-i) & 0 & 0 \\ \sqrt{3} & -i\sqrt{3} & -\sqrt{3} & i\sqrt{3} & -\sqrt{\frac{3}{2}}(1-i) & \sqrt{\frac{3}{2}}(1+i) & \sqrt{\frac{3}{2}}(1-i) & -\sqrt{\frac{3}{2}}(1+i) & 0 & 0 \\ \sqrt{3} & i\sqrt{3} & -\sqrt{3} & -i\sqrt{3} & \sqrt{\frac{3}{2}}(1+i) & -\sqrt{\frac{3}{2}}(1-i) & -\sqrt{\frac{3}{2}}(1+i) & \sqrt{\frac{3}{2}}(1-i) & 0 & 0 \\ 2 & 2 & 2 & 2 & 0 & 0 & 0 & 0 & -2 & -2 \\ 2 & -2 & 2 & -2 & 0 & 0 & 0 & 0 & -2 & 2 \end{pmatrix}, \tag{4.78}$$

with topological sectors label $j, j' = \{0, 1, 2, \ldots, 9\} = \left\{1, b, a, b^*, \bar{\sigma}_1, \bar{\tau}_2, \bar{\tau}_1, \bar{\sigma}_2, \bar{\phi}_2, \bar{\phi}_1\right\}$.

The primary fields' scaling dimensions and quantum dimensions of $\mathrm{SU}(4)_2$ are listed in table 4.6. The $\mathrm{SU}(4)_2$ theory and the $\mathbb{Z}_4$ parafermion CFT (see table 4.4) share identical primary field fusion rules. For example, the Abelian anyons $1, [b], [a], [b^*]$ in $\mathrm{SU}(4)_2$ and $1, \phi_3^1, j, \phi_3^2$ both form a $\mathbb{Z}_4$ fusion group. The metaplectic super-sector $[\bar{\phi}_2]$ forms the adjoint representation of $\mathrm{SU}(4)_2$. Therefore, it carries 15 primary fields since $\dim(\mathrm{SU}(4)) = 15$. In the $\mathrm{SU}(2)_4 \times \mathrm{SU}(4)_2 \subseteq \mathrm{SU}(8)_1$ conformal embedding, field products in $[j = 1] \times [\bar{\phi}_2]$ accounts for (a) the 45 local $\mathrm{SU}(8)_1$ currents J outside of $\mathrm{SU}(2)_4 \times \mathrm{SU}(4)_2$ (see (4.62)), as well as (b) the 45 non-local spin-1 vertex fields in $\mathcal{E}^4$ in $\mathrm{SU}(8)_1$ outside of the $[j = 2]$ super-sector in (4.69) from $\mathrm{SU}(2)_4$ and the $[a]$ super-sector in (4.75) from $\mathrm{SU}(4)_2$. As vector spaces, we have the decomposition

$$\begin{aligned} \mathrm{SU}(8)_1 &= \mathrm{SU}(2)_4 \oplus \mathrm{SU}(4)_2 \oplus \left([j = 1] \times [\bar{\phi}_2]\right), \\ \mathcal{E}^4 &= [j = 2] \oplus [a] \oplus \left([j = 1] \times [\bar{\phi}_2]\right). \end{aligned} \tag{4.79}$$

There are 45 fields in both cases because 45 equals $\dim(\mathrm{SU}(8)) - \dim(\mathrm{SU}(2)) - \dim(\mathrm{SU}(4))$ as well as $\#\mathcal{E}^4 - \#[j=2] - \#[a]$. Since there are 3 fields in $[j=1]$, there must be $15 = 45/3$ fields in $[\bar{\phi}_2]$.

According to the branching rules,

$$\begin{aligned} \mathcal{E}^2 &= [b] \oplus \left([j=1] \times [\bar{\phi}_1] \right) \\ \mathcal{E}^6 &= [b^*] \oplus \left([j=1] \times [\bar{\phi}_1] \right). \end{aligned} \tag{4.80}$$

field products in $[j=1] \times [\bar{\phi}_1]$ splits into components that belong to (a) the $\mathrm{SU}(8)_1$ vertex fields in $\mathcal{E}^2$ outside of the $[b]$ sector in (4.76) from $\mathrm{SU}(4)_2$, and (b) the $\mathrm{SU}(8)_1$ fields in $\mathcal{E}^6$ outside of $[b^*]$. There are 18 fields in each case because $18 = \#\mathcal{E}^2 - \#[b]$. Since $\#[j=1] = 3$, there are $6 = 18/3$ fields in $[\bar{\phi}_1]$. The $\mathrm{SU}(8)_1$ primary field super-sectors $\mathcal{E}^{1,3,5,7}$ with odd powers splits into $\mathrm{SU}(2)_4 \times \mathrm{SU}(4)_2$ components according to

$$\begin{aligned} \mathcal{E}^1 &= [j=1/2] \times [\bar{\sigma}_1], \\ \mathcal{E}^3 &= \left([j=1/2] \times [\bar{\tau}_2] \right) \oplus \left([j=3/2] \times [\bar{\sigma}_2] \right), \\ \mathcal{E}^5 &= \left([j=1/2] \times [\bar{\tau}_1] \right) \oplus \left([j=3/2] \times [\bar{\sigma}_1] \right), \\ \mathcal{E}^7 &= [j=1/2] \times [\bar{\sigma}_2]. \end{aligned} \tag{4.81}$$

Dimension counting from $\#\mathcal{E}^m = C^8_m$ and $\#[j] = 2j+1$ forces $\#[\sigma_{1,2}] = 4$ and $\#[\tau_{1,2}] = 20$. The branching rules (4.79), (4.80) and (4.81) allows us to construct strings of electron operators $\mathcal{S}^m = \prod_{y=y_1}^{y_2} \mathcal{E}_y^{L,m}(\mathsf{x}) \mathcal{E}_y^{R,m}(\mathsf{x})^\dagger$ (c.f. (4.66)) so that when operating on a ground state, it creates a conjugate excitation pair in an arbitrary anyon class in the $\mathrm{SU}(2)_4$ or $\mathrm{SU}(4)_2$

topological phase given an appropriate choice of the $\mathrm{SU}(8)_1$ primary field $\mathcal{E}^m$ (c.f. (4.63), (4.67) and (4.68)).

Table 4.6: The spin h, quantum dimension d, and number of fields # of each non-trivial primary sector of $\mathrm{SU}(4)_2$.

	$[a]$	$[b], [b^*]$	$[\bar{\sigma}_{1,2}]$	$[\bar{\tau}_{1,2}]$	$[\bar{\phi}_2]$	$[\bar{\phi}_1]$
h	1	$\frac{3}{4}$	$\frac{5}{16}$	$\frac{13}{16}$	$\frac{2}{3}$	$\frac{5}{12}$
d	1	1	$\sqrt{3}$	$\sqrt{3}$	2	2
#	20	10	4	20	15	6

We conclude this section by commenting on a few cases where the electrically neutral $\mathrm{SU}(m)_n$ topological sector contains a discrete gauge symmetry and the $\mathrm{SU}(m)_n$ WZW CFT on the edge can be identified with an orbifold CFT $\mathcal{G}_k/G$ [THF15b, TH23, LMT23], for some gauge group G and WZW algebra extension $\mathcal{G}_k$ of $\mathrm{SU}(m)_n$. These examples are

$$\begin{aligned}
\mathrm{SU}(2)_4 &= \mathrm{SO}(3)_2 = \frac{\mathrm{SU}(3)_1}{\mathbb{Z}_2}, \\
\mathrm{SU}(4)_2 &= \mathrm{SO}(6)_2 = \frac{\mathrm{SU}(6)_1}{\mathbb{Z}_2}, \\
\mathrm{SU}(8)_1 &= \frac{(E_7)_1}{\mathbb{Z}_2}, \\
\mathrm{SU}(9)_1 &= \frac{(E_8)_1}{\mathbb{Z}_3}, \quad \mathrm{SU}(3)_3 = \frac{\mathrm{SO}(8)_1}{\mathbb{Z}_3}.
\end{aligned} \tag{4.82}$$

In these examples, the gauge groups are the Abelian cyclic groups $\mathbb{Z}_2$ or $\mathbb{Z}_3$. The WZW algebra extensions $\mathcal{G}_k$ are simply-laced and have level $k = 1$. Therefore, the corresponding $\mathcal{G}_1$ topological order is Abelian and can be described by an Abelian Chern-Simons field theory whose K-matrix is the Cartan matrix of the $\mathcal{G}$ Lie algebra. The $\mathrm{SU}(m)_n$ topological order in the bulk is referred to as a twist liquid [THF15b] where the global G-symmetry in the $\mathcal{G}_1$ Abelian topological phase is gauged [BBCW19b].

The $\mathrm{SU}(m)_n$ WZW algebras in each example in (4.82) is the sub-algebra in $\mathcal{G}_1$ consisting with currents that are unchanged under the G symmetry. Moreover, there are bosonic $\mathrm{SU}(m)_n$ primary field(s) in super-selection sector(s) $[\mathcal{Z}]$ with spin $h_{\mathcal{Z}} = 1$ that carry gauge charges. They irreducibly and non-trivially represent the gauge group G. Since G here is cyclic, this means they transform according to $\mathcal{Z} \to -\mathcal{Z}$ if $G = \mathbb{Z}_2$, and $\mathcal{Z} \to e^{\pm 2\pi i/3}\mathcal{Z}$ if $G = \mathbb{Z}_3$. These spin-1 bosons would extend the $\mathrm{SU}(m)_n$ WZW algebra to $\mathcal{G}_1$, if they were local. This means $\mathrm{SU}(m)_n \oplus [\mathcal{Z}] = \mathcal{G}_1$ for $G = \mathbb{Z}_2$, or $\mathrm{SU}(m)_n \oplus [\mathcal{Z}] \oplus [\mathcal{Z}^*] = \mathcal{G}_1$ for $G = \mathbb{Z}_3$. For the examples listed in (4.82),

$$\begin{aligned}
&\mathrm{SU}(2)_4 \oplus [j=2] = \mathrm{SU}(3)_1, \\
&\mathrm{SU}(4)_2 \oplus [a] = \mathrm{SU}(6)_1, \\
&\mathrm{SU}(8)_1 \oplus \mathcal{E}^4 = (E_7)_1\,, \\
&\mathrm{SU}(9)_1 \oplus \mathcal{E}^3 \oplus \mathcal{E}^6 = (E_8)_1\,, \\
&\mathrm{SU}(3)_3 \oplus \mathbf{10} \oplus \overline{\mathbf{10}} = \mathrm{SO}(8)_1,
\end{aligned} \tag{4.83}$$

where $[j=2]$ and $[a]$ are bosonic primary fields in $\mathrm{SU}(2)_4$ and $\mathrm{SU}(4)_2$ (see table 4.5 and 4.6), $\mathcal{E}^{m=3,6}$ are the bosonic $\mathrm{SU}(9)_1$ primary fields defined in (4.51), and $\mathbf{10}$ and $\overline{\mathbf{10}}$ are the two Abelian bosonic $\mathrm{SU}(3)_3$ primary field super-sectors [THF15b] that form a ten-dimensional irreducible representation of the SU(3) Lie algebra. For instance, in each of these cases, the dimension of $\mathrm{SU}(m)$ and the number of fields in the gauge charge(s) $[\mathcal{Z}]$ add up to the dimension of the extended Lie algebra $\mathcal{G}$.

However, unlike the $\mathrm{SU}(m)_n$ currents, the primary fields in $[\mathcal{Z}]$ are *non-local* and are *not* integral combinations of electrons, despite being bosonic. Consequently, the $\mathrm{SU}(m)_n$ WZW CFT on the edge of the electronic topological phase does *not* extend to $\mathcal{G}_1$. The anyon class corresponding to $[\mathcal{Z}]$ does not condense (in the anyon condensation sense [BS09]) and the bulk $\mathrm{SU}(m)_n$ topological order remains. In particular, there are twist fields $[\Sigma]$ in the $\mathrm{SU}(m)_n$ CFT that correspond to deconfined gauge fluxes in the bulk. For $\mathrm{SU}(2)_4$, these gauge fluxes are $[j = \frac{1}{2}, \frac{3}{2}]$ (see table 4.5). For $\mathrm{SU}(4)_2$, they are $[\bar{\sigma}_{1,2}]$ and $[\bar{\tau}_{1,2}]$ (see table 4.6). For $\mathrm{SU}(9)_1$, they are $\mathcal{E}^{m=1,2,4,5,7,8}$ (see (4.51)), and for $\mathrm{SU}(3)_3$, they are $\mathbf{3}, \overline{\mathbf{3}}, \mathbf{6}, \overline{\mathbf{6}}, \mathbf{15}, \overline{\mathbf{15}}$ (see [THF15b]). These gauge fluxes $[\Sigma]$ and gauge charges $[\mathcal{Z}]$ have non-trivial mutual braiding monodromy phases -1 for $G = \mathbb{Z}_2$ or $e^{\pm 2\pi i/3}$ for $G = \mathbb{Z}_3$.

In general, the $\mathrm{SU}(m)_n$ WZW CFT on the edge of the topological phases constructed in this section always persists for any $m \geq 2$ and $n \geq 1$. Even if there are bosonic spin-1 primary fields $[\mathcal{Z}]$, they are always fractional. The non-locality is a result of the conformal embedding $\mathrm{SU}(m)_n \times \mathrm{SU}(n)_m \subseteq \mathrm{SU}(mn)_1$ used in the coupled wire construction. If the primary fields in $[\mathcal{Z}]$ were local and were to extend the $\mathrm{SU}(m)_n$ algebra, they would either (a) be currents living inside the $\mathrm{SU}(mn)_1$, or (b) belong in a spin-1 primary field super-sector of $\mathrm{SU}(mn)_1$ that extend the $\mathrm{SU}(m)_n$ algebra. First, case (a) does not apply because the only $\mathrm{SU}(mn)_1$ currents that live outside of $\mathrm{SU}(m)_n$ and $\mathrm{SU}(n)_m$ are in the tensor product $[A]_{\mathrm{SU}(m)_n} \times [A]_{\mathrm{SU}(n)_m}$ between the adjoint representations of $\mathrm{SU}(m)_n$ and $\mathrm{SU}(n)_m$ (see (4.62)). None of them are primary fields solely of $\mathrm{SU}(m)_n$ or $\mathrm{SU}(n)_m$. Second, case (b) is impossible as well. This is because the parton bundle construction dictates that all the $\mathrm{SU}(mn)_1$ primary fields $\mathcal{E}^j$ in (4.51) are non-local. Therefore, even if some of them are

bosonic, such as the ones in $\mathrm{SU}(8)_1$ and $\mathrm{SU}(9)_1$, they will never extend $\mathrm{SU}(m)_n$ to a larger local WZW algebra.

On the other hand, there are examples beyond $\mathrm{SU}(m)_n$ WZW algebras where the anyon condensation of gauge charges and the extension of WZW algebras occur. In the next section, we will see that the coupled-wire construction that uses backscattering of the KM currents in the orthogonal WZW algebras $\mathrm{SO}(n)_2$ will result in a topological phase with a different topological order. We will show that the $\mathbb{Z}_2$ gauge charge $[S]$ in $\mathrm{SO}(n)_2 = \mathrm{SU}(n)_1/\mathbb{Z}_2$ will in fact be local and will be an integral combination of electrons under the conformal embedding $\mathrm{SO}(2)_n \times \mathrm{SO}(n)_2 \subseteq \mathrm{SO}(2n)_1$. This is because the primary fields in $[S]$ are currents in $\mathrm{SO}(2n)_1$. On the edge, they will extend the WZW algebra to $\mathrm{SO}(n)_2 \oplus [S] = \mathrm{SU}(n)_1$. In the bulk, $[S]$ will anyon condense and reduce the topological order to the Abelian $\mathrm{SU}(n)_1$, where the $\mathbb{Z}_2$ symmetry is global rather than an internal gauge symmetry.

4.3 B_r and D_r series, emergent Dirac and Majorana fermions

In this section, we construct and study states with electrically neutral topological phases with a $\mathrm{SO}(m)_n$ topological order. These are superconducting or spin liquid phases of electrons. The $\mathrm{SO}(m)_n$ topological phase "partially occupies" the parent bosonic $\mathrm{SO}(mn)_1$ state where non-local Majorana fermions emerges. The construction relies on the $\mathrm{SO}(m)_n \times \mathrm{SO}(n)_m \subset \mathrm{SO}(mn)_1$ conformal embedding.

4.3.1 Coupled-Wire Construction of Topological Superconductors and Spin Liquids

We construct neutral topological phases with $\mathrm{SO}(N)_1$ topological order and chiral edge WZW CFT, where N is an arbitrary integer greater than 1. Following the strategy described previously, we consider a 2D array of bundles, each consisting of $\mathcal{N}$ wires. Each wire now hosts a single *spinful* electron with Rashba spin-orbit interaction, which, at low energies, decomposes into a Dirac electron $c^{\sigma}_{y,sj}$ with chirality $\sigma = R/L = +/-$, spin $s = \uparrow (\downarrow) = +(-)$, and $j = 1, \ldots, \mathcal{N}$ labels a given wire in the bundle y. The spin-orbit interaction, parameterized by momentum k_{SO}, splits the spin-degenerate Fermi points.

The Dirac electrons can be represented by vertex operators of chiral bosons $\Phi^{\sigma}_{y,sj}$ as follows:

$$c^{\sigma}_{y,sj}(\mathsf{x}) \sim \exp\left[i\Phi^{\sigma}_{y,sj}(\mathsf{x}) + i(\sigma k_f + s k_{SO})\mathsf{x}\right], \tag{4.84}$$

where $k^{\sigma}_s = \sigma k_f + s k_{SO}$ is the Fermi momentum about which $c^{\sigma}_{y,sj}$ is defined. The Luttinger liquid Lagrangian density is

$$\mathcal{L} = \frac{1}{4\pi} \sum_{y} \sum_{s,\sigma=\pm} \sum_{j=1}^{\mathcal{N}} \sigma \partial_t \Phi^{\sigma}_{y,sj} \partial_{\mathsf{x}} \Phi^{\sigma}_{y,sj} - \mathcal{H}_0, \tag{4.85}$$

where the free boson Hamiltonian density, including intra-bundle density-density interactions, is

$$\mathcal{H}_0 = \sum_{y} v^{jj',ss'}_{\sigma\sigma'} \partial_{\mathsf{x}} \Phi^{\sigma}_{y,sj} \partial_{\mathsf{x}} \Phi^{\sigma'}_{y,s'j'}. \tag{4.86}$$

Our first objective is to introduce an intra-bundle many-body interaction that gaps all local fermion excitations and leaves behind a non-chiral $\mathrm{SO}(N)_1$ bosonic CFT on each bundle. This can be achieved by either an Umklapp back-scattering or superconducting pairing potential [TH23]. On all bundle y, we impose one of the interactions below:

$$\begin{aligned} \mathcal{U}_{\text{Umklapp}} &= u\cos\theta_\rho \sim u\prod_{j=1}^{\mathcal{N}}\prod_{s=\uparrow,\downarrow} c_{sj}^{L\dagger}c_{sj}^{R} + h.c., \\ \mathcal{U}_{\text{SC}} &= \Delta\cos\varphi_\rho \sim \Delta\prod_{j=1}^{\mathcal{N}}\prod_{s=\uparrow,\downarrow} c_{sj}^{L}c_{sj}^{R} + h.c., \end{aligned} \tag{4.87}$$

where the sine-Gordon angle variables are

$$\theta_\rho = \sum_{sj}(\Phi_{sj}^R - \Phi_{sj}^L), \quad \varphi_\rho = \sum_{sj}(\Phi_{sj}^L + \Phi_{sj}^R). \tag{4.88}$$

When one of these interactions is present and is relevant, the charge degrees of freedom of each bundle are gapped. (1) In the Umklapp case, the potential is a $2\mathcal{N}$-body scattering process that violates momentum conservation. This interaction appears at low energies in the presence of a charge density wave with commensurate momentum. It can also arise in a 1D lattice with a commensurate filling so that the total momentum transfer $4\mathcal{N}k_f$ is an integer multiple of $2\pi/a$, where a is the microscopic lattice constant. $\mathcal{U}_{\text{Umklapp}}$ in (4.87) leads to a spin liquid state where all excitations with energy below u are electrically neutral. (2) In the superconducting case, the pairing potential preserves momentum, but violates charge conservation. It can be induced via the proximity effect by Cooper pair tunneling from a bulk superconductor. The U(1) symmetry is broken to $\mathbb{Z}_2$ by $\mathcal{U}_{\text{SC}}$ in (4.87) and a charge Q is indistinguishable from $Q + 2e$ because of the Cooper pair condensate.

Next, we perform a basis transformation of the bosons that isolates φ_ρ or θ_ρ and decouples it from the rest of the boson in each bundle. The basis transformation depends on whether the gapping potential is given by the Umklapp process or the superconducting pairing. In the Umklapp case, we define

$$2\phi_\rho^\sigma = \varphi_0 + \sigma\theta_\rho, \quad \phi_\ell^\sigma = \varphi_0 - \Phi_{s_\ell j_\ell}^\sigma, \tag{4.89}$$

whereas in the superconducting case, we define

$$2\phi_\rho^\sigma = \varphi_\rho + \sigma\theta_0, \quad \phi_\ell^\sigma = \theta_0 - \sigma\Phi_{s_\ell j_\ell}^\sigma. \tag{4.90}$$

In either case, the non-chiral conjugate bosons, in addition to φ_ρ and θ_ρ, are

$$\varphi_0 = \left(\Phi_{\uparrow 1}^R + \Phi_{\downarrow 1}^L\right)/2, \quad \theta_0 = \left(\Phi_{\uparrow 1}^R - \Phi_{\downarrow 1}^L\right)/2. \tag{4.91}$$

The above spin and wire index assignment (s_ℓ, j_ℓ) for a given ℓ are chosen to account for all the electron modes $\Phi_{s_\ell j_\ell}^\sigma$, except $\Phi_{\uparrow 1}^R$ and $\Phi_{\downarrow 1}^L$. For example, for a given chiral sector $\sigma = \pm$, they can be chosen to be

$$(s_\ell, j_\ell) = \begin{cases} (\sigma, \ell + 1), & \text{if } \ell = 1, \ldots, \mathcal{N} - 1 \\ (-\sigma, \ell - \mathcal{N} + 1), & \text{if } \ell = \mathcal{N}, \ldots, 2\mathcal{N} - 1 \end{cases}. \tag{4.92}$$

The charge boson ϕ_ρ^σ now decouples from the remaining $2\mathcal{N}-1$ non-local Dirac fermions $d_\ell^\sigma \sim e^{i\phi_\ell^\sigma}$, for $\ell = 1, \ldots, 2\mathcal{N}-1$. In this new basis, the free boson Lagrangian density is

$$\begin{aligned} \mathcal{L} &= \frac{1}{4\pi} \sum_{\sigma=R,L} \sigma \left[2\partial_x \phi_\rho^\sigma \partial_t \phi_\rho^\sigma + \sum_{\ell=1}^{2\mathcal{N}-1} \partial_x \phi_\ell^\sigma \partial_t \phi_\ell^\sigma \right] - \mathcal{H}_0, \\ \mathcal{H}_0 &= \frac{v}{4\pi} \sum_\sigma \sum_{\ell=1}^{2\mathcal{N}-1} (\partial_x \phi_\ell^\sigma)^2 + v_\rho \left[g_\rho (\partial_x \varphi)^2 + \frac{1}{g_\rho} (\partial_x \theta)^2 \right], \end{aligned} \tag{4.93}$$

where $2\phi_\rho^\sigma = \varphi + \sigma\theta$, i.e. $(\varphi, \theta) = (\varphi_0, \theta_\rho)$ in the Umklapp case, or $(\varphi, \theta) = (\varphi_\rho, \theta_0)$ in the superconducting case. The velocity tensor $v_{\sigma\sigma'}^{jj',ss'}$ in (4.86) is tuned so that the boson velocities in $\mathcal{H}_0$ are diagonal and isotropic among the Dirac fermions densities $\partial_x \phi_\ell^\sigma$, which are decoupled from $\partial_x \varphi$ and $\partial_x \theta$. This fine-tuning can be relaxed once a bulk energy gap opens up from the current backscattering interactions introduced later in this section. The Umklapp potential $\mathcal{U}_{\text{Umklapp}}$ in (4.87) is relevant in the RG sense, when $g_\rho < 4$. The pairing potential $\mathcal{U}_{\text{SC}}$ in (4.87) is relevant when $g_\rho > 1/4$. The Luttinger parameter g_ρ in either case can be tuned to the corresponding desired range by the presence of appropriate density interactions in the electron wires. In both cases, the potential $\mathcal{U}_{\text{Umklapp}}$ or $\mathcal{U}_{\text{SC}}$ gaps all local fermionic degrees of freedom and leaves behind the gapless ϕ_ℓ^σ modes. Each bundle is now at a low-energy fixed point described by the bosonic $\text{SO}(4\mathcal{N}-2)_1$ WZW CFT whose gapless excitations are bosonic pairs of Dirac fermions, $d_\ell^\sigma d_{\ell'}^{\sigma'}, d_\ell^{\sigma\dagger} d_{\ell'}^{\sigma'}, d_\ell^{\sigma\dagger} d_{\ell'}^{\sigma'\dagger}$, etc. There is a local fermion gap $E_g^f \sim u$ or Δ below which all odd fermion excitations are forbidden.

Using the basis transformation $\phi_\ell^\sigma = M_{\ell\sigma\sigma'}^{sj}\Phi_{sj}^{\sigma'}$ from (4.89) or (4.90), we see that Dirac fermion vertex operators,

$$d_\ell^\sigma \sim e^{i\phi_\ell^\sigma} = e^{iM_{\ell\sigma\sigma'}^{sj}\Phi_{sj}^{\sigma'}}, \tag{4.94}$$

are non-local. This is because $M_{\ell\sigma L}^{\uparrow 1}, M_{\ell\sigma R}^{\downarrow 1} = \pm 1/2$ are fractional (the rest of $M_{\ell\sigma\sigma'}^{sj} = \pm 1$). In addition, each Dirac fermion carries electric charge $Q = 0$ and angular spin $S = \pm 1/2$ in the Umklapp case, or $Q = \pm e \pmod{2e}$ and $S = 0, \pm 1$ in the superconducting case. Therefore, they must not be integral combinations of electrons, which has $Q = -e$ and $S = \pm 1$. This reflects the fact that there are no longer any low-energy single-fermion excitations below the fermion gap E_g^f. On the other hand, all fermion bilinears, such as $d_\ell^\sigma d_{\ell'}^{\sigma'}$, $d_\ell^{\sigma\dagger} d_{\ell'}^{\sigma'\dagger}$, $d_\ell^{\sigma\dagger} d_{\ell'}^{\sigma'}$, $d_\ell^\sigma d_{\ell'}^{\sigma'\dagger}$, are local. These Dirac fermions can be decomposed into real and imaginary Majorana components

$$d_\ell^\sigma = \left(\psi_{2\ell-1}^\sigma + i\psi_{2\ell}^\sigma\right)/\sqrt{2}, \tag{4.95}$$

where $\psi_j^{\sigma\,\dagger} = \psi_j^\sigma$. All Majorana fermion bilinears, $\psi_j^\sigma \psi_k^{\sigma'}$, for $1 \le j \le k \le 4\mathcal{N} - 2$, are also local. The momentum of these Majorana fermions are 0 (or π/a, where a is the microscopic lattice constant, for the Umklapp case) if $k_{SO} = k_f$ in the Umklapp case or $k_{SO} = 0$ in the superconducting case.

Apart from fermion bilinears, conjugate pairs of spinor fields are local operators as well up to ground state expectation values of θ_ρ or φ_ρ. Spinor primary fields $[s_\pm]$ in $\mathrm{SO}(4\mathcal{N}-2)_1$ are generated by vertex operators $s_{\boldsymbol{\varepsilon}}^\sigma = e^{i\sum_\ell \varepsilon^\ell \phi_\ell^\sigma/2}$, where $\varepsilon_\ell = \pm$. The sign $\prod_\ell \varepsilon_l = \pm$

sets the parity of the spinor field. A pair of spinor fields $s^\sigma_{\varepsilon_1} s^\sigma_{\varepsilon_2}$ in the same chiral sector σ but with opposite parity (i.e. $\prod_\ell \varepsilon_1^\ell \varepsilon_2^\ell = -1$) is an even product of fermions and thus is local. This shows $[s^\sigma_+] \times [s^\sigma_-] = 1$. A pair of spinor fields $s^R_{\varepsilon_1} s^L_{\varepsilon_2}$ from opposite chiral sectors but with the same parity (i.e. $\prod_\ell \varepsilon_1^\ell \varepsilon_2^\ell = 1$) is effectively local. It differs from $e^{i\theta_\rho/2}$ ($e^{i\varphi_\rho/2}$) by an integral product of electron operators, and $\langle\theta_\rho\rangle$ (resp. $\langle\varphi_\rho\rangle$) is pinned at its ground state expectation value by the Umklapp (resp. pairing) potential (4.87). This shows $[s^R_\pm] \times [s^L_\pm] = 1$.

The number of helical pairs of Majorana fermions can be reduced from $4\mathcal{N}-2$ to any integer N below by a momentum-preserving local backscattering potential.

$$\mathcal{U}_{\text{mass}} = im \sum_{j=N+1}^{4\mathcal{N}-2} \psi_j^L \psi_j^R. \tag{4.96}$$

This gaps out $\psi_j^{L,R}$ for $j = N+1, \ldots 4\mathcal{N}-2$, where $4\mathcal{N}-2 > N$. The low-energy effective Hamiltonian density can be written in terms of remaining N gapless non-chiral Majoranas as

$$\mathcal{H}_{\text{eff}} = \frac{iv}{2} \sum_y \sum_\sigma \sum_{j=1}^{N} \sigma \psi^\sigma_{yj} \partial_{\text{x}} \psi^\sigma_{yj}. \tag{4.97}$$

We stress that, despite appearances, (4.97) does *not* describe a collection of free Majorana fermions, since single-particle Majorana fermion operators are non-local.

The gapless modes in (4.97) in each bundle of wires are effectively described by the non-chiral $\text{SO}(N)_1$ WZW CFT, which can now be used to construct the $\text{SO}(N)_1$ coupled-

wire model for states with spin liquid or topological superconducting order. Within each bundle, the $\mathrm{SO}(N)_1$ WZW KM algebra for each chiral sector σ is spanned by $N(N-1)/2$ current operators $J^{\sigma}_{y,jk} = i\psi^{\sigma}_{ya}(X^{ab})_{jk}\psi^{\sigma}_{yb} = i\psi^{\sigma}_{yj}\psi^{\sigma}_{yk}$. Here, $(X^{ab})_{jk} \equiv \delta^a_j\delta^b_k$ is a matrix representation of $\mathrm{SO}(N)_1$ with $1 \leq j < k \leq N$ and $a, b = 1, \ldots, N$. Each bundle admits an internal $\mathbb{Z}_2$ symmetry:

$$\psi^{\sigma}_{yj} \to (-1)^{\delta_{yy'}}\psi^{\sigma}_{yj}, \quad \phi^{\sigma}_{ya} \to \phi^{\sigma}_{ya} + \sigma\pi\delta_{yy'}, \tag{4.98}$$

for each fixed y' that labels the bundle where this particular local $\mathbb{Z}_2$ symmetry applies. An operator is only local if it is unchanged by the internal $\mathbb{Z}_2$ symmetries for all y'. This internal symmetry is referred to as the local $\mathbb{Z}_2$ gauge symmetry. For example, all single-fermion tunneling $\psi_{y_1}\psi_{y_2}$ between bundles is non-local and forbidden. On the other hand, single-fermion tunneling within a given bundle, like those in (4.97) are local. Single-fermion tunneling between bundles is not local, however two-fermion scattering between bundles is also local. In particular, the current backscattering $\mathbf{J}^R_y \cdot \mathbf{J}^L_{y+1} = \sum_{j<k} J^R_{y,jk}J^L_{y,jk}$ in (4.100) below is an allowed process. In addition, counter-propagating pairs of spinor twist fields (with the same parity if $N \equiv 0 \bmod 4$ or opposite parity if $N \equiv 2 \bmod 4$) within the same bundle is effectively local at low energy because they differ from the local combination $s^R_{\boldsymbol{\varepsilon}}s^L_{\boldsymbol{\varepsilon}}$ of electron operators up to ground state expectation values of operators in the $\psi_{N+1,\ldots,4\mathcal{N}-2}$ sector, which is gapped by (4.96).

We construct the chiral $\mathrm{SO}(N)_1$ topological model,

$$\mathcal{H}\left[\mathrm{SO}(N)_1\right] = \mathcal{H}_{\mathrm{eff}} + \mathcal{H}_{\mathrm{inter}}^{\mathrm{SO(N)_1}}, \tag{4.99}$$

using the inter-bundle backscattering potential,

$$\begin{aligned} \mathcal{H}_{\mathrm{inter}}^{\mathrm{SO}(N)_1} &= u_{\mathrm{inter}} \sum_y \mathbf{J}_y^R \cdot \mathbf{J}_{y+1}^L \\ &= -u_{\mathrm{inter}} \sum_y \sum_{1 \le j < k \le N} \psi_{y,j}^R \psi_{y,k}^R \psi_{y+1,j}^L \psi_{y+1,k}^L, \end{aligned} \tag{4.100}$$

for $N \geq 3$. The potential between each neighboring pair of bundles is the $\mathrm{SO}(N)_1$ Gross-Neveu interaction [GN74], which is known to introduce a bulk excitation energy gap when $u_{\mathrm{inter}} > 0$. In terms of the bosonized variables defined by (4.94) and (4.95), the two-body interactions are

$$\begin{aligned} \mathcal{H}_{\mathrm{inter}}^{\mathrm{SO}(2r)_1} &= u_{\mathrm{inter}} \sum_y \sum_{a=1}^{r} \partial_{\mathsf{x}} \phi_{y,a}^R \partial_{\mathsf{x}} \phi_{y+1,a}^L - u_{\mathrm{inter}} \sum_y \sum_{\epsilon=\pm} \cos\left(\Theta_{y+1/2,a} + \epsilon \Theta_{y+1/2,b}\right), \\ \mathcal{H}_{\mathrm{inter}}^{\mathrm{SO}(2r+1)_1} &= \mathcal{H}_{\mathrm{inter}}^{\mathrm{SO}(2r)_1} - u_{\mathrm{inter}} \sum_y i \psi_{y,2r+1}^R \psi_{y+1,2r+1}^L \sum_{a=1}^{r} \cos \Theta_{y+1/2,a}, \end{aligned} \tag{4.101}$$

where the angle variables are $\Theta_{y+1/2,a} = \phi_{y,a}^R - \phi_{y+1,a}^L$. The sine-Gordon terms are relevant in the RG sense and do not mutually compete when $u_{\mathrm{inter}} > 0$. The ground state expectation values of the sine-Gordon variables are simultaneously pinned at $\langle \Theta_{y+1/2,a} \rangle \sim m_{y+1/2,a} \pi$. $m_{y+1/2,a}$ are either all odd or all even integers for all $a = 1, \ldots, r$. When $N = 2r+1$, the last term in (4.101) introduces a Majorana mass to ψ_{2r+1} and pins the expectation values of $\langle i \psi_{y,2r+1}^R(\mathsf{x}) \psi_{y+1,2r+1}^L(\mathsf{x}) \rangle \sim (-1)^{m_{y+1/2,a}}$. The model (4.99) now has a finite excitation

energy gap in the bulk and leaves behind chiral $\mathrm{SO}(N)_1$ WZW CFT along the boundary edges. The bulk carries the corresponding $\mathrm{SO}(N)_1$ topological order, which is explained in detail in ref. [Kit06, SZT16, TH23, LMT23].

We see that the current backscattering term (4.100) is a gapping potential only when $N \geq 3$. For $N = 1$, there is no two-fermion backscattering process and (4.100) is an empty sum. For $N = 2$, the two-fermion backscattering process is a density-density interaction $\partial_x \phi_y^R \partial_x \phi_{y+1}^L$, which only renormalizes the kinetic Hamiltonian without introducing an energy gap. Before moving on to the next section, here we present the alternative coupled wire models for these two cases that represent the chiral Ising and $\mathrm{SO}(2)_1$ topological phases.

First, we consider the case when there are $N = 2$ Majorana fermions on each bundle in each chiral sector. Instead of the inter-bundle current backscattering potential (4.100), we consider the sine-Gordon potential,

$$\mathcal{H}_{\text{inter}}^{\mathrm{SO}(2)_1} = -u_{\text{inter}} \sum_y \cos\left(2\phi_y^R - 2\phi_{y+1}^L\right), \tag{4.102}$$

where $e^{i\phi_y^\sigma} = (\psi_{y,1}^\sigma + i\psi_{y,2}^\sigma)/\sqrt{2}$. This term is symmetric under the internal $\mathbb{Z}_2$ symmetry (4.98) and is local. With a strong enough repulsive interaction $\partial_x \phi_y^R \partial_x \phi_{y+1}^L$, the sine-Gordon potential becomes RG relevant, gaps the bulk and leaves behind the chiral $\mathrm{SO}(2)_1$ WZW CFT on its edges.

Next, we consider the $N = 1$ case. This case is special because there is no local inter-bundle gapping potential if there is only one (non-chiral) Majorana fermion in each bundle. Instead, we begin with $N = 5$ gapless Majorana fermions $\psi_{y,j=1,\ldots,5}^\sigma$, and we now construct

a coupled wire model with a bulk gap that leaves behind a single chiral Majorana fermion on each edge. The model consists of two sets of backscattering potentials,

$$\begin{aligned}\mathcal{H}[\mathrm{SO}(1)_1] = \mathcal{H}_{\mathrm{eff}}^{N=5} - u_{\mathrm{inter}} \sum_y \cos\left(2\phi_y^R - 2\phi_{y-1}^L\right) \\ - u_{\mathrm{inter}} \sum_y \sum_{3\le j<k\le 5} \psi_{y,j}^R \psi_{y,k}^R \psi_{y+1,j}^L \psi_{y+1,k}^L,\end{aligned} \tag{4.103}$$

where $e^{i\phi_y^\sigma} = (\psi_{y,1}^\sigma + i\psi_{y,2}^\sigma)/\sqrt{2}$. Here, $\mathrm{SO}(1)_1$ stands for the Ising model, which is a minimal CFT and not a WZW CFT. The first potential is similar to the $\mathrm{SO}(2)_1$ sine-Gordon potential in (4.102) except with opposite chirality. The second potential is the $\mathrm{SO}(3)_1$ current backscattering that gaps $\psi_{j=3,4,5}$. With these together, the bulk is gapped and, on each boundary edge, there are three forward propagating fermions $\psi_{j=3,4,5}^R$ and two backward propagating ones $\psi_{j=1,2}^L$. These two sectors are correlated so that the fermion pairs $\psi_j^L\psi_k^R$, for $j = 1, 2$ and $k = 3, 4, 5$, are local and condensed in the anyon condensation sense. The counter-propagating fermions can be reduced by the edge potential,

$$\mathcal{H}_{\mathrm{edge}} = u_{\mathrm{edge}} i(\psi_1^L\psi_3^R + \psi_2^L\psi_4^R). \tag{4.104}$$

This leaves behind a single chiral non-local Majorana fermion ψ_5^R and the gapless theory is described by the chiral Ising CFT. Because of the anyon condensation of the fermion pairs $\psi_{j=1,2}^L\psi_{k=3,4,5}^R$, the bulk carries the Ising topological order ($\sigma \times \sigma = 1 + \psi$ and $h_\sigma = 1/16$) instead of the tensor product $\mathrm{SO}(3)_1 \times \overline{\mathrm{SO}(2)_1}$ topological order.

4.3.2 Conformal Embedding and Descendant Topological Order

Symmetry embedding

In the previous subsection, we constructed the bosonic $\mathrm{SO}(N)_1$ WZW CFT from electrons, where the chiral current algebra is generated by bilinears of emergent Majorana fermions, $J^{\sigma}_{y,jk} = i\psi^{\sigma}_{y,j}\psi^{\sigma}_{y,k} = i\psi^{\sigma}_{y,a}(X^{jk})_{ab}\psi^{\sigma}_{y,b}$. The matrix representation of the generators of the $\mathrm{SO}(N)$ Lie algebra, for arbitrary integer $N \geq 2$, are

$$(X^{jk})_{rs} = \frac{1}{2}\left(\delta^j_r\delta^k_s - \delta^k_r\delta^j_s\right), \tag{4.105}$$

where $r, s = 1, \ldots, N$ and $1 \leq j < k \leq N$.

Analogous to §4.2.3, we consider the conformal embedding $\mathrm{SO}(m)_n \times \mathrm{SO}(n)_m \subseteq \mathrm{SO}(mn)_1$, where we set $N = mn$ for $m, n \geq 2$. We will call $\mathrm{SO}(m)_n$ the A sector and $\mathrm{SO}(n)_m$ the B sector. The $m \times m$ matrix generators X^{pq} of $SO(m)$ can be embedded into $SO(mn)$ by taking $(X^A)^{pq}_{rs} \equiv (X^{pq} \otimes \mathbb{I}_n)_{rs} = (X^{pq})_{ab}\delta_{cd}\delta_r^{(a-1)n+c}\delta_s^{(b-1)n+d}$, where $r, s = 1, \ldots, mn$, $1 \leq p < q < m$, $a, b = 1, \ldots, m$, and $c, d = 1, \ldots, n$. The $\mathrm{SO}(m)_n$ current operators (for each chiral sector σ on each bundle y) are

$$\begin{aligned} J^A_{pq} &= i\sum_{r,s=1}^{mn}\psi_r\left(X^{pq}\otimes\mathbb{I}_n\right)_{rs}\psi_s \\ &= i\sum_{c=1}^{n}\psi_{(p-1)n+c}\psi_{(q-1)n+c}, \end{aligned} \tag{4.106}$$

which is a sum of n decoupled copies of the $\mathrm{SO}(m)_1$ currents. Similarly for the B sector, given any $n \times n$ anti-symmetric matrix X^{pq} that generates $\mathrm{SO}(n)$, we define $(X^B)^{pq}_{rs} \equiv (\mathbb{I}_m \otimes X^{pq})_{rs} = \delta_{ab}(X^{pq})_{cd}\delta_r^{(a-1)n+c}\delta_s^{(b-1)n+d}$, where $1 \le p < q \le n$ and a, b, c, d, r, s each has the same range as before. The $\mathrm{SO}(n)_m$ current operators are the fermion bilinears,

$$\begin{aligned} J^B_{pq} &= i \sum_{r,s=1}^{mn} \psi_r \left(\mathbb{I}_m \otimes X^{pq}\right)_{rs} \psi_s \\ &= i \sum_{a=1}^{m} \psi_{(a-1)n+p}\psi_{(a-1)n+q}. \end{aligned} \tag{4.107}$$

Descendant states

We now construct the coupled wire models for the $\mathrm{SO}(m)_n$ topological phases. These are spin liquids or superconducting phases that can be viewed as partially occupying the $\mathrm{SO}(mn)_1$ topological phases constructed before, and are descendant states of the $\mathrm{SO}(mn)_1$ states. This is because $\mathrm{SO}(m)_n$ is a WZW sub-algebra of $\mathrm{SO}(mn)_1$. They are the analog of the fractional quantum Hall $\mathrm{U}(1)_{mn}\times\mathrm{SU}(m)_n$ phases, studied in §4.2.3, that are descendants of the $\mathrm{U}(1)_{mn} \times \mathrm{SU}(mn)_1$ FQH state. Except, now there is no U(1) sector that supports electric charge response.

The coupled wire model begins with the effective Hamiltonian $\mathcal{H}_{\text{eff}}$ that describes $N = mn$ non-chiral emergent Majorana fermions on each bundle. The bosonic $\mathrm{SO}(N)_1$ WZW CFT on each bundle originates from a many-body Umklapp or superconducting pairing potential introduced in the previous subsection 4.3.1. Unlike the parent $\mathrm{SO}(N)_1$ state where the entire current algebra is back-scattered to the neighboring bundle, here $\mathrm{SO}(N)_1$ is split

into the decoupled $\mathrm{SO}(m)_n$ and $\mathrm{SO}(n)_m$ sectors by the level-rank duality, and the two are separately back-scattered between neighboring bundles or within a bundle. Following §4.2.3, we consider the Hamiltonian

$$\mathcal{H}\left[\mathrm{SO}(m)_n\right] = \mathcal{H}_{\mathrm{eff}} + \mathcal{H}_{\mathrm{inter}}^{\mathrm{SO(m)_n}} + \mathcal{H}_{\mathrm{intra}}^{\mathrm{SO(n)_m}}, \tag{4.108}$$

where the current backscattering potentials are

$$\begin{aligned}
\mathcal{H}_{\mathrm{inter}}^{\mathrm{SO}(m)_n} &= u_{\mathrm{inter}} \sum_y (\mathbf{J}_{\mathrm{SO}(m)_n})_y^R \cdot (\mathbf{J}_{\mathrm{SO}(m)_n})_{y+1}^L \\
&= -u_{\mathrm{inter}} \sum_y \sum_{c,c'=1}^{n} \sum_{1\le p<q\le m} \psi_{y,(p-1)n+c}^R \psi_{y,(q-1)n+c}^R \psi_{y+1,(p-1)n+c'}^L \psi_{y+1,(q-1)n+c'}^L, \\
\mathcal{H}_{\mathrm{intra}}^{\mathrm{SO}(n)_m} &= u_{\mathrm{intra}} \sum_y (\mathbf{J}_{\mathrm{SO}(n)_m})_y^R \cdot (\mathbf{J}_{\mathrm{SO}(n)_m})_{y+1}^L \\
&= -u_{\mathrm{intra}} \sum_y \sum_{a,a'=1}^{m} \sum_{1\le p<q\le n} \psi_{y,(a-1)n+p}^R \psi_{y,(a-1)n+q}^R \psi_{y+1,(a'-1)n+p}^L \psi_{y+1,(a'-1)n+q}^L.
\end{aligned} \tag{4.109}$$

Eq. (4.109) applies for any $m, n \geq 3$. Situations when $m = 2$ or $n = 2$ requires separate attention because the $\mathrm{SO}(2)_l$ current back-scattering interaction is not a gapping potential. We will present the modified model for this specific case in the following subsection. We conjecture that for $m, n \geq 3$, the potentials in (4.109) together create a finite excitation energy gap in the bulk and leave behind the gapless chiral $\mathrm{SO}(m)_n$ WZW CFT on each boundary edge. The presence of the bulk energy gap can be proven with the help of previous results in parafermions for small $m, n \leq 4$.

The $SO(3)_3$ case was proven in Ref. [SZT16] in the context of gapped topologically ordered surface states of topological superconductors. The $SO(3)_3$ KM current decomposes into $J^{\pm} = e^{\pm i\phi}\Psi$, where $e^{i\phi}$ is the vertex operator of the $SO(2)_3$ sub-algebra, and Ψ is the $\mathbb{Z}_6$ parafermion [ZF85] in the coset CFT $SO(3)_3/SO(2)_3$. Subsequently, the current backscattering also decomposes, $J_R^{\pm}J_L^{\mp} = \cos(\phi_R - \phi_L)\Psi^R\Psi^L$. The sine-Gordon part pins the angle variable $\phi_R - \phi_L$ and gaps the $SO(2)_3 = U(1)_{12}$ sector. The parafermion backscattering part gaps the $SO(3)_3/SO(2)_3$ coset CFT [FAT91]. A similar parafermion decomposition applies for $SO(3)_l = SO(2)_{\times}\mathbb{Z}_{2l}$ for any level $l \geq 2$, and the $SO(3)_l$ current backscattering potential in general gaps all degrees of freedom. (The level $l = 1$ case is a particular case of $SO(2r+1)_l$ and it was addressed previously below (4.101).) The energy gap of the $SO(4)_l$ current backscattering potential can be shown to be finite by identifying $SO(4)_l = SU(2)_l \times SU(2)_l$ and the parafermion decomposition $SU(2)_l = U(1)_{2l} \times \mathbb{Z}_l$ for each of the two $SU(2)_l$ components. The proof of the energy gap for $SO(m \geq 5)_n$ is beyond the scope of this paper and will be omitted.

4.3.3 Topological Order Examples

$SO(2)_n \times SO(n)_2 \subseteq SO(2n)_1$: anyon condensation, algebra extension, and $\mathbb{Z}_2$ gauge confinement

We present the coupled wire model for the $SO(n)_2$ and $SO(2)_n$ topological phases, for $n \geq 2$. The current back-scattering interactions considered previously in (4.109) are not gapping potentials for SO(2). Here we present a replacement for $\mathcal{H}^{SO(2)_n}_{\text{inter/intra}}$ using a sine-Gordon

potential that, together with the current back-scattering $\mathcal{H}^{\mathrm{SO}(n)_2}_{\mathrm{intra/inter}}$ in (4.109), opens a bulk excitation energy gap. Despite the suggestion of the conformal embedding $\mathrm{SO}(2)_n \times \mathrm{SO}(n)_2 \subseteq \mathrm{SO}(2n)_1$, the coupled wire model $\mathcal{H}^{\mathrm{SO}(2)_n}_{\mathrm{intra}} + \mathcal{H}^{\mathrm{SO}(n)_2}_{\mathrm{inter}}$ does *not* represent the non-Abelian $\mathrm{SO}(n)_2$ topological order. Instead, as a result of a WZW algebra extension and the anyon condensation of a $\mathbb{Z}_2$ gauge charge, the topological order is of the Abelian $\mathrm{SU}(n)_1$ type. The dual model $\mathcal{H}^{\mathrm{SO}(2)_n}_{\mathrm{inter}} + \mathcal{H}^{\mathrm{SO}(n)_2}_{\mathrm{intra}}$ only carries the $\mathrm{SO}(2)_n = \mathrm{U}(1)_{4n}$ topological order if n is odd. It reduces to $\mathrm{U}(1)_n$ when n is even. The reduction of topological orders in these special cases was previously reported in Ref. [TH23].

We begin with the bosonic $\mathrm{SO}(2n)_1$ bundles. Each decomposes according to the conformal embedding $\mathrm{SO}(2)_n \times \mathrm{SO}(n)_2 \subseteq \mathrm{SO}(2n)_1$. The $\mathrm{SO}(2)_n$ WZW algebra in the A sector has a single current operator, which is the Majorana fermion bilinear combination

$$\big[J_{\mathrm{SO}(2)_n}\big] = i\sum_{a=1}^{n} \psi_a \psi_{n+a} = \sum_{a=1}^{n} \partial_x \tilde{\phi}_a, \tag{4.110}$$

for each chiral sector $\sigma = R, L$ on each bundle y, where $e^{i\tilde{\phi}_a} = (\psi_a + i\psi_{n+a})/\sqrt{2}$. The current backscattering from (4.109) for $\mathrm{SO}(2)_n$ consists solely of the density interactions $\partial_x \tilde{\phi}^R_a \partial_x \tilde{\phi}^L_{a'}$, which only renormalizes the boson velocities and does not generate a mass gap. Instead we consider the sine-Gordon potential (c.f. (4.102) for $\mathrm{SO}(2)_1$ and similar construction in ref. [LMT23, SZT16, TH23]),

$$\begin{aligned}\mathcal{H}^{\mathrm{SO}(2)_n}_{y+\epsilon/2} = u_\epsilon \big[J_{\mathrm{SO}(2)_n}\big]^{R\dagger}_{y} \big[J_{\mathrm{SO}(2)_n}\big]^{L}_{y+\epsilon} \\ - u'_\epsilon \cos\big(\vartheta_{y+\epsilon/2}\big),\end{aligned} \tag{4.111}$$

where $\epsilon = 0$ or 1 represents an intra-bundle or inter-bundle back-scattering interaction, respectively. The sine-Gordon variable is

$$\vartheta_{y+\epsilon/2} = q \sum_{a=1}^{n} \left(\tilde{\phi}^R_{y,a} - \tilde{\phi}^L_{y+\epsilon,a} \right), \tag{4.112}$$

where $q = 1$ if $\epsilon = 0$ or n is even, or $q = 2$ if $\epsilon = 1$ and n is odd. q is the smallest positive number so that $\cos \vartheta_{y+\epsilon/2}$ is an integral combination of electrons. The sine-Gordon potential is RG relevant when $u_\epsilon < -v(q^2n^2 - 4)/[2\pi n(q^2n^2 + 4)]$. In this case, all $\mathrm{SO}(2)_n$ degrees of freedom are gapped. Together with the $\mathrm{SO}(n)_2$ current back-scattering potential presented in (4.109), for $n \geq 3$, we arrive at the fully gapped topological models

$$\begin{aligned} \mathcal{H}[\mathrm{U}(1)_l] &= \mathcal{H}_{\text{eff}} + \mathcal{H}^{\mathrm{SO}(n)_2}_{\text{intra}} + \sum_y \mathcal{H}^{\mathrm{SO}(2)_n}_{y+1/2}, \\ \mathcal{H}[\mathrm{SU}(n)_1] &= \mathcal{H}_{\text{eff}} + \mathcal{H}^{\mathrm{SO}(n)_2}_{\text{inter}} + \sum_y \mathcal{H}^{\mathrm{SO}(2)_n}_{y}, \end{aligned} \tag{4.113}$$

where $l = n$ when n is even, or $l = 4n$ when n is odd.

The topological orders and the WZW CFTs at a boundary are $\mathrm{U}(1)_l$ and $\mathrm{SU}(n)_1$, respectively. The former is distinct from $\mathrm{SO}(2)_n$ when n is even. The latter is different from $\mathrm{SO}(n)_2$ for all n. We here deduce the topological orders and prove that the result is a consequence of electron locality. We begin with the first model in (4.113). When n is even, the primitive local boson on the edge CFT is $\exp\left(i \sum_{a=1}^n \tilde{\phi}_a\right)$. It is an integral product of electrons because it is an even product of the Dirac fermions $\tilde{d}_a = (\psi_a + \psi_{n+a})/\sqrt{2} = e^{i\tilde{\phi}_a}$. The local boson has spin $h = n/2$, which sets the level of the U(1) CFT to be $l = n$. When n is odd, the vertex operator $\exp\left(i \sum_{a=1}^n \tilde{\phi}_a\right)$ is now an odd product of fermions and is there-

fore fractional. The primitive local boson is $\exp\left(2i\sum_{a=1}^{n}\tilde{\phi}_a\right)$ instead. The CFT is $\mathrm{U}(1)_{4n}$, which is identical to $\mathrm{SO}(2)_n$. The distinction between the even and odd n cases depends on the locality of the vertex operator $\exp\left(i\sum_{a=1}^{n}\tilde{\phi}_a\right)$. Its anyon condensation [BS09], when n is even, reduces the topological order from $\mathrm{SO}(2)_n$ to $\mathrm{U}(1)_n$.

Next, we move on to the second model in (4.113). The KM current algebra of the edge chiral WZW CFT consists of the $\mathrm{SO}(n)_2$ currents $J_{pq} = i\psi_p\psi_q + i\psi_{n+p}\psi_{n+q}$, for $1 \le p < q \le n$. They are local operators because they are even products of Majorana fermions. In addition, the following fermion bilinear are also local:

$$S_M = i\sum_{a,b=1}^{n}\psi_a M_{ab}\psi_{n+b}, \tag{4.114}$$

where $M = (M_{ab})_{n\times n}$ is a real symmetric matrix. The simplest examples of such combinations are $S_{ab} = i\psi_a\psi_{n+b} + i\psi_b\psi_{n+a}$, where $1 \le a \le b \le n$. The J and S fields obey the operator product expansions (including only singular terms)

$$\begin{aligned} J_{\mathrm{SO}(2)_n}(z)S_M(w) &= \frac{\mathrm{Tr}(M)}{(z-w)^2} + \dots, \quad J_{pq}(z)S_M(w) = \frac{i}{z-w}S_{[A_{pq},M]}(w) + \dots, \\ S_M(z)S_{M'}(w) &= \frac{\mathrm{Tr}(MM')}{(z-w)^2} - \frac{i}{z-w}\sum_{1\le p<q\le n}[M,M']_{pq}J_{pq}(w) + \dots, \end{aligned} \tag{4.115}$$

where $A_{pq} = \mathbf{e}_p\mathbf{e}_q^T - \mathbf{e}_q\mathbf{e}_p^T$ and $\mathbf{e}_p^T = (0,\dots,1,\dots,0)$ is the n-dimensional unit vector whose p^{th} entry is non-zero.

There are two differences in symmetries between J_{pq} and S_M. First, $J_{pq} = -J_{qp}$ is anti-symmetric, whereas $S_{ab} = S_{ba}$ is symmetric. Second, while both J and S are even under

the internal $\mathbb{Z}_2$ symmetry (4.98), they have opposite parities under the following global $\mathbb{Z}_2$ symmetry:

$$\mathbb{Z}_2 : \quad \psi_a \to \psi_a, \quad \psi_{n+a} \to -\psi_{n+a}, \tag{4.116}$$

for $a = 1, \ldots, n$. J_{pq} is even, while S_M is odd under (4.116). The diagonal symmetric combination $S_{\mathbb{I}} = \sum_{a=1}^{n} S_{aa}/2$ is identical to the $\mathrm{SO}(2)_n$ current (4.110), where $\mathbb{I}$ is the $n \times n$ identity matrix. Subtracting this diagonal component, traceless symmetric combinations span the primary field super-selection sector,

$$[S] = \mathrm{span}\left\{S_M : M \in \mathbb{R}^{n\times n}, M^T = M, \mathrm{Tr}(M) = 0\right\}, \tag{4.117}$$

that irreducibly represents $\mathrm{SO}(n)_2$ and has non-singular operator product expansions with $J_{\mathrm{SO}(2)_n}$. Since $[S]$ decouples from the $\mathrm{SO}(2)_n$, it is unaffected by the sine-Gordon potential (4.111) and remains gapless on the edge. The primary fields in $[S]$ are local and, according to (4.115), they extend the $\mathrm{SO}(n)_2$ KM algebra on the edge to $\mathrm{SU}(n)_1 = \mathrm{SO}(n)_2 \oplus [S]$.

In the bulk, the anyon class corresponding to $[S]$ anyon condenses [BS09] because fields in $[S]$ are local and should belong in the trivial vacuum class. Consequently, the anyon classes in $\mathrm{SO}(n)_2$ that carry a $\mathbb{Z}_2$ flux according to the $\mathbb{Z}_2$ symmetry (4.116) and have a π monodromy braiding phase with $[S]$ are confined. This reduces the non-Abelian $\mathrm{SO}(n)_2$ topological order to the Abelian $\mathrm{SU}(n)_1$ order. We notice in passing that a coupled-wire model with the $\mathrm{SO}(n)_2$ topological order can be constructed by starting with emergent Majorana fermion bundles with the $\mathbb{Z}_2$ symmetry (4.116) being an internal symmetry rather than a global

one. In this case, each bundle carries the $[\mathrm{SO}(n)_1]^2$ WZW CFT instead of $\mathrm{SO}(2n)_1$, and the non-Abelian topological model is constructed based on the coset decomposition $[\mathrm{SO}(n)_1]^2 = \mathrm{SO}(n)_2 \times [\mathrm{SO}(n)_1]^2/\mathrm{SO}(n)_2$ instead of the level-rank duality $\mathrm{SO}(2n)_1 \supseteq \mathrm{SO}(2)_n \times \mathrm{SO}(n)_2$. Such a construction has already been done in Ref. [TH23] and will not be repeated here.

Common primary fields and anyon excitations

We present some common primary field super-selection sectors that generically appear in the $\mathrm{SO}(m)_n$ WZW CFT. We discuss how they arise from branching rules of primary field sectors in $\mathrm{SO}(mn)_1 \supseteq \mathrm{SO}(m)_n \times \mathrm{SO}(n)_m$, and subsequently demonstrate how their corresponding anyon excitations can be created in the topological bulk. We begin with the fermion sector $[\psi]$ in $\mathrm{SO}(m)_1$. It is spanned by the m Majorana fermions $\psi_{1,\ldots,m}$ and it forms the vector representation of $\mathrm{SO}(m)$. For $\mathrm{SO}(m)_n$ with general level $n \geq 1$, we label the primary field sector associating with the vector representation by $[V] = \mathrm{span}\{V_a : a = 1, \ldots, m\}$. The quadratic Casimir operator of the vector representation of $\mathrm{SO}(m)$ is $C_V = m-1$. Therefore, the conformal scaling dimension of $[V]$ of $\mathrm{SO}(m)_n$ is $h_V = \frac{C_V/2}{m+n-2} = \frac{m-1}{2(m+n-2)}$. For $m = 2$, the vector representation is reducible and it decomposes into $[V] = [e^2] \oplus [e^{-2}]$, where $e^{\pm 2} = e^{\pm i \sum_{a=1}^{n} \tilde{\phi}_a/n}$ is the spin $h = \frac{1}{2n}$ vertex field in $\mathrm{SO}(2)_n = \mathrm{U}(1)_{4n}$. For $m \geq 3$, the vector representation is irreducible. For unit level $n = 1$, the vector $[\psi] = [V]$ is a spin-1/2 fermion and obeys the Abelian fusion rule $[\psi] \times [\psi] = 1$ because all fermion bilinear combinations are local $\mathrm{SO}(m)_1$ currents.

For higher levels $n \geq 2$, $[V]$ in $\mathrm{SO}(m)_n$ obeys the fusion rule $[V] \times [V] = 1 + [S] + [A]$, where $[S]$ is the traceless symmetric 2-tensor representation and $[A]$ is the anti-symmetric 2-tensor representation of $\mathrm{SO}(m)$. $[S]$ has dimension $\dim[S] = m(m+1)/2-1$ and quadratic Casimir $C_S = 2m$. In $\mathrm{SO}(m)_n$, it has conformal scaling dimension $h_S = m/(m+n-2)$. $[A]$ is identical to the adjoint representation. It has dimension $\dim[A] = m(m-1)/2$, quadratic Casimir $C_A = 2(m-2)$, and scaling dimension $h_A = (m-2)/(m+n-2)$ in $\mathrm{SO}(m)_n$. For $m = 2$, $[S]$ is reducible and decomposes as $[S] = [e^4] \oplus [e^{-4}]$, where $e^{\pm 4}$ is the vertex operator $= e^{\pm i2\sum_{a=1}^{n} \tilde{\phi}_a/n}$ of $\mathrm{SO}(2)_n$. $[A]$ rotates trivially under $\mathrm{SO}(2)$ and is identical to the vacuum sector 1. Except when $m = 4$, for which $[A]$ decomposes into the two spin-$j = 1$ isoclinic rotations of $\mathrm{SO}(4) = \mathrm{SU}(2) \times \mathrm{SU}(2)$, $[S]$ and $[A]$ are irreducible representations of $\mathrm{SO}(m)$ when $m \geq 3$.

In the conformal embedding $\mathrm{SO}(mn)_1 \supseteq \mathrm{SO}(m)_n \times \mathrm{SO}(n)_m$, we have the branching rules (as vector spaces of current operators)

$$\mathrm{SO}(mn)_1 = \mathrm{SO}(m)_n \oplus \mathrm{SO}(n)_m \oplus \left([S]_{\mathrm{SO}(m)_n} \times [A]_{\mathrm{SO}(n)_m}\right) \oplus \left([A]_{\mathrm{SO}(m)_n} \times [S]_{\mathrm{SO}(n)_m}\right). \tag{4.118}$$

This means the current operators in $\mathrm{SO}(mn)_1$ that are outside of $\mathrm{SO}(m)_n$ and $\mathrm{SO}(n)_m$ are combinations of tensor products between the traceless symmetric and anti-symmetric primary field sectors of $\mathrm{SO}(m)_n$ and $\mathrm{SO}(n)_m$. For instance, there are $mn(mn-1)/2$ fields on both sides of (4.118). Moreover, the conformal scaling dimensions of products in the

second and third line of (4.118) add up to

$$\frac{m}{m+n-2}+\frac{n-2}{m+n-2}=\frac{m-2}{m+n-2}+\frac{n}{m+n-2}=1. \tag{4.119}$$

In the particular case when $n=2$, $[A]_{\mathrm{SO}(2)_m}=1$ is trivial. Therefore, $[S]_{\mathrm{SO}(m)_2}$ belongs in the $\mathrm{SO}(2m)_1$ WZW algebra. It is local and extends $\mathrm{SO}(n)_2$ to $\mathrm{SU}(n)_1$. Level $n=2$ is the only situation where WZW algebra extension occurs. When $n\geq 3$, the branching rule (4.118) shows there cannot be local spin-1 primary fields in $\mathrm{SO}(m)_n$ that can extend the WZW algebra, and therefore the $\mathrm{SO}(m)_n$ CFT on the edge as well as the bulk $\mathrm{SO}(m)_n$ topological order persists.

Similar to the Fibonacci anyon creation by (4.63) (see figure 4.1) in $\mathrm{SU}(2)_3$, an anyon pair belonging to the vector class $[V]$ can be created by acting on the ground state of the $\mathrm{SO}(m)_n$ model with the string operator,

$$\mathcal{S}=\prod_{y=y_1}^{y_2} J_y^L(\mathsf{x})J_y^R(\mathsf{x})^\dagger, \tag{4.120}$$

where every J_y^σ is chosen to belong in either the second or the third component of the branching decomposition (4.118). If the J's belong in the second component in (4.118), the products $\left\langle \left(A_{\mathrm{SO}(n)_m}\right)_y^L \left(A_{\mathrm{SO}(n)_m}\right)_y^R \right\rangle$ and $\left\langle \left(S_{\mathrm{SO}(m)_n}\right)_y^R \left(S_{\mathrm{SO}(m)_n}\right)_{y+1}^L \right\rangle$ are pinned to their ground state expectation values at low energy. Dangling modes from $\left(S_{\mathrm{SO}(m)_n}\right)_{y_1}^L$ and $\left(S_{\mathrm{SO}(m)_n}\right)_{y_2}^R$ are left behind on the two ends of the string, creating the anyon pair of the $[S]$ class. If the currents J in the operator string (4.120) belong in the third component in (4.118), the string creates an anyon pair of class $[A]$ on both ends.

The vector representations in the conformal embedding $\mathrm{SO}(mn)_1 \supseteq \mathrm{SO}(m)_n \times \mathrm{SO}(n)_m$ follow the single-channel branching rule

$$[\psi]_{\mathrm{SO}(mn)_1} = [V]_{\mathrm{SO}(m)_n} \times [V]_{\mathrm{SO}(n)_m}. \tag{4.121}$$

There are mn fermions on both sides, and the scaling dimensions of the tensor product add up to

$$\frac{m-1}{2(m+n-2)} + \frac{n-1}{2(m+n-2)} = \frac{1}{2}. \tag{4.122}$$

Following (4.66), the string of conjugate Majorana pairs,

$$\mathcal{S}_\psi = \prod_{y=y_1}^{y_2} \psi_y^L(\mathsf{x})\psi_y^R(\mathsf{x}), \tag{4.123}$$

is an integral combination of electron operators because $\psi_y^L\psi_y^R$ on each bundle is local. When applied to the ground state of $\mathrm{SO}(m)_n$, the bulk of the string takes ground state expectation values according to the branching rule (4.121), but the dangling modes $\left(V_{\mathrm{SO}(m)_n}\right)_{y_1}^L$ and $\left(V_{\mathrm{SO}(m)_n}\right)_{y_2}^R$ are left behind, creating the anyon pair belonging to class $[V]$.

The WZW CFT also carries spinor primary fields, which are representations of the double cover $\mathrm{Spin}(m)$. However, the properties of these spinor fields are out of the scope of this paper and will be omitted.

4.4 C_r series and symplectic fermions

We now construct topological models with symplectic WZW symmetry group $\mathrm{Sp}(2n)$ on boundary edges. Previously, Ref. [Che18] studied surface topological order using the splitting of $\mathrm{SO}(4n^2)_1$ into two copies of $\mathrm{Sp}(2n)_n$, where the level and the rank of the algebra in each copy are identical. We will construct $\mathrm{Sp}(2m)_n$ spin liquids and topological superconductor models with arbitrary level and rank. This is achieved by a conformal embedding $\mathrm{Sp}(2m)_n \times \mathrm{Sp}(2n)_m \subseteq \mathrm{SO}(4mn)_1$ on each $\mathrm{SO}(4mn)_1$ wires from the previous section §4.3.1.

We begin with the matrix representation of the symplectic Lie algebra $\mathrm{Sp}(2n)$. It consists of $n \times n$ matrices X with quaternion entries that satisfy $X + X^\dagger = 0$. The matrices can be expressed in the combination $X = X_\mu \mathfrak{q}^\mu$, where $\mu = 0, \ldots, 3$ and X_μ are $n \times n$ real matrices. $\mathfrak{q}^{i=1,2,3}$ are the quaternions. $\mathfrak{q}^\mu$ can be represented in terms of the Pauli matrices

$$\mathfrak{q}^0 = \mathbb{I}_{2\times 2}, \quad \mathfrak{q}^1 = -i\sigma_x, \quad \mathfrak{q}^2 = -i\sigma_y, \quad \mathfrak{q}^3 = -i\sigma_z. \tag{4.124}$$

They satisfy the following properties:

$$\begin{gathered}(\mathfrak{q}^j)^\dagger = -\mathfrak{q}^j, \quad \mathfrak{q}^i\mathfrak{q}^j = -\delta^{ij}\mathbb{I}_{2\times 2} + \epsilon^{ijk}\mathfrak{q}^k, \\ \mathfrak{q}^1\mathfrak{q}^2\mathfrak{q}^3 = (\mathfrak{q}^j)^2 = -\mathbb{I}_{2\times 2},\end{gathered} \tag{4.125}$$

where $i, j, k = 1, 2, 3$, and ϵ^{ijk} is the anti-symmetric Levi-Civita symbol.

The Sp($2n$) Lie algebra is spanned by the following matrix generators $X_\mu(pq)$ (see also [Bak03]), whose matrix entries are

$$[X_\mu(pq)]_{rs} = \frac{1}{4(2)^{\delta_{p,q}/2}} (\delta^p_r \delta^q_s - \eta_{\mu\mu} \delta^q_r \delta^p_s) \tag{4.126}$$

where $r, s = 1, \ldots, n$. $\eta_{\mu\nu} = \text{diag}(1, -1, -1, -1)$ is the Minkowski metric. For $\mu = 0$, there are $n(n-1)/2$ real anti-symmetric matrices $X_0(pq)$, where $1 \le p < q \le n$. For $\mu \neq 0$, $X_{j=1,2,3}(pq)$ are real symmetric matrices, where in this case $1 \le p \le q \le n$. There are $3 \times n(n+1)/2$ such real symmetric matrices. Together, they generate the $n(2n+1)$ dimensional Sp($2n$) Lie algebra.

The chiral Sp$(2n)_1$ WZW algebra can be represented by fermion bilinear KM currents. We group $4n$ Majorana fermions $\psi^{r=1,\ldots,n}_\mu$ into a collection of symplectic fermions $\chi^r = \psi^r_\mu \mathfrak{q}^\mu$. Their complex conjugations are $(\chi^r)^\dagger = \eta_{\mu\mu} \psi^r_\mu \mathfrak{q}^\mu$. Conversely, the Majorana fields can be obtained from

$$\psi^r_\mu = \frac{1}{2} \eta_{\mu\nu} \, \text{Tr}[\chi^r \mathfrak{q}^\nu]. \tag{4.127}$$

We are now ready to describe the current algebra of Sp$(2n)_1$. The Hermitian current operators are defined by products of symplectic fermions:

$$\begin{aligned} J^\mu_{pq} &= \frac{i}{2} \, \text{Tr}\Big[\chi^\dagger X^\mu(pq) \mathfrak{q}^\mu \chi\Big] \\ &= \frac{i}{2} \sum_{\lambda,\nu,r,s} \eta_{\lambda\lambda} T^{\lambda\mu\nu} \psi^r_\lambda [X^\mu(pq)]_{rs} \psi^s_\nu. \end{aligned} \tag{4.128}$$

We refer to $T^{\lambda\mu\nu} \equiv \mathrm{Tr}\left[\mathfrak{q}^\lambda \mathfrak{q}^\mu \mathfrak{q}^\nu\right]$ as the trace of the product of three quaternions, or simply the quaternion trace. It takes the explicit form of

$$T^{\lambda\mu\nu} = 2\eta^{\lambda\mu}\delta^{\nu 0} + 2\eta^{\lambda\nu}\delta^{\mu 0} + 2\eta^{\mu\nu}\delta^{\lambda 0} - 4\delta^{\lambda 0}\delta^{\mu 0}\delta^{\nu 0} - 2\epsilon^{0\lambda\mu\nu} \tag{4.129}$$

with Greek letters $\lambda, \mu, \nu = 0, 1, 2, 3$ and lowercase alphabets $i, j, k = 1, 2, 3$. $\epsilon^{0\lambda\mu\nu}$ is the four dimensional the Levi-Civita symbol.

4.4.1 Conformal Embedding and Descendant Topological Order

Symmetry embedding

We then generalize the embedding of arbitrary levels symplectic current algebras into the $\mathrm{SO}(4mn)_1$ theory. We refer the A sector to $\mathrm{Sp}(2m)_n$, and the B sector to $\mathrm{Sp}(2n)_m$ in the symmetry or matrix embedding of $\mathrm{Sp}(2m)_n \times \mathrm{Sp}(2n)_m \subseteq \mathrm{SO}(4mn)_1$. The matrix embedding here is based on the tensor product over a real division algebra of quaternion that is equivalent to the identity $X^A \otimes X^B = (X^A_\mu \mathfrak{q}^\mu) \otimes (X^B_\nu \mathfrak{q}^\nu) = (X^A_\mu \otimes X^B_\nu)(\mathfrak{q}^\mu \mathfrak{q}^\nu)$.

The $m \times m$ matrix generator $X_\mu(pq)$, defined in (4.126), of $\mathrm{Sp}(2m)_n$ can be embedded into $\mathrm{SO}(4mn)$ by taking

$$\begin{aligned}
\left[X_\mu(pq)^A\right]_{rs} &= \left(X_\mu(pq) \otimes \mathbb{I}_n\right)_{rs} \\
&= \left[X_\mu(pq)\right]_{ab} \delta_{cd} \delta_r^{(a-1)n+c} \delta_s^{(b-1)n+d} \\
&= \frac{1}{4(2)^{\delta_{pq}/2}} \sum_{c=1}^{n} \left(\delta_r^{p'} \delta_s^{q'} - \eta^{\mu\mu} \delta_r^{q'} \delta_s^{p'}\right).
\end{aligned} \tag{4.130}$$

We denote $p' \equiv (p-1)n + c$ and $q' \equiv (q-1)n + c$, where the indices are subject to the following conditions: $r, s = 1, \ldots, mn$, $a, b = 1, \ldots, m$, and $c, d = 1, \ldots, n$. Additionally, the indices p and q follow these constraints: $1 \leq p < q \leq m$ when $\mu = 0$; and $1 \leq p \leq q \leq m$ when $\mu = 1, 2, 3$. For each chiral sector σ, the current operators of the A sector, under bilinear products of symplectic fermions, are

$$\begin{aligned} J^{A,\mu}_{pq} &= \frac{i}{2} \operatorname{Tr}\left[\chi^\dagger X_\mu(pq)^A \mathfrak{q}^\mu \chi\right] \\ &= \frac{i}{2} \sum_{\lambda,\nu,r,s} \eta_{\lambda\lambda} T^{\lambda\mu\nu} \psi^r_\lambda \left[X_\mu(pq)^A\right]_{rs} \psi^s_\nu, \end{aligned} \tag{4.131}$$

as a sum of n decoupled copies of $\mathrm{Sp}(2m)_1$ currents. Similarly for the B sector, given any $n \times n$ anti-Hermitian matrix $X_\mu(pq)$ that generates $\mathrm{Sp}(2n)$, we define

$$\begin{aligned} \left[X_\mu(pq)^B\right]_{rs} &= (\mathbb{I}_m \otimes (X_\mu(pq))_{rs} \\ &= \delta_{ab} \left[X_\mu(pq)\right]_{cd} \delta_r^{(a-1)n+c} \delta_s^{(b-1)n+d} \\ &= \frac{1}{4(2)^{\delta_{pq}/2}} \sum_{a=1}^{m} \left(\delta_r^{p'} \delta_s^{q'} - \eta^{\mu\mu} \delta_r^{q'} \delta_s^{p'}\right) \end{aligned} \tag{4.132}$$

with $p' = (a-1)n + p$ and $q' = (a-1)n + q$. The indexes are subject to $r, s = 1, \ldots, mn$, $a, b = 1, \ldots, m$, and $c, d = 1 \ldots, n$. Additionally, the indices p and q follow these constraints: $1 \leq p < q \leq n$ when $\mu = 0$, and $1 \leq p \leq q \leq n$ when $\mu = 1, 2, 3$. The current operators of the B sector are symplectic fermions bilinears

$$\begin{aligned} J^{B,\mu}_{pq} &= \frac{i}{2} \operatorname{Tr}\left[\chi^\dagger X_\mu(pq)^B \mathfrak{q}^\mu \chi\right] \\ &= \frac{i}{2} \sum_{\lambda,\nu,r,s} \eta_{\lambda\lambda} T^{\lambda\mu\nu} \psi^r_\lambda \left[X_\mu(pq)^B\right]_{rs} \psi^s_\nu. \end{aligned} \tag{4.133}$$

We assume that the KM current-current backscatterings in (4.135) and (4.136) generate finite mass gaps.

Descendant states

We begin with the $SO(4mn)_1$ wires discussed in Sec.4.3.1. The $4mn$ chiral Majorana fermions $\psi^{\sigma}_{y,j=1,\ldots,4mn}$ in each $\mathrm{SO}(4mn)_1$ wire are relabeled, as $\psi^{\sigma,r}_{y,\mu} = \psi^{\sigma}_{y,j=mn\mu+r}$ with $\mu = 0,1,2,3$ and $r = 1,\ldots,mn$, to fit into $\mathrm{Sp}(2m)_n \times \mathrm{Sp}(2n)_m$. For a given bundle y, According to the discussion in Sec. 4.3.1, an operator is local if it is invariant under the internal $\mathbb{Z}_2$ symmetry in (4.98). Consequently, the current operators, given in equations (4.128), (4.131), and (4.133), are local.

We now use these current operators to build the theories of $\mathrm{Sp}(2m)_n$ or $\mathrm{Sp}(2n)_m$ spin liquids and topological superconductor. We recall that the charge sector has previously been gapped out through Umklapp backscattering or superconducting pairing described by (4.87). Extra degree of freedom of Majoranas were removed using fermions backscattering in (4.96). Leaving us with the neutral $\mathrm{SO}(N = 4mn)_1$ theory and $4mn$ Majoranas. Hence, the embedded theories inherit two important features, which are the charge neutrality and the kinetic Hamiltonian $\mathcal{H}_0$ of (4.97). The microscopic Hamiltonian

$$\mathcal{H}\left[\mathrm{Sp}(2m)_n\right] = \mathcal{H}_0 + \mathcal{H}^{\mathrm{Sp}(2m)_n}_{\mathrm{inter}} + \mathcal{H}^{\mathrm{Sp}(2n)_m}_{\mathrm{intra}} \tag{4.134}$$

supports the edge CFT of $\mathrm{Sp}(m)_n$ in an open geometry, with current-current backscattering potentials given by/

$$\begin{aligned}\mathcal{H}_{\text{inter}}^{\mathrm{Sp}(2m)_n} &= u_{\text{inter}} \sum_{y,\mu} \sum_{1\le p,q\le m} \left(J^{\mathrm{Sp}(2m)_n}\right)^{R,\mu}_{y,pq} \left(J^{\mathrm{Sp}(2m)_n}\right)^{L,\mu}_{y+1,pq} \\ &= -\frac{u_{\text{inter}}}{4} \sum_{y,\mu} \sum_{1\le p,q\le m} \sum_{r,s=1}^{mn} \mathrm{Tr}\left[\chi^R_{y,r}\left[X^\mu(pq)^{\mathrm{Sp}(2m)_n}\right]_{rs} \mathfrak{q}^\mu \chi^R_{y,s}\right] \\ &\times \mathrm{Tr}\left[\chi^L_{y+1,r}\left[X^\mu(pq)^{\mathrm{Sp}(2m)_n}\right]_{rs} \mathfrak{q}^\mu \chi^L_{y+1,s}\right],\end{aligned} \tag{4.135}$$

and

$$\begin{aligned}\mathcal{H}_{\text{intra}}^{\mathrm{Sp}(2n)_m} &= u_{\text{intra}} \sum_{y,\mu} \sum_{1\le p,q\le n} \left(J^{\mathrm{Sp}(2n)_m}\right)^{R,\mu}_{y,pq} \left(J^{\mathrm{Sp}(2n)_m}\right)^{L,\mu}_{y,pq} \\ &= -\frac{u_{\text{intra}}}{4} \sum_{y,\mu} \sum_{1\le p,q\le n} \sum_{r,s=1}^{mn} \mathrm{Tr}\left[\chi^R_{y,r}\left[X^\mu(pq)^{\mathrm{Sp}(2n)_m}\right]_{rs} \mathfrak{q}^\mu \chi^R_{y,s}\right] \\ &\times \mathrm{Tr}\left[\chi^L_{y,r}\left[X^\mu(pq)^{\mathrm{Sp}(2n)_m}\right]_{rs} \mathfrak{q}^\mu \chi^L_{y,s}\right].\end{aligned} \tag{4.136}$$

4.4.2 Topological Order Examples

In this subsection, we discuss examples of the resulting topological order. The simplest conformal embedding in the $\mathrm{SO}(4mn)_1$ family is $\mathrm{SO}(4)_1 = \mathrm{Sp}(2)_1 \times \mathrm{Sp}(2)_1$, where $\mathrm{Sp}(2)_1 = \mathrm{SU}(2)_1$. This embedded algebra supports the same Abelian topological order as the $\mathrm{SU}(2)_1$.

In the remainder of this section, we will examine two interesting examples of non-Abelian topological orders: $\mathrm{SO}(8)_1 \supseteq \mathrm{Sp}(2)_2 \times \mathrm{Sp}(4)_1$, which follows a special branching rule of (4.137), distinct from the general case of (4.137), and $\mathrm{SO}(16)_1 \supseteq \mathrm{Sp}(2)_4 \times \mathrm{Sp}(8)_1$, which exhibits orbifold structures.

$\mathrm{SO}(8)_1 \supseteq \mathrm{Sp}(2)_2 \times \mathrm{Sp}(4)_1$

We begin by considering the conformal embedding of the 3-dimensional $\mathrm{Sp}(2)_2$ algebra and the 10-dimensional $\mathrm{Sp}(4)_1$ algebra into the 28-dimensional $\mathrm{SO}(8)_1$.

The emergent topological order of $\mathrm{Sp}(2)_2$ includes of a one-dimensional vacuum sector, a three-dimensional fermion superselection sector, and a two-dimensional twist field supersector, with conformal scaling dimension 3/16. Since $\mathrm{Sp}(2)_2$ is isomorphic to $\mathrm{SO}(3)_1$, the topological order is Ising-like. The fermion supersector $[f]_{\mathrm{Sp}(2)_2} = [f]_{\mathrm{SO}(3)_1}$ corresponds to the adjoint representation, or equivalently, the skew-Hermitian quaternion 2-tensor $[A]_{\mathrm{Sp}(2)_2} = [f]_{\mathrm{Sp}(2)_2}$ of $\mathrm{Sp}(2)_2$.

Similarly, $\mathrm{Sp}(4)_1$ also exhibits Ising-like topological order, as it is isomorphic to $\mathrm{SO}(5)_1$. Its anyon structure consists of a vacuum sector, a five-dimensional fermion sector, and a four-dimensional Ising-like twist field, with conformal scaling dimension 5/16. Unlike $\mathrm{Sp}(2)_2$, $\mathrm{Sp}(4)_1$ lacks a primary field supersector associated with its adjoint representation. Instead, its fermion supersector $[f]_{\mathrm{Sp}(4)_1} = [f]_{\mathrm{SO}(5)_1}$ corresponds to its traceless-Hermitian quaternion 2-tensor $[S]_{\mathrm{Sp}(4)_1} = [f]_{\mathrm{Sp}(4)_1}$.

In each chiral sector, the product of the fields $[A]_{\mathrm{Sp}(2)_2} \times [S]_{\mathrm{Sp}(4)_1}$ forms local spin 1 bosons with conformal scaling dimension $h = 1/2 + 1/2 = 1$. The dimensional difference between $\mathrm{SO}(8)_1$ and $\mathrm{Sp}(2)_2 \times \mathrm{Sp}(4)_1$ is $28 - 3 - 10 = 3 \times 5$, which is accounted for by all possible combinations of primary field pairing between $[A]_{\mathrm{Sp}(2)_2}$ and $[S]_{\mathrm{Sp}(4)_1}$. These resulting bosons extend the $\mathrm{Sp}(2)_2 \times \mathrm{Sp}(4)_1$ WZW algebra to the full $\mathrm{SO}(8)_1$ WZW algebra, in agreement

with the branching rules:

$$\begin{aligned} \mathrm{SO}(8)_1 &= \mathrm{SO}(3)_1 \oplus \mathrm{SO}(5)_1 \oplus \left([f]_{\mathrm{SO}(3)_1}\right) \times \left([f]_{\mathrm{SO}(5)_1}\right) \\ &= Sp(2)_2 \oplus Sp(4)_1 \oplus \left([f]_{Sp(2)_2}\right) \times \left([f]_{Sp(4)_1}\right). \end{aligned} \tag{4.137}$$

In Sec. 4.4.2, we will explore how anyon excitations can emerge from the branching rules and how they can be generated within the topological bulk.

$\mathrm{SO}(16)_1 \supseteq \mathrm{Sp}(2)_4 \times \mathrm{Sp}(8)_1$

We present here another symmetry embedding, $\mathrm{Sp}(2)_4 \times \mathrm{Sp}(8)_1$, which again exhibits orbifold structures: $\mathrm{Sp}(2)_4 = \mathrm{SU}(3)_1/\mathbb{Z}_2$ and $\mathrm{Sp}(8)_1 = (E_6)_1/\mathbb{Z}_2$.

To understand how the orbifold structure arise in $\mathrm{Sp}(2)_4$, we must examine whether local $\mathbb{Z}_2$ gauge charges exist that could extend the $\mathrm{Sp}(2)_4$ to $\mathrm{SU}(3)_1$. Given the isomorphism between $\mathrm{Sp}(2)_4$ and $\mathrm{SO}(3)_2$, we can rewrite the $\mathrm{Sp}(2)_4$ current operators in the form of the $\mathrm{SO}(3)_2$. Following from (4.115), we derive the corresponding $\mathbb{Z}_2$ gauge charge for $\mathrm{Sp}(2)_4$ from (4.114) and analyze its locality.

We start by showing that $\left[J_{\mathrm{Sp}(2)_4}\right]_{pq=11}^{\mu=1,2,3}$ is equivalent to $\left[J_{\mathrm{SO}(3)_2}\right]_{pq} = i\psi_p\psi_q + i\psi_{3+p}\psi_{3+q}$, where $1 \le p < q \le 3$. Using the angle sum rules, we obtain:

$$\begin{aligned}
\left[J_{\mathrm{Sp}(2)_4}\right]_{11}^{\mu=1} &\sim \cos(\tilde{\varphi}_1)\cos(\tilde{\varphi}_2) + \cos(\tilde{\varphi}_4)\cos(\tilde{\varphi}_5) \\
&\simeq i\tilde{\psi}_1\tilde{\psi}_2 + i\tilde{\psi}_4\tilde{\psi}_5, \\
\left[J_{\mathrm{Sp}(2)_4}\right]_{11}^{\mu=2} &\sim \cos(\tilde{\varphi}_1)\cos(\tilde{\varphi}_3) + \cos(\tilde{\varphi}_4)\cos(\tilde{\varphi}_6) \\
&\simeq i\tilde{\psi}_1\tilde{\psi}_3 + i\tilde{\psi}_4\tilde{\psi}_6, \\
\left[J_{\mathrm{Sp}(2)_4}\right]_{11}^{\mu=3} &\sim \cos(\tilde{\varphi}_2)\cos(\tilde{\varphi}_3) + \cos(\tilde{\varphi}_5)\cos(\tilde{\varphi}_6) \\
&\simeq i\tilde{\psi}_2\tilde{\psi}_3 + i\tilde{\psi}_5\tilde{\psi}_6,
\end{aligned} \tag{4.138}$$

with angle variables $\tilde{\varphi}$ defined by

$$\begin{aligned}
\tilde{\varphi}_1 &= \frac{\phi_1 - \phi_3 - \phi_5 + \phi_7}{2}, \quad \tilde{\varphi}_4 = \frac{\phi_2 - \phi_4 - \phi_6 + \phi_8}{2}, \\
\tilde{\varphi}_2 &= \frac{\phi_1 - \phi_3 + \phi_5 - \phi_7}{2}, \quad \tilde{\varphi}_5 = \frac{\phi_2 - \phi_4 + \phi_6 - \phi_8}{2}, \\
\tilde{\varphi}_3 &= \frac{\phi_1 - \phi_5 + \phi_3 - \phi_7}{2}, \quad \tilde{\varphi}_6 = \frac{\phi_2 - \phi_6 + \phi_4 - \phi_8}{2}.
\end{aligned} \tag{4.139}$$

Here for simplicity, we have temporarily suppressed the y and σ indexes. The notation "$\simeq$" indicates equivalence up to a normalization factor after refermionization. In the refermionization process, given by $e^{i\tilde{\varphi}_j} = (\tilde{\psi}_j + i\tilde{\psi}_{6+j})/\sqrt{2}$, we can match $\tilde{\psi}_j$ with $\cos\tilde{\varphi}_j$ for $j = 1, \ldots, 6$. This yields the $\mathrm{SU}(3)_2$-like current operator, as well as the gapped Hamiltonian in (4.113).

We can now write down a $\mathrm{Sp}(2)_4$-$\mathbb{Z}_2$ gauge charge from (4.114). Take for example the gauge charge $S_{11} = 2i\tilde{\psi}_1\tilde{\psi}_4$. This fermion pairs can be expressed using the angle sum rules as:

$$i\tilde{\psi}_1\tilde{\psi}_4 \simeq \cos(\tilde{\varphi}_1 + \tilde{\varphi}_4) + \cos(\tilde{\varphi}_1 - \tilde{\varphi}_4). \tag{4.140}$$

Since $\tilde{\varphi}_1 \pm \tilde{\varphi}_4$ are sums involving half-integer multiples of linearly independent bosonized variables of Dirac fermions defined by (4.94), the cosine terms correspond to pairs of fractional Dirac fermions. Therefore the $\mathbb{Z}_2$ gauge charge S_{11} is non-local and does not condense in the anyon condensation sense. Consequently, $\mathrm{Sp}(2)_4$ remains unchanged and does not extend to $\mathrm{SU}(3)_1$.

A similar non-local gauge charges construction applies to $\mathrm{Sp}(8)_1 = (E_6)_1/\mathbb{Z}_2$, which does not extended $\mathrm{Sp}(8)_1$ to $(E_6)_1$. Thus, both WZW algebras exhibit $\mathbb{Z}_2$ gauge theory with an orbifold structure.

Common primary fields and anyon excitations

In closing, we discuss the branching rules for $\mathrm{SO}(4mn)_1 \supseteq \mathrm{Sp}(2m)_n \times \mathrm{Sp}(2n)_m$, and how anyon excitations associated with the embedded sub-algebras arise from string operators within the topological bulk.

In the simplest cases, $\mathrm{SO}(4)_1 = \mathrm{Sp}(2)_1 \times \mathrm{Sp}(2)_1$. Because $\mathrm{Sp}(2)_1$ is identical to $\mathrm{SU}(2)_1$, its fusion group of Abelian anyons is the vacuum and two semions. The vector representation of $\mathrm{Sp}(2)_1$ is simply the semion, which obeys the fusion rule $[V] \times [V] = 1$.

For general $Sp(2m)$, we label the primary field sector corresponding to the vector representation $[V] = \text{span}\{V_a : a = 1, \ldots, 2m\}$. The quadratic Casimir of $[V]$ is $C_V = 2(2m+1)/4$. The dual Coxeter of $Sp(2m)$ is $g = m + 1$. Therefore, the scaling dimension of $[V]$ in $Sp(2m)_n$ is $h_V = \frac{C_V/2}{m+n+1} = \frac{2m+1}{4(m+n+1)}$. The vector representation of $Sp(2m)$ is irreducible for $m \geq 1$ [FMS12].

For higher levels $n \geq 2$, there exists $[V]$ in $Sp(2m)_n$ that obey the fusion rule $[V] \times [V] = 1 + [A] + [S]$. The adjoint representation $[A]$ of $Sp(2m)$ is the skew-Hermitian quaternion 2-tensor with dimension $\dim[A] = 2m^2 + m$ and quadratic Casimir $C_A = 2(m + 1)$. It has conformal scaling dimension $h_A = (m + 1)/(m + n + 1)$ in $Sp(2m)_n$. The traceless Hermitian quaternion 2-tensor $[S]$ has dimension $\dim[S] = m(2m - 1) - 1$ and quadratic Casimir $C_S = 2m$. It has scaling dimension $h_S = m/(m + n + 1)$ in $Sp(2m)_n$. In general, the conformal embedding $SO(4mn)_1 \supseteq Sp(2m)_n \times Sp(2n)_m$ obeys the branching rule

$$\begin{aligned} SO(4mn)_1 = {} & Sp(2m)_n \oplus Sp(2n)_m \\ & \oplus \left([S]_{Sp(2m)_n} \times [A]_{Sp(2n)_m}\right) \\ & \oplus \left([A]_{Sp(2m)_n} \times [S]_{Sp(2n)_m}\right). \end{aligned} \tag{4.141}$$

So there are $2mn(4mn-1)$ fields on both sides of (4.141). The $(2m+1)(2n+1)(2mn-m-n)$ current operators of $\text{SO}(4mn)_1$ that lie outside $\text{Sp}(2m)_n$ and $\text{Sp}(n)_m$ are constructed form combinations of tensor products between the skew-Hermitian and the traceless Hermitian quaternion primary field sectors of $\text{Sp}(2m)_n$ and $\text{Sp}(n)_m$. Additionally, the conformal scal-

ing dimensions of products in the second and third line of (4.141) sum up to

$$\frac{m+1}{m+n+1}+\frac{n}{m+n+1}=\frac{n+1}{m+n+1}+\frac{m}{m+n+1}=1. \tag{4.142}$$

In the special case where $m=1$ and $n\geq 2$, the isomorphism between $Sp(2)$ and $SU(2)$ tells us that $Sp(2)_n$ only has the skew-Hermitian quanternion representation $[A]$, and not the $[S]$ representation. This reduces the branching rule in (4.141) to

$$SO(4n)_1 = Sp(2)_n \oplus Sp(2n)_1 \oplus \left([A]_{Sp(2)_n} \times [S]_{Sp(2n)_1}\right), \tag{4.143}$$

as demonstrated in the example of (4.137).

The dimension difference between $\mathrm{SO}(4n)_1$ and $\mathrm{Sp}(2)_n \times \mathrm{Sp}(2m)_1$ is accounted for by the dimension of primary field tensor products $[A]_{Sp(2)_n} \times [S]_{Sp(2n)_1}$, with the conformal scaling dimensions from these two primary field sectors add up to unity:

$$h_A^{Sp(2)_n} + h_S^{Sp(2n)_1} = \frac{2}{n+2}+\frac{n}{n+2}=1. \tag{4.144}$$

Using the same reasoning as in 4.3.3, an anyon pair of the vector representation $[V]$ in $Sp(m)_n$ can be generated by applying a string operator, similar to that in (4.120). However, each current operator J_y^σ must be selected from either the second or third component of the branching rules in (4.141). If the J operators are in the second component of (4.141), dangling modes from $\left(S_{Sp(2m)_n}\right)_{y_1}^L$ and $\left(S_{Sp(2m)_n}\right)_{y_2}^R$ remain at both ends of the string op-

erator, leading to the creation of an anyon pair of the $[S]$ class. Conversely, if the currents J belong to the third component in (4.141), the string operator generates a pair of anyon excitation of the $[A]$ class.

Moreover, in the conformal embedding of $SO(4mn)_1 \supseteq Sp(2m)_n \times Sp(2n)_m$, the vector representations obey a single-channel branching rule:

$$[\psi]_{SO(4mn)_1} = [V]_{Sp(2m)_n} \times [V]_{Sp(2n)_m}, \tag{4.145}$$

with $4mn$ fermions on both sides. The corresponding conformal scaling dimensions of the single channel tensor products sum to

$$\frac{2m+1}{4(m+n+1)} + \frac{2n+1}{4(m+n+1)} = \frac{1}{2}. \tag{4.146}$$

Since the operators $\psi_y^L \psi_y^R$ originate from the $SO(4mn)_1$ family, they remain local within each wire bundle. Consequently, we can construct an identically local string of conjugate Majorana pairs, as shown in (4.123). In the lower-energy sector of the $Sp(m)_n$ model, the bulk of the string is pinned to its ground state expectation value according to (4.145). This leaves behind the dangling modes $\left(V_{Sp(m)_n}\right)_{y_1}^L$ and $\left(V_{Sp(n)_m}\right)_{y_2}^R$ at both ends of the string, creating an anyon pair of the $[V]$ class.

4.5 Discussion and Conclusion

We construct exactly solvable coupled-wire Hamiltonians for topological phases characterized by classical Lie algebras at arbitrary levels. These topological phases include chiral states of quantum Hall liquids, topological superconductors and spin liquids. We assume that the current-current backscattering of $\mathrm{SU}(m)_n$, $\mathrm{SO}(m)_n$ and $\mathrm{Sp}(2m)_n$ WZW algebras opens up a bulk excitation energy gap. These bulk excitations are corresponding to the chiral CFT primary fields that appear on the edge.

Our construction demonstrates how various Abelian and non-Abelian anyons, associated with primary field superselection sectors, emerge from string operators. This occurs by pinning their ground state expectation values according to their branching rules, such as those in (4.61),(4.64), (4.118), and (4.141), at the lower-energy of the coupled-wire models.

An open question remains as to whether current-current backscattering in WZW KM algebra generally leads to finite bulk excitation gaps. Our assumption is based on a concrete mass gap analysis of the $\mathrm{SU}(2)_n$ model. In this model, current-current interactions can be expressed through backscattering of opposite chiral $\mathbb{Z}_n$ parafermions, coupled to sine-Gordon potential. The sine-Gordon potential is pinned at its finite ground state expectation values, which subsequently opens up a mass gap for the counter-propagating $\mathbb{Z}_n$ parafermions.

We can extended the analysis of finite mass gaps to models involving SO(3) and Sp(2) at various level by utilizing their isomorphisms with the SU(2) algebra. Additionally, we can

determine the presence of a finite excitation gap in the $\mathrm{Sp}(4)_1$ by examining its conformal embedding as a product of two $\mathrm{Sp}(2)_1$ models, since $\mathrm{Sp}(4)_1$ is equivalent to $\mathrm{Sp}(2)_1 \times \mathrm{Sp}(2)_1$. This approach allows us to generalize the analysis by exploring isomorphisms between gapped models and their conformal embeddings.

So far in this work, we have applied the coupled-wire construction for topological phases characterized by classical Lie algebras at arbitrary levels, while the construction for exceptional Lie algebras at level-1 was addressed in [LMT23]. It will be of interest to construct coupled-wire models for exceptional Lie algebras at arbitrary levels and investigate what topological phases they may represent.

Furthermore, it would be of particular interest to explore coupled-wire construction for parent symmetries that can host various conformal embeddings among exceptional and classical Lie algebras at arbitrary levels, characterizing different topological phases. This exploration may provide a unifying theme, or suggest a classification scheme in the study of chiral states of matter.

In addition to using coupled-wire models to generate various topological phases, we can analyze the entanglement properties of these topological states by solving their ground state wavefunctions for the proposed microscopic Hamiltonians. As demonstrated in our previous work in [LATM21], this approach could offer new insights into the disentangling behavior of topological states. By understanding how entanglement manifests and is structured in these states, we establish a connection between the fields of quantum information and topolgoical states of matter.

Chapter 5

Topological Defects in quantum LDPC codes

This chapter was previous published as [Pak Kau Lim, Kirill Shtengel, Leonid P. Pryadko, "Topological defects in general quantum LDPC codes", Memorial Volume for Shoucheng Zhang, pp. 1-17 (2021)]

5.1 Introduction

One of the many advantages of surface codes is the flexibility they offer in the code parameters and the structure of logical operators. To add an extra qubit one may simply create a hole in the surface. A larger hole, well separated from other defects, offers better protec-

tion (larger minimal code distance). Pairs of such holes can be moved around to perform encoded Clifford gates, etc[DKLP02, BMD09, Bom10].

On the other hand, a substantial disadvantage of surface codes, or any stabilizer code with generators local on a D-dimensional Euclidean lattice, is that such codes necessarily have small rates $R = k/n$ whenever the code distance d gets large[BT09, BPT10]. Here k is the number of encoded qubits and n is the block length of the code. To get a finite asymptotic rate, one needs more general quantum codes. In particular, any family of *w-bounded quantum LDPC codes* with stabilizer generators of weight not exceeding $w > 0$ and distances divergent as a logarithm or a power of n has a non-zero asymptotic error correction threshold even in the presence of measurement errors[KP13a, DKP15]. Several families of bounded-weight quantum LDPC codes with finite rates have been constructed. Best-known constructions are quantum hypergraph-product (qHP) and related codes[TZ09, KP13b, ZP19], and various hyperbolic codes[Zém09, Del13, GL14, BT16].

The biggest obstacle to practical use of finite-rate quantum LDPC codes is that their stabilizer generators must include far separated qubits, regardless of the qubit layout in a D-dimensional space[BT09, BPT10]. Error correction requires frequent measurement of all stabilizer generators, and measuring such non-local generators just isn't practical if the hardware only allows local measurements. Nevertheless, there is a question of whether other advantages of surface codes, e.g., the ability to perform protected Clifford gates by code deformations, can be extended to more general quantum LDPC codes.

Such a construction generalizing the surface-code defects and gates by code deformations to the family of qHP codes[TZ09] has been recently proposed by Krishna and Poulin[KP19]. However, their defect construction is very specific to qHP codes. Second, Krishna and Poulin do not discuss the distance of the defect codes they construct, even though it is important for the accuracy of the resulting gates. Indeed, since gates by code deformation are relatively slow, the distance has to be large enough to suppress logical errors.

The purpose of this work is to give a general defect construction applicable to any stabilizer code. In the simplest form, one may just remove a stabilizer generator which produces an additional logical qubit, $k \to k+1$. However, the distance d' of such a code will not exceed the maximum stabilizer generator weight, $d' \leq w$. Given a degenerate quantum LDPC code with the stabilizer generator weights bounded by w and a distance $d > w$, we would actually like to construct a related code encoding more qubits but retaining degeneracy, i.e., with a distance $d' > w$. We propose a three-step defect construction: remove qubits in an erasable region to obtain a subsystem code, do gauge-fixing to obtain a stabilizer code with some generators of weight exceeding w, and promote one or more such generators of the resulting code to logical operators. The choice of the gauge-fixing prescription is easier in the case of Calderbank, Shor, and Steane (CSS) codes[CS96, Ste96], which makes the construction more explicit. For such codes, with some additional assumptions, we give a lower bound on the distance of the defect code. This shows that defect codes with unbounded distances can be constructed, as is also the case with surface codes.

An interesting and a rather unexpected application of this analysis is the relation of qubit-carrying capacity of a defect to its (generalized) topological entanglement entropy[KP06b,

LW06, GTV11] (TEE), denoted γ. Namely, a degenerate defect code with distance $d' > w$ can only be created when $\gamma > 0$. Further, when distance d' is large, the TEE γ acquires stability: it remains non-zero whenever the defect is deformed within certain bounds.

5.2 Defect construction

Generally, an n-qubit quantum code is a subspace of the n-qubit Hilbert space $\mathbb{H}_2^{\otimes n}$. A quantum $[[n, k, d]]$ stabilizer code is a 2^k-dimensional subspace $\mathcal{Q} \subseteq \mathbb{H}_2^{\otimes n}$ specified as a common $+1$ eigenspace of all operators in an Abelian *stabilizer* group $\mathcal{S} \in \mathcal{P}_n$, $-\mathbf{1} \notin \mathcal{S}$, where $\mathcal{P}_n$ denotes the n-qubit Pauli group generated by tensor products of single-qubit Pauli operators. The stabilizer is typically specified in terms of its generators, $\mathcal{S} = \langle S_1, \ldots, S_r \rangle$. If the number of independent generators is $r \equiv \operatorname{rank} \mathcal{S}$, the code encodes $k = n - r$ qubits. The weight of a Pauli operator is the number of qubits that it affects. The distance d of a quantum code is the minimum weight of a Pauli operator $L \in \mathcal{P}_n$ which commutes with all operators from the stabilizer $\mathcal{S}$, but is not a part of the stabilizer, $L \notin \mathcal{S}$. Such operators act non-trivially in the code and are called logical operators.

An n-qubit CSS stabilizer code $\mathcal{Q} \equiv \operatorname{css}(P, Q)$ is specified in terms of two n-column binary stabilizer generator matrices $H_X \equiv P$ and $H_Z \equiv Q$. Rows of the matrices correspond to stabilizer generators of X- and Z-type, respectively, and the orthogonality condition $PQ^T = 0$ is required to ensure commutativity. The code encodes $k = n - \operatorname{rank} P - \operatorname{rank} Q$

qubits, and has the distance $d = \min(d_X, d_Z)$,

$$d_X = \min_{b \in \mathcal{C}_Q^\perp \setminus \mathcal{C}_P} \mathrm{wgt}(b), \quad d_Z = \min_{c \in \mathcal{C}_P^\perp \setminus \mathcal{C}_Q} \mathrm{wgt}(c). \tag{5.1}$$

Here $\mathcal{C}_Q \in \mathbb{F}_2^{\otimes n}$ is the binary linear code (linear space) generated by the rows of Q, and $\mathcal{C}_Q^\perp$ is the corresponding dual code formed by all vectors in $\mathbb{F}_2^{\otimes n}$ orthogonal to the rows of Q. Matrix Q is the parity check matrix of the code $\mathcal{C}_Q^\perp$. A generating matrix of $\mathcal{C}_Q^\perp$, Q^*, has $\operatorname{rank} Q^* = n - \operatorname{rank} Q$ and is called *dual* to Q. Also, if $V = \{1, \ldots, n\}$ is the set of indices and $B \subset V$ its subset, for any vector $b \in \mathbb{F}_2^{\otimes n}$, we denote $b[B]$ the corresponding *punctured* vector with positions outside B dropped. Similarly, $Q[B]$ (with columns outside of B dropped) generates the code $\mathcal{C}_Q$ *punctured* to B. We will also use the notion of a binary code $\mathcal{C}$ *shortened* to B, which is formed by puncturing only vectors in $\mathcal{C}$ supported inside B,

$$\text{Code } \mathcal{C} \text{ shortened to } B = \{c[B] : \ c \in \mathcal{C} \ \wedge \ (c) \in B\}.$$

We will denote Q_B a generating matrix of the code $\mathcal{C}_Q$ shortened to B. If G and $H = G^*$ is a pair of mutually dual binary matrices, i.e., $GH^T = 0$ and $\operatorname{rank} G + \operatorname{rank} H = n$, then H_B is a parity check matrix of the punctured code $\mathcal{C}_{G[B]}$, and[MS83]

$$\operatorname{rank} G[B] + \operatorname{rank} H_B = |B|. \tag{5.2}$$

The distance d of a linear code $\mathcal{C}$ is the minimal Hamming weight of a non-zero vector in $\mathcal{C}$. In general puncturing reduces the code distance. More precisely, if d and d' are the distances of the original and the punctured code, respectively, they satisfy $d - |A| \le d' \le d$.

On the other hand, the minimum distance d'' of a shortened code is not smaller than that of the original code, $d'' \geq d$.

For a quantum code, if A is a set of qubits and $B = V \setminus A$ its complement, the stabilizer group $\mathcal{S}$ can also be punctured to B, by dropping all positions outside B. With the exception of certain special cases[Rai99, Sar08], the resulting group $\mathcal{G} \equiv \mathcal{S}[B]$ will not be Abelian, and can be viewed as a gauge group of a subsystem code[Pou05, Bac06] called the *erasure* code. A stabilizer code can be obtained by removing some of the generators from $\mathcal{G}$ to make it Abelian; such a procedure is called gauge-fixing. In the case of a CSS code with stabilizer generator matrices $H_X = P$ and $H_Z = Q$, the punctured group has generators $P[B]$ and $Q[B]$, while a gauge-fixed stabilizer code can be obtained, e.g., by replacing punctured matrix $Q[B]$ with the corresponding shortened matrix, Q_B. This latter construction can be viewed as a result of measuring qubits outside B in the X basis. Qubits in an erasable set A can be removed without destroying quantum information. In this case, according to the cleaning Lemma[BPT10], the logical operators of the original code can all be chosen with the support outside A. From here, with the help of Eqs. (5.1) and (5.2), one obtains

Statement 1. *Consider a CSS code $\mathcal{Q} \equiv \mathrm{css}(P, Q)$ on qubit set V of cardinality $|V| = n$, encoding k qubits and with the CSS distances d_X, d_Z. Let $A \subset V$ be an erasable in $\mathcal{Q}$ set of qubits, and $B \equiv V \setminus A$ its complement. Then, the length-$|B|$ code $\mathcal{Q}' \equiv \mathrm{css}(P[B], Q_B)$ encodes the same number of qubits, $k' = k$, and has the CSS distances d'_X, d'_Z such that:*

$$d_X - |A| \leq d'_X \leq d_X, \quad d'_Z \geq d_Z. \tag{5.3}$$

The statement about the number of encoded qubits is true in general: an erasure code and any of the corresponding gauge-fixed codes encode the same number of qubits as the original code as long as the set A of removed qubits is erasable. (And, of course, we want to stick to erasable sets since we do not want to lose quantum information). To construct a code that encodes $k'' > k$ qubits, it is not sufficient to just remove some qubits, one has to also remove some group generators. If we do not care about the weight of stabilizer generators and start with a generic stabilizer code, a code with a decent distance may be obtained simply by dropping one of the existing stabilizer generators. Our general construction below is focused on quantum LDPC codes with weight-limited stabilizer generators:

Construction 1. *Given an original* $[[n, k, d]]$ *degenerate code with stabilizer generator weights bounded by some* $w < d$*, in order to create a degenerate "defect" code with* $k' > k$ *and* $d' > w$*,* (**i**) *remove some qubits in an erasable set,* (**ii**) *gauge fix the resulting subsystem code, and then* (**iii**) *drop one or more stabilizer generators with weights bigger than* w*.*

The gauge group $\mathcal{G} = \mathcal{S}[B]$ of the erasure code in step (**i**) has generators of weights w or smaller; generators of weight greater than w are obtained after gauge fixing in step (**ii**). This construction does not guarantee whether we get a degenerate code or not. Below, with the help of some additional assumptions, we prove several inequalities that guarantee the existence of not only degenerate defect codes with $d' > w$, but also highly-degenerate defect codes with unbounded distances.

5.3 Distance bounds for a defect in a CSS code

First, let us get general expressions for the distances d'_X, d'_Z of a CSS code with a removed Z-type generator. Given the original code $\mathrm{css}(P, Q)$, we choose a linearly-independent row of Q, u_0, as the additional type-Z logical operator, and denote Q' the corresponding matrix with the row dropped (and of the rank reduced by one). Denote

$$d_Z^{(0)} = \min_{\alpha} \mathrm{wgt}(u_0 + \alpha Q'), \tag{5.4}$$

the minimum weight of a linear combination of u_0 with the rows of Q'. Then, Eq. (5.1) gives

$$d'_Z = \min(d_Z, d_Z^{(0)}). \tag{5.5}$$

The additional type-X logical operator has to be taken from the set of detectable errors of the original code. Specifically, it has to anticommute with the element of the stabilizer being removed, but commute with the remaining operators in the stabilizer and all logical operators of the original code. In addition to the X-type logical operators of the original code, the logical operators of the new code include all errors with the same syndrome as the chosen canonical operator. Respectively, the expression for the distance reads:

$$d'_X = \min(d_X, d_X^{(0)}), \quad d_X^{(0)} = \min_{b\,:\,u_0 b^T = 1 \,\wedge\, Q' b^T = 0} \mathrm{wgt}(b). \tag{5.6}$$

The lower bounds constructed in the following two subsections both rely on geometry in a bipartite (Tanner) graph associated with the type-Z generator matrix $H_Z = Q$. Namely,

given its row-set U (check-nodes) and column-set V (value-nodes), the Tanner graph has the union $U \cup V$ as its vertex set, and an undirected edge $(u, v) \in U \times V$ for each non-zero matrix element Q_{uv}. On a graph there is a natural notion of the distance between a pair of nodes, the number of edges in the shortest path between them; a ball $\Omega_R(u_0)$ of radius R centered around u_0 is the set of all vertices at distance R or smaller from u_0. Then, an erasable region $A = \Omega_R(u_0) \cap V$ is chosen as a set of value nodes within the radius R from a check node $u_0 \in U$, subject to the condition that a row of the shortened matrix Q_B contains u_0 in its expansion over the rows of Q.

The condition is not a trivial one, as it is actually equivalent to region A being erasable in the code $\mathrm{css}(P, Q')$ formed by the original matrix $H_X \equiv P$ and the matrix Q', the original matrix Q with the row u_0 (considered linearly independent) dropped, same code as in Eqs. (5.4) to (5.6). As an equivalent but easier to check condition, one may request that row $u_0[A]$ be a linear combination of the rows of the punctured matrix $Q'[A]$ (remember that the support of u_0 is a subset of A, while u_0 is linearly independent from the rows of Q'). In addition, we use a corresponding sufficient condition as a part of lower X-distance bound in Statement 2, and formulate a related necessary condition in terms of the topological entanglement entropy associated with the defect A in Sec. 5.4.

5.3.1 Code with locally linearly-independent generators

We need a condition to guarantee a lower bound on the weight of the operator conjugate to the row u_0 removed from the matrix Q_B, see Eq. (5.6). Here, we will assume that the set

of Z-type stabilizer generators forming the rows of the matrix $H_Z = Q$ be overcomplete. That is, there be one or more linear relations between the rows of Q, and that we start with a row u_0 which takes part in such a relation.

In the case of the toric code (or any surface code on a locally planar graph without boundaries), see Fig. 5.1(a), the linear relation is simply the statement that the sum of all rows of H_Z be zero (necessarily so since each column has weight two). Such a relation exists for any matrix with even column weights, e.g., qHPs from (ℓ, m)-regular binary codes with both ℓ and m even. Further, many such linear relations exist for CSS codes forming chain complexes of length 3 or more, e.g., the D-dimensional hyperbolic[GL14, Bre18] and higher-dimensional qHP codes[ZP19] with $D > 2$.

Statement 2. *Given a CSS code* $\mathrm{css}(P, Q)$ *and a natural* R_1*, consider the bipartite Tanner graph associated with the matrix* Q*, and a ball* $W = \Omega_{2R_1}(u_0)$ *of radius* $2R_1$ *centered around the row* $u_0 \in U$*. Assume* (**a**) *that the row* u_0 *is involved in at least one linear relation with other rows of* Q*, and* (**b**) *there exists* $R_2 > R_1$ *such that all rows within radius* $2R_2$ *from the center be linearly independent of each other. Let* Q_1 *denote a full-row-rank matrix obtained from* Q *by removing some (linearly-dependent) rows outside* W*. Then weight of any* $b \in \mathbb{F}_2^{\otimes n}$ *such that the syndrome* $Q_1 b^T$ *has the only non-zero bit at the check node* u_0 *satisfies* $\mathrm{wgt}(b) \geq R_2$*, and for the complement* $B = V \setminus A$ *of any region* $A \subseteq W$*,* $\mathrm{wgt}(b[B]) \geq R_2 - R_1$.

The punctured vector $b[B]$ is a representative of the new X-type codeword in the defect code $\mathrm{css}(P[B], Q'_B)$, where Q' is obtained from Q_1 by removing u_0; the constructed bound gives $d_X^{(0)} \geq R_2 - R_1$ for the distance in Eq. (5.6).

We also note that additional, linearly-dependent with u_0, rows in Q need not have bounded weight, as long as on the Tanner graph they are located outside the ball W_2. The corresponding requirement is of course equivalent to any of the two conditions above the subsection 5.3.1 title, with $A = W_2 \cap V$. In the case of a surface code with smooth boundary, see Fig. 5.1 (b) and (c), the extra row may be chosen as the product of all plaquette generators, with the support along the actual boundary. In such a case, the lower distance bound in Statement 2 is saturated.

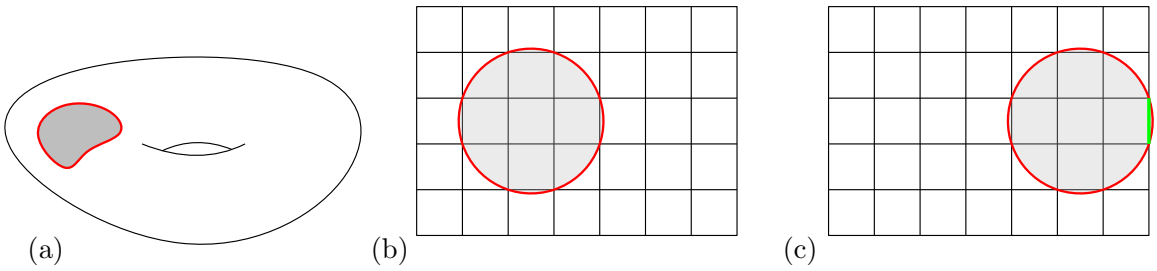

Figure 5.1: (a) Homologically trivial hole on a torus. (b) Surface code with a smooth boundary. Removing qubits (edges) inside of the circle we get a non-trivial defect. (c) This circle contains a boundary edge with no neighboring plaquette; removing the corresponding edges we again get a trivial defect.

5.3.2 Stabilizer group with an expansion

Here we construct a simple lower bound on the Z-distance of the defect, in essence, relying on the monotonicity of the distance d_Z with respect to X-basis measurement of qubits in an erasable set, see Statement 1. To make it non-trivial, we assume that Z-type stabilizer

generators of the original code satisfy an expansion condition, namely, there exists an increasing real-valued function f such that a product Π_m of any m distinct generators has weight bounded by $f(m)$,

$$\mathrm{wgt}(\Pi_m) \geq f(m), \quad f(m+1) > f(m). \tag{5.7}$$

Such a *global* condition on code generators guarantees that the boundary condition is good for the defect we are trying to construct. For example, in case of the toric code on an $L \times L$ square lattice with periodic boundary conditions, there are L^2 plaquette generators but only $L^2 - 1$ of them are independent. Namely, the product of all plaquette generators is an identity, so $m \to L^2 - m$ is a symmetry of the weight distribution. Necessarily, the function f in Eq. (5.7) has a trivial maximum, $f(L^2) \leq 0$. Respectively, a single hole in Fig. 5.1(a) has a homologically trivial boundary—meaning that it can be pushed out and eventually contracted to nothing by a sequence of single-plaquette steps. On the other hand, for a planar smooth-boundary surface code configuration as in Fig. 5.1(b), one gets $f(m)$ scaling as a perimeter of m plaquettes with a non-trivial maximum.

Generally, as one increases the set A of removed qubits, there will be rows in the shortened matrix Q_B formed as linear combinations of increasing numbers of rows of the original matrix Q. The expansion condition (5.7) with $\max_m f(m) > 0$ guarantees that the corresponding rows cannot be contracted to nothing. For example, when we remove a single qubit corresponding to a weight-ℓ column of Q, if the corresponding adjacent rows all have weights w and do not overlap (in the case of a surface code $\ell \leq 2$ and w is the number of

sides in the corresponding plaquette), the shortened matrix Q_B necessarily has $\kappa = \ell - 1$ rows of weight $2w - 2$. Assuming $f(2) = 2w - 2$, at any $w > 2$ this is already sufficient to guarantee the existence of a degenerate defect code with $d'_Z > w$.

With larger defects, combinations of larger numbers of rows may become necessary. If so, the expansion condition (5.7) will also guarantee that codes with Z-type distances (5.5) much greater than w can be constructed (assuming big enough original code distance d_Z).

Statement 3. *Given a code* $\mathrm{css}(P, Q)$ *and a natural* R_1*, consider the bipartite Tanner graph associated with the matrix* Q*, and a ball* $W = \Omega_{2R_1}(u_0)$ *of radius* $2R_1$ *centered around the row* $u_0 \in U$*. Denote* Q' *the matrix obtained by removing* u_0 *from* Q*. Assume* (**a**) *that* $A \equiv W \cap V$ *is erasable in the code* $\mathrm{css}(P, Q')$*, and* (**b**) *that the set of* Z*-generators defined by the rows of matrix* Q *satisfies the expansion condition (5.7) with* $f(2) \geq 1$*. Then, weight of any linear combination of* u_0 *with rows of the matrix* Q' *supported on the complement* $B \equiv V \setminus A$ *satisfies* $d_Z^{(0)} \geq f(R_1)$*.*

Notice that the condition (**a**) here is the same as discussed above the Section 5.3.1 title; the corresponding sufficient condition is a part of Statement 2, where any $R_2 > R_1$ will do.

5.3.3 Defect codes with arbitrary large distances

Notice that Statement 2 requires a linear *dependence* between generators of Q, while Statement 3 requires the expansion condition (5.7) with non-trivial f which is stronger than just linear *independence*. Nevertheless, these conditions are not necessarily incompatible. The condition in Statement 2 only needs to be satisfied for some parent code. For example, in

the case of a toric code, *two* distinct holes are needed in order to create a defect code with distance $d' = \min(d'_Z, d'_X) > 4$. Here a linear dependence between plaquette operators can be found in the parent toric code, one hole is needed to satisfy the conditions of Statement 3, while the other one is the actual erasable set in Construction 1.

Generally, suppose we have a parent CSS code $\mathrm{css}(H_X, H_Z)$ with bounded-weight generators, sufficiently large distance, and matrix H_Z with even-weight columns so that the sum of all rows be zero. Such a pair of matrices satisfies conditions of Statement 2 but not of Statement 3. Similar to the toric code, where one needs two holes to create a single-qubit defect, here we also may need to take an erasable set A formed by two or more disjoint erasable defects, e.g., balls as in Statement 3; that the set A be erasable can be guaranteed by the union Lemma (Lemma 2 in Ref. [BT09]). Then, one (or more if needed) balls can be used to ensure the existence of the function f in Eq. (5.7) with sufficiently large $\max_m f(m)$, while the qubits in the last remaining ball would be used as the erasable set.

Explicitly, as a parent code family, one can use, e.g., qHP codes[TZ09] created from random matrices with even-valued row and column weights. For example, $(4, 6)$-regular random matrices would do well, leading to qHP codes with asymptotically finite rates, whose CSS generator matrices have column weights 4 and 6, regular row weights $w = 10$, and $\mathcal{O}(n^{1/2})$ linear relations between the rows of generator matrices with number of non-zero coefficients in each linear relation scaling linearly with block length n of the resulting code. The distance of such parent codes grows as $\mathcal{O}(n^{1/2})$; this is sufficient to ensure that for any $d_0 > 0$ one can choose n large enough so that sufficiently large erasable balls exist to guarantee the existence of defect codes with $d' \equiv \max(d'_X, d'_Z) \geq d_0$.

5.4 Relation with topological entanglement entropy

There exists a suggestive parallel between the structure of a large-distance qubit-carrying defect we discussed, and (generalized) topological entanglement entropy (TEE) which can be associated with such a defect[KP06b, LW06]. The latter may be defined in terms of the usual entanglement entropy (EE), which characterizes what happens when some of the qubits carrying a normalized quantum state $|\psi\rangle \in \mathcal{H}_2^{\otimes n}$ are erased (traced over). Namely, if the set of qubits is decomposed into A and its complement $B = V \setminus A$, one considers the binary von Neumann entropy $\Upsilon(A;B) \equiv -\operatorname{tr}_B \rho_B \log_2 \rho_B$, where the density matrix $\rho_B = \operatorname{tr}_A |\psi\rangle\langle\psi|$ is obtained by tracing over the qubits in A. The definition is actually symmetric with respect to interchanging A and B, $\Upsilon(A;B) = \Upsilon(B;A)$.

When $|\psi\rangle$ is a stabilizer state[FCY+04], the entanglement entropy has a particularly simple form. Such a state is just a stabilizer code encoding no qubits, so that its dimension is $2^0 = 1$. With $n = |V|$ total qubits, this requires a stabilizer group with n independent generators. According to Fattal et al.[FCY+04], the EE of any stabilizer state $|\psi\rangle \in \mathcal{Q}$ is uniquely determined by the decomposition of the stabilizer group $\mathcal{S} = \mathcal{S}_A \times \mathcal{S}_B \times \mathcal{S}_{AB}$, where non-trivial elements of subgroups $\mathcal{S}_A$ and $\mathcal{S}_B$ are supported only on A and only on B, respectively, and those of $\mathcal{S}_{AB}$ are necessarily split between A and B. Namely, $\operatorname{rank} \mathcal{S}_{AB} = 2p$ is always even, and it is this p (or, equivalently, the number of EPR pairs split between A and B) that determines the entanglement entropy,

$$\Upsilon(A;B) = p \equiv \frac{1}{2} \operatorname{rank} \mathcal{S}_{AB}. \tag{5.8}$$

Given a stabilizer code $\mathcal{Q}$ with parameters $[[n, k, d]]$ and a stabilizer group $\mathcal{S}$ of rank $n-k$, a stabilizer state $|\psi\rangle \in \mathcal{Q}$ can be formed by adding any k mutually commuting logical Pauli operators to the stabilizer group. Then, if set $A \subset V$ is erasable, according to the cleaning lemma[BPT10], we can select all logical operators with the support in $B = V \setminus A$. With the logical operators in $\mathcal{S}_B$, both $\mathcal{S}_A$ and $\mathcal{S}_{AB}$ are subgroups of the stabilizer group $\mathcal{S}$ of our original code, and the entanglement entropy is given by the same Eq. (5.8). The same quantity p can also be expressed in terms of the punctured stabilizer group $\mathcal{S}[B] = \mathcal{S}_B \times \mathcal{S}_{AB}[B]$ (gauge group of the subsystem erasure code), written as a product of its center, the (shortened) stabilizer group $\mathcal{S}_B$, and p pairs of canonically conjugated "gauge" qubits which generate the (punctured) subgroup $\mathcal{S}_{AB}[B]$.

In the case of a CSS code, such a decomposition exists for both X-type and Z-type subgroups of the stabilizer, e.g., $\mathcal{S}^{(Z)} = \mathcal{S}_A^{(Z)} \times \mathcal{S}_B^{(Z)} \times \mathcal{S}_{AB}^{(Z)}$, with $\operatorname{rank} \mathcal{S}_{AB}^{(Z)} = \operatorname{rank} \mathcal{S}_{AB}^{(X)} = p$. These p independent generators are obtained from the rows of the original generator matrices that are split between A and B. In a weight-limited LDPC code, the total number of such rows, e.g., in H_Z, can be called the perimeter $L(A; B)$ of the cut. However, the number of generators of $\mathcal{S}_{AB}^{(Z)}$ can actually be smaller than $L(A; B)$ since some linear combination(s) of the generators split between A and B combined with other generators may form an element of $\mathcal{S}_A$ or $\mathcal{S}_B$. Thus, we can write EE as

$$\Upsilon(A; B) = L - \gamma, \tag{5.9}$$

with $L = L(A;B)$ the perimeter of the cut and some integer $\gamma \equiv \gamma(A;B) \geq 0$. While this expression strongly resembles the Kitaev-Preskill definition of TEE [KP06b, LW06], for now γ is just a parameter associated with the particular cut.

Let us now consider weights of generators of $\mathcal{S}_B^{(Z)}$. These correspond to the rows of Q_B. Clearly, each row of the original matrix Q may be supported in A, or in B, or be split between the two sets. Rows already supported in B can be moved directly to Q_B and preserve their original weights. Thus no more than $\gamma \geq 0$ generators of $\mathcal{S}_B^{(Z)}$ may need to have larger weights. Necessarily, if we want to construct a defect forming a degenerate code with the distance $d' > w$, the additional number of qubits is bounded by

$$\kappa \equiv k' - k \leq \gamma. \tag{5.10}$$

Thus, with $\gamma = 0$, the defect cannot support a degenerate code with $\kappa > 0$. However, whether or not a particular defect does, in fact, support $\kappa > 0$, also depends on the global structure of the code, e.g., the boundary conditions.

Now, let us imagine that we have a defect code with a sufficiently large distance d. Then, such a defect is also *stable* to small deformations, e.g., when B is changed to some B' as a result of up to $M < d$ steps, where at each step a single position is added or removed from the set. That is, our defect code retains the same number κ of additional qubits when we change the set B to a set B', $|B \triangle B'| \leq M$, where $B \triangle B' = (B \setminus B') \cup (B' \setminus B)$ is the symmetric set difference. For deformations such that $M + w < d$, the inequality $\gamma \geq \kappa$ must be satisfied in the course of deformations.

Now, TEE is normally considered a property of ground-state wave function of some many-body Hamiltonian, while our focus was on quantum LDPC codes with bounded-weight but not necessarily local generators. Different terms in a Hamiltonian can be viewed as generators of the code. However, in the absence of locality, why would we care about weights of terms in a quantum spin Hamiltonian?

In a physical system, multi-qubit Pauli operators may appear as terms in an n-spin quantum Hamiltonian, e.g.,

$$H_0 = -A \sum_a P_a - B \sum_b Q_b, \tag{5.11}$$

where and $A > 0$ and $B > 0$ are the coupling constants, and, to connect with our discussion of CSS codes, P_a and Q_b could be Pauli operators of X- and Z-type, respectively, specified by rows of the binary matrices P and Q. Then, if all terms in the Hamiltonian commute, i.e., $PQ^T = 0$, the ground state space of H_0 is exactly the code with the stabilizer group generated by these operators.

Any simple spin Hamiltonian (5.11) is usually just the leading-order approximation to a real problem. Even at zero temperature, additional interaction terms are virtually always present. Such terms may break the degeneracy of the ground state of the Hamiltonian H_0. The effect is weak if the code has a large distance, while perturbations be small and local. The standard example is the effect of an external magnetic field $\mathbf{h} = (h_x, h_y, h_z)$, which can be introduced as an additional perturbation Hamiltonian

$$H_1 = -\frac{1}{2} \sum_i (h_x X_i + h_y Y_i + h_z Z_i). \tag{5.12}$$

For a code with distance d, only a Pauli operator of weight d or larger may act within the code. Respectively, assuming the magnetic field small, degenerate perturbation theory gives the ground state subspace energy splitting scaling as $\mathcal{O}(h^d)$, where $h = |\mathbf{h}|$ is the field magnitude.

However, the code distance d gives only a part of the story. Large-weight operators appearing in H_0 make the ground-state order particularly susceptible to local perturbations such as the magnetic field. In this case the relevant scale for the magnetic field is $Wh \sim \max(A, B)$, that is, the effect of the magnetic field may be magnified by the operator weight W. Indeed, if we start with the spin-polarized ground state of H_1, a weight-W Pauli operator will generically flip W spins, producing a state with the energy increased by $\mathcal{O}(Wh)$. The effect of such a perturbation will be small as long as the corresponding coefficient, A or B in Eq. (5.11), remains small compared to Wh. Thus, with W large, the ground state of the spin Hamiltonian H_0 gets destroyed already with very small $h \sim \max(A, B)/W$. The same estimate can be also obtained with the help of an exact operator map similar to that used by Trebst et al.[TWT+07].

5.5 Discussion and Conclusions

To summarize, we discussed a general approach to adding logical qubits to an existing quantum stabilizer code, with the focus on quantum LDPC codes with weight-limited stabilizer generators. In short, a stabilizer generator needs to be promoted to a logical operator, which puts a bound on the distance of the obtained code in terms of the generator weight

w. As in a surface code, a degenerate code can be obtained by removing some qubits in an erasable set, and gauge-fixing the resulting subsystem code in such a way as to ensure that stabilizer generators of sufficiently large weight be created. We also constructed some lower bounds on the distance of thus obtained defect codes which show that construction can in principle be used to obtain highly degenerate codes with distances much larger than w.

An interesting observation is a relation between the ability of a particular defect (erasable set of qubits) to support an additional logical qubit in a degenerate code, and a quantity analogous to TEE, γ. A degenerate defect code can be only created with $\gamma > 0$. Further, when a defect code has a large distance d', a lower bound on $\gamma > 0$ is maintained in the course of deformations, not unlike for the conventionally defined TEE.

Many open problems remain. First, our lower distance bounds are constructed by analogy with surface codes. In particular, the lower bound in Statement 2 applies only for a single qubit. In addition, we do not have good lower distance bounds for defects in non-CSS codes.

Second, the notion of generalized TEE γ in Eq. (5.9) needs to be cleaned up. Here we are working with lattice systems, not necessarily local, and the usual expansions in term of $1/L$ do not necessarily help. Further, as defined, γ certainly depends of the chosen set of generators. Redundant sets of small-weight generators imply the existence of higher homologies, as in higher-dimensional toric codes; it would be nice to be able to interpret values of γ, as, e.g., was done by Grover et al. in a field theory setting[GTV11].

Third, if we start with a finite-rate family of codes, are there defects of size $|A|$ with $\gamma = \mathcal{O}(|A|)$? Coming back to defect codes, it appears that a typical defect with large γ

would generically lead to an entire spectrum of operator weights in the generators of $\mathcal{S}_B$. Is there a situation when there is a large gap in this weight distribution, as in the surface codes with $\gamma = 1$, where only one high-weight operator may exist?

Chapter 6

Summary and Outlook

This thesis investigates four distinct but interconnected studies. One of the focuses is on disentangling conditions in multipartite Abelian and non-Abelian topological fluids, such as the general Laughlin and Moore-Read states. By studying the inseparability of the density of states of Ising twisted fields that arise in multipartite entanglement, we suspect that such obstructions generally occur in non-Abelian topological states. These obstructions are likely caused by the scrambling of the density matrix associated with the super-selection sectors of non-Abelian anyons.

In a separate work, we refines the notion of generalized topological entanglement entropy (TEE) and its relation to quantum error correction, which enables the addition of logical qubits to quantum LDPC codes through topological defects. Therefore, advancing our understanding of how much entanglement is required for non-local quantum error correction.

In terms of implications for future applications in topological quantum computing, we have developed a universal framework using symmetry factorization and the coupled-wire model construction to predict novel bosonic fractional quantum Hall states, unified spin liquids, superconducting states, and fractional quantum Hall states. All of these can be traced back to the electronic origin of 1D quantum wires, which host fractional quasiparticles emerging from strongly interacting bosonic and electronic states.

Additionally, we discovered branching rules that allow us to construct various anyon chains explicitly out of local electronic states. These particles consist of emergent non-local Dirac fermions, Majorana fermions, Ising, Fibonacci, and metaplectic anyons, some of which are capable of building anyon qubits and universal quantum gates.

It remains unknown whether there exists a single gapless parent state that may host various fractional E_8 states, spin liquids, and superconducting states. Finding such a gapless parent state candidate is of significant interest in theoretical physics. Besides, by solving ground states of such a unified, exactly solvable model, we can prove the conjecture that non-Abelian topological fluids are generally unable to disentangle due to the presence of long-range entangled quasiparticle excitations, even if the disentangling conditions (2.4) are satisfied. Moreover, it is of practical interest to construct various anyon qubits and topological quantum gates explicitly using the branching rules we discovered.

To make scalable quantum computers a reality, we must look for novel materials and experimental breakthroughs. Promising candidates for realizing the coupled-wire model include Gallium Arsenide, superconducting thin slab devices, carbon nanotubes, or possible exper-

iments in cold atom setting. However, it remains crucial and urgent to develop efficient quantum error correction algorithms or schemes to help reduce the overhead of current quantum processors.

Bibliography

[aFLH+22] Yu ang Fan, Yingcheng Li, Yuting Hu, Yishan Li, Xinyue Long, Hongfeng Liu, Xiaodong Yang, Xinfang Nie, Jun Li, Tao Xin, Dawei Lu, and Yidun Wan. Experimental realization of a topologically protected hadamard gate via braiding fibonacci anyons, 2022.

[Bac06] Dave Bacon. Operator quantum error-correcting subsystems for self-correcting quantum memories. *Phys. Rev. A*, 73:012340, Jan 2006.

[Bak03] A. Baker. *Matrix Groups: An Introduction to Lie Group Theory*. Springer, 2003.

[BB87] F. Alexander Bais and Peter G. Bouwknegt. A Classification of Subgroup Truncations of the Bosonic String. *Nucl. Phys. B*, 279:561, 1987.

[BBCW19a] Maissam Barkeshli, Parsa Bonderson, Meng Cheng, and Zhenghan Wang. Symmetry fractionalization, defects, and gauging of topological phases. *Phys. Rev. B*, 100:115147, Sep 2019.

[BBCW19b] Maissam Barkeshli, Parsa Bonderson, Meng Cheng, and Zhenghan Wang. Symmetry fractionalization, defects, and gauging of topological phases. *Phys. Rev. B*, 100:115147, Sep 2019.

[BCDP96] David Beckman, Amalavoyal N. Chari, Srikrishna Devabhaktuni, and John Preskill. Efficient networks for quantum factoring. *Phys. Rev. A*, 54:1034–1063, Aug 1996.

[BMD09] H Bombin and M A Martin-Delgado. Quantum measurements and gates by code deformation. *Journal of Physics A: Mathematical and Theoretical*, 42(9):095302, feb 2009.

[Bom10] H. Bombin. Topological subsystem codes. *Phys. Rev. A*, 81:032301, Mar 2010.

[BPT10] Sergey Bravyi, David Poulin, and Barbara Terhal. Tradeoffs for reliable quantum information storage in 2d systems. *Phys. Rev. Lett.*, 104:050503, Feb 2010.

[Bre18] Nikolas P. Breuckmann. Phd thesis: Homological quantum codes beyond the toric code, 2018.

[BRU16] On the classification of weakly integral modular categories. *Journal of Pure and Applied Algebra*, 220(6):2364–2388, 2016.

[BS09] F. A. Bais and J. K. Slingerland. Condensate-induced transitions between topologically ordered phases. *Phys. Rev. B*, 79:045316, Jan 2009.

[BT09] Sergey Bravyi and Barbara Terhal. A no-go theorem for a two-dimensional self-correcting quantum memory based on stabilizer codes. *New Journal of Physics*, 11(4):043029, apr 2009.

[BT16] Nikolas P. Breuckmann and Barbara M. Terhal. Constructions and noise threshold of hyperbolic surface codes. *IEEE Transactions on Information Theory*, 62(6):3731–3744, 2016.

[Bur18] F. J. Burnell. Anyon Condensation and Its Applications. *Annual Review of Condensed Matter Physics*, 9:307–327, March 2018.

[Cas13] C. Castelnovo. Negativity and topological order in the toric code. *Phys. Rev. A*, 88:042319, Oct 2013.

[CCM+14] Jennifer Cano, Meng Cheng, Michael Mulligan, Chetan Nayak, Eugeniu Plamadeala, and Jon Yard. Bulk-edge correspondence in (2+ 1)-dimensional abelian topological phases. *Physical Review B*, 89(11):115116, 2014.

[CCT12] Pasquale Calabrese, John Cardy, and Erik Tonni. Entanglement negativity in quantum field theory. *Phys. Rev. Lett.*, 109:130502, Sep 2012.

[CCT14] Pasquale Calabrese, John Cardy, and Erik Tonni. Finite temperature entanglement negativity in conformal field theory. *Journal of Physics A: Mathematical and Theoretical*, 48(1):015006, dec 2014.

[CER20] Valentin Crépel, Benoit Estienne, and Nicolas Regnault. Microscopic study of the coupled-wire construction and plausible realization in spin-dependent optical lattices. *Phys. Rev. B*, 101:235158, Jun 2020.

[CGLW13] Xie Chen, Zheng-Cheng Gu, Zheng-Xin Liu, and Xiao-Gang Wen. Symmetry protected topological orders and the group cohomology of their symmetry group. *Phys. Rev. B*, 87:155114, Apr 2013.

[CGS18] Eyal Cornfeld, Moshe Goldstein, and Eran Sela. Imbalance entanglement: Symmetry decomposition of negativity. *Phys. Rev. A*, 98:032302, Sep 2018.

[Che18] Meng Cheng. Microscopic theory of surface topological order for topological crystalline superconductors. *Phys. Rev. Lett.*, 120:036801, Jan 2018.

[CHM15] Jennifer Cano, Taylor L. Hughes, and Michael Mulligan. Interactions along an entanglement cut in 2 + 1D abelian topological phases. *Phys. Rev. B*, 92:075104, Aug 2015.

[CHR14] Horacio Casini, Marina Huerta, and José Alejandro Rosabal. Remarks on entanglement entropy for gauge fields. *Phys. Rev. D*, 89:085012, Apr 2014.

[CHRB11] Anushya Chandran, M. Hermanns, N. Regnault, and B. Andrei Bernevig. Bulk-edge correspondence in entanglement spectra. *Phys. Rev. B*, 84:205136, Nov 2011.

[CHZ02] Andrea Cappelli, Marina Huerta, and Guillermo R. Zemba. Thermal transport in chiral conformal theories and hierarchical quantum Hall states. *Nuclear Physics B*, 636(3):568–582, August 2002.

[CKS14] Anushya Chandran, Vedika Khemani, and S. L. Sondhi. How universal is the entanglement spectrum? *Phys. Rev. Lett.*, 113:060501, Aug 2014.

[CKW00] Valerie Coffman, Joydip Kundu, and William K. Wootters. Distributed entanglement. *Phys. Rev. A*, 61:052306, Apr 2000.

[CRTR17] Xiao Chen, Abhishek Roy, Jeffrey C. Y. Teo, and Shinsei Ryu. From orbifolding conformal field theories to gauging topological phases. *Phys. Rev. B*, 96:115447, Sep 2017.

[CS96] A. R. Calderbank and Peter W. Shor. Good quantum error-correcting codes exist. *Phys. Rev. A*, 54:1098–1105, Aug 1996.

[CS13] John Horton Conway and Neil James Alexander Sloane. *Sphere packings, lattices and groups*, volume 290. Springer Science & Business Media, 2013.

[CTC14] Andrea Coser, Erik Tonni, and Pasquale Calabrese. Entanglement negativity after a global quantum quench. *Journal of Statistical Mechanics: Theory and Experiment*, 2014(12):P12017, dec 2014.

[CW15] Shawn X. Cui and Zhenghan Wang. Universal quantum computation with metaplectic anyons. *Journal of Mathematical Physics*, 56(3):032202, 03 2015.

[Del13] Nicolas Delfosse. Tradeoffs for reliable quantum information storage in surface codes and color codes. In *2013 IEEE International Symposium on Information Theory*, pages 917–921, 2013.

[DF84] Vl.S. Dotsenko and V.A. Fateev. Conformal algebra and multipoint correlation functions in 2d statistical models. *Nuclear Physics B*, 240(3):312–348, 1984.

[DFLN08a] Shiying Dong, Eduardo Fradkin, Robert G. Leigh, and Sean Nowling. Topological entanglement entropy in chern-simons theories and quantum hall fluids. *Journal of High Energy Physics*, 2008(05):016, may 2008.

[DFLN08b] Shiying Dong, Eduardo Fradkin, Robert G. Leigh, and Sean Nowling. Topological entanglement entropy in Chern-Simons theories and quantum Hall fluids. *Journal of High Energy Physics*, 2008(5):016, May 2008.

[DHVW85] L. Dixon, J.A. Harvey, C. Vafa, and E. Witten. Strings on orbifolds. *Nuclear Physics B*, 261:678–686, 1985.

[DHVW86] L. Dixon, J. Harvey, C. Vafa, and E. Witten. Strings on orbifolds (ii). *Nuclear Physics B*, 274(2):285–314, 1986.

[DKLP02] Eric Dennis, Alexei Kitaev, Andrew Landahl, and John Preskill. Topological quantum memory. *Journal of Mathematical Physics*, 43(9):4452–4505, 09 2002.

[DKP15] Ilya Dumer, Alexey A. Kovalev, and Leonid P. Pryadko. Thresholds for correcting errors, erasures, and faulty syndrome measurements in degenerate quantum codes. *Phys. Rev. Lett.*, 115:050502, Jul 2015.

[DQW21] Xi Dong, Xiao-Liang Qi, and Michael Walter. Holographic entanglement negativity and replica symmetry breaking. *Journal of High Energy Physics*, 2021(6), June 2021.

[DVC00] W. Dür, G. Vidal, and J. I. Cirac. Three qubits can be entangled in two inequivalent ways. *Phys. Rev. A*, 62:062314, Nov 2000.

[DVV88] Robbert Dijkgraaf, Erik Verlinde, and Herman Verlinde. $C = 1$ conformal field theories on Riemann surfaces. *Communications in Mathematical Physics*, 115(4):649 – 690, 1988.

[DVVV89] Robbert Dijkgraaf, Cumrun Vafa, Erik Verlinde, and Herman Verlinde. The operator algebra of orbifold models. *Communications in Mathematical Physics*, 123(3):485 – 526, 1989.

[EMSS89a] Shmuel Elitzur, Gregory Moore, Adam Schwimmer, and Nathan Seiberg. Remarks on the canonical quantization of the chern-simons-witten theory. *Nuclear Physics B*, 326(1):108–134, 1989.

[EMSS89b] Shmuel Elitzur, Gregory W. Moore, Adam Schwimmer, and Nathan Seiberg. Remarks on the Canonical Quantization of the Chern-Simons-Witten Theory. *Nucl. Phys. B*, 326:108–134, 1989.

[EZ14] Viktor Eisler and Zoltán Zimborás. Entanglement negativity in the harmonic chain out of equilibrium. *New Journal of Physics*, 16(12):123020, dec 2014.

[FAT91] V.A. FATEEV. Integrable deformations in zn-symmetrical models of the conformal quantum field theory. *International Journal of Modern Physics A*, 06(12):2109–2132, 1991.

[FCY+04] David Fattal, Toby S. Cubitt, Yoshihisa Yamamoto, Sergey Bravyi, and Isaac L. Chuang. Entanglement in the stabilizer formalism, 2004.

[FGB13] Chen Fang, Matthew J. Gilbert, and B. Andrei Bernevig. Entanglement spectrum classification of C_n-invariant noninteracting topological insulators in two dimensions. *Phys. Rev. B*, 87:035119, Jan 2013.

[Fid10] Lukasz Fidkowski. Entanglement spectrum of topological insulators and superconductors. *Phys. Rev. Lett.*, 104:130502, Apr 2010.

[FMS12] Philippe Francesco, Pierre Mathieu, and David Sénéchal. *Conformal field theory*. Springer Science & Business Media, 2012.

[FW53] R. Franz and G. Wiedemann. Ueber die wärme-leitungsfähigkeit der metalle. *Annalen der Physik*, 165(8):497–531, 1853.

[Gep87] Doron Gepner. New conformal field theories associated with lie algebras and their partition functions. *Nuclear Physics B*, 290:10–24, 1987.

[GG18] Gilad Gour and Yu Guo. Monogamy of entanglement without inequalities. *Quantum*, 2:81, August 2018.

[Gia03] Thierry Giamarchi. *Quantum physics in one dimension*, volume 121. Clarendon press, 2003.

[Gin88] P. Ginsparg. Curiosities at c = 1. *Nuclear Physics B*, 295(2):153–170, 1988.

[GL14] Larry Guth and Alexander Lubotzky. Quantum error correcting codes and 4-dimensional arithmetic hyperbolic manifolds. *Journal of Mathematical Physics*, 55(8):082202, 08 2014.

[GN74] David J. Gross and André Neveu. Dynamical symmetry breaking in asymptotically free field theories. *Phys. Rev. D*, 10:3235–3253, Nov 1974.

[GPW05] Berry Groisman, Sandu Popescu, and Andreas Winter. Quantum, classical, and total amount of correlations in a quantum state. *Phys. Rev. A*, 72:032317, Sep 2005.

[GSF21] Hart Goldman, Ramanjit Sohal, and Eduardo Fradkin. Composite particle construction of the fibonacci fractional quantum hall state. *Phys. Rev. B*, 103:235118, Jun 2021.

[GTV11] Tarun Grover, Ari M. Turner, and Ashvin Vishwanath. Entanglement entropy of gapped phases and topological order in three dimensions. *Phys. Rev. B*, 84:195120, Nov 2011.

[GWW91] Martin Greiter, Xiao-Gang Wen, and Frank Wilczek. Paired hall state at half filling. *Phys. Rev. Lett.*, 66:3205–3208, Jun 1991.

[Hal95] F. D. M. Haldane. Stability of chiral luttinger liquids and abelian quantum hall states. *Phys. Rev. Lett.*, 74:2090–2093, Mar 1995.

[HC18] O. Hart and C. Castelnovo. Entanglement negativity and sudden death in the toric code at finite temperature. *Phys. Rev. B*, 97:144410, Apr 2018.

[HCRB11] M. Hermanns, A. Chandran, N. Regnault, and B. Andrei Bernevig. Haldane statistics in the finite-size entanglement spectra of $1/m$ fractional quantum hall states. *Phys. Rev. B*, 84:121309, Sep 2011.

[HD15] Marianne Hoogeveen and Benjamin Doyon. Entanglement negativity and entropy in non-equilibrium conformal field theory. *Nuclear Physics B*, 898:78 – 112, 2015.

[HHH96] Michał Horodecki, Paweł Horodecki, and Ryszard Horodecki. Separability of mixed states: necessary and sufficient conditions. *Physics Letters A*, 223(1):1–8, 1996.

[HIZ05] Alioscia Hamma, Radu Ionicioiu, and Paolo Zanardi. Ground state entanglement and geometric entropy in the kitaev model. *Physics Letters A*, 337(1):22 – 28, 2005.

[HJPW04] Patrick Hayden, Richard Jozsa, Denes Petz, and Andreas Winter. Structure of states which satisfy strong subadditivity of quantum entropy with equality. *Communications in Mathematical Physics*, 246(2):359–374, Apr 2004.

[HKM19] Aaron Hui, Eun-Ah Kim, and Michael Mulligan. Non-abelian bosonization and modular transformation approach to superuniversality. *Phys. Rev. B*, 99:125135, Mar 2019.

[HNW13] Matthew B. Hastings, Chetan Nayak, and Zhenghan Wang. Metaplectic anyons, majorana zero modes, and their computational power. *Phys. Rev. B*, 87:165421, Apr 2013.

[HNW14] Matthew B. Hastings, Chetan Nayak, and Zhenghan Wang. On metaplectic modular categories and their applications. *Communications in Mathematical Physics*, 330(1):45–68, April 2014.

[HS16] Po-Shen Hsin and Nathan Seiberg. Level/rank Duality and Chern-Simons-Matter Theories. *JHEP*, 09:095, 2016.

[HST] Yichen Hu, Ramanjit Sohal, and Jeffrey C. Y. Teo. to appear soon.

[HV15] Huan He and Guifre Vidal. Disentangling theorem and monogamy for entanglement negativity. *Phys. Rev. A*, 91:012339, Jan 2015.

[IBM22] IBM Newsroom. IBM Unveils 400+ Qubit Quantum Processor and Next Generation IBM Quantum System Two, 2022.

[Jai20] J. K. Jain. Thirty Years of Composite Fermions and Beyond. *arXiv e-prints*, page arXiv:2011.13488, November 2020.

[Kac68] V. G. Kac. Simple irreducible graded lie algebras of finite growth. *Math. USSR-Izv.*, 2(6):1271–1311, 1968.

[KF97] C. L. Kane and Matthew P. A. Fisher. Quantized thermal transport in the fractional quantum hall effect. *Phys. Rev. B*, 55:15832–15837, Jun 1997.

[KFNRT20] Jonah Kudler-Flam, Masahiro Nozaki, Shinsei Ryu, and Mao Tian Tan. Quantum vs. classical information: operator negativity as a probe of scrambling. *Journal of High Energy Physics*, 2020(1):31, 2020.

[Kia06] A. Kiaev. Anyons in an exactly solved model and beyond. *Annals of Physics*, 321(2), 2006.

[Kit] A. Kitaev. http://online.kitp.ucsb.edu/online/topomat11/kitaev.

[Kit03] A. Yu. Kitaev. Fault-tolerant quantum computation by anyons. *Annals of Physics*, 303(1):2–3–0, January 2003.

[Kit06] Alexei Kitaev. Anyons in an exactly solved model and beyond. *Annals of Physics*, 321(1):2–111, 2006.

[KML02] C. L. Kane, Ranjan Mukhopadhyay, and T. C. Lubensky. Fractional quantum hall effect in an array of quantum wires. *Phys. Rev. Lett.*, 88:036401, Jan 2002.

[KP06a] Alexei Kitaev and John Preskill. Topological entanglement entropy. *Phys. Rev. Lett.*, 96:110404, Mar 2006.

[KP06b] Alexei Kitaev and John Preskill. Topological entanglement entropy. *Phys. Rev. Lett.*, 96:110404, 2006.

[KP13a] Alexey A. Kovalev and Leonid P. Pryadko. Fault tolerance of quantum low-density parity check codes with sublinear distance scaling. *Phys. Rev. A*, 87:020304, Feb 2013.

[KP13b] Alexey A. Kovalev and Leonid P. Pryadko. Quantum kronecker sum-product low-density parity-check codes with finite rate. *Phys. Rev. A*, 88:012311, Jul 2013.

[KP19] A. Krishna and D. Poulin. Fault-tolerant gates on hypergraph product codes. Unpublished, 2019.

[KTH14] Mayukh Nilay Khan, Jeffrey C. Y. Teo, and Taylor L. Hughes. Anyonic symmetries and topological defects in abelian topological phases: An application to the *ade* classification. *Phys. Rev. B*, 90:235149, Dec 2014.

[LATM21] Pak Kau Lim, Hamed Asasi, Jeffrey C. Y. Teo, and Michael Mulligan. Disentangling $(2+1)$D topological states of matter with entanglement negativity. *Phys. Rev. B*, 104:115155, Sep 2021.

[Lau83] R. B. Laughlin. Anomalous quantum hall effect: An incompressible quantum fluid with fractionally charged excitations. *Phys. Rev. Lett.*, 50:1395–1398, May 1983.

[LBH10] Andreas M Läuchli, Emil J Bergholtz, and Masudul Haque. Entanglement scaling of fractional quantum hall states through geometric deformations. *New Journal of Physics*, 12(7):075004, jul 2010.

[LFFO13] Rex Lundgren, Yohei Fuji, Shunsuke Furukawa, and Masaki Oshikawa. Entanglement spectra between coupled tomonaga-luttinger liquids: Applications to ladder systems and topological phases. *Phys. Rev. B*, 88:245137, Dec 2013.

[LG20] Tsung-Cheng Lu and Tarun Grover. Structure of quantum entanglement at a finite temperature critical point. *Phys. Rev. Res.*, 2:043345, Dec 2020.

[LH08] Hui Li and F. D. M. Haldane. Entanglement spectrum as a generalization of entanglement entropy: Identification of topological order in non-abelian fractional quantum hall effect states. *Phys. Rev. Lett.*, 101:010504, Jul 2008.

[LHG20] Tsung-Cheng Lu, Timothy H. Hsieh, and Tarun Grover. Detecting topological order at finite temperature using entanglement negativity. *Phys. Rev. Lett.*, 125:116801, Sep 2020.

[LHR07] Michael Levin, Bertrand I. Halperin, and Bernd Rosenow. Particle-hole symmetry and the pfaffian state. *Phys. Rev. Lett.*, 99:236806, Dec 2007.

[LMC91] Michael Lässig, Giuseppe Mussardo, and John L. Cardy. The scaling region of the tricritical ising model in two dimensions. *Nuclear Physics B*, 348(3):591–618, 1991.

[LMT23] Pak Kau Lim, Michael Mulligan, and Jeffrey C. Y. Teo. Partial fillings of the bosonic E_8 quantum hall state. *Phys. Rev. B*, 108:035136, Jul 2023.

[LQHT19] Pedro L. S. Lopes, Victor L. Quito, Bo Han, and Jeffrey C. Y. Teo. Non-abelian twist to integer quantum hall states. *Phys. Rev. B*, 100:085116, Aug 2019.

[LRNF07] Sung-Sik Lee, Shinsei Ryu, Chetan Nayak, and Matthew P. A. Fisher. Particle-hole symmetry and the $\nu = \frac{5}{2}$ quantum hall state. *Phys. Rev. Lett.*, 99:236807, Dec 2007.

[LSP21] Pak Kau Lim, Kirill Shtengel, and Leonid P. Pryadko. *Topological Defects in General Quantum LDPC Codes*, page 1–17. WORLD SCIENTIFIC, September 2021.

[LV12] Yuan-Ming Lu and Ashvin Vishwanath. Theory and classification of interacting integer topological phases in two dimensions: A chern-simons approach. *Phys. Rev. B*, 86:125119, Sep 2012.

[LV13] Yirun Arthur Lee and Guifre Vidal. Entanglement negativity and topological order. *Phys. Rev. A*, 88:042318, Oct 2013.

[LW06] Michael Levin and Xiao-Gang Wen. Detecting topological order in a ground state wave function. *Phys. Rev. Lett.*, 96:110405, Mar 2006.

[MCA+14] Roger S.K. Mong, David J. Clarke, Jason Alicea, Netanel H. Lindner, Paul Fendley, Chetan Nayak, Yuval Oreg, Ady Stern, Erez Berg, Kirill Shtengel, and Matthew P.A. Fisher. Universal topological quantum computation from a superconductor-abelian quantum hall heterostructure. *Phys. Rev. X*, 4:011036, Mar 2014.

[Moo68] Robert V Moody. A new class of lie algebras. *Journal of Algebra*, 10(2):211–230, 1968.

[MR91a] Gregory Moore and Nicholas Read. Nonabelions in the fractional quantum hall effect. *Nuclear Physics B*, 360(2):362–396, 1991.

[MR91b] Gregory Moore and Nicholas Read. Nonabelions in the fractional quantum hall effect. *Nuclear Physics B*, 360(2):362 – 396, 1991.

[MR96] M. Milovanović and N. Read. Edge excitations of paired fractional quantum hall states. *Phy. Rev. B*, 53(13559), 1996.

[MS83] F.J. MacWilliams and N.J.A. Sloane. *The Theory of Error-Correcting Codes*, volume 16. Elsevier, 1983.

[MS89] Gregory Moore and Nathan Seiberg. Taming the conformal zoo. *Physics Letters B*, 220(3):422–430, 1989.

[MSC+22] Xiuqi Ma, Wilbur Shirley, Meng Cheng, Michael Levin, John McGreevy, and Xie Chen. Fractonic order in infinite-component chern-simons gauge theories. *Phys. Rev. B*, 105:195124, May 2022.

[NH19] Rahul M. Nandkishore and Michael Hermele. Fractons. *Annual Review of Condensed Matter Physics*, 10(Volume 10, 2019):295–313, 2019.

[NS90] Stephen G. Naculich and Howard J. Schnitzer. Duality between su(n)k and su(k)n wzw models. *Nuclear Physics B*, 347(3):687–742, 1990.

[NSS+08a] Chetan Nayak, Steven H. Simon, Ady Stern, Michael Freedman, and Sankar Das Sarma. Non-abelian anyons and topological quantum computation. *Rev. Mod. Phys.*, 80:1083–1159, Sep 2008.

[NSS+08b] Chetan Nayak, Steven H. Simon, Ady Stern, Michael Freedman, and Sankar Das Sarma. Non-abelian anyons and topological quantum computation. *Rev. Mod. Phys.*, 80:1083–1159, Sep 2008.

[NT92] Tomoki Nakanishi and Akihiro Tsuchiya. Level-rank duality of wzw models in conformal field theory. *Communications in Mathematical Physics*, 144(2):351–372, 1 1992.

[NW96] Chetan Nayak and Frank Wilczek. 2n quasihole states realize 2n-1-dimensional spinor braiding statistics in paired quantum hall states. *Nuclear Physics B*, 479(3):529–553, 1996.

[OF07] Yong-Cheng Ou and Heng Fan. Monogamy inequality in terms of negativity for three-qubit states. *Phys. Rev. A*, 75:062308, Jun 2007.

[OKS+07] Masaki Oshikawa, Yong Baek Kim, Kirill Shtengel, Chetan Nayak, and Sumanta Tewari. Topological degeneracy of non-abelian states for dummies. *Annals of Physics*, 322(6):1477–1498, 2007.

[OT15] Kantaro Ohmori and Yuji Tachikawa. Physics at the entangling surface. *Journal of Statistical Mechanics: Theory and Experiment*, 2015(4):P04010, apr 2015.

[OV06] Tobias J. Osborne and Frank Verstraete. General monogamy inequality for bipartite qubit entanglement. *Phys. Rev. Lett.*, 96:220503, Jun 2006.

[PacBR11] Z. Papić, B. A. Bernevig, and N. Regnault. Topological entanglement in abelian and non-abelian excitation eigenstates. *Phys. Rev. Lett.*, 106:056801, Feb 2011.

[Per96] Asher Peres. Separability criterion for density matrices. *Phys. Rev. Lett.*, 77:1413–1415, Aug 1996.

[PG90] R. E. Prange and S. M Girvin. *The quantum Hall effect*. New York: Springer-Verlag, 1990.

[PHB10] Emil Prodan, Taylor L. Hughes, and B. Andrei Bernevig. Entanglement spectrum of a disordered topological chern insulator. *Phys. Rev. Lett.*, 105:115501, Sep 2010.

[PMN13] Eugeniu Plamadeala, Michael Mulligan, and Chetan Nayak. Short-range entangled bosonic states with chiral edge modes and t duality of heterotic strings. *Physical Review B*, 88(4):045131, 2013.

[Pou05] David Poulin. Stabilizer formalism for operator quantum error correction. *Phys. Rev. Lett.*, 95:230504, Dec 2005.

[PTBO10] Frank Pollmann, Ari M. Turner, Erez Berg, and Masaki Oshikawa. Entanglement spectrum of a topological phase in one dimension. *Phys. Rev. B*, 81:064439, Feb 2010.

[PV05] Martin B. Plenio and S. Virmani. An introduction to entanglement measures. *arXiv e-prints*, pages quant–ph/0504163, April 2005.

[QKL12] X.-L. Qi, H. Katsura, and A. W. W Ludwig. General relationship betwen the entanglement spectrum an the edge state spectrum of topologial quantum states. *Phys. Rev. Lett.*, 108(196402), 2012.

[Rai99] E.M. Rains. Nonbinary quantum codes. *IEEE Transactions on Information Theory*, 45(6):1827–1832, 1999.

[RBH09] N. Regnault, B. A. Bernevig, and F. D. M. Haldane. Topological entanglement and clustering of jain hierarchy states. *Phys. Rev. Lett.*, 103:016801, Jun 2009.

[RDSS13] Iván D. Rodríguez, Simon C. Davenport, Steven H. Simon, and J. K. Slingerland. *Entanglement spectrum of composite fermion states in real space*, volume 88. American Physical Society, Oct 2013.

[Rou20] Mohamed Taha Rouabah. Compiling single-qubit braiding gate for fibonacci anyons topological quantum computation, 2020.

[RR99] N. Read and E. Rezayi. Beyond paired quantum hall states: Parafermions and incompressible states in the first excited landau level. *Phys. Rev. B.*, 59:8084, 1999.

[RR14] Mukund Rangamani and Massimiliano Rota. Comments on entanglement negativity in holographic field theories. *Journal of High Energy Physics*, 2014(10), October 2014.

[Sar08] Pradeep Kiran Sarvepalli. *Quantum stabilizer codes and beyond*. Doctoral dissertation, Texas A&M University, 2008. Available electronically from https://hdl.handle.net/1969.1/86011.

[SB01] J.K. Slingerland and F.A. Bais. Quantum groups and non-abelian braiding in quantum hall systems. *Nuclear Physics B*, 612(3):229–290, 2001.

[SCMA15] E. M. Stoudenmire, David J. Clarke, Roger S. K. Mong, and Jason Alicea. Assembling fibonacci anyons from a F_3 parafermion lattice model. *Phys. Rev. B*, 91:235112, Jun 2015.

[SCMH18] Luiz H. Santos, Jennifer Cano, Michael Mulligan, and Taylor L. Hughes. Symmetry-protected topological interfaces and entanglement sequences. *Phys. Rev. B*, 98:075131, Aug 2018.

[SDC21] Joseph Sullivan, Arpit Dua, and Meng Cheng. Fractonic topological phases from coupled wires. *Phys. Rev. Res.*, 3:023123, May 2021.

[SDL20] Bowen Shi, Xin Dai, and Yuan-Ming Lu. Entanglement negativity at the critical point of measurement-driven transition. *arXiv e-prints*, page arXiv:2012.00040, November 2020.

[Sho97] Peter W. Shor. Polynomial-time algorithms for prime factorization and discrete logarithms on a quantum computer. *SIAM Journal on Computing*, 26(5):1484–1509, 1997.

[SHST20] Ramanjit Sohal, Bo Han, Luiz H. Santos, and Jeffrey C. Y. Teo. Entanglement entropy of generalized moore-read fractional quantum hall state interfaces. *Phys. Rev. B*, 102:045102, Jul 2020.

[SIW21] Joseph Sullivan, Thomas Iadecola, and Dominic J. Williamson. Planar p-string condensation: Chiral fracton phases from fractional quantum hall layers and beyond. *Phys. Rev. B*, 103:205301, May 2021.

[SL13] T. Senthil and Michael Levin. Integer quantum hall effect for bosons. *Phys. Rev. Lett.*, 110:046801, Jan 2013.

[SLKFV21] Hassan Shapourian, Shang Liu, Jonah Kudler-Flam, and Ashvin Vishwanath. Entanglement negativity spectrum of random mixed states: A diagrammatic approach. *PRX Quantum*, 2:030347, Sep 2021.

[SLZ+20] Shengqi Sang, Yaodong Li, Tianci Zhou, Xiao Chen, Timothy H. Hsieh, and Matthew P. A. Fisher. Entanglement Negativity at Measurement-Induced Criticality. *arXiv e-prints*, page arXiv:2012.00031, November 2020.

[SP08] Sankar Das Sarma and Aron Pinczuk. *Perspectives in quantum hall effects: Novel quantum liquids in low-dimensional semiconductor structures*. John Wiley & Sons, 2008.

[SRRC19] Hassan Shapourian, Paola Ruggiero, Shinsei Ryu, and Pasquale Calabrese. Twisted and untwisted negativity spectrum of free fermions. *SciPost Phys.*, 7:037, 2019.

[SSC19] Wilbur Shirley, Kevin Slagle, and Xie Chen. Universal entanglement signatures of foliated fracton phases. *SciPost Phys.*, 6:015, 2019.

[SSCT19] Alexander Sirota, Sharmistha Sahoo, Gil Young Cho, and Jeffrey C. Y. Teo. Paired parton quantum hall states: A coupled wire construction. *Phys. Rev. B*, 99:245117, Jun 2019.

[SSR17] Hassan Shapourian, Ken Shiozaki, and Shinsei Ryu. Partial time-reversal transformation and entanglement negativity in fermionic systems. *Phys. Rev. B*, 95:165101, Apr 2017.

[Ste96] A. M. Steane. Simple quantum error-correcting codes. *Phys. Rev. A*, 54:4741–4751, Dec 1996.

[SW86] A. N. Schellekens and N. P. Warner. Conformal subalgebras of kac-moody algebras. *Phys. Rev. D*, 34:3092–3096, Nov 1986.

[SZT16] Sharmistha Sahoo, Zhao Zhang, and Jeffrey C. Y. Teo. Coupled wire model of symmetric majorana surfaces of topological superconductors. *Phys. Rev. B*, 94:165142, Oct 2016.

[Teo16] Jeffrey C. Y. Teo. Globally symmetric topological phase: from anyonic symmetry to twist defect. *Journal of Physics: Condensed Matter*, 28(14):143001, 2016.

[TH23] Jeffrey C. Y. Teo and Yichen Hu. Dihedral twist liquid models from emergent majorana fermions. *Quantum*, 7:967, Mar 2023.

[THF15a] Jeffrey C.Y. Teo, Taylor L. Hughes, and Eduardo Fradkin. Theory of twist liquids: Gauging an anyonic symmetry. *Annals of Physics*, 360(0):349 – 445, 2015.

[THF15b] Jeffrey C.Y. Teo, Taylor L. Hughes, and Eduardo Fradkin. Theory of twist liquids: Gauging an anyonic symmetry. *Annals of Physics*, 360:349–445, 2015.

[TK14a] Jeffrey C. Y. Teo and C. L. Kane. From luttinger liquid to non-abelian quantum hall states. *Phys. Rev. B*, 89:085101, Feb 2014.

[TK14b] Jeffrey C.Y. Teo and C.L. Kane. From luttinger liquid to non-abelian quantum hall states. *PHYSICAL REVIEW B*, 89(085101), 2014.

[TKV16] Jeffrey C. Y. Teo, Mayukh Nilay Khan, and Smitha Vishveshwara. Topologically induced fermion parity flips in superconductor vortices. *Phys. Rev. B*, 93:245144, Jun 2016.

[TSRB10] R. Thomale, A. Sterdyniak, N. Regnault, and B. Andrei Bernevig. Entanglement gap and a new principle of adiabatic continuity. *Phys. Rev. Lett.*, 104:180502, May 2010.

[TTWL08] Simon Trebst, Matthias Troyer, Zhenghan Wang, and Andreas W. W. Ludwig. A Short Introduction to Fibonacci Anyon Models. *Progress of Theoretical Physics Supplement*, 176:384–407, 06 2008.

[TWT+07] Simon Trebst, Philipp Werner, Matthias Troyer, Kirill Shtengel, and Chetan Nayak. Breakdown of a topological phase: Quantum phase transition in a loop gas model with tension. *Phys. Rev. Lett.*, 98:070602, Feb 2007.

[TZ09] Jean-Pierre Tillich and Gilles Zemor. Quantum ldpc codes with positive rate and minimum distance proportional to $n^{\frac{1}{2}}$. In *2009 IEEE International Symposium on Information Theory*, pages 799–803, 2009.

[Ver88] Erik Verlinde. Fusion rules and modular transformations in 2d conformal field theory. *Nucl. Phys. B*, 300:360, 1988.

[VW02] G. Vidal and R. F. Werner. Computable measure of entanglement. *Phys. Rev. A*, 65:032314, Feb 2002.

[WCR15] Xueda Wen, Po-Yao Chang, and Shinsei Ryu. Entanglement negativity after a local quantum quench in conformal field theories. *Phys. Rev. B*, 92:075109, Aug 2015.

[Wen91a] X. G. Wen. Gapless boundary excitations in the quantum hall states and in the chiral spin states. *Phys. Rev. B*, 43:11025–11036, May 1991.

[Wen91b] X. G. Wen. Non-abelian statistics in the fractional quantum hall states. *Phys. Rev. Lett.*, 66:802–805, Feb 1991.

[WEN92a] XIAO-GANG WEN. Theory of the edge states in fractional quantum hall effects. *International Journal of Modern Physics B*, 06(10):1711–1762, 1992.

[Wen92b] Xiao-Gang Wen. Theory of the edge states in fractional quantum hall effects. *International journal of modern physics B*, 6(10):1711–1762, 1992.

[Wen13] Xiao-Gang Wen. Topological order: From long-range entangled quantum matter to a unified origin of light and electrons. *ISRN Condensed Matter Physics*, 2013:1–20, March 2013.

[Wil90] Frank Wilczek. *Fractional Statistics and Anyon Superconductivity.* World Scientific, 1990.

[Wit83] Edward Witten. Global aspects of current algebra. *Nuclear Physics B*, 223(2):422 – 432, 1983.

[Wit84] Edward Witten. Nonabelian bosonization in two dimensions. *Comm. Math. Phys.*, 92(4):455–472, 1984.

[WMR16] Xueda Wen, Shunji Matsuura, and Shinsei Ryu. Edge theory approach to topological entanglement entropy, mutual information, and entanglement negativity in chern-simons theories. *Phys. Rev. B*, 93:245140, Jun 2016.

[WN90] X.G. Wen and Q. Niu. Ground-sttate degeneracy of the fractional quantum hall states in the presence of a random potential and on high-genus riemann surface. *Phys. Rev. B*, 41(13), 1990.

[WZ71] J. Wess and B. Zumino. Consequences of anomalous ward identities. *Physics Letters B*, 37(1):95 – 97, 1971.

[WZ92] Xiao-Gang Wen and A. Zee. Classification of abelian quantum hall states and matrix formulation of topological fluids. *Phys. Rev. B*, 46:2290, 1992.

[Zam90] A. B. Zamolodchikov. Conformal field theory and 2-D critical phenomena. 4. Minimal models. 7 1990.

[Zém09] Gilles Zémor. On cayley graphs, surface codes, and the limits of homological coding for quantum error correction. In Yeow Meng Chee, Chao Li, San Ling, Huaxiong Wang, and Chaoping Xing, editors, *Coding and Cryptology*, pages 259–273, Berlin, Heidelberg, 2009. Springer Berlin Heidelberg.

[ZF85] A B Zamolodchikov and V A Fateev. Nonlocal (parafermion) currents in two-dimensional conformal quantum field theory and self-dual critical points in z/sub n/-symmetric statistical systems. *Sov. Phys. - JETP (Engl. Transl.), United States*, 62, 8 1985.

[ZGT+12] Yi Zhang, Tarun Grover, Ari Turner, Masaki Oshikawa, and Ashvin Vishwanath. Quasiparticle statistics and braiding from ground-state entanglement. *Phys. Rev. B*, 85:235151, Jun 2012.

[ZP19] Weilei Zeng and Leonid P. Pryadko. Higher-dimensional quantum hypergraph-product codes with finite rates. *Phys. Rev. Lett.*, 122:230501, Jun 2019.

Appendix A

Appendix

A.1 Topological data

In this appendix, we collect the charge assignment tables for current operators and quasiparticle excitations for the conformal embeddings $\mathcal{G}_A \times \mathcal{G}_B \subset E_8$ studied in the main text. Except for $SU(8)_1 \times U(1)_8 \subset (E_8)_1$, all conformal embeddings involve algebras at level 1. Therefore, aside from this case, we will not specify the levels of the algebras in the tables below to simplify the notation. In these tables, the numbers in each term $*$ $(\star)$ specify the dimension $*$ of the subspace consisting of fields with charge $\star$.

Table A.1: Current operator charge assignments for the conformal embeddings $\mathcal{G}_A \times \mathcal{G}_B \subset E_8$, where $\mathcal{G}_A$ or $\mathcal{G}_B$ is an exceptional group.

ν_{G_2}	ν_{F_4}	$\#Q_{G_2}$	$\#Q_{F_4}$
0	16	$14(0)$	$22(0), 8(\pm 2), 7(\pm 4)$
8	8	$4(0), 4(\pm 2), 1(\pm 4)$	$22(0), 14(\pm 2), 1(\pm 4)$
$\nu_{SU(2)}$	ν_{E_7}	$\#Q_{SU(2)}$	$\#Q_{E_7}$
0	16	$3(0)$	$49(0), 32(\pm 2), 10(\pm 4)$
2	14	$1(0), 1(\pm 2)$	$49(0), 35(\pm 2), 7(\pm 4)$
8	8	$1(0), 1(\pm 4)$	$67(0), 32(\pm 2), 1(\pm 4)$
$\nu_{SU(3)}$	ν_{E_6}	$\#Q_{SU(3)}$	$\#Q_{E_6}$
0	16	$8(0)$	$30(0), 16(\pm 2), 8(\pm 4)$
8/3	40/3	$4(0), 2(\pm 2)$	$28(0), 20(\pm 2), 5(\pm 4)$
8	8	$2(0), 2(\pm 2), 1(\pm 4)$	$36(0), 20(\pm 2), 1(\pm 4)$
32/3	16/3	$4(0), 2(\pm 4)$	$46(0), 16(\pm 2)$

Table A.2: Quasiparticle charge assignments for the conformal embedding $G_2 \times F_4 \subset E_8$. Below, τ refers to the nontrivial super-selection sector of the G_2 topological phase and $\bar{\tau}$ refers to the nontrivial super-selection sector of the F_4 topological phase.

ν_{G_2}	ν_{F4}	$\#(Q_\tau)_{G_2}$	$\#(Q_{\bar{\tau}})_{F_4}$
0	16	$7(0)$	$8(0), 8(\pm 2), 1(\pm 4)$
8	8	$3(0), 2(\pm 2)$	$14(0), 6(\pm 2)$

Table A.3: Quasiparticle charge assignments for the conformal embedding $SU(2) \times E_7 \subset E_8$. Below, $\mathcal{S}$ refers to the nontrivial superselection sectors of the $SU(2)$ and E_7 topological phases.

$\nu_{SU(2)}$	ν_{E_7}	$\#(Q_\mathcal{S})_{SU(2)}$	$\#(Q_\mathcal{S})_{E_7}$
0	16	$2(0)$	$20(0), 16(\pm 2), 2(\pm 4)$
2	14	$1(\pm 1)$	$21(\pm 1), 7(\pm 3)$
8	8	$1(\pm 2)$	$32(0), 12(\pm 4)$

Table A.4: Quasiparticle charge assignments for the conformal embedding $SU(3) \times E_6 \subset E_8$. Below, $\mathcal{E}$ and $\overline{\mathcal{E}}$ refer to the nontrivial superselection sectors of the $SU(3)$ and E_6 topological phases.

$\nu_{SU(3)}$	ν_{E_6}	$\#(Q_\mathcal{E})_{SU(3)}$	$\#(Q_\mathcal{E})_{E_6}$	$\#(Q_{\bar{\mathcal{E}}})_{SU(3)}$	$\#(Q_{\bar{\mathcal{E}}})_{E_6}$
0	16	$3(0)$	$9(0), 8(\pm 2), 1(\pm 4)$	$3(0)$	$9(0), 8(\pm 2), 1(\pm 4)$
8/3	40/3	$1(-\frac{4}{3}), 2(\frac{2}{3})$	$5(-\frac{8}{3}), 10(-\frac{2}{3}), 10(\frac{4}{3}), 2(\frac{10}{3})$	$2(-\frac{2}{3}), 1(\frac{4}{3})$	$2(-\frac{10}{3}), 10(-\frac{4}{3}), 10(\frac{2}{3}), 5(\frac{8}{3})$
8/3	40/3	$2(-\frac{2}{3}), 1(\frac{4}{3})$	$2(-\frac{10}{3}), 10(-\frac{4}{3}), 10(\frac{2}{3}), 5(\frac{8}{3})$	$1(-\frac{4}{3}), 2(\frac{2}{3})$	$5(-\frac{8}{3}), 10(-\frac{2}{3}), 10(\frac{4}{3}), 2(\frac{10}{3})$
8	8	$1(0), 1(\pm 2)$	$15(0), 6(\pm 2)$	$1(0), 1(\pm 2)$	$15(0), 6(\pm 2)$
32/3	16/3	$1(-\frac{8}{3}), 2(\frac{4}{3})$	$10(-\frac{4}{3}), 16(\frac{2}{3}), 1(\frac{8}{3})$	$2(-\frac{4}{3}), 1(\frac{8}{3})$	$1(-\frac{8}{3}), 16(-\frac{2}{3}), 10(\frac{4}{3})$
32/3	16/3	$2(-\frac{4}{3}), 1(\frac{8}{3})$	$1(-\frac{8}{3}), 16(-\frac{2}{3}), 10(\frac{4}{3})$	$1(-\frac{8}{3}), 2(\frac{4}{3})$	$10(-\frac{4}{3}), 16(\frac{2}{3}), 1(\frac{8}{3})$

Table A.5: Current operator charge assignments for the conformal embedding $SU(5)^A \times SU(5)^B \subseteq E_8$.

$\nu_{SU(5)^A}$	$\nu_{SU(5)^B}$	$\#(Q)_{SU(5)^A}$	$\#(Q)_{SU(5)^B}$
0	16	$24(0)$	$8(0), 4(\pm 2), 4(\pm 4)$
16/5	64/5	$16(0), 4(\pm 2)$	$16(0), 4(\pm 4)$
16/5	64/5	$16(0), 4(\pm 2)$	$10(0), 4(\pm 2), 3(\pm 4)$
24/5	56/5	$12(0), 6(\pm 2)$	$8(0), 6(\pm 2), 2(\pm 4)$
8	8	$10(0), 6(\pm 2), 1(\pm 4)$	$10(0), 6(\pm 2), 1(\pm 4)$

Table A.6: Charge assignments of the $SU(5)_1$ primary fields in $\mathcal{E}^{m=-2,-1,0,1,2}$. Here, $\mathcal{E}^0$ is the vacuum and $\mathcal{E}^{-m} = (\mathcal{E}^m)^\dagger$. We only list the charge assignments of fields in $\mathcal{E}^m$ for $m = 1, 2$.

$\nu_{SU(5)}$	$\#(Q_{\mathcal{E}^1})_{SU(5)}$	$\#(Q_{\mathcal{E}^2})_{SU(5)}$
0	$5(0)$	$10(0)$
16/5	$1(-8/5), 4(2/5)$	$4(-6/5), 6(4/5)$
16/5	$4(-2/5), 1(8/5)$	$6(-4/5), 4(6/5)$
24/5	$2(-6/5), 3(4/5)$	$1(-12/5), 6(-2/5), 3(8/5)$
24/5	$3(-4/5), 2(6/5)$	$3(-8/5), 6(2/5), 1(12/5)$
8	$3(0), 1(\pm 2)$	$4(0), 3(\pm 2)$
56/5	$1(-12/5), 2(-2/5), 2(8/5)$	$2(-14/5), 3(-4/5), 4(6/5), 1(16/5)$
56/5	$2(-8/5), 2(2/5), 1(12/5)$	$1(-16/5), 4(-6/5), 3(4/5), 2(14/5)$
64/5	$1(-16/5), 4(4/5)$	$4(-12/5), 6(8/5)$
64/5	$4(-4/5), 1(16/5)$	$6(-8/5), 4(12/5)$
64/5	$1(-14/5), 1(-4/5), 3(6/5)$	$1(-18/5), 3(-8/5), 3(2/5), 3(12/5)$
64/5	$3(-6/5), 1(4/5), 1(14/5)$	$3(-12/5), 3(-2/5), 3(8/5), 1(18/5)$
16	$1(0), 2(\pm 2)$	$4(0), 2(\pm 2), 1(\pm 4)$

Table A.7: Current operator charge assignments for the conformal embeddings $SU(8)_1 \times U(1)_8 \subseteq (E_8)_1$ and $Sp(8)_1 \times SU(2)_4 \subseteq (E_8)_1$ that involve the orbifold theories. The charge assignment in $U(1)_8$ is obtained from $b = \exp\left[\pm 2i(\tilde{\phi}_1 - \tilde{\phi}_2)\right] = \exp[\pm i(2\phi_1 - \phi_2 - \phi_4 - \phi_6 - \phi_8)]$.

$\nu_{SU(8)_1}$	$\nu_{U(1)_8}$	$\#Q_{SU(8)_1}$	$\#Q_{U(1)_8}$
7/2	25/2	$49(0), 7(\pm 2)$	$1(\pm 10)$
8	8	$31(0), 16(\pm 2)$	$1(\pm 8)$
23/2	9/2	$29(0), 15(\pm 2), 2(\pm 4)$	$1(\pm 6)$
14	2	$25(0), 16(\pm 2), 3(\pm 4)$	$1(\pm 4)$
14	2	$49(0), 7(\pm 4)$	$1(\pm 4)$
31/2	1/2	$37(0), 7(\pm 2), 6(\pm 4)$	$1(\pm 2)$
31/2	1/2	$25(0), 15(\pm 2), 4(\pm 4)$	$1(\pm 2)$
16	0	$23(0), 16(\pm 2), 4(\pm 4)$	$2(0)$
$\nu_{Sp(8)_1}$	$\nu_{SU(2)_4}$	$\#Q_{Sp(8)_1}$	$\#Q_{SU(2)_4}$
16	0	$14(0), 8(\pm 2), 3(\pm 4)$	$3(0)$

Table A.8: Quasiparticle charge assignments for the conformal embedding $SU(8)_1 \times U(1)_8 \subset (E_8)_1$. We denote the super-selection sectors of the $SU(8)_1$ and $U(1)_8$ topological phases by $\mathcal{E}^m$ with $m = -3, \ldots, 4$. Here, $\mathcal{E}^0$ is the vacuum. Because the charge assignments for $\mathcal{E}^m$ and $\mathcal{E}^{-m} = (\mathcal{E}^m)^\dagger$ are opposite, we only list the charge assignments of $\mathcal{E}^m$ sectors with $m = 1, \ldots, 4$.

$\nu_{SU(8)}$	$\nu_{U(1)_8}$	$\#(Q_{\mathcal{E}^1})_{SU(8)}$	$\#(Q_{\mathcal{E}^1})_{U(1)_8}$	$\#(Q_{\mathcal{E}^2})_{SU(8)}$	$\#(Q_{\mathcal{E}^2})_{U(1)_8}$
7/2	25/2	$7(-\frac{1}{4}), 1(\frac{7}{4})$	$1(-\frac{5}{4})$	$21(-\frac{1}{2}), 7(\frac{3}{2})$	$1(-\frac{5}{2})$
7/2	25/2	$1(-\frac{7}{4}), 7(\frac{1}{4})$	$1(\frac{5}{4})$	$7(-\frac{3}{2}), 21(\frac{1}{2})$	$1(\frac{5}{2})$
8	8	$4(\pm 1)$	$1(1)$	$6(\pm 2), 16(0)$	$1(2)$
8	8	$4(\pm 1)$	$1(-1)$	$6(\pm 2), 16(0)$	$1(-2)$
23/2	9/2	$1(-\frac{9}{4}), 5(-\frac{1}{4}), 2(\frac{7}{4})$	$1(\frac{3}{4})$	$5(-\frac{5}{2}), 12(-\frac{1}{2}), 10(\frac{3}{2}), 1(\frac{7}{2})$	$1(\frac{3}{2})$
23/2	9/2	$2(-\frac{7}{4}), 5(\frac{1}{4}), 1(\frac{9}{4})$	$1(-\frac{3}{4})$	$1(-\frac{7}{2}), 10(-\frac{3}{2}), 12(\frac{1}{2}), 5(\frac{5}{2})$	$1(-\frac{3}{2})$
14	2	$1(-\frac{5}{2}), 4(-\frac{1}{2}), 3(\frac{3}{2})$	$1(-\frac{1}{2})$	$4(-3), 9(-1), 12(1), 3(3)$	$1(-1)$
14	2	$3(-\frac{3}{2}), 4(\frac{1}{2}), 1(\frac{5}{2})$	$1(\frac{1}{2})$	$3(-3), 12(-1), 9(1), 4(3)$	$1(1)$
14	2	$7(-\frac{1}{2}), 1(\frac{7}{2})$	$1(-\frac{1}{2})$	$21(-1), 7(3)$	$1(-1)$
14	2	$1(-\frac{7}{2}), 7(\frac{1}{2})$	$1(\frac{1}{2})$	$7(-3), 21(1)$	$1(1)$
31/2	1/2	$6(-\frac{3}{4}), 1(\frac{5}{4}), 1(\frac{13}{4})$	$1(\frac{1}{4})$	$15(-\frac{3}{2}), 6(\frac{1}{2}), 6(\frac{5}{2}), 1(\frac{9}{2})$	$1(\frac{1}{2})$
31/2	1/2	$1(-\frac{13}{4}), 1(-\frac{5}{4}), 6(\frac{3}{4})$	$1(-\frac{1}{4})$	$1(-\frac{9}{2}), 6(-\frac{5}{2}), 6(-\frac{1}{2}), 15(\frac{3}{2})$	$1(-\frac{1}{2})$
31/2	1/2	$4(-\frac{5}{4}), 3(\frac{3}{4}), 1(\frac{11}{4})$	$1(-\frac{1}{4})$	$6(-\frac{5}{2}), 12(-\frac{1}{2}), 7(\frac{3}{2}), 3(\frac{7}{2})$	$1(-\frac{1}{2})$
31/2	1/2	$1(-\frac{11}{4}), 3(-\frac{3}{4}), 4(\frac{5}{4})$	$1(\frac{1}{4})$	$3(-\frac{7}{2}), 7(-\frac{3}{2}), 12(\frac{1}{2}), 6(\frac{5}{2})$	$1(\frac{1}{2})$
16	0	$2(\pm 2), 4(0)$	$1(0)$	$1(\pm 4), 8(\pm 2), 10(0)$	$1(0)$
$\nu_{SU(8)}$	$\nu_{U(1)_8}$	$\#(Q_{\mathcal{E}^3})_{SU(8)}$	$\#(Q_{\mathcal{E}^3})_{U(1)_8}$	$\#(Q_{\mathcal{E}^4})_{SU(8)}$	$\#(Q_{\mathcal{E}^4})_{U(1)_8}$
7/2	25/2	$35(-\frac{3}{4}), 21(\frac{5}{4})$	$1(-\frac{15}{4})$	$35(\pm 1)$	$1(-5)$
7/2	25/2	$21(-\frac{5}{4}), 35(\frac{3}{4})$	$1(\frac{15}{4})$	$35(\pm 1)$	$1(5)$
8	8	$4(\pm 3), 24(\pm 1)$	$1(3)$	$1(\pm 4), 16(\pm 2), 36(0)$	$1(4)$
8	8	$4(\pm 3), 24(\pm 1)$	$1(-3)$	$1(\pm 4), 16(\pm 2), 36(0)$	$1(-4)$
23/2	9/2	$10(-\frac{11}{4}), 20(-\frac{3}{4}), 21(\frac{5}{4}), 5(\frac{13}{4})$	$1(\frac{9}{4})$	$10(\pm 3), 25(\pm 1)$	$1(3)$
23/2	9/2	$5(-\frac{13}{4}), 21(-\frac{5}{4}), 20(\frac{3}{4}), 10(\frac{11}{4})$	$1(-\frac{9}{4})$	$10(\pm 3), 25(\pm 1)$	$1(-3)$
14	2	$6(-\frac{7}{2}), 16(-\frac{3}{2}), 21(\frac{1}{2}), 12(\frac{5}{2}), 1(\frac{9}{2})$	$1(-\frac{3}{2})$	$4(\pm 4), 19(\pm 2), 24(0)$	$1(-2)$
14	2	$1(-\frac{9}{2}), 12(-\frac{5}{2}), 21(-\frac{1}{2}), 16(\frac{3}{2}), 6(\frac{7}{2})$	$1(\frac{3}{2})$	$4(\pm 4), 19(\pm 2), 24(0)$	$1(2)$
14	2	$35(-\frac{3}{2}), 21(\frac{5}{2})$	$1(-\frac{3}{2})$	$35(\pm 2)$	$1(-2)$
14	2	$21(-\frac{5}{2}), 35(\frac{3}{2})$	$1(\frac{3}{2})$	$35(\pm 2)$	$1(2)$
31/2	1/2	$20(-\frac{9}{4}), 15(-\frac{1}{4}), 15(\frac{7}{4}), 6(\frac{15}{4})$	$1(\frac{3}{4})$	$15(\pm 3), 20(\pm 1)$	$1(1)$
31/2	1/2	$6(-\frac{15}{4}), 15(-\frac{7}{4}), 15(\frac{1}{4}), 20(\frac{9}{4})$	$1(-\frac{3}{4})$	$15(\pm 3), 20(\pm 1)$	$1(-1)$
31/2	1/2	$4(-\frac{15}{4}), 18(-\frac{7}{4}), 18(\frac{1}{4}), 13(\frac{9}{4}), 3(\frac{17}{4})$	$1(-\frac{3}{4})$	$1(\pm 5), 12(\pm 3), 22(\pm 1)$	$1(-1)$
31/2	1/2	$3(-\frac{17}{4}), 13(-\frac{9}{4}), 18(-\frac{1}{4}), 18(\frac{7}{4}), 4(\frac{15}{4})$	$1(\frac{3}{4})$	$1(\pm 5), 12(\pm 3), 22(\pm 1)$	$1(1)$
16	0	$4(\pm 4), 14(\pm 2), 20(0)$	$1(0)$	$6(\pm 4), 16(\pm 2), 26(0)$	$1(0)$

Table A.9: Quasiparticle charge assignments for $Sp(8)_1$.

$\nu_{Sp(8)_1}$	$\#Q_\sigma$	$\#Q_{\mathsf{E}}$	$\#Q_\tau$	$\#Q_S$
16	$4(0), 2(\pm 2)$	$9(0), 8(\pm 2), 1(\pm 4)$	$16(0), 12(\pm 2), 4(\pm 4)$	$16(0), 8(\pm 2), 5(\pm 4)$

Table A.10: Current operator charge assignments for the conformal embeddings $SO(2r+1) \times SO(15-2r) \subset E_8$ for $r = 1, 2, 3$ and Ising $\times\, SO(15) \subset E_8$.

$\nu_{SO(7)}$	$\nu_{SO(9)}$	$\#Q_{SO(7)}$	$\#Q_{SO(9)}$
0	16	$21(0)$	$22(0), 7(\pm 4)$
0	16	$21(0)$	$16(0), 4(\pm 2), 6(\pm 4)$
4	12	$11(0), 5(\pm 2)$	$12(0), 9(\pm 2), 3(\pm 4)$
8	8	$7(0), 6(\pm 2), 1(\pm 4)$	$14(0), 10(\pm 2), 1(\pm 4)$
12	4	$9(0), 3(\pm 2), 3(\pm 4)$	$22(0), 7(\pm 2)$
16	0	$11(0), 5(\pm 4)$	$36(0)$
$\nu_{SO(5)}$	$\nu_{SO(11)}$	$\#Q_{SO(5)}$	$\#Q_{SO(11)}$
0	16	$10(0)$	$37(0), 9(\pm 4)$
0	16	$10(0)$	$19(0), 12(\pm 2), 6(\pm 4)$
4	12	$4(0), 3(\pm 2)$	$19(0), 15(\pm 2), 3(\pm 4)$
8	8	$4(0), 2(\pm 2), 1(\pm 4)$	$25(0), 14(\pm 2), 1(\pm 4)$
16	0	$4(0), 3(\pm 4)$	$55(0)$
$\nu_{SO(3)}$	$\nu_{SO(13)}$	$\#Q_{SO(3)}$	$\#Q_{SO(13)}$
0	16	$3(0)$	$56(0), 11(\pm 4)$
0	16	$3(0)$	$26(0), 20(\pm 2), 6(\pm 4)$
4	12	$1(0), 1(\pm 4)$	$30(0), 21(\pm 2), 3(\pm 4)$
16	0	$1(0), 1(\pm 8)$	$78(0)$
ν_{Ising}	$\nu_{SO(15)}$	$\#Q_{\text{Ising}}$	$\#Q_{SO(15)}$
0	16	N/A	$79(0), 13(\pm 4)$
0	16	N/A	$37(0), 28(\pm 2), 6(\pm 4)$

Table A.11: Quasiparticle charge assignments for the conformal embeddings $SO(2r+1) \times SO(15-2r) \subset E_8$ for $r = 1, 2, 3$ and Ising $\times\, SO(15) \subset E_8$. Below, f and σ denote the nontrivial super-selection sectors of the $SO(2r+1)$ and $SO(15-2r)$ topological phases.

$\nu_{SO(7)}$	$\nu_{SO(9)}$	$\#(Q_f)_{SO(7)}$	$\#(Q_f)_{SO(9)}$	$\#(Q_\sigma)_{SO(7)}$	$\#(Q_\sigma)_{SO(9)}$
0	16	$7(0)$	$7(0), 1(\pm 4)$	$8(0)$	$8(\pm 2)$
0	16	$7(0)$	$1(0), 4(\pm 2)$	$8(0)$	$6(0), 4(\pm 2), 1(\pm 4)$
4	12	$5(0), 1(\pm 2)$	$3(0), 3(\pm 2)$	$4(\pm 1)$	$6(\pm 1), 2(\pm 3)$
8	8	$3(0), 2(\pm 2)$	$5(0), 2(\pm 2)$	$4(0), 2(\pm 2)$	$8(0), 4(\pm 2)$
12	4	$1(0), 3(\pm 2)$	$7(0), 1(\pm 2)$	$3(\pm 1), 1(\pm 3)$	$8(\pm 1)$
16	0	$5(0), 1(\pm 4)$	$9(0)$	$4(\pm 2)$	$16(0)$
$\nu_{SO(5)}$	$\nu_{SO(11)}$	$\#(Q_f)_{SO(5)}$	$\#(Q_f)_{SO(11)}$	$\#(Q_\sigma)_{SO(5)}$	$\#(Q_\sigma)_{SO(11)}$
0	16	$5(0)$	$9(0), 1(\pm 4)$	$4(0)$	$16(\pm 2)$
0	16	$5(0)$	$3(0), 4(\pm 2)$	$4(0)$	$12(0), 8(\pm 2), 2(\pm 4)$
4	12	$3(0), 1(\pm 2)$	$5(0), 3(\pm 2)$	$2(\pm 1)$	$12(\pm 1), 4(\pm 3)$
8	8	$1(0), 2(\pm 2)$	$7(0), 2(\pm 2)$	$2(0), 1(\pm 2)$	$16(0), 8(\pm 2)$
16	0	$3(0), 1(\pm 4)$	$11(0)$	$2(\pm 2)$	$32(0)$
$\nu_{SO(3)}$	$\nu_{SO(13)}$	$\#(Q_f)_{SO(3)}$	$\#(Q_f)_{SO(13)}$	$\#(Q_\sigma)_{SO(3)}$	$\#(Q_\sigma)_{SO(13)}$
0	16	$3(0)$	$11(0), 1(\pm 4)$	$2(0)$	$32(\pm 2),$
0	16	$3(0)$	$5(0), 4(\pm 2)$	$2(0)$	$24(0), 16(\pm 2), 4(\pm 4)$
4	12	$1(0), 1(\pm 2)$	$7(0), 3(\pm 2)$	$1(\pm 1)$	$24(\pm 1), 8(\pm 3)$
16	0	$1(0), 1(\pm 4)$	$13(0)$	$1(\pm 2)$	$64(0)$
ν_{Ising}	$\nu_{SO(15)}$	$\#(Q_f)_{\text{Ising}}$	$\#(Q_f)_{SO(15)}$	$\#(Q_\sigma)_{\text{Ising}}$	$\#(Q_\sigma)_{SO(15)}$
0	16	$1(0)$	$13(0), 1(\pm 4)$	$1(0)$	$64(\pm 2),$
0	16	$1(0)$	$7(0), 4(\pm 2)$	$1(0)$	$48(0), 32(\pm 2), 8(\pm 4)$

Table A.12: Current operator charge assignments for the conformal embeddings $SO(2r) \times SO(16-2r) \subset E_8$ for $r = 4, 3, 2, 1$.

$\nu_{SO(8)}$	$\nu_{SO(8)}$	$\#(Q)_{SO(8)}$	$\#(Q)_{SO(8)}$
0	16	$28(0)$	$16(0), 6(\pm 4)$
4	12	$16(0)$,$6(\pm 2)$	$10(0), 6(\pm 2), 3(\pm 4)$
8	8	$10(0)$,$8(\pm 2)$,$1(\pm 4)$	$10(0), 8(\pm 2), 1(\pm 4)$
12	4	$10(0), 6(\pm 2), 3(\pm 4)$	$16(0)$,$6(\pm 2)$
16	0	$16(0), 6(\pm 4)$	$28(0)$
$\nu_{SO(6)}$	$\nu_{SO(10)}$	$\#(Q)_{SO(6)}$	$\#(Q)_{SO(10)}$
0	16	$15(0)$	$29(0), 8(\pm 4)$
0	16	$15(0)$	$17(0), 8(\pm 2), 6(\pm 4)$
3	13	$9(0), 3(\pm 2)$	$17(0), 10(\pm 2), 4(\pm 4)$
4	12	$7(0), 4(\pm 2)$	$15(0), 12(\pm 2), 3(\pm 4)$
8	8	$5(0), 4(\pm 2), 1(\pm 4)$	$19(0), 12(\pm 2), 1(\pm 4)$
11	5	$5(0), 3(\pm 2), 2(\pm 4)$	$25(0), 10(\pm 2)$
12	4	$9(0), 3(\pm 4)$	$29(0), 8(\pm 2)$
16	0	$7(0), 4(\pm 4)$	$45(0)$
$\nu_{SO(4)}$	$\nu_{SO(12)}$	$\#(Q)_{SO(4)}$	$\#(Q)_{SO(12)}$
0	16	$6(0)$	$46(0), 10(\pm 4)$
0	16	$6(0)$	$22(0), 16(\pm 2), 6(\pm 4)$
2	14	$4(0), 1(\pm 2)$	$26(0), 15(\pm 2), 5(\pm 4)$
4	12	$2(0), 2(\pm 2)$	$24(0), 18(\pm 2), 3(\pm 4)$
8	8	$4(0), 1(\pm 4)$	$32(0), 16(\pm 2), 1(\pm 4)$
10	6	$2(0), 1(\pm 2), 1(\pm 4)$	$36(0), 15(\pm 2)$
16	0	$2(0), 2(\pm 4)$	$66(0)$
$\nu_{SO(2)}$	$\nu_{SO(14)}$	$\#(Q)_{SO(2)}$	$\#(Q)_{SO(14)}$
0	16	$2(0)$	$67(0), 12(\pm 4)$
0	16	$2(0)$	$31(0), 24(\pm 2), 6(\pm 4)$
1	15	$1(\pm 2)$	$37(0), 21(\pm 2), 6(\pm 4)$
4	12	$1(\pm 4)$	$37(0), 24(\pm 2), 3(\pm 4)$
9	7	$1(\pm 6)$	$49(0), 21(\pm 2)$
16	0	$1(\pm 8)$	$91(0)$

Table A.13: Quasiparticle charge assignments for the conformal embeddings $SO(2r) \times SO(16-2r) \subset E_8$ for $r = 4, 3, 2, 1$. Below, f, $s+$, and $s-$ denote the nontrivial super-selection sectors of the $SO(2r)$ and $SO(16-2r)$ topological phases.

$\nu_{SO(8)}$	$\nu_{SO(8)}$	$\#(Q_f)_{SO(8)}$	$\#(Q_f)_{SO(8)}$	$\#(Q_{s+})_{SO(8)}$	$\#(Q_{s+})_{SO(8)}$	$\#(Q_{s-})_{SO(8)}$	$\#(Q_{s-})_{SO(8)}$
0	16	$8(0)$	$6(0), 1(\pm 4)$	$8(0)$	$4(\pm 2)$	$8(0)$	$4(\pm 2)$
0	16	$8(0)$	$4(\pm 2)$	$8(0)$	$6(0), 1(\pm 4)$	$8(0)$	$4(\pm 2)$
0	16	$8(0)$	$4(\pm 2)$	$8(0)$	$4(\pm 2)$	$8(0)$	$6(0), 1(\pm 4)$
4	12	$6(0), 1(\pm 2)$	$2(0), 3(\pm 2)$	$4(\pm 1)$	$3(\pm 1), 1(\pm 3)$	$4(\pm 1)$	$3(\pm 1), 1(\pm 3)$
4	12	$4(\pm 1)$	$3(\pm 1), 1(\pm 3)$	$6(0), 1(\pm 2)$	$2(0), 3(\pm 2)$	$4(\pm 1)$	$3(\pm 1), 1(\pm 3)$
4	12	$4(\pm 1)$	$3(\pm 1), 1(\pm 3)$	$4(\pm 1)$	$3(\pm 1), 1(\pm 3)$	$6(0), 1(\pm 2)$	$2(0), 3(\pm 2)$
8	8	$4(0), 2(\pm 2)$	$4(0), 2(\pm 2)$	$4(0), 2(\pm 2)$	$4(0), 2(\pm 2)$	$4(0), 2(\pm 2)$	$4(0), 2(\pm 2)$
12	4	$2(0), 3(\pm 2)$	$6(0), 1(\pm 2)$	$3(\pm 1), 1(\pm 3)$	$4(\pm 1)$	$3(\pm 1), 1(\pm 3)$	$4(\pm 1)$
12	4	$3(\pm 1), 1(\pm 3)$	$4(\pm 1)$	$2(0), 3(\pm 2)$	$6(0), 1(\pm 2)$	$3(\pm 1), 1(\pm 3)$	$4(\pm 1)$
12	4	$3(\pm 1), 1(\pm 3)$	$4(\pm 1)$	$3(\pm 1), 1(\pm 3)$	$4(\pm 1)$	$2(0), 3(\pm 2)$	$6(0), 1(\pm 2)$
16	0	$6(0), 1(\pm 4)$	$8(0)$	$4(\pm 2)$	$8(0)$	$4(\pm 2)$	$8(0)$
16	0	$4(\pm 2)$	$8(0)$	$6(0), 1(\pm 4)$	$8(0)$	$4(\pm 2)$	$8(0)$
16	0	$4(\pm 2)$	$8(0)$	$4(\pm 2)$	$8(0)$	$6(0), 1(\pm 4)$	$8(0)$
$\nu_{SO(6)}$	$\nu_{SO(10)}$	$\#(Q_f)_{SO(6)}$	$\#(Q_f)_{SO(10)}$	$\#(Q_{s+})_{SO(6)}$	$\#(Q_{s+})_{SO(10)}$	$\#(Q_{s-})_{SO(6)}$	$\#(Q_{s-})_{SO(10)}$
0	16	$6(0)$	$8(0), 1(\pm 4)$	$4(0)$	$8(\pm 2)$	$4(0)$	$8(\pm 2)$
0	16	$6(0)$	$2(0), 4(\pm 2)$	$4(0)$	$6(0), 4(\pm 2), 1(\pm 4)$	$4(0)$	$6(0), 4(\pm 2), 1(\pm 4)$
3	13	$3(\pm 1)$	$4(\pm 1), 1(\pm 3)$	$1(-\frac{3}{2}), 3(\frac{1}{2})$	$4(-\frac{5}{2}), 5(-\frac{1}{2}), 6(\frac{3}{2}), 1(\frac{7}{2})$	$3(-\frac{1}{2}), 1(\frac{3}{2})$	$1(-\frac{7}{2}), 6(-\frac{3}{2}), 5(\frac{1}{2}), 4(\frac{5}{2})$
3	13	$3(\pm 1)$	$4(\pm 1), 1(\pm 3)$	$3(-\frac{1}{2}), 1(\frac{3}{2})$	$1(-\frac{7}{2}), 6(-\frac{3}{2}), 5(\frac{1}{2}), 4(\frac{5}{2})$	$1(-\frac{3}{2}), 3(\frac{1}{2})$	$4(-\frac{5}{2}), 5(-\frac{1}{2}), 6(\frac{3}{2}), 1(\frac{7}{2})$
4	12	$4(0), 1(\pm 2)$	$4(0), 3(\pm 2)$	$2(\pm 1)$	$6(\pm 1), 2(\pm 3)$	$2(\pm 1)$	$6(\pm 1), 2(\pm 3)$
8	8	$2(0), 2(\pm 2)$	$6(0), 2(\pm 2)$	$2(0), 1(\pm 2)$	$8(0), 4(\pm 2)$	$2(0), 1(\pm 2)$	$8(0), 4(\pm 2)$
11	5	$2(\pm 1), 1(\pm 3)$	$5(\pm 1)$	$1(-\frac{5}{2}), 1(-\frac{1}{2}), 2(\frac{3}{2})$	$5(-\frac{3}{2}), 10(\frac{1}{2}), 1(\frac{5}{2})$	$2(-\frac{3}{2}), 1(\frac{1}{2}), 1(\frac{5}{2})$	$1(-\frac{5}{2}), 10(-\frac{1}{2}), 5(\frac{3}{2})$
11	5	$2(\pm 1), 1(\pm 3)$	$5(\pm 1)$	$2(-\frac{3}{2}), 1(\frac{1}{2}), 1(\frac{5}{2})$	$1(-\frac{5}{2}), 10(-\frac{1}{2}), 5(\frac{3}{2})$	$1(-\frac{5}{2}), 1(-\frac{1}{2}), 2(\frac{3}{2})$	$5(-\frac{3}{2}), 10(\frac{1}{2}), 1(\frac{5}{2})$
12	4	$3(\pm 2)$	$8(0), 1(\pm 2)$	$1(-3), 3(1)$	$8(\pm 1)$	$3(-1), 1(3)$	$8(\pm 1)$
12	4	$3(\pm 2)$	$8(0), 1(\pm 2)$	$3(-1), 1(3)$	$8(\pm 1)$	$1(-3), 3(1)$	$8(\pm 1)$
16	0	$4(0), 1(\pm 4)$	$10(0)$	$2(\pm 2)$	$16(0)$	$2(\pm 2)$	$16(0)$
$\nu_{SO(4)}$	$\nu_{SO(12)}$	$\#(Q_f)_{SO(4)}$	$\#(Q_f)_{SO(12)}$	$\#(Q_{s+})_{SO(4)}$	$\#(Q_{s+})_{SO(12)}$	$\#(Q_{s-})_{SO(4)}$	$\#(Q_{s-})_{SO(12)}$
0	16	$4(0)$	$10(0), 1(\pm 4)$	$2(0)$	$16(\pm 2)$	$2(0)$	$16(\pm 2)$
0	16	$4(0)$	$4(0), 4(\pm 2)$	$2(0)$	$12(0), 8(\pm 2), 2(\pm 4)$	$2(0)$	$12(0), 8(\pm 2), 2(\pm 4)$
2	14	$2(\pm 1)$	$5(\pm 1), 1(\pm 3)$	$1(\pm 1)$	$11(\pm 1), 5(\pm 3)$	$2(0)$	$10(0), 10(\pm 2), 1(\pm 4)$
2	14	$2(\pm 1)$	$5(\pm 1), 1(\pm 3)$	$2(0)$	$10(0), 10(\pm 2), 1(\pm 4)$	$1(\pm 1)$	$11(\pm 1), 5(\pm 3)$
4	12	$2(0), 1(\pm 2)$	$6(0), 3(\pm 2)$	$1(\pm 1)$	$12(\pm 1), 4(\pm 3)$	$1(\pm 1)$	$12(\pm 1), 4(\pm 3)$
8	8	$2(\pm 2)$	$8(0), 2(\pm 2)$	$1(\pm 2)$	$16(0), 8(\pm 2)$	$2(0)$	$16(0), 8(\pm 2)$
8	8	$2(\pm 2)$	$8(0), 2(\pm 2)$	$2(0)$	$16(0), 8(\pm 2)$	$1(\pm 2)$	$16(0), 8(\pm 2)$
10	6	$1(\pm 1), 1(\pm 3)$	$6(\pm 1)$	$1(\pm 2)$	$20(0), 6(\pm 2)$	$1(\pm 1)$	$15(\pm 1), 1(\pm 3)$
10	6	$1(\pm 1), 1(\pm 3)$	$6(\pm 1)$	$1(\pm 1)$	$15(\pm 1), 1(\pm 3)$	$1(\pm 2)$	$20(0), 6(\pm 2)$
16	0	$2(0), 1(\pm 4)$	$12(0)$	$1(\pm 2)$	$32(0)$	$1(\pm 2)$	$32(0)$
$\nu_{SO(2)}$	$\nu_{SO(14)}$	$\#(Q_f)_{SO(2)}$	$\#(Q_f)_{SO(14)}$	$\#(Q_{s+})_{SO(2)}$	$\#(Q_{s+})_{SO(14)}$	$\#(Q_{s-})_{SO(2)}$	$\#(Q_{s-})_{SO(14)}$
0	16	$2(0)$	$12(0), 1(\pm 4)$	$1(0)$	$32(\pm 2)$	$1(0)$	$32(\pm 2)$
0	16	$2(0)$	$6(0), 4(\pm 2)$	$1(0)$	$24(0), 16(\pm 2), 4(\pm 4)$	$1(0)$	$24(0), 16(\pm 2), 4(\pm 4)$
1	15	$1(\pm 1)$	$6(\pm 1), 1(\pm 3)$	$1(-\frac{1}{2})$	$6(-\frac{7}{2}), 21(-\frac{3}{2}), 21(\frac{1}{2}), 15(\frac{5}{2}), 1(\frac{9}{2})$	$1(\frac{1}{2})$	$1(-\frac{9}{2}), 15(-\frac{5}{2}), 21(-\frac{1}{2}), 21(\frac{3}{2}), 6(\frac{7}{2})$
1	15	$1(\pm 1)$	$6(\pm 1), 1(\pm 3)$	$1(\frac{1}{2})$	$1(-\frac{9}{2}), 15(-\frac{5}{2}), 21(-\frac{1}{2}), 21(\frac{3}{2}), 6(\frac{7}{2})$	$1(-\frac{1}{2})$	$6(-\frac{7}{2}), 21(-\frac{3}{2}), 21(\frac{1}{2}), 15(\frac{5}{2}), 1(\frac{9}{2})$
4	12	$1(\pm 2)$	$8(0), 3(\pm 2)$	$1(-1)$	$24(\pm 1), 8(\pm 3)$	$1(1)$	$24(\pm 1), 8(\pm 3)$
4	12	$1(\pm 2)$	$8(0), 3(\pm 2)$	$1(1)$	$24(\pm 1), 8(\pm 3)$	$1(-1)$	$24(\pm 1), 8(\pm 3)$
9	7	$1(\pm 3)$	$7(\pm 1)$	$1(-\frac{3}{2})$	$7(-\frac{5}{2}), 35(-\frac{1}{2}), 21(\frac{3}{2}), 1(\frac{7}{2})$	$1(\frac{3}{2})$	$1(-\frac{7}{2}), 21(-\frac{3}{2}), 35(\frac{1}{2}), 7(\frac{5}{2})$
9	7	$1(\pm 3)$	$7(\pm 1)$	$1(\frac{3}{2})$	$1(-\frac{7}{2}), 21(-\frac{3}{2}), 35(\frac{1}{2}), 7(\frac{5}{2})$	$1(-\frac{3}{2})$	$7(-\frac{5}{2}), 35(-\frac{1}{2}), 21(\frac{3}{2}), 1(\frac{7}{2})$
16	0	$1(\pm 4)$	$14(0)$	$1(-2)$	$64(0)$	$1(2)$	$64(0)$
16	0	$1(\pm 4)$	$14(0)$	$1(2)$	$64(0)$	$1(-2)$	$64(0)$